Applications of Macrocycles: From Nucleic Acid Sensors to Controlling Molecular Motion

Edward Alexander Wilkinson

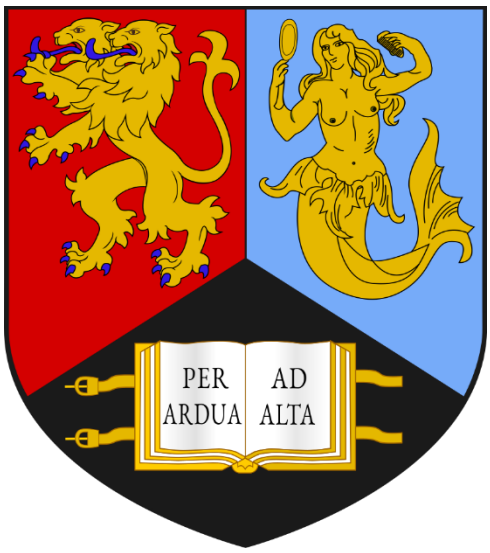

UNIVERSITY OF BIRMINGHAM

A thesis submitted to the
University of Birmingham
for the degree of
DOCTOR OF PHILOSOPHY

School of Chemistry
College of Engineering and Physical Sciences
University of Birmingham
September 2020

Abstract

Macrocycles have long been key molecular cornerstones of many fundamental processes found in nature and have risen to prominence over the last 60 years in the field of chemistry research, with their rich coordination chemistry seeing them used for a variety of applications. The work herein employs macrocycles and their complexes in two areas; firstly in the development of a switchable system which exhibits controlled molecular-level motion, and secondly as a component of a electrochemical nucleic acid sensing system capable of detecting important cancer biomarkers.

Harnessing molecular motion is considered vital for the development of next generation nanotechnology. In this thesis, the design, synthesis and study of a novel ball-bearing rotary system is described that employs the coordination chemistry of crown ethers to control the rate of rotation about the axis of a (η^4-tetraarylcyclobutadiene)(η^5-cyclopentadienyl)cobalt(I) sandwich complex core. Chemical inputs, in the form of pH changes and metal cations, were employed to exert switchable control over molecular motion, as evidenced by variable temperature ^{1}H NMR experiments and the subsequent calculation of kinetic parameters.

In 2016, Tucker and co-workers reported a nucleic acid probe modified with a copper cyclidene complex capable of electrochemically distinguishing between target DNA strands containing the four canonical nucleobases at one locus. The work herein details the synthesis of the cyclidene macrocycle and its transition metal complexes, and establishes the synthetic route for their incorporation into DNA. The sensing ability of the previously reported sensing system is explored as part of a SAM on the electrode surface, leading to the synthesis and study of a hetero-bimetallic and ratiometric sensing probe that can rapidly detect key cancer

biomarkers at low femtomolar levels. The ability to discriminate between nucleobases at such low concentrations raises the exciting possibility of biomarker detection without the need for amplification, highlighting the potential of this sensing system to act as a valuable medical tool in the diagnosis and management of genetic diseases.

Additionally, a variety of other cyclidene-modified DNA systems are synthesised and characterised, with strands varying in length and number of metal atoms, whilst the previously problematic electrochemical visualisation of the nickel complex is addressed. This research expands the previously reported family of metal-modified nucleic acids and provides the foundations for their electrochemical properties to be explored in a wider range of applications such as molecular wires.

Acknowledgements

Firstly, a huge thank you to my supervisors Prof. Jim Tucker and Dr Sarah Horswell. Jim, thank you for encouraging me to take every opportunity and for your unconditional support. You provided the platform for me to grow as not only a scientist but as a person over the last few years and I am truly grateful. Most importantly, you never gloated on one of the many occasions that QPR beat Blues! Sarah, thank you for your endless patience teaching me electrochemistry, for our varied discussions on everything and anything, and always giving me your support. I have also learnt more about gramma and the English language from you than I ever learnt at school!

A massive thank you to all past and present members of the Tucker Group; thank you for contributing to a thoroughly enjoyable, supportive and collaborative environment to perform some incredible science. A special thank you to Dr Francia Allabush for teaching me everything she knows and being a fantastic lab mentor. Thank you to Dr Holly Roberts for teaching me electrochemistry and always finding the time to answer any of my queries. Thank you to Dr Jon Kedge for always pushing my understanding and listening to any problems; I always valued our chats. Dr Aysha Ali, it's a miracle really that any of this work got done whilst you were around distracting us all! Thank you to Sam Todd for being the best lab assistant around. Finally, thank you to all the members of the Grainger and Cox groups who completed Office 408, especially Russell Wood, Connor Prior and Izzy Barker.

Thank you to Dr Chris Richards and Dr Ross Arthurs for hosting me at the University of East Anglia and for their help with the cobalt project. A big thank you to Dr Cecile Le Duff for your help with the VT NMR experiments, but just as importantly all your talks and cups of tea.

Thank you to Dr Chi Tsang and Peter Ashton for all their help and advice with mass spectrometry over the years. Thank you to Dr Louise Male for her work with the crystal structure, and Dr Allen Bowden for his help with HPLC. Thank you to the administrative team, Helen Vahey, Stuart Arkless, Bernard Tudor, Iain Wilkinson and colleagues for always being willing to help with a problem, no matter how big or small. You guys really are the glue of the department and it could not function without you. A special thank you to Dr Adrian Wright, who has been a valuable mentor since my first day at the University 8 years ago. I look forward to seeing you back at St Andrews.

To the guys at Lodge Hill; Mat Wakeling, Sajni Haria, Dr Nick Cundy and Dr Effie Pearson, it's been a privilege to share this journey, and a lot of pizza, with you. To the Gym Team boys, the Harborne Lane family and what can only be described as Joesef Baker's support network, thank you for always pretending to be interested in my work, never failing to provide humour and joy, and some important relief from the academic bubble. Joe, I hope this thesis answers a few of your questions.

A special thank you to my family, especially my amazing parents for all their support. You both are the perfect role models and I would not be in a position to complete this without your guidance through the years. Finally, to G, thank you for your unconditional love and support over the last couple of years. You are a wonderful partner and truly the best.

Table of Contents

1. Introduction 1

1.2.1. The Macrocyclic Effect 5

1.2.2. Crown Ethers 6

1.2.3. Cryptands and Lariat Ethers 7

1.2.4. Tetraaza Macrocycles 8

1.2.4.1. Porphyrins and Derivatives 8

1.2.4.2. Cyclams 10

1.2.4.3. Cyclidenes 11

1.2.5. Cavitands: Cyclodextrins, Calixarenes and Pillarenes 12

1.3.1. Crown Ether Synthesis 15

1.3.2. Cyclam Synthesis 16

1.3.3. Cyclidene Synthesis 17

1.4.1. Pharmaceuticals 19

1.4.2. Sensors 21

1.4.3. Logic Gates 24

1.4.4. Switchable Systems 25

1.4.5. Nanostructures 27

1.4.6. Mechanically Interlocked Structures: Catenanes and Rotaxanes 29

2. Controlling the Rotary Motion of Cobalt Sandwich Complexes 36

2.1.1. Controlled Molecular Motion 36

2.1.2. Metallocenes 41

2.1.2.1. Ferrocene 41

2.1.2.2. Metallocenes and Controllable Molecular Motion 42

2.1.2.3. Cobalt Sandwich Complexes 43

2.1.2.4. Synthesis of Sandwich Complexes 44

2.1.3. Variable Temperature NMR 45

2.1.3.1. Overview 45

2.1.3.2. Environmental Exchange 46

2.1.3.3. Temperature of Coalescence and Kinetics 48

2.4.1. Synthesis of 4'-(*o*-tolylethynyl)benzo-18-crown-6 ether 53

2.4.2. Cobalt Sandwich Complex Synthesis 54

2.4.3. Functionalisation of Cyclopentadienyl Ring 58

2.4.4. Synthesis of Control Compounds 62

2.5.1. Protonation of the Primary Amine Tether 66

2.5.2. Solvent Effects: Protic *vs* Aprotic 67

2.6.1. Initial VT Studies on the Rotary System 2.10 71

2.6.1.1. Acetonitrile at Neutral pH 71

2.6.1.2. Acetonitrile at Acidic pH 72

2.6.1.3. Methanol at Neutral pH 76

2.6.1.4. Methanol at Acidic pH 77

2.6.1.5. Summary 78

2.6.2. Variable Temperature NMR Studies with the Control Compounds 79

2.6.2.1. Absence of the Amine Tether 79

2.6.2.2. Absence of the Crown Ethers 81

2.6.2.3. Absence of the Amine Tether and the Crown Ethers 82

2.6.2.4. Crown Ethers replaced with Methoxy Units 83

2.6.2.5. Control Compounds Summary 84

2.6.3. Reversibility 85

2.6.4. Calculation of Activation Parameters 88

2.6.5. Probing the Nature of the Non-covalent Interactions 92

2.7.1. Potassium Titrations 95

2.7.2. Variable Temperature NMR Studies 98

2.7.2.1. Rotary System 2.10 98

2.7.2.2. Control Compound 2.11 101

2.7.3. Reversibility Studies 102

3. Metal-Modified Nucleic Acids 111

3.1.1. Deoxyribonucleic Acid 111

3.1.2. DNA in the Human Genome 114

3.1.3. Single Point Variants 116

3.1.3.1. Single Nucleotide Polymorphisms 116

3.1.3.2. Epigenetic Mutations 118

3.1.4. Automated Solid-Phase DNA Synthesis 120

3.1.4.1. Preparation of Nucleobase Phosphoramidites 121

3.1.4.2. The DNA Synthesis Cycle 122

3.1.4.3. Ultra-mild DNA Synthesis Conditions 124

3.1.5. Modified DNA 126

3.1.5.1. Nucleobase Modifications 126

3.1.5.2. Sugar Ring Modifications 128

3.1.5.3. Backbone Modifications 129

3.1.6. Incorporating Metals into DNA for Electrochemical Applications 131

3.1.6.1. Metal-Base Pairs 132

3.1.6.2. Ligand-Metal Coordination Complexes 134

3.1.6.3. Metallocenes 136

3.1.6.4. Direct Incorporation of Metals into the DNA Backbone 137

3.1.7. Electrochemistry 141

3.1.7.1. Electrochemical Set Up 141

3.1.7.2. Cyclic Voltammetry 142

3.3.1. Synthesis of Cyclidene Macrocycle 147

3.3.2. Metal Complexation 149

3.3.3. Synthesis of Cyclidene Link System 151

3.3.3.1. Synthesis of Link Diol 151

3.3.3.2. Preparation for DNA Synthesis: DMT Protection 152

3.3.3.3. Preparation for DNA Synthesis: Phosphitylation 153

3.3.4. Synthesis of Cyclidene Tag System 154

3.3.4.1. Synthesis of Tag Diol 154

3.3.4.2. Preparation for DNA Synthesis: DMT Protection 155

3.3.4.3. Preparation for DNA Synthesis: Phosphitylation 156

3.4.1. DNA Synthesis 157

3.4.2. Purification and Characterisation 157

3.5.1. Introduction 158

3.5.1.1. Redox Activity of Cyclidene Complexes 158

3.5.1.2. Redox Activity in DNA 159

3.5.2. Synthesised DNA Strands 160

3.5.3. Visualising the Nickel Redox Signal 161

3.5.3.1. Varying the Buffer Conditions 161

3.5.3.2. Varying the Working Electrode: Boron Doped Diamond 164

3.5.4. Conclusion 167

3.6.1. Previous Work 168

3.6.2. Synthesis of Triple Cyclidene DNA 169

3.6.3. UV-vis Characterisation 170

3.6.4. Electrochemical Analysis 171

3.6.5. Conclusion 172

4. Electrochemical Sensing with Metal-Modified Nucleic Acid Probes 179

4.1.1. Overview of Nucleic Acid Probes 179

4.1.2. DNA Sequencing 180

4.1.3. Commercial Sensing Probes 180

4.1.3.1. Overview 180

4.1.3.2. Molecular Beacons 181

4.1.3.3. TaqMan Assay 182

4.1.4. Electrochemical Methods 184

4.3.1. Probe Design and Synthesis 190

4.3.2. Purification and Characterisation 191

4.3.3. Thermal Melting Studies 193

4.3.4. Electrochemical Sensing 195

4.3.4.1. An Introduction to Surface-Based Electrochemistry 195

4.3.4.2. Self-Assembled Monolayer Formation 198

4.3.4.3. Detecting Binding Events 199

4.3.4.4. Nucleobase Discrimination 200

4.3.4.5. Reusability Studies 202

4.4.1. Probe Design and Synthesis 205

4.4.2. Characterisation and Purification 206

4.4.3. Thermal Melting Studies 207

4.4.4. Electrochemical Sensing 208

4.4.4.1. Initial Studies: Cyclic Voltammetry 208

4.4.4.2. Initial Studies: Square Wave Voltammetry 212

4.4.4.3. Determining the Cyclidene:Ferrocene Current Ratio 215

4.4.4.4. Varying the Nucleobase Target 216

4.4.4.5. Selectivity Studies 220

4.4.4.6. Limit of Detection 222

4.4.4.7. Reusability and Unbound Probe Regeneration 224

4.4.4.8. Epigenetic Sensing 227

4.4.4.9. Sensing with (*S*)-FcCycNINA 228

4.4.4.10. Summary 229

4.5.1. Sequence Selection 230

4.5.2. Thermal Melting Studies 232

4.5.3. Electrochemical Sensing 233

4.5.3.1. BRAF V600E 233

4.5.3.2. KRAS G12V and G12D 235

4.5.4. Summary 238

5. Experimental 242

5.1.1. Synthesis of Alkyne Precursors: 243

5.1.1.1. Trimethyl(*o*-tolylethynyl)silane: 243

5.1.1.2. 1-Ethynyl-2-methylbenzene: 244

5.1.2. Alkyne Functionalisation: 244

5.1.2.1. 4'-(*o*-tolylethynyl)benzo-18-crown-6 ether: 244

5.1.2.2. 4'-(*o*-tolylethynyl)veratrole: 246

5.1.3. Sandwich Complex Formation: 247

5.1.3.1. Chlorotris(triphenylphosphine) Cobalt 247

5.1.3.2. (η^4-1,3-*o*-Tolyl-2,4-benzo-18-crown-6-ether-cyclobutadiene)(η^5-carbomethoxycyclopentadienyl) Cobalt: 247

5.1.4. Synthesis of Cobalt Sandwich Complex Rotary System: 252

5.1.4.1. (η^4-1,3-*o*-Tolyl-2,4-benzo-18-crown-6-ether-cyclobutadiene)(η^5-*N*-3-(aminomethyl)benzylaminecyclopentadienyl) Cobalt: 252

5.1.5. Synthesis of Cobalt Sandwich Complex Control Compounds: 253

5.1.5.1. (η^4-1,3-o-Tolyl-2,4-veratrole-cyclobutadiene) (η^5-*N*-3-(amino-methyl)benzylaminecyclopentadienyl) Cobalt: 253

5.1.5.4. (η^4-1,3-*o*-Tolyl-2,4-benzo-18-crown-6-ether-cyclobutadiene)(η^5-*N*-(3-methylbenzylaminecyclopentadienyl) Cobalt: 258

5.1.6. X-Ray Diffraction 261

5.2.1. General Procedure: 261

5.2.1.1. Controlling Rotary Motion Through Protonation 261

5.2.1.2. Controlling Rotary Motion Through Metal Cation Binding 262

5.3.1. Synthesis of Cyclidene Macrocycle: 262

5.3.1.1. Methyl Diformylacetate: 262

5.3.1.2. Cyclidene Macrocycle: 263

5.3.2. Metal Complexation: 264

5.3.2.1. Nickel (II) Cyclidene Complex: 264

5.3.2.2. Copper (II) Cyclidene Complex: 265

5.3.3. Cyclidene Tag Complex Synthesis: 266

5.3.3.1. Cyclidene Tag Copper Complex: 266

5.3.3.2. Tritylation of Copper Cyclidene Tag Diol: 267

5.3.3.2.1. Regeneration of Copper Cyclidene Tag from Bistrityl Tag 268

5.3.3.3. Phosphitylation of Monotrityl Copper Cyclidene Tag: 269

5.3.4. Cyclidene Link Complex Synthesis: 270

5.3.4.1. Cyclidene Link Nickel Complex: 270

5.3.4.2. Tritylation of Nickel Cyclidene Link Diol: 271

5.3.4.3. Phosphitylation of Monotrityl Nickel Cyclidene Link: 273

5.3.4.4. Cyclidene Link Copper Complex: 274

5.3.4.5. Tritylation of Copper Cyclidene Link Diol: 275

5.3.4.6. Phosphitylation of Monotrityl Copper Cyclidene Link: 276

5.4.1. Phosphitylation of Monotrityl Ferrocene: 277

5.5.1. Oligonucleotide Synthesis: 278

5.5.2. Oligonucleotide Purification: 279

5.5.2.1. Unmodified Oligonucleotide Sensing Probes and Targets: 280

5.5.2.2. Modified Oligonucleotide Sensing Probes: 281

5.5.2.3. Nickel Cyclidene Modified Oligonucleotides: 282

5.5.3. Thermal Melting Studies: 282

5.6.1. Equipment and Preparation: 283

5.6.2. Solution-based Electrochemistry 283

5.6.3. Surface-based Electrochemistry 284

5.6.3.1. Self-Assembled Monolayer Preparation: 285

5.6.3.2. Electrochemical Sensing Procedure: 285

5.6.3.3. Regeneration of the Unbound Probe: 286

6. Appendix 288

6.1.1. Crystal Data for 2.15 288

6.1.2. Variable Temperature NMR 289

6.1.2.1. Rotary System 2.10 in Methanol at Acidic pH 289

6.1.2.2. Rotary System 2.10 T_c in Acetonitrile at Acidic pH 290

6.1.2.3. Rotary System 2.10 Under Cationic Control: Reversibility 291

6.2.1. DNA Characterisation 292

6.2.2. HPLC Traces: 292

6.2.2.1. NiLink10mer 292

6.2.2.2. NiLink40mer 293

6.2.2.3. 3NiLink30mer 293

6.2.3. Electrochemistry 294

6.2.3.1. Nilink10mer 294

6.2.3.2. NiLink40mer 294

6.3.1. DNA Characterisation 295

6.3.1.1. Unmodified DNA 295

6.3.1.2. Modified DNA 296

6.3.2. HPLC Traces: 297

6.3.2.1. FcCycNINA Probe: 297

6.3.2.2. CycNINA Probe: 298

6.3.2.3. FcNINA Modified Probe: 298

6.3.2.4. FcCycBRAF Probe: 299

6.3.2.5. FcCycKRAS Probe: 299

6.3.3. Electrochemical Sensing Summary 300

6.3.4. Cyclic Voltammograms 301

6.3.4.1. FcCycNINA..... 301

6.3.4.2. FcCycBRAF..... 303

6.3.4.3. FcCycKRAS..... 304

6.3.5. Electrochemical Sensing Buffer Summary..... 305

6.3.6. Control Studies:..... 305

List of Abbreviations:

A	Adenine
Aq.	Aqueous
Bpy	Bipyridine
C	Cytosine
Cb	Cyclobutadiene ring
Cp	Cyclopentadiene ring
CPG	Controlled pore glass
CV	Cyclic voltammetry
Cyc	Cyclidene
DCM	Dichloromethane
DIPEA	N,N-diisopropylethylamine
DMAP	4-Dimethylaminopyridine
DMF	Dimethylformamide
DMT	Dimethoxytrityl
DNA	Deoxyribonucleic acid
ES	Electrospray
ESI	Electrospray ionisation
Equiv.	Equivalents
Fc	Ferrocene
G	Guanine
H-bonding	Hydrogen bonding

HIV	Human Immuno Virus
HPLC	High-performance liquid chromatography
HRMS	High resolution mass spectrometry
IR	Infrared
LC	Liquid chromatography
LoD	Limit of detection
m/z	Mass (m) to charge (z) ratio
MALDI	Matrix assisted laser desorption ionisation
mC	5-methylcytosine
MS	Mass spectrometry
NMR	Nuclear magnetic resonance
PAGE	Polyacrylamide gel electrophoresis
PCR	Polymerase chain reaction
PNA	Peptide Nucleic Acid
R_f	Retention factor
RNA	Ribonucleic acid
RP	Reverse phase
RT	Room temperature
SAM	Self-assembled monolayer
Sat.	Saturated
SEM	Standard error of the mean
SNP	Single Nucleotide Polymorphism

SPV	Single Point Variant
SW	Square wave voltammetry
T	Thymine
TCA	Trichloroacetic acid
TCEP	Tris(2-carboxyethyl)phosphine
TEA	Triethylamine
TEAA	Triethylammonium acetate
TFA	Trifluoroacetic acid
THF	Tetrahydrofuran
TLC	Thin layer chromatography
T_m	Thermal melting temperature
TMS	Trimethylsilane
TOF	Time of flight
Tris	Tris(hydroxymethyl)aminomethane
UV/vis	Ultraviolet/visible

1. Introduction

1.1. An Introduction to Macrocycles

Macrocycles are a broad class of molecule, defined as cyclic structures with 12 or more atoms, that have found applications in a wide range of areas in modern chemistry.[1] Long before they attracted the attention of scientists, nature had crafted intricate and precise designs employing macrocycles and implemented them as the cornerstones of life on Earth. Some of these specialist macrocycles perform a crucial role in the lives of humans, animals and plants. Chlorophylls play a critical role in photosynthesis in plants and bacteria, the process by which sunlight is converted into the energy used by the plant to live and grow. These naturally occurring macrocycles are photoreceptors that are involved in the three main elements of photosynthesis: light harvesting, energy transfer and energy conversion.[2]

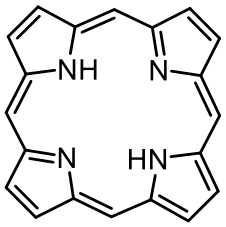

Figure 1.1: The chemical structure of porphyrin.

Porphyrins are a class of macrocycle with a similar structure to chlorophylls, consisting of four pyrroles linked together to form a rigid, square planar ring, Figure 1.1. The most famous porphyrin derivative is haem, which comprises the macrocycle and an iron cation bound at its centre. The haem unit is an essential component of haemoglobin, a globular protein found in red blood cells that transports oxygen around the body and is vital in the metabolism of living organisms.[3] Siderophores are another class of natural molecules that bind and transport

iron but, unlike porphyrins, are only found in fungi and bacteria. They have an exceptionally high affinity for Fe^{3+}. In fact, their name is derived from the Greek word for 'iron bearer'.[4] Although they are not exclusively macrocycles there are many macrocyclic examples including alcaligin, ferrichrome and enterobactin, shown below in Figure 1.2.[5, 6]

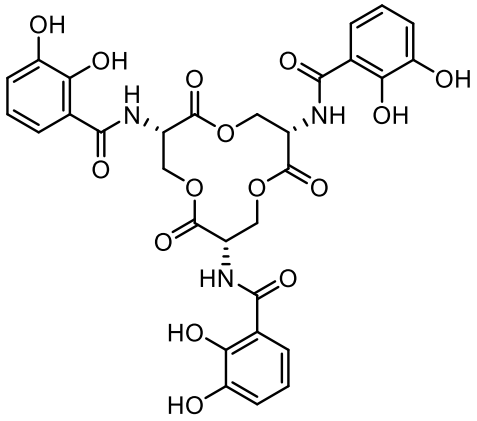

Figure 1.2: The chemical structure of enterobactin, a siderophore used in the transportation of iron in cells.

Despite being widely utilised in nature, there was only a limited interest in macrocycles from chemists in the first half of the 20th century. This was due in part to the difficulty in synthesising them, with methods generally long, difficult to control and poorly yielding. However, emphasis started to shift in the early 1960s when Curtis[7] and Busch[8] synthesised macrocyclic coordination complexes which used nitrogen and both nitrogen and sulfur respectively as donor atoms to coordinate a nickel cation. The work uses Ni^{2+} as a template to facilitate the formation of the macrocycle, with the individual components of the macrocycle coming together about the metal cation. Without the cationic template, the formation of the macrocycle fails because of competing reactions. This method, taking advantage of template effects to construct the macrocycle, is termed template synthesis.[8]

The development of templated synthesis suddenly made a range of macrocyclic compounds far more accessible and by the mid-1960s there had been a rapid increase in research into the synthesis of macrocycles, as well as their reactivity and coordination chemistry. Busch was influential in this, synthesising a series of ligands and coordination complexes that were often variations of his initial four-coordinate nitrogen and sulfur complex, before carrying out further studies on their properties and reactivity.[9-12] The drawback to this approach of modifying the same basic macrocycle template was that although the field of macrocycles was expanding, it was a narrow and restricted expansion. A novel idea was needed.

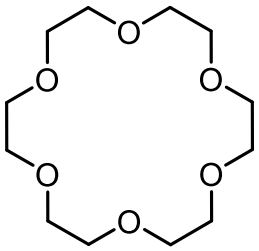

Figure 1.3: One of Pedersen's crown ethers. The names assigned to each crown ether are informative as to its size and structure. This is an 18-crown-6 ether: 18 atoms in the ring, 6 donor atoms.

When Pedersen published work in 1967 detailing the synthesis of no fewer than 33 novel cyclic polyethers with a variety of ring sizes, number of oxygen donor atoms and substituents, he administered the uplift that the field craved.[13] This was the birth of a species known as the crown ether, Figure 1.3, and a discovery that provided a new source of inspiration for researchers in the area. These crown ethers were found to strongly coordinate to a wide variety of alkali metal and alkaline earth ions, including ones which had not been researched previously.[14, 15] At the time, it was proving a significant challenge to find a neutral complexing agent which could bind alkali metal cations. Pedersen's discovery of crown ethers subsequently provided huge advances in fields such as biological ion transport, anionic synthetic reagents, and phase-transfer catalysis.[16]

Lehn built on this fundamental discovery in 1969 by developing a series of compounds called cryptands, bicyclic compounds of crown ether origin, which have three polyether strands connected to two bridge head nitrogen atoms. They were found to be even more selective with regards to metal ion binding than their crown ether cousins.[17] Pedersen and Lehn went on to share the 1987 Nobel Prize in Chemistry for this ground-breaking research, along with Donald Cram.

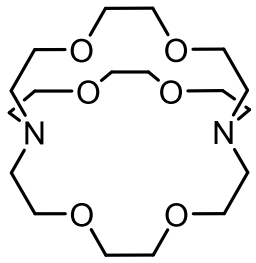

Figure 1.4: Lehn's Cryptand. The additional polyether arm increases the selectivity of the macrocycle towards metal cations.

Cram devoted his research to the field of macrocycles following Pedersen's creation of crown ethers and made a large contribution to what he called Host-Guest chemistry, more widely known as Supramolecular Chemistry. His research with cavitands, macrocycles with enforced cavities comparable to a bowl or vase, used Host-Guest chemistry to investigate substrate binding sites in enzymes.[18] He synthesised macrocycles which could selectively bind organic cations that varied in structure or chirality.[19-21] Some of these complexes acted as models to simulate the high selectivity exhibited by enzymes with their substrates, and demonstrated the role of selectivity and specificity in catalysis and other reactions of biological importance.[18, 19] Such model systems are of significant value in furthering our understanding of some of nature's more intricate processes.[22]

1.2. Coordination Chemistry of Macrocycles

1.2.1. The Macrocyclic Effect

As alluded to above, the rich coordination chemistry of macrocycles is vital in many aspects of nature. Porphyrins and siderophores both form strong and stable complexes with iron, and the subsequent properties of these complexes prove pivotal to their applications. The complexes are so thermodynamically and kinetically stable that the biological process is not impaired by a competing process that may break up the complex, such as demetallation. This detail is crucial and is why macrocycles execute this role in nature ahead of their acyclic counterparts.

It has long been known that the complex obtained from the reaction between a multidentate ligand and a metal ion is far more thermodynamically stable than a complex containing the equivalent monodentate ligands. This phenomenon is termed the 'chelate effect' and is primarily entropic in origin. Macrocycles have been found to form even more stable complexes with metal ions in comparison with those formed by the equivalent acyclic ligands. The name attributed to this is the 'macrocyclic effect'.[23] Like the chelate effect, the macrocyclic effect has entropic origins because macrocycle ligands are less flexible and possess a far more restricted geometry, and so are more preorganised for binding. This is more favourable entropically as macrocycles have less disorder to lose when forming a complex. Macrocycles are also less heavily solvated than acyclic ligands, which is enthalpically favourable for complex formation as less energy is required for desolvation. This gives a complex which has increased thermodynamic and kinetic stability.[22-24]

1.2.2. Crown Ethers

The structure of crown ethers consists of a core that has several oxygen donor atoms connected by ethylene bridges. They can form coordination complexes with alkali metal salts and salts which have similar cations through electrostatic attractions between the positively charged cation and the negative end of the carbon-oxygen dipole. If the guest species is an organic cation, such as an ammonium ion, hydrogen bonds contribute to the formation of the complex. There is an optimum arrangement which generates the most hydrogen bonds between the organic cation and crown ether. Crown ethers can also contain nitrogen or sulfur donor atoms, forming azo- or thio-crown ethers respectively.[13, 15]

The stability of crown ether complexes depends greatly on the relative sizes of the cation and the cavity of the ring. There is an optimal spatial fit when the cavity is of similar size to the cation. Factors such as charge density, steric hindrance in the ring and the solvating power of the solvent used can also have an effect.[15, 16] Varying the size of the crown ether cavity will change which cation is favoured to form the most stable complex. If the ion is too large to sit in the hole of the ring, a stable complex will not be formed. For example, in acetonitrile a 12-crown-4 ether forms its most stable complex with lithium cations, whereas the larger 15-crown-5 favours sodium, which is much bigger. Whilst complexes can also be formed with sodium cations, potassium is the ideal size for 18-crown-6 ethers and so forms the most stable complex.[25] Generally, complexes form with a stoichiometry of 1:1 between the bound cation and the crown ether ligand. However, there have been some instances of 2:1 and even 3:2 crown ether:cation complexes, with larger cations held between two crown ether units in what Pedersen speculated to be a possible ‘sandwich’ structure.[14]

Alongside cavity size, the identity of the donor atoms in the macrocycle have a strong influence on complexation. Donor atoms have specific preferences towards the type of metal ion that they prefer to bind, and these can be explained by the Hard-Soft Acid Base Theory. It states that a hard Lewis acid preferentially binds a hard Lewis base, whilst a soft Lewis acid favours a soft Lewis base. Hard acids are usually small or highly charged ions, and so have a high charge density, whereas soft acids tend to be larger ions or have a low charge and are more polarizable than their hard base counterparts.[26] As oxygen is a hard base, crown ethers preferentially bind metal ions from groups 1 and 2, for example Na^+ or K^+. In a thio-crown ether, where the oxygen atoms have been replaced with sulfur, a soft base, the stability of complexes with transition metal cations such as Ag^+ or Hg^+ is markedly increased, whilst it is reduced for complexes with Tl^+ or Pb^{2+}.[14, 25]

1.2.3. Cryptands and Lariat Ethers

Discovered by Lehn shortly after Pedersen released the details of his crown ether discovery, cryptands are enveloping hetero-macrocycles composed of three polyether strands connected to two bridge head nitrogen atoms.[17] This combination of oxygen and nitrogen atoms, as well as extra donor atoms, led to cryptands being far more selective than crown ethers in their preference for cations to bind. Having these extra donor atoms also results in exclusion of molecules of solvent from the solvation sphere of the cation, something that is rarely the case with crown ether complexes.[16] Whilst crown ethers form two-dimensional complexes which have fast kinetics when binding and unbinding cations, the envelope-like complexes favoured by cryptands are more three-dimensional. This results in slower complexation kinetics.[16, 27]

Lariat crown ethers are similar to cryptands in that they also have an extra polyether strand but, rather than forming a bridge over the crown ether cavity, that extra strand is a free arm connected to the crown ether by just the one bridgehead nitrogen atom. Importantly, the free polyether arm still takes part in binding. This gives lariat crown ethers a flexibility that cryptands do not possess, which gives them faster complexing kinetics, whilst still forming enveloping complexes.[16, 27, 28]

1.2.4. Tetraaza Macrocycles

Macrocycles containing solely nitrogen donor atoms do not have the same selectivity that crown ethers can have over the metal cations that they can bind. This is partly due to the hard/soft base properties of the nitrogen donor atoms. As nitrogen lies somewhere in the middle of the two extremes this leads to a wider range of potential binding targets, with M^{2+} and M^{3+} cations generally favoured.

1.2.4.1. Porphyrins and Derivatives

Consequently, a range of porphyrin derivatives are seen complexing different metals in nature. The oxygen transport expertise of haemoglobin centres around the porphyrin-iron complex of the haem unit, whilst plants rely on chlorophyll to harvest sunlight to power the

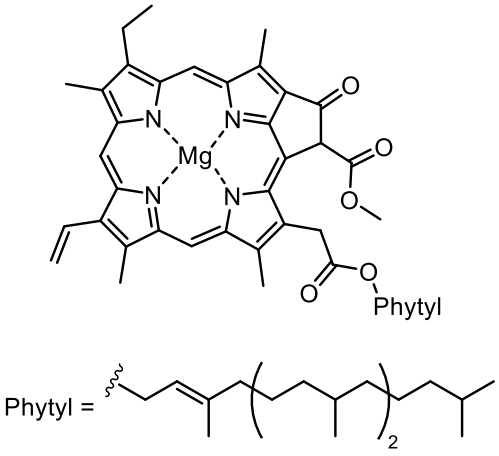

Figure 1.5: Structure of Chlorophyll A.

plant. All chlorophylls contain the chlorin ligand, a porphyrin derivative that complexes Mg^{2+}, Figure 1.5. Vitamin B_{12} is a corrinoid; the corrin ring at its core is a pyrrole-based macrocycle very similar to porphyrins.[12] It uses the nitrogen donor atoms of its four pyrrole units along with its benzimidazole-derived side arm to coordinate cobalt in an octahedral geometry, Figure 1.6. The final coordination site acts as a catalytic centre.[29]

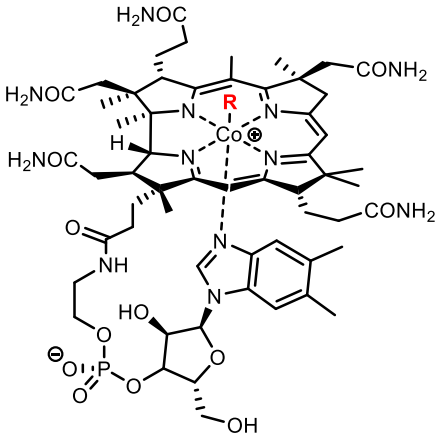

Figure 1.6: The octahedral geometry of the cobalt complex in vitamin B_{12}.

It is not just cations that these porphyrin derivatives are limited to binding. Sapphyrins are expanded porphyrins, discovered accidently during an attempted synthesis of vitamin B_{12}, that possess five pyrrole units. They have a 22 π-electron core compared to the 18 π-electron core of porphyrins and corroles, and unlike their tetrapyrrole counterparts, they commonly exist in their protonated state. It is the protonation of two of the core nitrogen donor atoms that allows for the complexation of a range of anions through hydrogen bonding, with targets including a range of phosphates and halogen anions. They are capable of forming 1:1 and 2:1 complexes, with the anion commonly situated above or below the central cavity.[30, 31]

1.2.4.2. Cyclams

Cyclams possess a core of four nitrogen atoms that sit in a square planar conformation with an empty cavity between them. Like porphyrins, the nature of the nitrogen donor atoms and size of the cavity allows them to bind a variety of metal cations, including Ni^{2+}, Cu^{2+}, Pb^{2+}, Zn^{2+}, Co^{2+}, Cd^{2+} and Hg^{2+} with high thermodynamic and kinetic stability.[32-34] Often the bound metal sits in the square planar cavity between the nitrogen donor atoms but the flexibility of the ethylene and propylene bridges can lead to square pyramidal and sometimes trigonal bipyramidal confirmations to be adopted. Bridged cyclams are molecules where an internal ethylene bridge is used to connect two of the nitrogen atoms and give additional structural rigidity. This added structure can lead to stronger complexes forming on reaction with a metal ion.

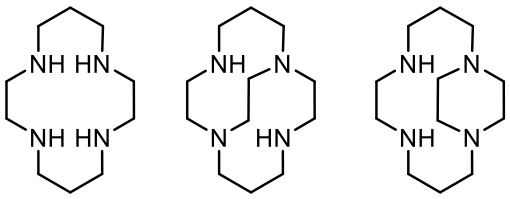

Figure 1.7: The traditional cyclam (left) and its bridged derivatives: cross bridged cyclam (centre) and side bridged cyclam (right).

There are two different variations, cross-bridged and side-bridged cyclams, Figure 1.7.[34-36] Unlike the original cyclam, bridged cyclams do not form planar coordination complexes with metal ions, instead forming an envelope around the metal ion.[35] Cyclam complexes are also pH sensitive, as the nitrogen donor atoms can be protonated and lead to decomplexation, something not experienced by macrocyclic complexes with oxygen or sulfur donors.[34]

1.2.4.3. Cyclidenes

Cyclidenes are neutral macrocycles whose core of four nitrogen atoms connected by ethylene and propylene bridges have a striking structural resemblance to cyclam. Where cyclidenes differ is that the propylene bridges are composed of conjugated double bonds. This structural diversion greatly alters the properties of the macrocycle. Firstly, the conjugated system gives cyclidenes a rigidity and they adopt an almost planar structure, which is also observed in their coordination complexes.[37] Secondly, the conjugation increases the stability of the complexes formed. For example, complexes are more stable in acidic conditions, with the coordinating nitrogen atoms less prone to protonation and subsequent decomplexation than cyclams.

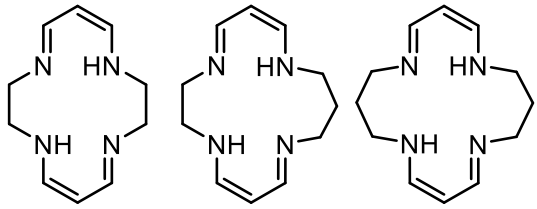

Figure 1.8: The traditional 14 atom cyclidene (left) alongside the expanded [15] (centre) and [16] (right) derivatives.

Like other tetraaza macrocycles, cyclidenes form complexes with a range of metal ions, with Cu^{2+} and Ni^{2+} coordination complexes being common, as well as Fe^{2+}, Co^{2+} and Zn^{2+}.[38] Rare examples even include palladium and platinum complexes.[39] When a coordination complex is formed, the amino nitrogen atoms in the macrocycle ligand are deprotonated, allowing neutral complexes to be formed with M^{2+} cations.[38-42] The core cyclidene structure usually consists of 14 atoms, because of the two ethylene and two propylene bridges, but 15 and 16 atom variations exist, with additional propylene bridges replacing the ethylene bridge, Figure 1.8. These larger 15 and 16 membered macrocycles are slightly more flexible and deviations from planarity are observed as ring size increases.[42] They also possess a more versatile coordination chemistry, and have been shown to coordinate in three equatorial positions and

one axial position in an octahedral Fe^{2+} complex, as well as a conventional square planar arrangement.[40, 41, 43]

That Co^{2+} and Ni^{2+} coordination complexes are some of the most common can be partially explained by the Irving-Williams Series, which refers to the relative stabilities of coordination complexes formed between a metal ion and ligand. It states that the stability constants of the first-row transitions metal ions are as follows:

$$Mn^{2+} < Fe^{2+} < Co^{2+} < Ni^{2+} < Cu^{2+} > Zn^{2+}$$

The trend can be explained by several factors, including the decrease in ionic radius across the period from Mn^{2+} to Zn^{2+}. This follows the general increase in coordination complex stability across the period. The Crystal Field Stabilization Energy (CFSE) increases across the period, starting at zero for Mn^{2+} to a maximum at Ni^{2+}, before decreasing again for Cu^{2+} and finally returning to zero for Zn^{2+}. The higher the CFSE, the higher the stability of the complex. Although Cu^{2+} has a lower CFSE than Ni^{2+}, octahedral Cu^{2+} coordination complexes gain additional stability due to the Jahn-Teller effect, leading to the high stability constant for Cu^{2+}.[44]

1.2.5. Cavitands: Cyclodextrins, Calixarenes and Pillarenes

Cavitands are container-like molecules with a hydrophobic binding pocket which allows an appropriately sized hydrophobic guest to dock. They include cyclodextrins, shown in Figure 1.9, which are naturally occurring cyclic oligosaccharides that adopt a cone-like structure with a hydrophobic interior that can bind non-polar molecules. They have long been employed as a solubilizing agent for drug compounds, enhancing the delivery of the drug and subsequently increasing bioavailability.[45]

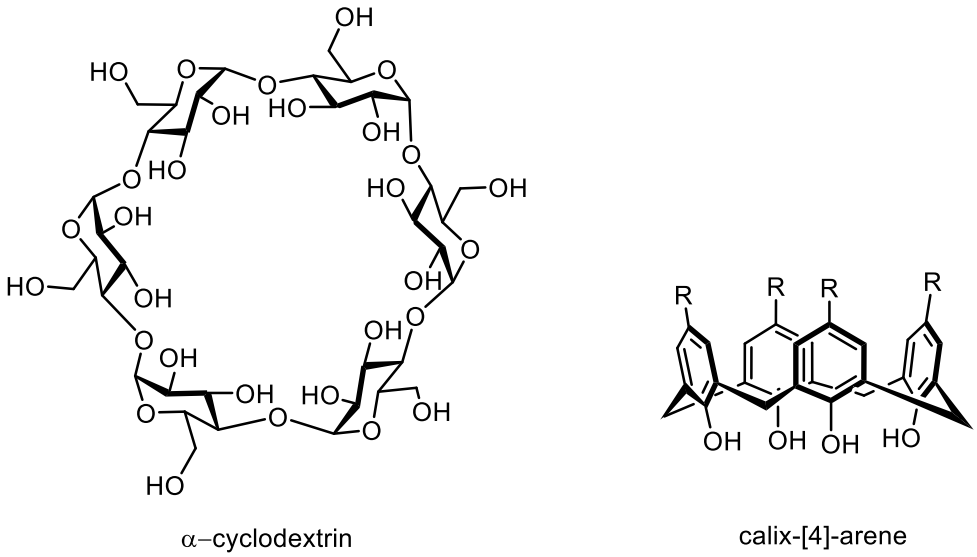

Figure 1.9: Examples of a naturally occurring cyclodextrin (left) and a calixarene (right).

Calixarenes are synthetic macrocycles which derive their name from the chalice shape adopted by their phenol monomer units. The specificity of the hydrophobic cavity has been used to mimic the active sites of enzymes whilst its ability to bind small ions such as Cu^{2+} and Zn^{2+} has been employed in catalysis.[46, 47] Their discovery led to the construction of a range of macrocycles with a rich host-guest chemistry including pillararenes and resorcinarenes, which consist of hydroquinone and 1,3-dihydroxylbenzene, respectively.[48, 49] Like cyclodextrins, pillararenes have proven useful drug delivery systems and can release their cargo on demand through changes in pH.[50, 51]

An extensive review of the host-guest chemistry of crown ethers, cyclodextrins, calixarenes and other systems has been reported by Stoddart *et al.*[52]

1.3. Macrocycle Synthesis

One of the main challenges that impeded early research into macrocycles was the difficulty to synthesise them. Macrocycle synthesis is a delicate business and an art; the optimum conditions are needed to encourage the individual components to come together and form a ring, rather than the more favourable chain.

Early methods of macrocycle synthesis were based around high dilution techniques. Long chains with reactive groups were reacted together in a very dilute solution to minimise any competing polymerisation reaction, affording the macrocycle as the kinetic product. High dilution can also be achieved through the very slow addition of one of the reactive species to the reaction solution.[53-56] Whilst this delicate balancing of conditions achieved macrocycle synthesis, early yields were often very low and reaction times long. They were not suitable in a practical sense.[57]

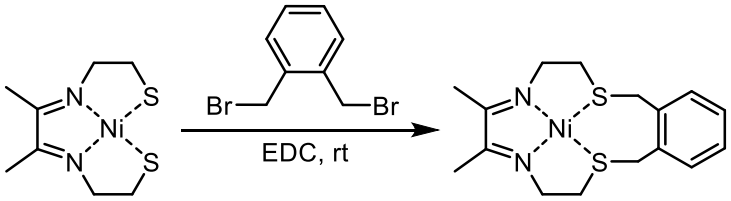

Scheme 1.1: Busch's early investigations of the template effect used a Ni^{2+} cation as the template.

The discovery by Curtis and Busch of the template effect revolutionised macrocycle synthesis. They observed that the coordination sphere of a template, often a metal cation, could be used to induce an optimum spatial arrangement of the reacting species that would encourage the formation of the macrocycle over any competing polymerisation reactions. Without the presence of the template, macrocycle formation would be highly disfavoured. Busch's early investigations into the template effect utilised a Ni^{2+} cation to control reactions between mercapto groups and alkyl halides, Scheme 1.1.[8, 11]

1.3.1. Crown Ether Synthesis

When populating his initial library of crown ether derivatives, Pedersen used some general methods including templating with sodium cations, which gave mixed results in terms of yields. Some dibenzo- and cyclohexyl-derivatives were afforded in respectable yields but others including 18-crown-6 ether gave the very low yields and so these were not viable methods for future crown ether synthesis. Since then, templating and high dilution techniques have been developed to synthesise crown ethers, with template effects proving to be popular.[13]

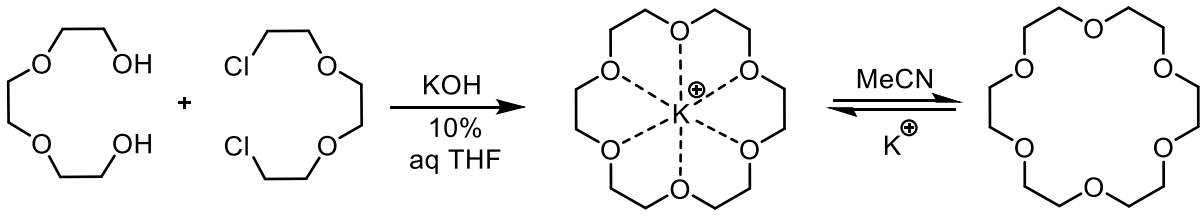

Scheme 1.2: The template synthesis of 18-crown-6 ether by Cram.

Greene first observed that the presence of a potassium cation enhanced the formation of 18-crown-6 ether from a diol and a ditosylate.[58] Cram then reported a simple template synthesis of 18-crown-6 from triethylene glycol and triethylene glycol dichloride in 1974 that has remained popular to this day.[59] The method, outlined in Scheme 1.2, uses an inorganic base, potassium hydroxide. The base has two roles. Firstly, it generates a better nucleophile by deprotonating the alcohol groups, encouraging nucleophilic attack towards the triethylene glycol dichloride. Secondly, the potassium cation acts as the template and encourages cyclisation, bringing the reactive sites into close proximity so a nucleophilic substitution reaction can occur and close the ring. This yields a crown ether-potassium complex. To remove the template ion and yield the free crown ether, demetallation is performed. Cram's method uses acetonitrile to do this, as the cyanide anion that is subsequently formed is a strongly coordinating ligand and so will compete for the metal ion with the macrocycle.[59]

The premise of conformational preorganisation is the basis of syntheses for many crown ether derivatives, such as polythioethers, polyaza macrocycles and cryptands.[13, 15, 60] Despite the formation of crown ethers and their derivatives being so well investigated historically, it is still an active area of research, with studies championing the benefits of templated or non-templated methods or the use of different templates to make gains in yields and efficiency.[61, 62]

1.3.2. Cyclam Synthesis

After it was first reported by van Alphen, where it was found in the high boiling point fractions of mixtures of polyamines,[63] Stetter and Mayer reported a cyclam synthesis that was long and gave a yield of merely 24%.[64] In what is proving to be a familiar theme, cyclam synthesis was then reinvigorated by Barefield *via* the use of a Ni^{2+} template cation. The cation coordinates tetraazadodecane, before glyoxal is added to form the macrocycle. Sodium cyanide is used to remove the nickel, with the cyanide anion competing with the freshly made cyclam ligand over binding of the cation ion. Barefield's template synthesis of cyclam acts as the basis of the methods widely used today.[65]

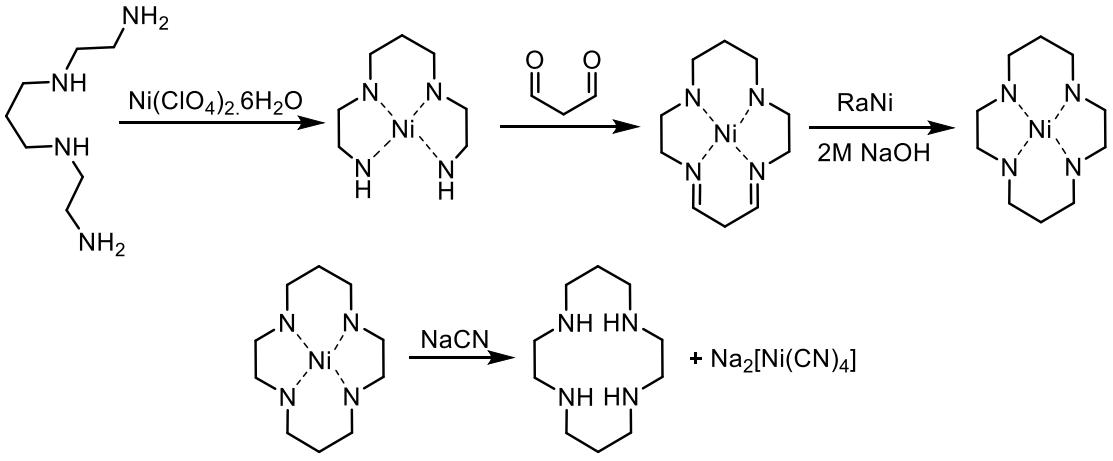

Scheme 1.3: Barefield's template synthesis of cyclam with a Ni^{2+} cation.

1.3.3. Cyclidene Synthesis

There are several different methods to synthesise cyclidene derivatives and the pathway chosen often depends on the application of the final product and which substituent groups are desired. The conjugated propylene bridges are often formed using a formyl acetate derivative, the choice of which can introduce methyl groups to the first and third carbon of the propylene bridge, and an ester or aldehyde in the central carbon position, Scheme 1.4.[42, 43, 66] Incorporating this functionality offers a simple synthetic pathway to other functional groups and allows the cyclidene to be incorporated into a larger molecule[37] or tagged to another structure such as DNA.[67] Another consideration is the desired size of the cyclidene ring.

Template syntheses have employed Cu^{2+} and Ni^{2+} ions to facilitate the synthesis of the 14-, 15- and 16- membered macrocycles.[42, 43] Jager's copper-templated method pictured in Scheme 1.4 gives a 14-cyclidene core with ethyl ester derivatives on the middle carbon atom

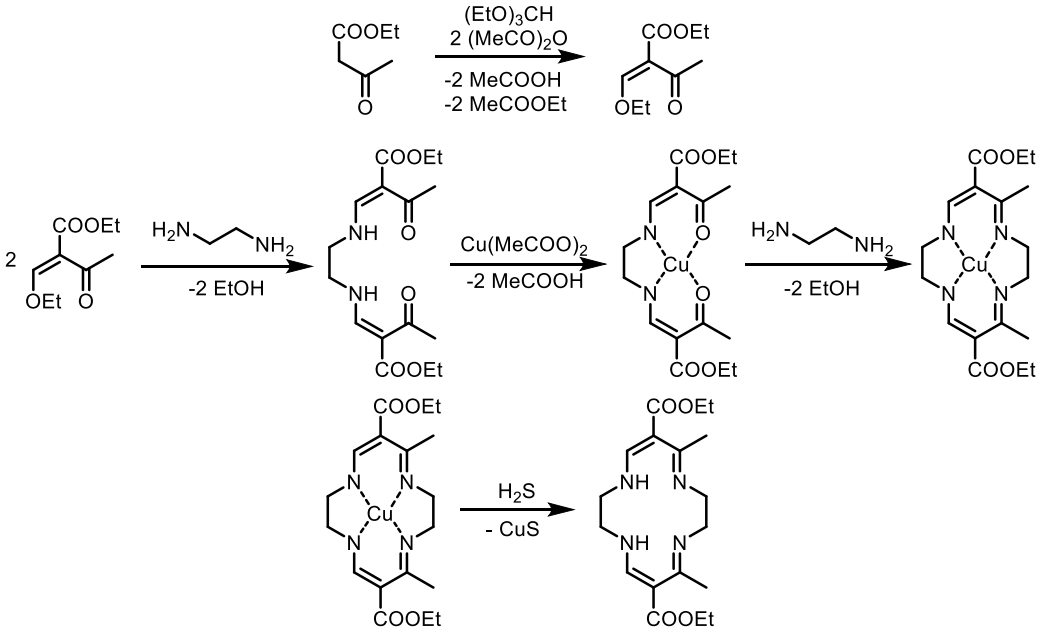

Scheme 1.4: The Cu^{2+} templated synthesis of cyclidene by Jager and co-workers.

of the propylene bridge. The propylene bridges also have methyl groups on the first carbon atom.

One disadvantage of the template method is that the cyclidene complexes can be so stable that the metal template can be difficult to remove and harsh demetallation conditions must be employed. For example, Jager used either hydrogen sulfide or concentrated sulfuric acid, whilst Rybka *et al.* turned to methanesulfonic acid and ammonium hexafluorophosphate. Not only are these harsh conditions unpleasant to work with but they can destroy the newly formed ligand.

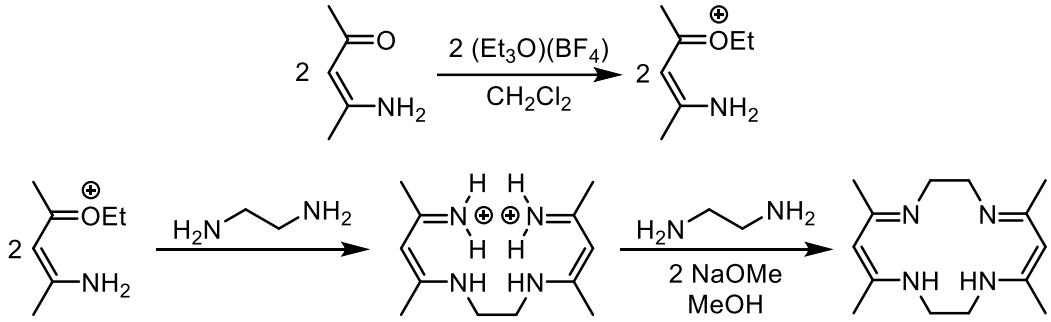

Scheme 1.5: This high dilution synthesis of a cyclidene derivative by Holm and Truex gives the ligand in a 35% yield.

Consequently, non-template syntheses have also been developed. Holm has developed a couple of high dilution methods, one outlined above in Scheme 1.5. High dilution was achieved by slow, dropwise addition of the diamine, which itself had been diluted prior to addition. The method can be modified to give 15- and 16- membered cyclidenes by replacing ethylene diamine with diaminopropane in either step, albeit at lower yields. Copper and nickel complexes have subsequently been formed.[38, 68]

1.4. Applications of Macrocycles and their Complexes

1.4.1. Pharmaceuticals

Macrocycles are now utilised in a variety of roles in modern research. They feature strongly in pharmaceuticals, where inspiration for drug compounds is often gleaned from nature.[69] Verteporfin is a porphyrin derivative that is routinely used in phototherapy for age-related degeneration of blood vessels in the eye, generating oxygen radicals upon irradiation to combat tumour cells.[70] Recent research has suggested that it could also be used to treat hypoxic glioma cells; highly malignant brain tumours which currently prove to be therapy-resistant. The generation of reactive oxygen species proves again to be the method of action, induced here through the complexation of free iron.[71]

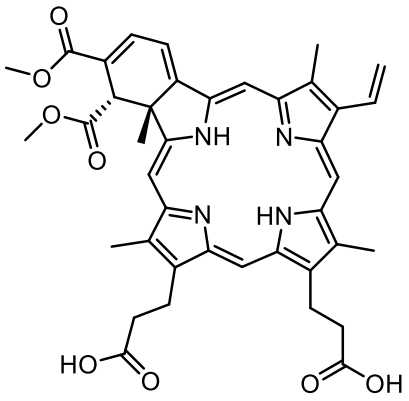

Figure 1.10: Verteporfin is a photosensitizer drug used in photodynamic therapy.

With their high affinity for almost any transition metal cation, cyclams were never going to be effective selective chelating agents. Instead they have found roles in pharmaceuticals. Unbound cyclam, alongside Ni^{2+} and Zn^{2+} cyclam complexes, displays anti-HIV activity and research has been conducted into using them as HIV entry inhibitors.[34] Entry inhibitors focus on stopping the initial binding of the viral glycoprotein to the cell receptors, usually by blocking and preventing the binding event. Disrupting the glycoprotein binding prohibits it

from infiltrating the cell and beginning the process of replicating viral DNA that spreads the HIV virus.[72]

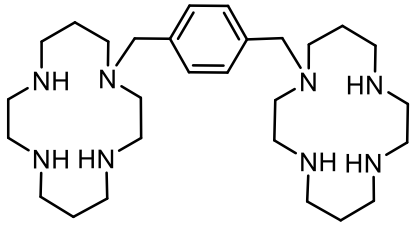

Figure 1.11: A bicyclam compound that exhibits anti-HIV activity. Zinc and nickel complexes enhance its anti-HIV activity, whilst copper, cobalt and palladium complexes decrease its activity.

Bicyclam compounds have exhibited an even greater potency and interact with the CXCR4 co-receptor, one of the docking points for the HIV glycoprotein.[34, 73] The bicyclam compound's anti-HIV activity increased further upon the formation of Zn^{2+} and Ni^{2+} complexes, Figure 1.11. It is thought that the presence of Zn^{2+} and Ni^{2+} ions enhance the cyclam's affinity for the CXCR4 co-receptor, increasing its effectiveness as an inhibitor.[34, 73, 74]

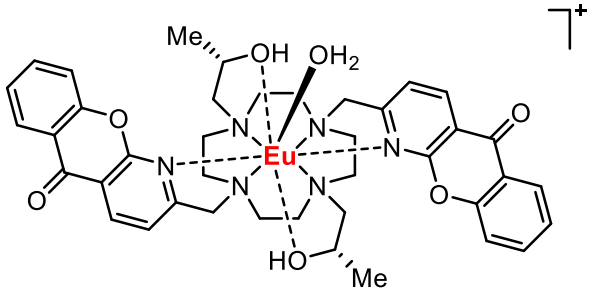

Figure 1.12: A europium tetraaza macrocyclic complex developed by Parker.

Parker and co-workers have reported a variety of aza macrocycles which form lanthanide coordination complexes with strong, long-lived luminescent properties that can be employed as cell imaging agents. Cellular uptake occurs readily with the complexes and their strong optical signals enable the examination of live cells, providing information on their functions. Unsurprisingly such powerful imaging agents are of huge value in diagnostic medical imagining and subsequent therapies.[75-77] Archibald has extensively reviewed the use of macrocyclic coordination complexes for imaging and other biomedical applications.[78]

1.4.2. Sensors

The selectivity demonstrated by crown ethers towards the binding of cations, as well as the relative ease to synthesise and modify them has led to their playing an integral part as the recognition element in supramolecular sensors.[16] A redox active group such as ferrocene can be tagged to the crown ether or even be implemented as part of the ring system, allowing electrochemical techniques, such as cyclic voltammetry, to be used to identify when a complex has been formed with a target analyte.[79, 80] A reversible change in the redox potential is observed when the crown ether-containing sensor binds the target. In the example of ferrocene, the iron is oxidised from Fe(II) to Fe(III) and a potential (*E*) is measured for this change. A change in peak characteristics, such as a change in position or magnitude, is observed upon binding the analyte, thus identifying its presence.

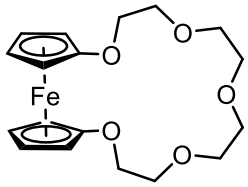

Figure 1.13: A ferrocene unit tagged with a 15-crown-5 ether.

The first reported example of ferrocene crown ethers exhibiting a change in redox potential when binding an analyte was by Saji, who incorporated a ferrocene unit into the ring system of a 15-crown-5 ether, Figure 1.13.[81] Upon addition of the appropriate alkali metal salt, a clear change in peak characteristics was observed as lithium and sodium cations were bound by the crown ether. Saji also found that upon oxidation of the ferrocene unit, the binding constants for lithium and sodium decreased drastically due to electrostatic repulsion between the positive charges of the cations and the ferrocenium ion, which enabled binding to be controlled electrochemically.[81, 82] This is an example of a switchable system and Saji and Kinoshita utilized it to transport metal ions across liquid membranes.[82, 83]

Redox-active anion sensors have also been developed, with Sessler and Kim reporting a calixarene system that could bind a range of anions, including halides and phosphates, important analytes for a range of chemical and biological processes.[84] This was followed by a ferrocene-tagged calixarene developed by Bekhradnia and colleagues for selective fluoride detection, Figure 1.14. The halide is associated with tooth decay and osteoporosis, making its detection of significant medical interest.[85] Selective anion binding has proved more challenging than for their cationic counterparts due to poorly defined coordination preferences and relatively low charge-to-radius ratios.[86] The host-guest chemistry of macrocycles has proven vital for anion recognition and other supramolecular approaches are detailed in a recent review by Beer *et al*.[87]

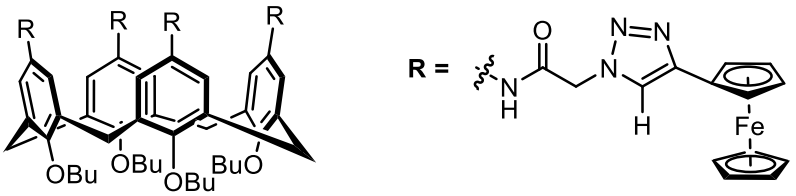

Figure 1.14: A ferrocene-tagged calix-[4]-arene for anion sensing.

The nature of the group attached to the macrocycle to form a viable supramolecular sensor is not limited to redox active groups. Fluorophores, such as anthracene, are luminescent and are well suited to be the recognition element of sensors, allowing sensing to be carried out through the detection of fluorescent photo-induced electron transfer (PET) processes. It is important to note that the process, be it a luminescence or redox change, must be chemically reversible so the sensor can be regenerated.[88]

One of the pioneers of fluorescence-based sensing is de Silva, who developed an anthracene-tagged crown ether, Figure 1.15, among many other sensors.[16, 89, 90] When there is no target bound, fluorescence is quenched by the lone pair of electrons on the nitrogen atom in the

crown ether and the signal is heavily suppressed. When the analyte is bound by the sensor, the lone pair is involved in the binding event and so the PET stops. Consequently, an enhancement of the fluorescence signal is observed, betraying the presence of the analyte.[16, 89] Sensors of this type are popular in the detection of sodium ions near micelle surfaces. The fluorescent anthracene tag is highly hydrophobic which facilitates its uptake by micelles. Benzo-15-crown-5 ether was used as the recognition element as it is the ideal size to bind sodium and contains no pH-sensitive groups, so is unaffected by pH changes as its environment varies.[90]

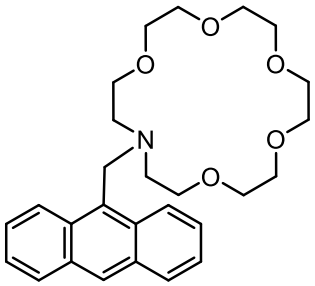

Figure 1.15: De Silva was the first to create a crown ether based molecule that could be used for fluorescence sensing, by using an anthracene tag.

Tetraaza macrocycles including cyclam have been utilised by de Silva in fluorescence-based sensors that can detect Zn^{2+}, Figure 1.16. Zinc sensors are required to monitor its role in degenerative diseases and neurophysiology. Cadmium cations can interfere with the sensing of zinc and so it is important that there are sensors that bind zinc cations preferentially. This cyclam-containing sensor addresses this issue with the triazole group, conveniently formed by coupling the cyclam and benzo isoquinoline-1,3-dione species through azide-alkyne click

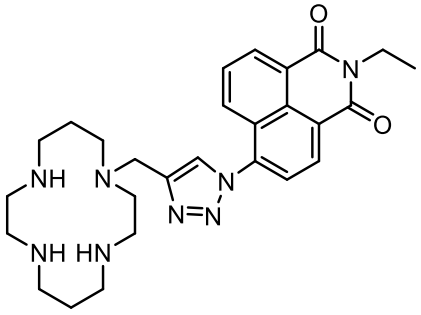

Figure 1.16: A fluorescence-based sensor which includes a cyclam moiety as the recognition element.

chemistry to act as a receptor that causes selective binding of Zn^{2+} that would not be achieved with the cyclam alone.[91]

De Silva's fluorescent PET sensors have had huge success as portable diagnostic tools and are used by ambulance crews to analyse a patient's blood electrolyte levels.[92] In an environment where every second counts, it is crucial that the sensors act fast, and these fluorescent PET sensors can relay information to paramedics in just 30 seconds. With metal cations, including Na^+ and K^+, the target analytes, macrocyclic systems like crown ethers contribute significantly to the success of these devices because of their selectivity and rapid signal output.[93]

1.4.3. Logic Gates

Fluorescent molecules capable of specific molecular recognition are ideally suited to being utilised as molecular logic gates. Such research is vital in the development of molecular information processing and chemical computation. Molecules are needed that can confirm simple commands: yes, no, and, or. Pass (YES) logic gates register a binding event (the 'input') and convert it into a change in fluorescence signal (the 'output'), often a clear "off-on" response. These logic gates are essential but are simple in that they have only one input and one output. The sensors developed by de Silva are capable of being used in complex logic operations, requiring two inputs. The receptor in Figure 1.17a is suitable to be used as an OR logic gate. The cryptand has poor selectivity and is capable of complexing rubidium or potassium cations from the ion pool, with the presence of either ion capable of triggering a fluorescent output signal.[94]

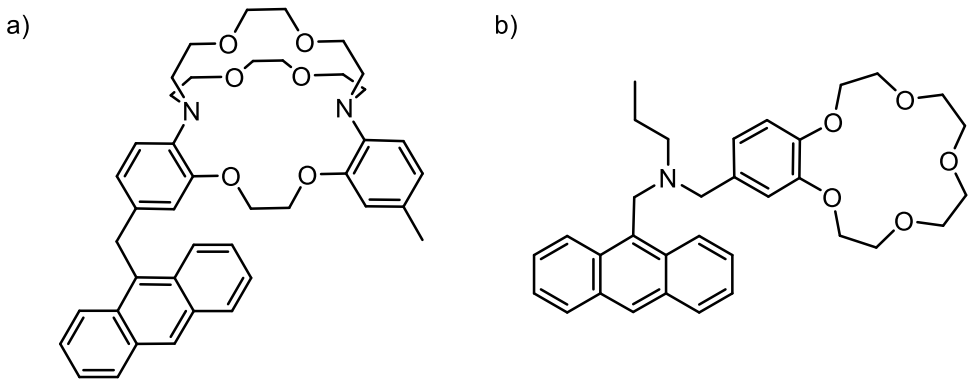

Figure 1.17: a) An anthracene tagged cryptand used as an OR logic gate. b) An AND logic gate.

The receptor displayed in Figure 1.17b is an AND logic gate. As the name suggests, it requires the presence of both the inputs in order to elicit an output signal.[94] The 15-crown-5 ether binds sodium cations whilst the tertiary amine component binds protons, and both do so with such high selectivity that they will ignore all other inputs to favour their pre-programmed targets. An AND logic gate developed by de Silva set a world record for the smallest computational act.[95] Alongside their applications in nanoelectronics and in traditional circuit set ups, the future of logic gates is thought to include processing information in biological environments, much like the fluorescent and redox-active sensors described above.[94]

1.4.4. Switchable Systems

Molecular switches can be reversibly transformed between two states *via* the application of an external input, such as a change in pH or irradiation with light. As with sensors, the field of molecular switches expanded rapidly upon the discovery of crown ethers because of their ability to selectively bind cations. They have found a role as the recognition element in molecules that possess the ability to switch the binding of a guest molecule on and off. This can be done through a change in the conformation, structure or charge that then enables or prevents the cation from binding with the crown ether.[16, 96]

Azobenzenes are photochromic molecules which can switch between *cis* and *trans* arrangements upon irradiation with light of the appropriate wavelength. The rearrangement can be reversed by photo irradiation at a different wavelength or through heating, Figure 1.18a.[16, 97]

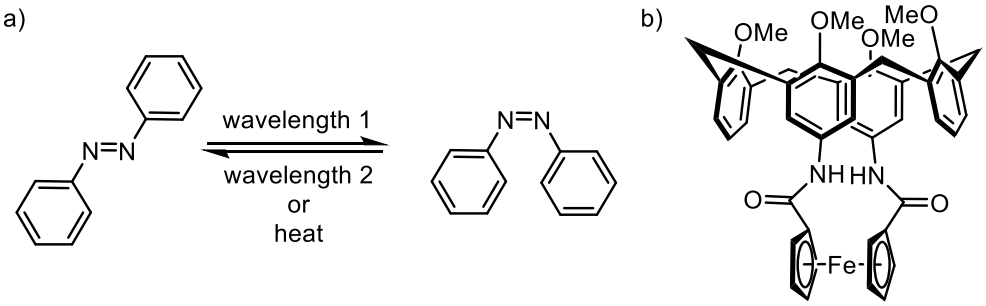

Figure 1.18: a) The photoinduced rearrangement of azobenzene. The trans form is the more stable arrangement. b) a calix-[4]-arene capped with a ferrocene to make a redox-controlled switchable system.

Azobenzene has been attached to crown ethers and other macrocycles in a way that they bridge over the cavity and govern its binding ability. When the nitrogen-nitrogen double bond is in the *trans* configuration the cavity is completely blocked, no binding event can take place. Upon switching to the *cis* configuration, the steric obstruction is removed and the cavity is accessible again so binding can occur.[98] Other groups including ferrocene have been employed in similar roles. In Figure 1.18b the redox properties of the metallocene are used to control the binding preferences of the calixarene through electrostatic interactions. Oxidising the ferrocene to create the positively charged ferrocenium ion enhances the affinity of the calixarene for negatively charged anions.[96, 99]

Nabeshima *et al.* reported switchable binding controlled through a dithiol-disulfide switch, Scheme 1.6. With the disulfide bond intact, rotation about the biphenyl bond is prevented, positioning the two 12-crown-4 ethers in close proximity to enable binding of the *p*-bromobenzylammonium cation through hydrogen bonding interactions. Reducing the

disulfide bond enables rotation about the central axis and greatly reduces the binding affinity for the cationic guest, with the crown ethers no longer able to work together.[100]

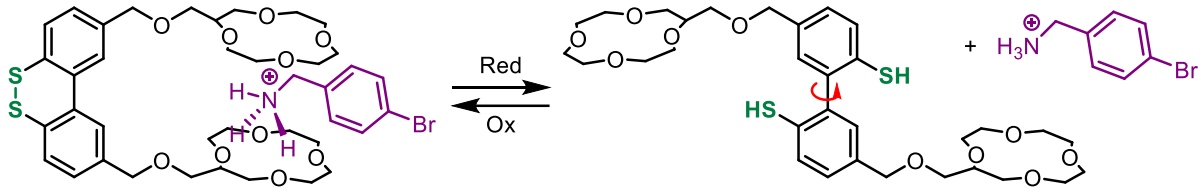

Scheme 1.6: A redox controlled switchable system for the binding of p-bromobenzylammonium.

Switchable systems were early demonstrations of controlled molecular motion, an area of research that expanded dramatically towards the end of the 20th century with the advent of molecular machines. The controlled movement of azobenzene has subsequently been utilized alongside polymers, driving the contractions and expansion of a system that has been compared to an artificial muscle.[101] The topic of controlled molecular motion is covered further in *Chapter 2.*

1.4.5. Nanostructures

The coordination chemistry of macrocycles has enabled the construction of a wide variety of nanostructures, often through supramolecular self-assembly. Hunter and co-workers synthesised a series of heterodimeric tetralactam macrocycles whose construction was directed by non-covalent zinc porphyrin-pyridine interactions which guided the porphyrin

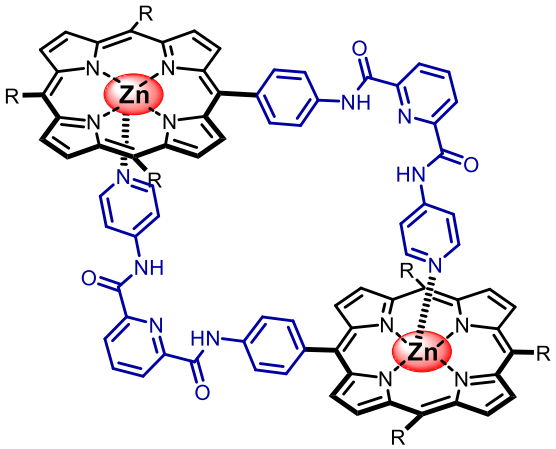

Figure 1.19: A heterodimeric tetralactam macrocycle synthesised by Hunter and co-workers containing Zn-porphyrin complexes.

building blocks into position to afford the cyclic product. The linker units can be varied to alter the geometry of the ring, with the system shown in Figure 1.19 adopting a rectangular shape complete with right-angled corners.[102] This coordination chemistry underpins Anderson's creation of vast molecular nanorings which are assembled by templating porphyrin complexes about a central scaffold. The example in Figure 1.20 employs a β-cyclodextrin as the template to construct a nanoring containing seven Zn-porphyrin complexes through the same porphyrin-pyridine interactions. The macrocyclic scaffold is the perfect size and geometry to align the porphyrin units before Pd-catalysed ring closure completes the nanostructure.[103, 104]

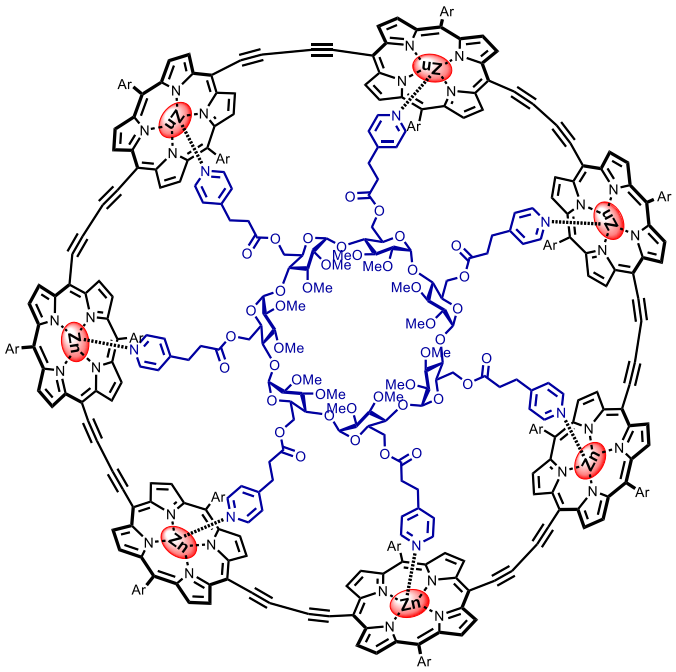

Figure 1.20: A nanoring designed by Anderson which contains seven Zn-porphyrin complexes in the outer ring and a cyclodextrin at its centre.

Coordination chemistry has also been used extensively to mould macrocycles into a variety of shapes and conformations. A range of geometries can be programmed into a molecule through the careful selection of donor atoms and choice of metal cation, with key considerations including coordination number, geometry and preferential bond length. This

has been used to populate a vast library of molecular knots, including a trefoil knot, a single interwoven macrocycle, and Borromean rings, which comprise three, mechanically interlocked macrocycles.[105, 106]

1.4.6. Mechanically Interlocked Structures: Catenanes and Rotaxanes

Macrocycles play a key role in mechanically interlocked systems. Catenanes consist of two or more interlocked rings,[107] whilst a rotaxane comprises a linear axle threading a macrocycle. Bulky groups called stoppers are placed at either end of the axle to trap the macrocycle, giving the rotaxane a unique appearance which has drawn comparisons with a dumbbell.[108] The components of such interlocked architectures are held together by what has been dubbed the mechanical bond. This bond is not a physical bond like a covalent bond, but the molecules are interlocked, or "bonded", in such a way that the only way to prise them apart would be the destruction of one or more of their covalent bonds.

Synthesis of the first catenane was first achieved through a statistical approach; long carbon chains in solution would interlock if the two ends of the chain were stuck together, for example *via* acyloin formation. Unsurprisingly, these early methods required many synthetic steps and gave the product in a miniscule yield.[107] Early syntheses of rotaxanes threw up similar issues, with numerous repetitions having to be carried out to obtain a sample of any substance.[108] Consequently, research into these systems was minimal.

Research into interlocked systems was revolutionised by Sauvage's metal-templated synthesis of catenanes.[109] Using very similar principles to those previously detailed for the template synthesis of macrocycles, a Cu^{+} cation was used to hold two molecules together to mediate the interlocking process. Sauvage outlined two strategies to do this; one involved

using the cation to help thread a strand through a macrocycle, before clipping the strand together to form two interlocked macrocycles. The other brought two strands together about the cation before clipping them both to interlock them. The macrocycles used resembled crown ethers, with much of the looping chain consisting of poly ethers, Scheme 1.7.

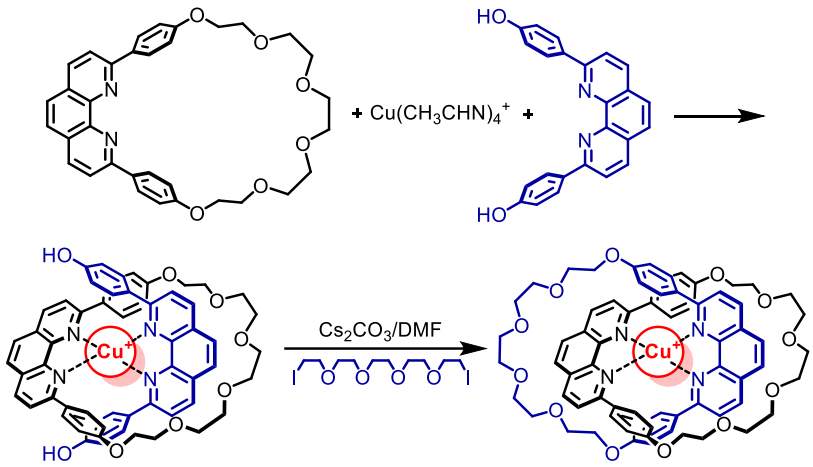

Scheme 1.7: Copper templated Synthesis of Catenanes by Sauvage using the threading method.

The crucial part in the macrocycle's design however was the incorporation of a 1,10-phenanthroline unit which could coordinate with the Cu^{2+} cation *via* the two nitrogen atoms. The rest of the interlocked system could be built around this central coordination complex through poly ethers.[109] Suddenly, these complex, mechanically interlocked molecules were accessible in just a couple of steps and in workable yields. It is no surprise that a surge in research interest followed.

Mechanically interlocked structures quickly rose to prominence in research into controlled molecular motion, switchable systems and the development of molecular machines.[110-112] With their research interest growing, further elegant syntheses were developed.[113-115] How many components could be interlocked became a synthetic challenge and methods of synthesis had to be modified to link several units. This included Stoddart's creation of the [5]catenane, five interlocked macrocyclic rings which resembled the Olympic rings, named

Olympiadane.[116] Recent publications by Goldup *et al.* have explored using these unusual systems in other fields including catalysis, sensing and self-assembly.[117-119]

1.5. Thesis Outline

This thesis explores the use of macrocycles and their coordination complexes in two areas of research. The first, detailed in *Chapter 2*, employs an 18-crown-6 ether as the key component in a novel switchable system. The second area incorporates cyclidene transition metal complexes into the backbone of deoxyribonucleic acid (DNA) and utilises their redox chemistry for detection of important cancer biomarkers. The synthesis of these complexes and the subsequent nucleic acid conjugates is described in *Chapter 3*, alongside some other potential applications for these systems, whilst *Chapter 4* details the development of these systems into a functional electrochemical sensor.

1.6. References

1. A. K. Yudin, *Chem. Sci.*, 2015, **6**, 30.
2. J. J. Katz, J. R. Norris, L. L. Shipman, M. C. Thurnauer and M. R. Wasielewski, *Ann. Rev. Biophys. Bioeng.*, 1978, **7**, 393.
3. M. Biesaga, K. Pyrzynska and Trojanowicz, *Talanta*, 2000, **51**, 209.
4. J. B. Neilands, *J. Biol. Chem.*, 1995, **270**, 26723.
5. R. Saha, N. Saha, R. S. Donofrio and L. L. Bestervelt, *J. Basic Microbiol.*, 2013, **53**, 303.
6. K. N. Raymond, E. A. Dertz and S. S. Kim, *Proc. Natl. Acad. Sci. U.S.A.*, 2003, **100**, 3584.
7. N. F. Curtis, *J. Chem. Soc.*, 1960, 4409.
8. M. C. Thompson and D. H. Busch, *Chem. Eng. News*, 1962, **84**, 1762.
9. M. C. Thompson and D. H. Busch, *J. Am. Chem. Soc.*, 1964, **86**, 213.
10. J. C. Curry and D. H. Busch, *J. Am. Chem. Soc.*, 1964, **86**, 592.
11. M. C. Thompson and D. H. Busch, *J. Am. Chem. Soc.*, 1964, **86**, 3651.
12. G. A. Melson and D. H. Busch, *J. Am. Chem. Soc.*, 1964, **86**, 4834.
13. C. J. Pedersen, *J. Am. Chem. Soc.*, 1967, **89**, 7017.
14. C. J. Pedersen, *J. Am. Chem. Soc*, 1970, **92**, 386.
15. C. J. Pedersen and H. K. Frensdorff, *Angew. Chem. Internat. Edit.*, 1972, **11**, 16.
16. G. W. Gokel, W. M. Leevy and M. E. Weber, *Chem. Rev.*, 2004, **104**, 2723.
17. J. M. Lehn, *Angew. Chem.*, 1970, **9**, 175.
18. D. J. Cram, *Science*, 1983, **219**, 1177.
19. D. J. Cram and J. M. Cram, *Science*, 1974, **183**, 803.
20. D. J. Cram, R. C. Helgeson, L. R. Sousa, J. M. Timko, M. Newcomb, P. Moreau, F. DeJong, G. W. Gokel, D. H. Hoffman, L. A. Domeier, S. C. Peacock, K. Madan and L. kaplan, *Pure. Appl. Chem.*, 1975, **43**, 327.
21. D. J. Cram, *Applications of Biochemical Systems in Organic Chemistry*, John Wiley and Sons, New York, 2nd edn., 1976.
22. G. Melson, *Coordination chemistry of macrocyclic compounds*, Springer Science & Business Media, 2012.
23. D. K. Cabbiness and D. W. Margerum, *J. Am. Chem. Soc.*, 1969, **91**, 6540.
24. R. D. Hancock and G. J. McDougal, *Advances in Molecular Relaxation and Interaction Processes*, 1980, **18**, 99.
25. R. M. Izatt, J. S. Bradshaw, S. A. Nielsen, J. D. Lamb and J. J. Christensen, *Chem. Rev.*, 1985, **85**, 271.
26. R. G. Pearson, *J. Am. Chem. Soc*, 1963, **85**, 3533.
27. G. W. Gokel, *Chem. Soc. Rev.*, 1992, **21**, 39.
28. G. W. Gokel, D. M. Dishong and C. J. Diamond, *J.C.S. Chem. Comm.*, 1980, 1053.
29. M. Giedyk, K. Goliszewskaab and D. Gryko, *Chem. Soc. Rev.*, 2015, **44**, 3391.
30. J. L. Sessler and J. M. Davis, *Acc. Chem. Res.*, 2001, **34**, 989.
31. J. L. Sessler, J. M. Davis, V. Král, T. Kimbrough and V. Lynch, *Org. Biomol. Chem.*, 2003, **1**, 4113.
32. B. Bosnich, C. K. Poon and M. L. Tobe, *Inorg. Chem.*, 1965, **4**, 1102.
33. B. Bosnich, M. L. Tobe and G. A. Webb, *Inorg. Chem.*, 1965, **4**, 1109.
34. X. Liang and P. J. Sadler, *Chem. Soc. Rev.*, 2004, **33**, 246.
35. E. H. Wong, G. R. Weisman, D. C. Hill, D. P. Reed, M. E. Rogers, J. S. Condon, M. A. Fagan, J. C. Calabrese, K. C. Lam, I. A. Guzei and A. L. Rheingold, *J. Am. Chem. Soc*, 2000, **122**, 10561.
36. K. P. Wainwright, *Inorg. Chem.*, 1980, **19**, 1398.
37. B. Korybut-Daszkiewicz, A. Wieckowska, R. Bilewicz, S. Domagała and K. Wozniak, *J. Am. Chem. Soc*, 2001, **123**, 9356.
38. T. J. Truex and R. H. Holm, *J. Am. Chem. Soc*, 1972, **94**, 4529.

39. M. E. Lopez-Morales and J. Gomez-Lara, *Inorg. Chim. Acta.*, 1985, **101**, 141.
40. D. P. Riley, J. A. Stone and D. H. Busch, *J. Am. Chem. Soc*, 1977, **99**, 767.
41. D. P. Riley, J. A. Stone and D. H. Busch, *J. Am. Chem. Soc*, 1976, **98**, 1752.
42. A. Rybka, R. Kolinski, J. Kowalski, R. Szmigielski, S. Domagała, K. Wozniak, A. Wieckowska, R. Bilewicz and B. Korybut-Daszkiewicz, *Euro. J. Inorg. Chem.*, 2007, 172.
43. B. Weber, I. Käpplinger, H. Görls and E. G. Jäger, *Eur. J. Inorg. Chem.*, 2005, 2794.
44. H. Irving and R. J. P. Williams, *J. Chem. Soc*, 1953, 3192.
45. G. Tiwari, R. Tiwari and A. K. Rai, *J. Pharm. Bioallied Sci.* , 2010, **2**, 72.
46. J.-N. Rebilly and O. Reinaud, *Supramol. Chem.*, 2014, **26**, 454.
47. R. Cacciapaglia, S. D. Stefano, L. Mandolini and R. Salvio, *Supramol. Chem.*, 2013, **25**, 537.
48. T. Ogoshi, S. Kanai, S. Fujinami, T. Yamagishi and Y. Nakamoto, *J. Am. Chem. Soc*, 2008, **130**, 5022.
49. Y. Aoyama, Y. Tanaka, H. Toi and H. Ogoshi, *J. Am. Chem. Soc*, 1998, **110**, 364.
50. Y. Sun, Y. Yang, D. Chen, G. Wang, Y. Zhou, C. Wang and J. F. Stoddart, *Small*, 2013, **9**, 3224.
51. Q. Duan, Y. Cao, Y. Li, X. Hu, T. Xiao, C. Lin, Y. Pan and L. Wang, *J. Am. Chem. Soc*, 2013, **135**, 10542.
52. Z. Liu, S. K. M. Nalluri and J. F. Stoddart, *Chem. Soc. Rev.*, 2017, **46**, 2459.
53. B. Dietrich, J. M. Lehn, J. P. Sauvage and J. Blanzat, *Tetrahedron.*, 1973, **29**, 1629.
54. S. J. Rodgers, C. Y. Ng and K. N. Raymond, *J. Am. Chem. Soc*, 1985, **107**, 4094.
55. P. Ruggli, *Ann.*, 1912, **392**, 92.
56. R. Adams and L. N. Whitehill, *J. Am. Chem. Soc*, 1941, **63**, 2073.
57. M. Fujita, *Chem. Soc. Rev.*, 1998, **27**, 417.
58. R. N. Greene, *Tetrahedron Lett.*, 1972, 1793.
59. G. W. Gokel and D. J. Cram, *J. Org. Chem.*, 1974, **39**, 2445.
60. J. M. Lehn, *Acc. Chem. Res.*, 1978, **11**, 49.
61. W. Jiang and C. A. Schalley, *Beilstein J. Org. Chem.*, 2010, **6**, 1.
62. V. Martí-Centelles, M. D. Pandey, M. I. Burguete and S. V. Luis, *Chem. Rev.*, 2015, **115**, 8736.
63. J. V. Alphen, *Rec. Tray. Chim. Pays-Bas.*, 1936, **55**, 835.
64. H. Stetterand and K. H. Mayer, *Chem. Ber.*, 1961, **94**, 1410.
65. E. K. Barefield, *Inorg. Chem.*, 1972, **11**, 2273.
66. M. Nakane, H. Gollman, C. R. Hutchinson and P. L. Knutson, *J. Org. Chem.*, 1980, **45**, 2536.
67. J.-L. H. A. Duprey, J. Carr-Smith, S. L. Horswell, J. Kowalski and J. H. R. Tucker, *J. Am. Chem. Soc*, 2016, **138**, 746.
68. S. C. Tang, S. Koch, G. N. Weinstein, R. W. Lane and R. H. Holm, *Inorg. Chem.*, 1973, **12**.
69. J. Mallinson and I. Collins, *Future Med. Chem.*, 2012, **4**, 1409.
70. L. J. Scott and K. L. Goa, *Drugs Aging*, 2000, **16**, 139–146.
71. K. L. Eales, E. A. Wilkinson, G. Cruickshank, J. H. R. Tucker and D. A. Tennant, *Sci. Rep.*, 2018, **8**, 14358.
72. Y. Mehellou and E. d. Clercq, *J. Med. Chem.*, 2010, **53**, 521.
73. G. J. Bridger, R. T. Skerlj, S. Padmanabhan, S. A. Martellucci, G. W. Henson, M. J. Abrams, H. C. Joao, M. Witvrouw, K. D. Vreese, R. Pauwels and E. D. Clercq, *J. Med. Chem.*, 1996, **39**, 109.
74. A. R. Lam, S. Bhattacharya, K. Patel, S. E. Hall, A. Mao and N. Vaidehi, *J. Chem. Inf. Model.*, 2011, **51**, 139.
75. C. P. Montgomery, B. S. Murray, E. J. New, R. Pal and D. Parker, *Acc. Chem. Res.*, 2009, **42**, 925.
76. S. J. Butler, L. Lamarque, R. Pal and D. Parker, *Chem. Sci.*, 2014, **5**, 1750.
77. J. W. Walton, A. Bourdolle, S. J. Butler, M. Soulie, M. Delbianco, B. K. McMahon, R. Pal, H. Puschmann, J. M. Zwier, L. Lamarque, O. Maury, C. Andraud and D. Parker, *Chem. Commun.*, 2013, **49**, 1600.
78. R. E. Mewis and S. J. Archibald, *Coord. Chem. Rev.*, 2010, **254**, 1686.
79. P. D. Beer, C. Blackburn, J.F. McAleer and H. Sikanyika, *Inorg. Chem.*, 1990, **29**, 378.

80. D. A. Gustowski, L. Echegoyen, D. M. Goli, A. Kaifer, R. A. Schultz and G. W. Gokel, *J. Am. Chem. Soc*, 1984, **106**, 1633.
81. T. Saji, *Chem. Lett.*, 1986, 275.
82. P. D. Beer, *Chem. Soc. Rev.*, 1989, **18**, 409.
83. T. Saji and I. Kinoshita, *J. Chem. Soc., Chem. Commun.*, 1986, 716.
84. M. H. Lee, Q.-Y. Cao, S. K. Kim, J. L. Sessler and J. S. Kim, *J. Org. Chem.* , 2011, **76**, 870.
85. R. Hosseinzadeh, F. Maliji, H. Golchoubian and A. Bekhradnia, *ChemistrySelect*, 2019, **4**, 3914.
86. A. Brown and P. D. Beer, *Chem. Commun.*, 2016, **52**, 8645.
87. R. Hein, P. D. Beer and J. J. Davis, *Chem. Rev.*, 2020, **120**, 1888.
88. B. Daly, J. Ling and A. P. d. Silva, *Chem. Soc. Rev.*, 2015, **44**, 4203.
89. A. P. d. Silva and S. A. d. Silva, *J. Chem. Soc. Commun.*, 1986, 1709.
90. S. Uchiyama, E. Fukatsu, G. D. McClean and A. P. d. Silva, *Angew. Chem. Int. Ed.*, 2016, **55**, 768.
91. A. P. d. Silva, T. S. Moody and G. D. Wright, *Analyst*, 2009, **134**, 2385.
92. J. K. Tusa and H. He, *J. Mater. Chem.*, 2005, **15**, 2640.
93. J. F. Callan, A. P. d. Silva and D. C. Magri, *Tetrahedron*, 2005, **61**, 8551–8588.
94. S. Erbas-Cakmak, S. Kolemen, A. C. Sedgwick, T. Gunnlaugsson, T. D. James, J. Yoon and E. U. Akkaya, *Chem. Soc. Rev.*, 2018, **47**, 2221.
95. S. Uchiyama, G. D. McClean, K. Iwai and A. P. d. Silva, *J. Am. Chem. Soc*, 2005, **127**, 8920.
96. A. Blanco-Gomez, P. Corton, L. Barravecchia, I. Neira, E. Pazos, C. Peinador and M. D. Garcia, *Chem. Soc. Rev.*, 2020, **49**, 3719.
97. T. Ikeda and O. Tsutsumi, *Science*, 1995, **268**, 1873.
98. S. Shinkai, T. Nakaji, Y. Nishida, T. Ogawa and O. Manabe, *J. Am. Chem. Soc*, 1980, **102**, 5860.
99. B. Tomapatanaget, T. Tuntulani and O. Chailapakul, *Org. Lett.*, 2003, **5**, 1539.
100. T. Nabeshima, A. Sakiyama, A. Yagyu and N. Furukawa, *Tetrahedron Lett.*, 1989, **30**, 5287.
101. F. Lancia, A. Ryabchun, A. Nguindjel, S. Kwangmettatam and N. Katsonis, *Nat. Commun.*, 2019, **10**, 1.
102. P. Ballester, A. Costa, P. M. Deya, A. Frontera, R. M. Gomila, A. I. Oliva, J. K. M. Sanders and C. A. Hunter, *J. Org. Chem.*, 2005, **70**, 6616.
103. P. S. Bols and H. L. Anderson, *Acc. Chem. Res.*, 2018, **51**, 2083.
104. P. Liu, P. Neuhaus, D. V. Kondratuk, T. S. Balaban and H. L. Anderson, *Angew. Chem. Int. Ed.*, 2014, **53**, 7770.
105. K. S. Chichak, S. J. Cantrill, A. R. Pease, S. Chiu, G. W. V. Cave, J. L. Atwood and J. F. Stoddart, *Science*, 2004, **304**, 1308.
106. S. D. P. Fielden, D. A. Leigh and S. L. Woltering, *Angew. Chem. Int. Ed.*, 2017, **56**, 11166.
107. E. Wasserman, *J. Am. Chem. Soc*, 1960, **82**, 4433.
108. I. T. Harrison and S. Harrison, *J. Am. Chem. Soc*, 1967, **89**, 5723.
109. C. O. Dietrich-Buchecker, J.-P. Sauvage and J. P. Kintzinger, *Tetrahedron Lett.*, 1983, **24**, 5095.
110. M. R. Wilson, J. Solà, A. Carlone, S. M. Goldup, N. Lebrasseur and D. A. Leigh, *Nature*, 2016, **534**, 235.
111. R. A. Bissell, E. Cordova, A. E. Kaifer and J. F. Stoddart, *Nature*, 1994, **369**, 133.
112. M. Alvarez-Perez, S. M. Goldup, D. A. Leigh and A. M. Z. Slawin, *J. Am. Chem. Soc*, 2008, **130**, 1836.
113. P. R. Ashton, C. L. Brown, E. J. T. Chrystal, T. T. Goodnow, A. E. Kaifer, K. P. Parry, D. Philp, A. M. Z. Slawin, N. Spencer, J. F. Stoddart and D. J. Williams, *J. Chem. Soc. Chem. Commun.*, 1991, 634.
114. S. M. Goldup, D. A. Leigh, P. J. Lusby, R. T. McBurney and A. M. Z. Slawin, *Angew. Chem. Int. Ed.*, 2008, **47**, 6999.
115. V. Aucagne, J. Berna, J. D. Crowley, S. M. Goldup, K.D. Hanni, D. A. Leigh, P. J. Lusby, V. E. Ronaldson, A.M. Z. Slawin, A. Viterisi and D.B. Walker, *J. Am. Chem. Soc*, 2007, **129**, 11950.

116. D. B. Amabilino, P. R. Ashton, A. S. Reder, N. Spencer and J. F. Stoddart, *Angew. Chem. Int. Ed. Engl.*, 1994, **33**, 1286.
117. M. Galli, J. E. M. Lewis and S. M. Goldup, *Angew. Chem. Int. Ed.* , 2015, **54**, 13545.
118. J. E. M. Lewis, M. Galli and S. M. Goldup, *Chem. Commun.*, 2017, **53**, 298.
119. A. W. Heard and S. M. Goldup, *Chem*, 2020, **6**, 994.

2. Controlling the Rotary Motion of Cobalt Sandwich Complexes

2.1. Introduction

2.1.1. Controlled Molecular Motion

Controlled motion at the molecular level is a fundamental component of many biological processes, yet so far it has not been exploited in our own technologies or society.[1, 2] The motor protein Kinesin walks along microtubule filaments, acting like a molecular shuttle and harnesses this movement to transport cargo. Similarly, myosins move along actin filaments and have a wide range of roles, including in muscle contraction, membrane trafficking and signal transduction.[3, 4] Perhaps the most well-known biological molecular machine is the ribosome, which uses controlled molecular movements to synthesise proteins.[5]

Richard Feynman famously drew attention to this untapped potential late in 1959[2] but it was not until the mid-1980s that the challenge of creating such a system on the nanoscale began to capture the mind of many a supramolecular chemist. Macroscopic machines often provided inspiration, with chemists looking to replicate their intricacies and mechanisms on a molecular level. Subsequently, a catalogue of molecular machines that demonstrate a range of controllable simple movements and functionalities have been created. Metal cations have been employed as the switch for the rotation of a wheel in a molecular brake,[6] the direction of rotation can be controlled in a molecular gear,[7] whilst one of the more creative designs brings four different elements together to mimic a pedal.[8] Wilcox's molecular torsion balance

harnessed its internal motion to successfully probe specific, weak supramolecular interactions which are otherwise difficult to quantify.[9]

Many of these creations were inspired by the work of Jean-Pierre Sauvage, Sir Fraser Stoddart and Ben Feringa, three of the pioneers of the field and the recipients of the 2016 Nobel Prize in Chemistry. Sauvage's template synthesis of catenanes, drawing on similar principles observed in the templated synthesis of macrocycles, sparked a surge in the synthesis of interlocked molecules due to the relative ease in accessing such designs.[10] Interlocked systems suddenly became a focal point for controlled molecular motion and thus began the rise of the molecular machine. Stoddart shrewdly used a rotaxane as the scaffold for a molecular shuttle. He installed two docking stations into its axle, whilst also designing the interlocked macrocycle in such a way that it would have a preference over which station to rest at. A change in pH or redox state could alter this preference, resulting in the shuttling of the macrocycle to the other docking station, Scheme 2.1.[11]

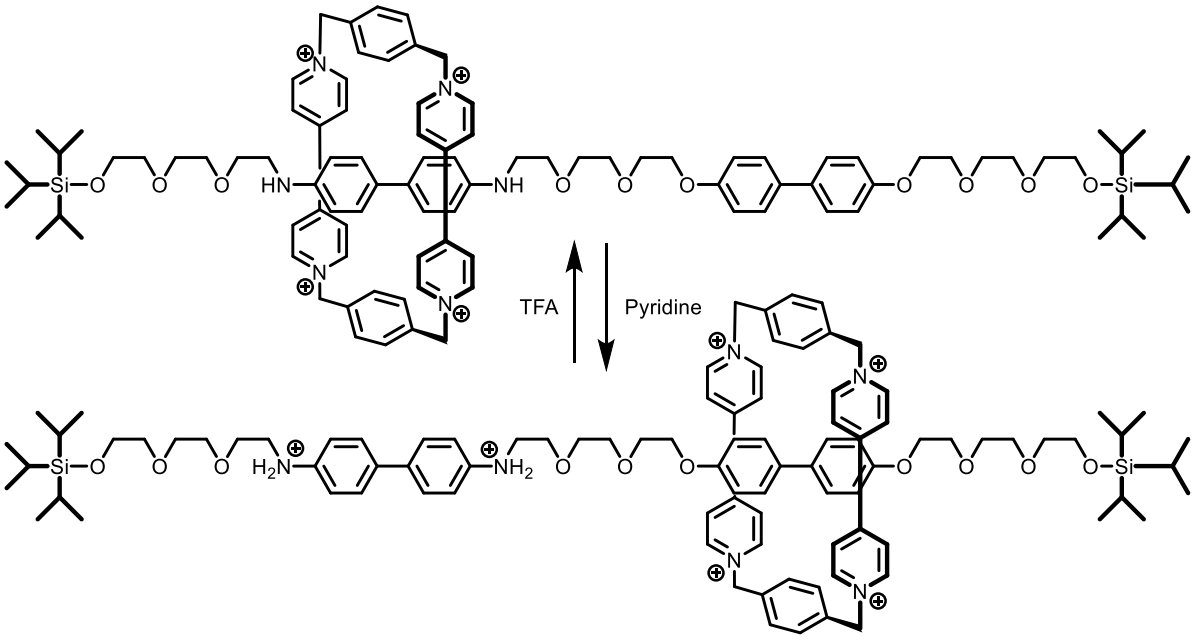

Scheme 2.1: The structure of a switchable rotaxane where the position of the macrocycle is controlled by proton concentration changes. Protonation of the benzidine station causes the positively charged macrocycle to shift and dock at the biphenol site in order to avoid unfavourable electrostatic interactions. Addition of a base such as pyridine deprotonates the benzidine unit and the macrocycle can dock there once more, returning to its resting state.

Feringa crafted the first molecular rotor, a molecular machine that was capable of repetitive 360° rotation about a carbon-carbon double bond when held above a certain temperature and irradiated with light, Scheme 2.2.

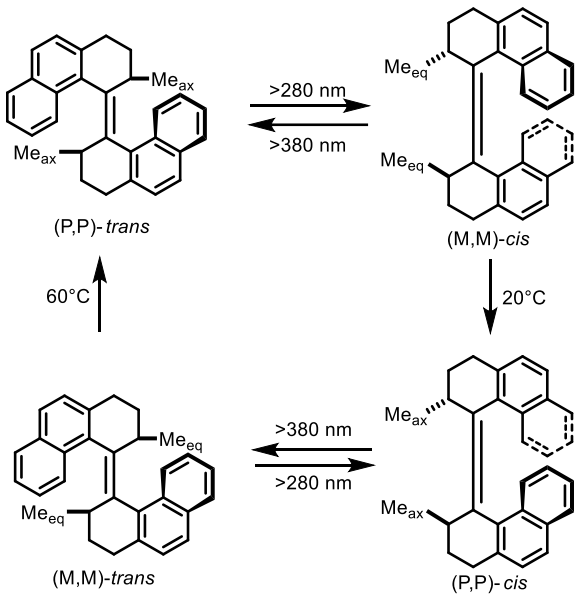

Scheme 2.2: A heat and light controlled molecular rotor by Feringa et al.

This was an invention that took controlled molecular motion in a new direction. Light is capable of inducing *trans* to *cis* isomerism in the double bond, a fast and reversible process that causes a 180° rotation. A small amount of heat is then applied to change the helicity of the molecule, transforming (M,M)-*cis* to (P,P)-*cis,* before further irradiation with light causes another change in stereochemistry about the double bond, this time *cis* to *trans.* Further heating again alters the helicity and completes the 360° rotation. Due to the irreversibility of the heat-induced helicity changes, the system is limited to unidirectional rotation.[12] What is significant about Feringa and Stoddart's creations is the ability to control the molecular movement by using an external input.

Kelly *et al.* achieved controlled, multidirectional 120° rotation with their design, shown in Figure 2.1. The rotor comprises a bulky [4]helicene attached to a three-bladed triptycene unit

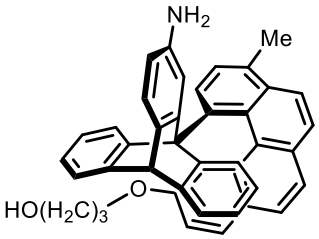

Figure 2.1: A molecular rotor capable of unidirectional molecular motion by Kelly et al.

by a single carbon-carbon bond which is the point of rotation. Rotation about this bond is limited by the bulky groups attached to it. Rotation is induced upon heating the system and occurs equally in the clockwise and anti-clockwise direction. The genius of the design is that the direction of rotation can be selectively controlled *via* reacting the system with carbonyl dichloride to give an isocyanate, which lowers the energy barrier of rotation for one specific direction. With less thermal energy required to overcome the energy barrier, gentle heating induces uniform rotation in the now favoured direction. The isocyanate can be removed, thus returning the system to a state where rotation in either direction is equally favoured.[13]

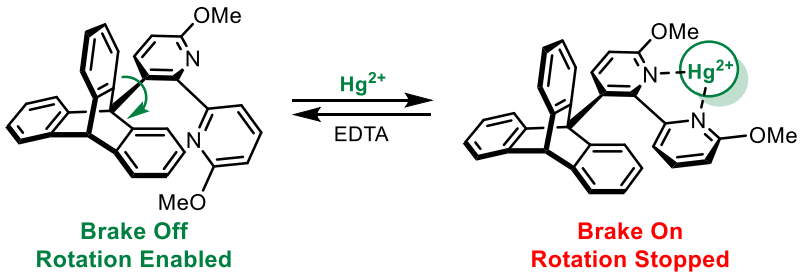

Scheme 2.3: Kelly's molecular brake.

Kelly adapted the system to function as a molecular brake, pictured in Scheme 2.3, with rotation about the central carbon-carbon single bond under switchable control. With the brake 'off', the molecule is in a state of free rotation. Addition of a mercury(II) cation causes the bpy unit to assume a particular conformation to complex the cation. The spatial arrangement adopted creates a steric restriction that inhibits the rotation, turning the brake

on. Addition of the chelating agent EDTA removes the cation and allows rotation to resume with the system returned to its original state.[6, 14]

David Leigh has emerged as one of the forerunners over the past decade or so in the design of molecular machines. His focus has been on interlocked molecules, for example combining peptides and rotaxanes to make a molecular shuttle,[15] achieving controlled unidirectional motion in a catenane-based molecular rotor[16] and utilising rotaxanes as the basis of a molecular information ratchet.[17] Attention turned to applying molecular machines to solve problems or provide outputs. One particular aspect of his work has been the use of molecular shuttles to transport macroscopic cargo, including a water droplet along a surface.[18] The significance of this work is that in utilising controlled motion on the molecular level to affect our macroscopic environment, we are starting to emulate something that is intrinsic and routine in nature. The potential of such technology is huge.

Pushing the boundaries further, a molecular walker was developed that uses its 'two legs' to walk along a linear four-part track one step at a time, mimicking the motion of biological motor proteins. Each foot has two potential binding sites along the track and each step can be controlled by changes in pH to selectively maintain or break the bonds between foot and track.[19] Turberfield and co-workers utilised the complementary nature of DNA to develop a walker that could be guided along a DNA track by adenosine triphosphate hydrolysis and enzymatic ligation.[20] The implementation of a system of dynamic covalent bonding provided the foundation for a molecule transporter. This consisted of a 'robotic' arm that acted like a crane, picking up its cargo and moving it from one site to another. As with the molecular

walker, the 'switch' was pH-responsive. This was one of the first synthetic examples of controlled molecular level construction.[21]

2.1.2. Metallocenes

2.1.2.1. Ferrocene

Metallocenes are organometallic compounds that consist of a transition metal sandwiched between two planar cyclopentadiene anions. The most famous is the iron-containing metallocene, ferrocene, whose accidental discovery in the early 1950s inspired a whole new field of organometallic chemistry.[22, 23] Whilst its precise structure was initially a mystery, Wilkinson deduced the familiar sandwich structure,[24] before Fischer quickly provided crystallography data to confirm the hypothesis. Fischer also detailed the identification of cobalt and nickel metallocenes, and suddenly the foundations were put in place for a new class of molecule.[25] The duo were awarded the 1973 Nobel Prize in Chemistry for these contributions.

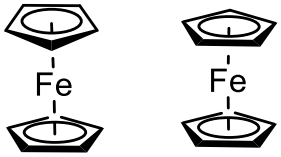

Figure 2.2: The staggered (left) and eclipsed (right) conformations of ferrocene.

Ferrocene is very stable, surprisingly so for an organometallic compound. Its individual components combine perfectly to fulfil the 18-electron rule, with the cyclopentadiene rings providing six electrons apiece in the complexation with iron(II), which itself contributes six d-electrons to give a stable 18-electron configuration. It also has a well-studied electrochemistry, readily undergoing a reversible, single-electron redox conversion to give ferrocenium, a positively charged ion where the iron(II) centre has been oxidised to iron(III). This reliable redox chemistry has made it an attractive component of electrochemical

sensors,[26] including with macrocycles, as discussed in *Chapter 1*,[27, 28] and DNA, which is covered in *Chapters 3* and *4*. Ferrocene derivatives have also shown considerable potential in medicinal chemistry.[29-33]

2.1.2.2. Metallocenes and Controllable Molecular Motion

In the solid state, the cyclopentadiene (Cp) rings of ferrocene can exist in two conformations, shown previously in Figure 2.2, with the lower energy 'eclipsed' conformation preferred. These rings have a barrier of rotation of 0.9(3) kcal mol^{-1} and so are rapidly rotating in solution, even when cooled to low temperatures.[34, 35] This rotary motion about the central iron atom sees the iron act as a molecular ball-bearing.[36] Rotation about the ball-bearing axis of metallocenes has been utilised as part of several systems demonstrating controlled molecular motion.

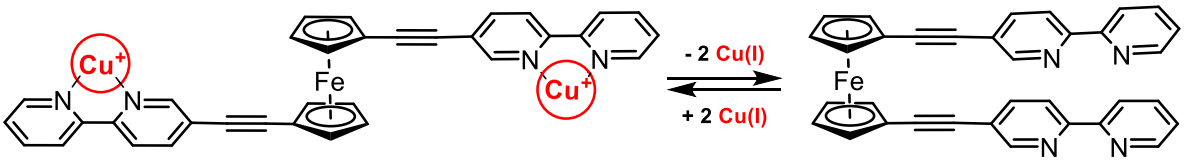

Scheme 2.4: A ferrocene system investigating the use of metallocenes in developing electrostatic drivers for molecular motors.

Binding interactions have been used to control the conformations adopted in ferrocenes by attaching bipyridine derivatives to the Cp rings, as shown in Scheme 2.4. Various chemical inputs such as changes in pH and metal cations have been investigated. In neutral conditions or with no cation present, the ferrocene adopts the conformation pictured on the right-hand side, with the two bipyridine units positioned over one another, a favourable arrangement due to π-π stacking interactions. However upon the addition of Cu^{+} or protonation of the pyridine units, unfavourable electrostatic interactions resulted in the ferrocene adopting the left-hand conformation with the bipyridine units positioned apart from one another.[35, 37]

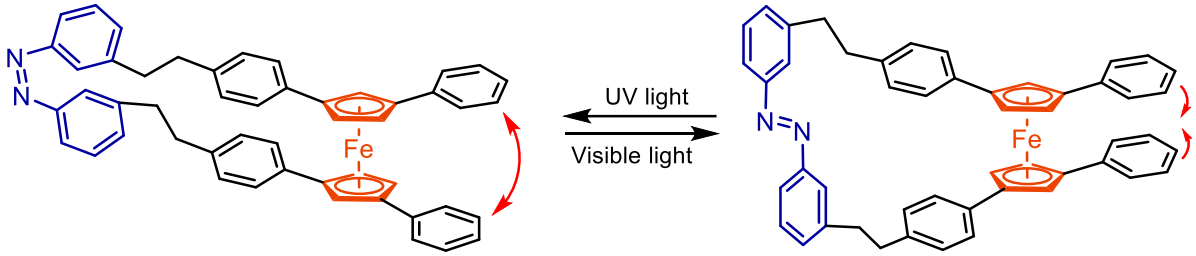

Scheme 2.5: A pair of molecular scissors by Aida et al. Photoisomerism of the azobenzene units results in the opening and closing of the scissors.

Multiple units of this ferrocene system have been joined together to create a folding molecular ruler, where extension can be controlled by the presence of copper cations.[38] Other molecular machines involving ferrocene include using it as a pivot point in molecular scissors or pliers, with both creations utilising the movement about the ball-bearing axis in tandem with isomerism changes in an azobenzene unit to open and close the 'blades', pictured in Scheme 2.5.[8, 39]

2.1.2.3. Cobalt Sandwich Complexes

Ferrocene proves a good point of reference when examining cobalt sandwich complexes. Its remarkable stability is in part a result of its fulfilment of the 18-electron rule, a trend that is also observed with other group 8 transition metal metallocenes such as ruthenocene, the ruthenium-containing analogue of ferrocene. However, the cobalt equivalent of ferrocene, cobaltocene, is much less stable and air sensitive because of its extra electron. As a result, it is used as a one-electron reducing agent.[40]

However, cobalt's additional electron can be beneficial as it allows for the formation of alternative sandwich species, including (η^4-tetraphenylcyclobutadiene) (η^5-cyclopentadienyl) cobalt, Figure 2.3. They deviate from the familiar metallocene structure by possessing only one cyclopentadiene ring, with the other replaced by a cyclobutadiene ring. Like ferrocene, these sandwich compounds are air, heat and moisture stable, benefiting from the stability

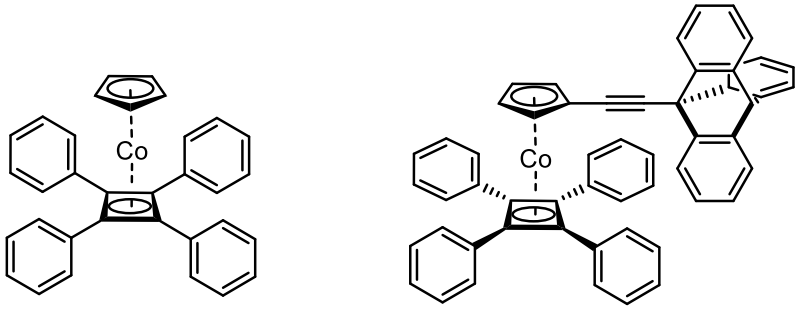

Figure 2.3: (η^4-tetraphenyl-cyclobutadiene) (η^5-cyclo-pentadienyl) cobalt metallocene (left). This metallocene core has been developed in a molecular gear (right) by Richards and co-workers.

gained from satisfying the 18-electron rule. Derivatives of these unique compounds have been employed as asymmetric catalysts, proving to be more active than their ferrocene counterparts.[41, 42] They also act as prototype molecular machine components, including gears[43] and rotors.[44]

2.1.2.4. Synthesis of Sandwich Complexes

Modern methods for ferrocene synthesis proceed through reacting iron(II) chloride with freshly cracked cyclopentadiene, Scheme 2.6. The pure metallocene product is then obtained through a simple recrystallisation.[45] Functionalisation of the cyclopentadiene rings can be achieved through lithiation followed by subsequent reactions with a range of electrophiles, as well as electrophilic substitutions such as Friedel-Craft acylation and alkylation.[46, 47]

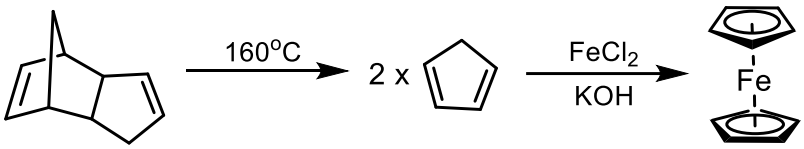

Scheme 2.6: Ferrocene Synthesis. The cyclopentadiene is freshly prepared by cracking dicyclopentadiene. Potassium hydroxide is added to deprotonate it before the iron chloride is added slowly.

Cobalt complexes containing η^4-tetraphenylcyclobutadiene and η^5-cyclopentadiene are prepared through mixing sodium cyclopentadienide, freshly prepared cobalt(I) and acetylene.

The cobalt cation forms a piano stool intermediate with the cyclopentadiene, which guides two acetylene units into the optimum position to cyclise and form the cyclobutadiene ring.

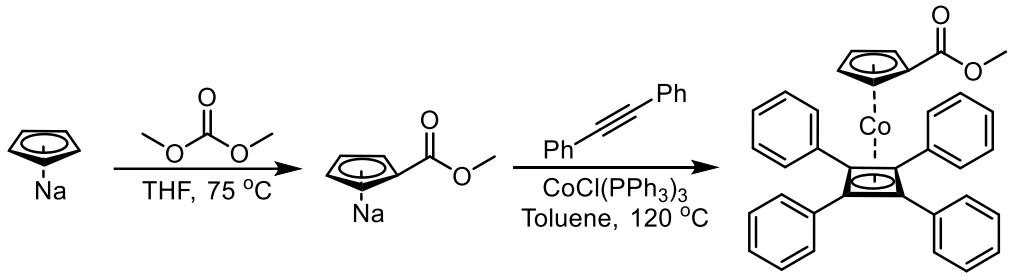

Scheme 2.7: The synthesis of a (η^4-tetraphenylcyclobutadiene) (η^5-cyclopentadienyl) cobalt sandwich core with an ester-functionalised cyclopentadiene ring.

Different acetylene derivatives can be used to add structural variety about the cyclobutadiene ring, whilst the cyclopentadienide is often functionalised with a ketone or ester beforehand to provide a synthetic pathway to other functional groups, as shown in Scheme 2.7.[48, 49] This is advantageous as it allows installation of a versatile synthetic handle during sandwich complex formation.

2.1.3. Variable Temperature NMR

2.1.3.1. Overview

NMR spectroscopy has long been a powerful tool of chemists to probe dynamic processes in supramolecular systems.[11, 16, 21] In some cases, for example where different conformations or orientations are brought about through bond formation[19, 21] or changes in solvent,[15] NMR experiments at ambient temperature are sufficient for identifying such processes. However, these processes can be under conditions of fast exchange at ambient temperature, and require cooling to slow the rate of environmental exchange to the point where spectral changes can be observed.[11] As outlined below, variable temperature NMR studies can be

employed for the determination of quantitative information regarding the kinetics of such exchange processes.[50]

2.1.3.2. Environmental Exchange

Certain molecules possess a signal in their ^{1}H NMR spectrum that is a single line at one temperature, indicating that it represents protons that are in equivalent magnetic environments, but two separate signals at a lower temperature, indicating that the protons are in separate environments. Dimethylformamide (DMF) is one such molecule. Its NMR spectrum gives two different signals for its two methyl groups at ambient temperature because of the carbon-nitrogen bond having some partial double bond character, as shown by the resonance structures in Scheme 2.8, which slows the rotation about the C-N bond. At higher temperatures, only one signal for the two methyl groups is observed.

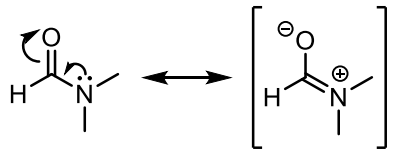

Scheme 2.8: Dimethylformamide (left) and its resonance form (right). The π-bonding between the nitrogen atom and the carbonyl carbon slows the C-N bond rotation.

Central to this phenomenon is the rate at which the proton resonances exchange between the different proton environments, given by the temperature-dependent rate constant, k_{ex}. At one extreme (essentially no exchange), the protons may appear as two sharp, separate peaks, Figure 2.4a, with a frequency separation, $\Delta\nu$. The rate of exchange relative to the magnitude of the frequency separation governs the appearance of the signal or signals at a given temperature.[50]

In the case of DMF, its two methyl resonances are in a state of slow exchange relative to the NMR timescale at ambient temperature.[50] As the temperature is raised, the rate of rotation

about the C-N bond increases, which increases the rate of exchange. As it becomes comparable to the frequency separation, the signals start to broaden, flatten out and shift closer together, Figure 2.4b and c. Eventually, the two signals converge and become one, Figure 2.4d, a process called coalescence.[50]

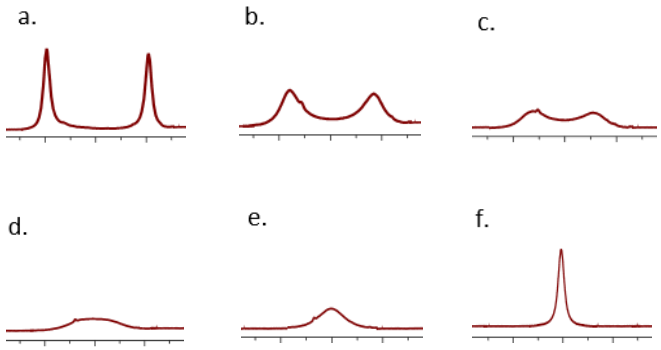

Figure 2.4: The appearance of a signal that represents protons in multiple environments is influenced by the rate of exchange k_{ex} and the frequency separation, Δv. When $k_{ex} << \Delta v$, separate signals are observed (a). When $k_{ex} >> \Delta v$, a single, averaged peak is seen (f). In between these two extremes, the signals appear broader and less defined, as k_{ex} and Δv are closer in magnitude. Eventually the two separate signals coalesce, (d).

Further heating leads to the now single signal sharpening to a pointed, well-resolved peak as the rate of rotation about the bond reaches a maximum, Figure 2.4e and f. This is a state of fast exchange on the NMR timescale, where the rate of exchange is far greater than the frequency separation. This single signal is an average of the two previously observed resonances and has a chemical shift that is in the middle of the two individual signals.[50]

2.1.3.3. Temperature of Coalescence and Kinetics

When a signal in an NMR spectrum splits into two environments that are equally populated upon cooling, the rate constant for the environmental exchange, k_{ex}, at the coalescence temperature, T_c, can be calculated using Equation 2.1.[50]

Equation 2.1 $$k_{ex} = \frac{\pi \Delta v}{\sqrt{2}}$$

Equation 2.2 shows the relationship between the temperature of coalescence, T_c, the molar gas constant, R, and the frequency of separation, Δv, and the free energy of activation for the dynamic process, $\Delta G^{\ddagger}$.[50] If multiple coalescence events are observed in an NMR spectrum, calculating the free energy of activation can inform as to whether the events are associated with the same exchange process or independent.

Equation 2.2 $$\Delta G^{\ddagger} = RT_c[23 + \ln\left(\frac{T_c}{\Delta v}\right)]$$

2.2. Aims and Objectives

Tucker and co-workers previously constructed a series of switchable systems based on the inversion displayed by the nitrogen atom in aziridine.[51-53] One system[51] was designed to study non-covalent interactions between functionalised arms containing hydrogen bond donor (HBD) and acceptor (HBA) units attached to the three-membered ring system of aziridine, as shown in Scheme 2.9. With each inversion, the HBA *X* swung back and forth between HBD groups, *Y*. Small modifications to the design of *X* and *Y* also allowed other non-covalent interactions and external inputs, including metal cations, to be used to explore their effect on nitrogen inversion.[51-53]

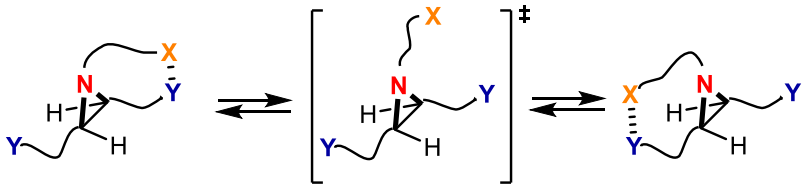

Scheme 2.9: The aziridine system designed by Tucker et al. is one of the smallest known switchable systems. 'X' is a hydrogen bond acceptor, 'Y' is a hydrogen bond donor. The dashed line represents a hydrogen bond.

Drawing on these non-covalent interactions for inspiration, the aim of this work was to combine the ball-bearing axis of metal sandwich complexes with the binding properties of crown ethers to develop a novel switchable rotary system. A (η^4-tetraarylcyclobutadiene) (η^5-cyclopentadienyl)cobalt(I) core is an appropriate scaffold for the rotary system; its two rings rotate independently of one another but if functionalised appropriately, the hypothesis was that they could interact with one another under certain conditions to affect the rate of rotation about the ball-bearing axis.

The basic design of the system, outlined below in Scheme 2.10, equips the cyclobutadiene (cb) ring of the cobalt sandwich complex core with two benzo-18-crown-6 ethers, whilst the

binding group *R* is connected *via* a suitable linker group to the cyclopentadiene (cp) ring. The orthogonal geometry of the cb ring allows the two crown ether units to be stationed directly opposite each other, allowing the possibility of 180° rotation. Both ring systems can also be functionalised during the synthesis of the cobalt sandwich complex, making it more appealing than a traditional metallocene such as ferrocene. Upon the application of a chemical input, such as a change in pH or the addition of a metal ion, the hypothesis was that the non-covalent interactions between the binding group and a crown ether would be affected, subsequently impeding or facilitating the rate of rotation about the ball-bearing axis.

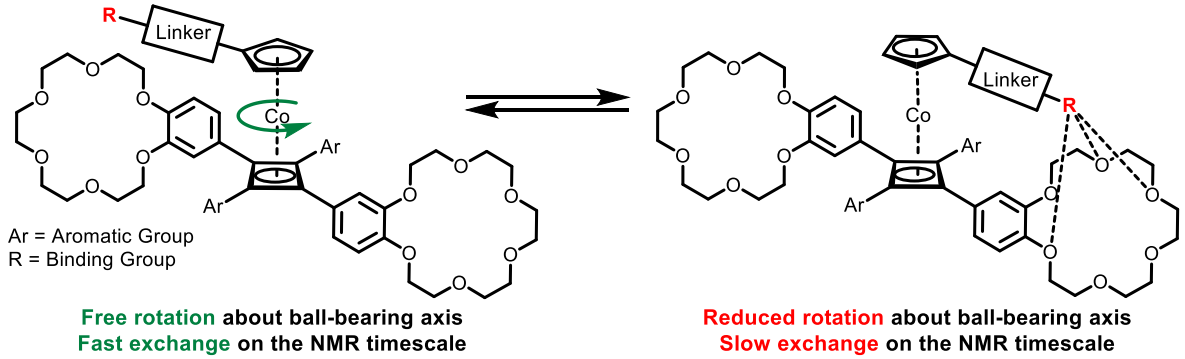

Scheme 2.10: A schematic representation of the switchable molecular rotor in action. The rotation process could be fast or slow on the NMR timescale, depending on the strength of the interaction between the binding group R and the crown ether.

Following this blueprint, the first objective of this project was to design and synthesise a rotary system with an appropriate binding group. Variable temperature ^{1}H NMR experiments would subsequently be conducted to provide evidence of the impact on the rotary motion of applying different chemical inputs to the system. The rotation process could be fast or slow on the NMR timescale, depending on the strength of the interaction between the binding group and the crown ethers. To complement these studies, a control compound would also be synthesised and subjected to testing.

2.3. Rotary System Design Rationale

The first generation of rotary system sees the cyclopentadienyl ring functionalised with a primary amine tether, Scheme 2.11, allowing molecular motion to be controlled by a change in pH. In this system, the expectation is that lowering the pH will protonate the amine, forming a strong hydrogen bond donor unit which can form hydrogen bonds with the oxygen atoms of the crown ethers. This in turn will stop or reduce the rotation about the ball-bearing axis of the metallocene core, in a similar fashion to the molecular brake discussed in 2.1.1.[6, 14] Increasing the pH sufficiently will deprotonate the amine, weakening the interaction between the amine and the crown ether and thus returning to the faster rotation state.

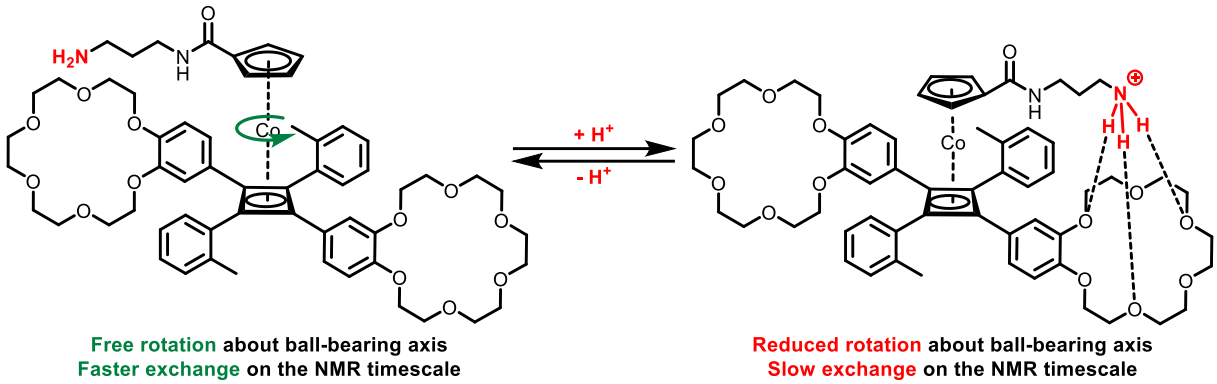

Scheme 2.11: The first generation metallocene rotary system. At neutral pH (LHS), the amine weakly interacts with the crown ethers and rotation about the ball-bearing axis is enabled. At a low pH (RHS), the amine is protonated and interacts strongly with the crown ethers, hydrogen bond acceptors, hindering the rotation.

The arm of the cyclopentadienyl ring comprises a stable amide linkage with a primary amine capable of interacting with the benzocrown ethers on the cyclobutadiene ring. The length of the linker between amide and amine is crucial, as the amine must be positioned above the crown ether in a way that maximises the interactions between the two. A basic model system indicated that a three-carbon linker chain is the optimum length.

2.4. Synthesis of Rotary System

The η^4-tetraarylcyclobutadiene ring of the cobalt core was formed *via* the cyclisation of two diphenylacetylene derivatives, as detailed in section 2.1.2.4. The design of the alkyne is crucial to achieving the desired geometry of crown ethers about the cyclobutadiene ring. Previous work by Richards and co-workers shows an unsymmetrical diphenylacetylene derivative is ideal but yields both *cis* and *trans* products.[48] They found that stationing an *ortho*-tolyl group at one end of the alkyne promoted the formation of the sterically favourable *trans* stereoisomer over the *cis* in a 2.5:1 ratio. Preference for the *trans* isomer was increased to 6:1 by substituting the methyl group in the *ortho* position of the benzene ring for an isopropyl group.[48]

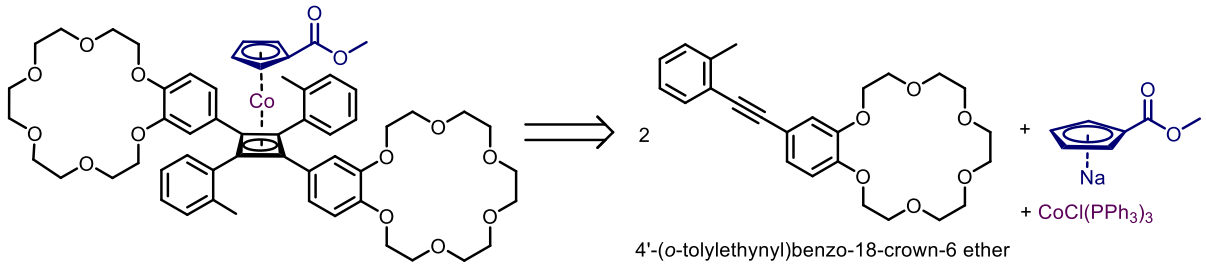

Scheme 2.12: Retrosynthetic analysis of the cobalt sandwich complex-crown ether core.

The retrosynthetic analysis in presented in Scheme 2.12 showed that 4'-(*o*-tolylethynyl)benzo-18-crown-6 ether was a suitable alkyne precursor for the sandwich complex and was the first synthetic target of the project. A benzo-18-crown-6 ether is positioned at one end of the alkyne, whilst an *ortho*-tolyl unit is stationed at the other. Whilst the *o*-methyl derivative was found not to favour the formation of the desired *trans* conformation to the same extent as an *o*-isopropyl derivative, in this project it was expected that the presence of the bulky crown ether would also promote the *trans* conformation. This would also be the first time that such a bulky acetylene unit would be utilised in the formation

of these cobalt complexes. Therefore, taking these factors into account, an *o*-methyl derivative was chosen over an *o*-isopropyl group to limit the steric hinderance.

2.4.1. Synthesis of 4'-(*o*-tolylethynyl)benzo-18-crown-6 ether

It was envisaged that benzocrown alkyne **2.3** could be synthesised in three steps, Scheme 2.13, utilising methods previously established by Richards for the development of asymmetric alkynes.[48] The initial two steps were followed as detailed in the literature, first employing a Sonogashira reaction to couple 2-iodotoluene with ethynyl trimethylsilane to give the protected alkyne **2.1** in a near quantitative yield. Use of the protected acetylene derivative ensured the formation of only the monosubstituted alkyne product. Deprotection to **2.2** was achieved through stirring in a basic solution of potassium carbonate in methanol.

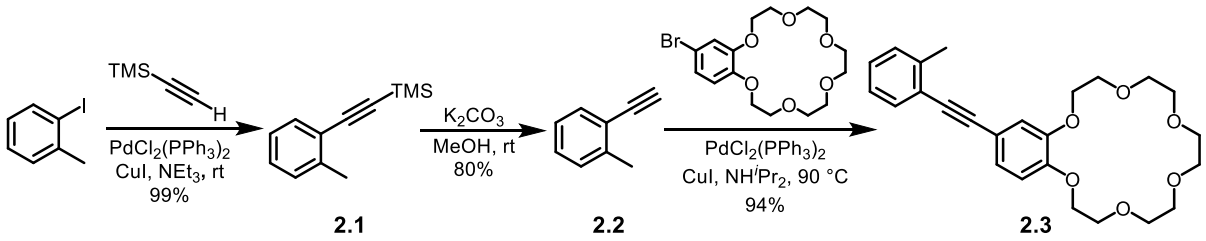

Scheme 2.13: The three-step synthesis of 4'-(o-tolylethynyl)benzo-18-crown-6 ether, ***2.3****.*

Synthesis of benzocrown alkyne **2.3** proved more of a challenge. A second Sonogashira coupling was proposed, but the only commercial reagent available to provide the benzocrown ether was 4-bromo-benzo-18-crown-6 ether. Ideally, an aryl iodide unit would be used instead of an aryl bromide due to its higher reactivity. Consequently, the coupling conditions used to form **2.1** were unsuccessful, with competing reactions including homo coupling of the alkyne occurring instead of the desired hetero coupling. However, fortunately, substituting triethylamine for the far more basic and less sterically hindered diisopropylamine,[54] along

with heating and a lower catalytic loading of copper iodide, afforded benzocrown alkyne **2.3** in high yield.

2.4.2. Cobalt Sandwich Complex Synthesis

The major hurdle en route to forming the rotary system is the construction of the cobalt sandwich complex core, and in particular the steric hinderance imposed by the bulky crown ethers that may restrict the formation of the cyclobutadiene ring. The conditions used were again based on previous metallocene syntheses by Richards *et al.*[48] to devise the formation of sandwich complex **2.4**, Scheme 2.14. Sodium cyclopentadienylide was first reacted with dimethyl carbonate to generate (η^5-carbomethoxycyclopentadienyl) sodium. The methyl ester was chosen to provide a synthetic pathway to the primary amine tether. The four hour reaction time allowed for fresh chlorotris(triphenylphosphine) cobalt(I) to be prepared alongside it.[55] The chocolate-brown powder was air-sensitive and so was added immediately to the reaction mixture alongside a solution of **2.3** in toluene and refluxed.[48, 49]

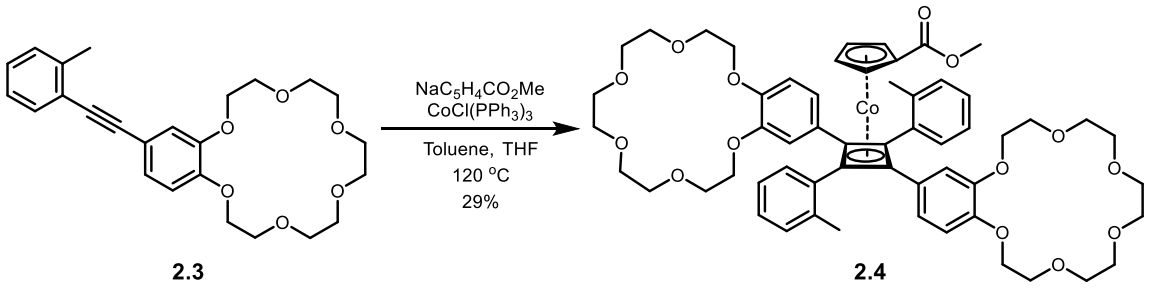

Scheme 2.14: Synthesis of the ester-functionalised benzocrown cobalt metallocene.

Cobalt sandwich complex **2.4** was successfully formed but its synthesis presented a number of challenges that needed to be overcome to yield workable amounts of product. The biggest challenge was purification of the crude reaction mixture, which was a complex concoction of several species, pictured in Figure 2.5 below. Alongside the desired organometallic product (the strong, yellow spot **4**) a significant quantity of benzocrown alkyne **2.3** remained

unreacted (spot **3**) along with sodium cyclopentadienylide species **1** and a possible decomposition product of the alkyne, **2**. Even with very polar eluent conditions employed, product spot **4** barely moved from the baseline. Despite the complex mixture, column chromatography with a carefully planned eluent system appeared to be a suitable purification method.

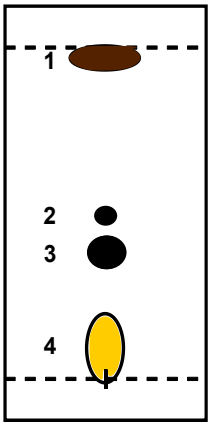

Figure 2.5: Depiction of the TLC plate of the reaction mixture. 1) sodium cyclopentadienylide derivatives 2) minor side product 3) unreacted crown alkyne 4) metallocene product mixture. Eluent 6:4:1 DCM:hexane:methanol.

Besides obtaining pure **2.4** from the mixture, efficient recovery of alkyne **2.3** would allow it to be subsequently reacted again. Therefore a gradient eluent system was employed to achieve this. A 6:4:1 DCM:hexane:methanol eluent mixture was sufficient to remove spot **1**, whilst slowly increasing the proportion of DCM to 8:2:1 removed spot **2**, before gradually eluting spot **3**. The presence of hexane in the eluent kept the product spot **4** near the baseline, allowing recovery of pure alkyne **2.3**. Finally, increasing the polarity of the eluent to 9:1 DCM:methanol allowed a mixture of benzocrown cobalt sandwich complexes to be slowly eluted from the column. Although this process took several hours, the *cis* and *trans* isomers could be partially separated with some coelution, with the *trans* isomer eluting first, as evidenced by NMR spectroscopy.

NMR analysis of many of the fractions from spot **4** revealed that in addition to the expected *cis* and *trans* isomers of the product, isomers of an unexpected side product where the cyclopentadiene ring was not functionalised were also observed, Figure 2.6. This indicated that either the first reaction was not always proceeding to completion, or there was some degradation of the ester unit during the reaction. The additional two isomers increased the retention time of the organometallic mixture, complicating effective removal of the desired product from the column.

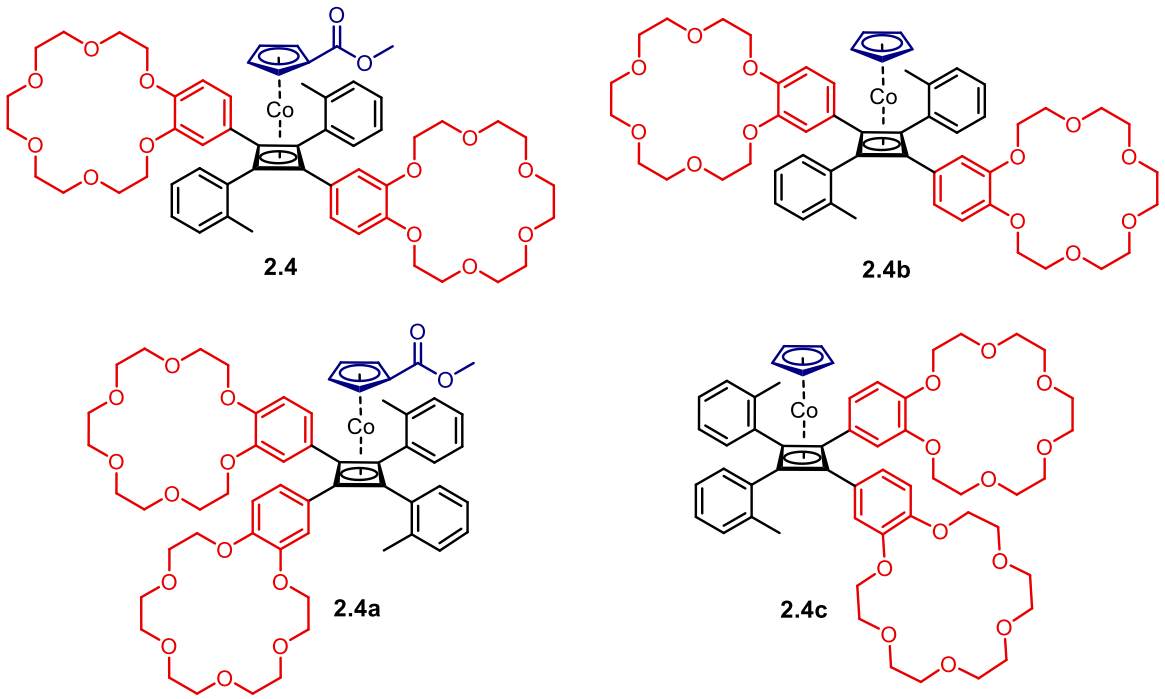

*Figure 2.6: Mixture of sandwich complex products eluted from the column; trans and cis isomers of the desired product (**2.4** and **2.4a**, respectively), alongside trans and cis isomers with an unfunctionalised Cp ring (**2.4b** and **2.4c**, respectively).*

Adding a small amount of Triethylamine (TEA) to the eluent (and subsequent removal of its protonated form from the collected fractions using a water wash) was partially successful in that the purification time and amount of solvent required was reduced, although complete separation of the desired *trans* product from its *cis* isomer continued to prove a challenge.

HPLC was therefore employed to purify the isomer mixture using an acetonitrile:water gradient eluent system and a C18 column. Figure 2.7 displays the HPLC trace of the crude organometallic mixture. Fortunately, the first main peak in the chromatogram corresponded to the desired *trans* isomer **2.4**, which could be isolated pure relatively easily, albeit in low yield (29%).

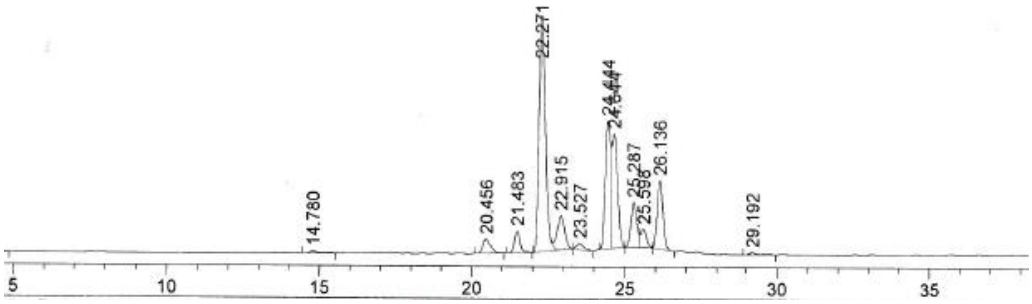

*Figure 2.7: HPLC trace of isomer mixture (TLC spot 4); 22.2 mins is **2.4**, 24.4 mins is **2.4a**, 24.6 mins is **2.4b** and 26.1 mins is **2.4c**. C18 column used with a gradient eluent system starting with 50:50 water:acetonitrile increasing to 100 % acetonitrile over 30 mins. Trace pictured uses a wavelength of 254 nm to visualise components of the mixture, whilst 375 nm was also used to exclusively visualise cobalt sandwich complex peaks.*

It was thought that the low yield could be attributed to the longer reaction time, which contributed to the decomposition of the ester-functionalised cyclopentadiene ring and the formation of side products **2.4b** and **2.4c**. The solvent ratio used was also a factor, with an 8:1 ratio (toluene:THF) found to give the optimum yield. Nevertheless, given that the literature quotes a yield of 34% for a far simpler unsymmetrical diarylacetylene derivative,[48] the reaction was overall deemed a success, with sufficient quantities obtained for characterisation, analysis and further reaction.

Surprisingly, the *trans*:*cis* ratio for the reaction was still 2.5:1 by NMR, Figure 2.8, the same selectivity observed in previous work by Richards and co-workers on similar systems.[48] This indicates that the presence of the bulky crown ethers in the *meta* and *para* positions had little to no impact on the distribution of stereoisomers. As previously discussed, replacing the

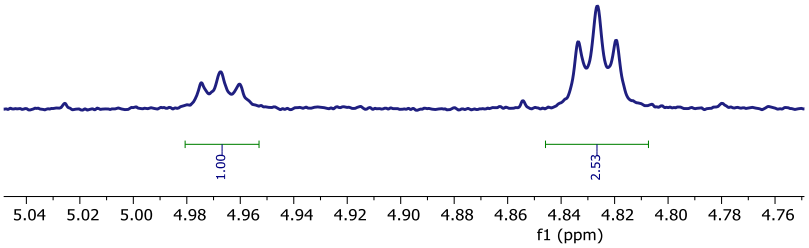

Figure 2.8: ^{1}H NMR integrals of one of the Cp ring proton environments of the cis (triplet at 4.98-4.99 ppm) and the trans (triplet at 4.84-4.81 ppm) stereoisomers. The NMR solvent was deuterated chloroform.

ortho-methyl group of the benzene ring with an *ortho*-isopropyl substituent was expected to increase the efficiency of the reaction by favouring the desired *trans* isomer.

2.4.3. Functionalisation of Cyclopentadienyl Ring

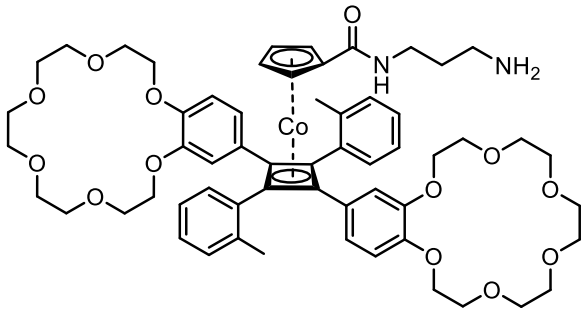

2.5

Figure 2.9: The synthetic target: the benzocrown rotary system.

Given that the benzocrown ethers hindered the facile purification of the cobalt sandwich species **2.4**, it was desirable to achieve the necessary functionalisation of the cyclopentadiene ring in as few synthetic steps as possible. It was envisaged that reacting ester **2.4** with 1,3-diaminopropane would lead directly to the target rotary system **2.5**, containing an arm with a stable amide group as well as a free amine capable of interacting with the benzocrown ethers on the lower cyclobutadiene ring. In order to preserve stocks of the hard earned **2.4**, unsubstituted sandwich complex **2.6** was synthesised from diphenylacetylene[49] to act as test compound.

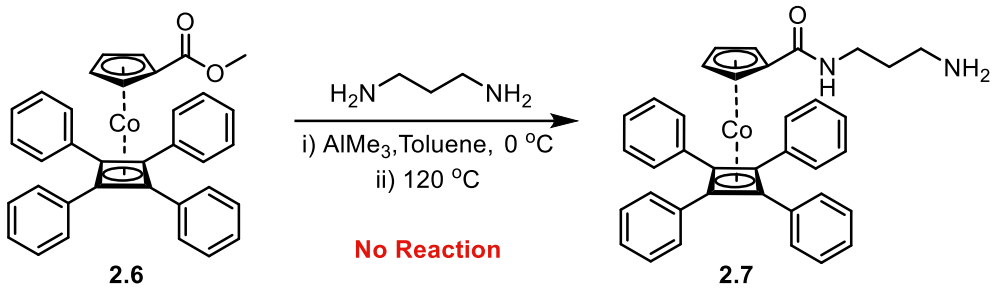

Scheme 2.15: Proposed one-step synthetic route to functionalise the cyclopentadiene ring with amine arm.

After several failed attempts to form **2.7** directly from the reaction between **2.6** and 1,3-diaminopropane, it was clear that more forcing conditions would be required to convert the ester directly into the coveted amide. Trimethylaluminium promotes the formation of amides from esters or carboxylic acids and amines through reacting with primary and secondary amines to give a dimethylaluminium amide intermediate.[56, 57] There is literature precedent of it being employed in the synthesis of ferrocene amides, demonstrating its suitability for use in this organometallic system.[58, 59] However, employing the conditions as detailed in Scheme 2.15 still failed to obtain amide **2.7**.

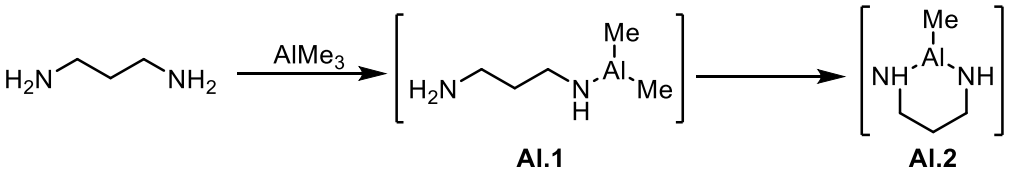

Scheme 2.16: Proposed formation of cyclic-aluminium intermediate Al.2.

It was proposed that the failure of the reaction centred around the formation of the dimethylaluminium intermediate. Upon reaction of trimethyl aluminium with 1,3-diaminopropane, **Al.1** was formed. Due to the presence of a second amine in the molecule at the end of a flexible alkyl chain, it is possible that this amine could coordinate to the same aluminium ion as its amine neighbour to give the cyclic intermediate **Al.2**. The formation of a six-membered ring system is enthalpically favoured due to the low ring-strain in the cyclic

product and the system was seemingly stable enough to prevent subsequent reaction with the ester.

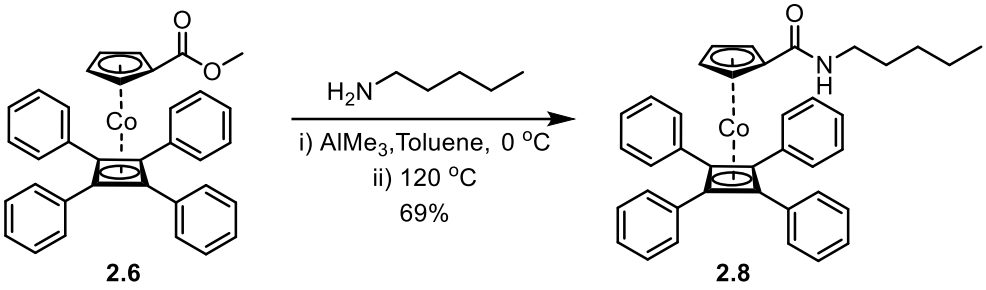

2.6 **2.8**

Scheme 2.17: Test trimethylaluminium-mediated ester to amide conversion with pentylamine.

To test the hypothesis, **2.6** was reacted with the readily available pentylamine. Reaction with the alkyl mono-amine was expected to proceed due to the absence of the second amine and therefore no possibility of a cyclic aluminium intermediate inhibiting the reaction. As expected, the reaction was successful, with the conversion of the ester into amide **2.8** proceeding quickly and in good yield, Scheme 2.17.

With the chemistry in place, it was apparent that a redesign of the amine arm was necessary. The benzene derivative *m*-xylylene diamine seemed an appropriate diamine with which to functionalise the cyclopentadienyl ring. The 1,3-spacing of the aminomethyl groups about the inflexible benzene core would separate the amine units sufficiently to prevent cyclisation, whilst a basic model indicated that there would still be sufficient flexibility to allow the amine arm to position itself above the crown's cavity to maximise non-covalent interactions. This

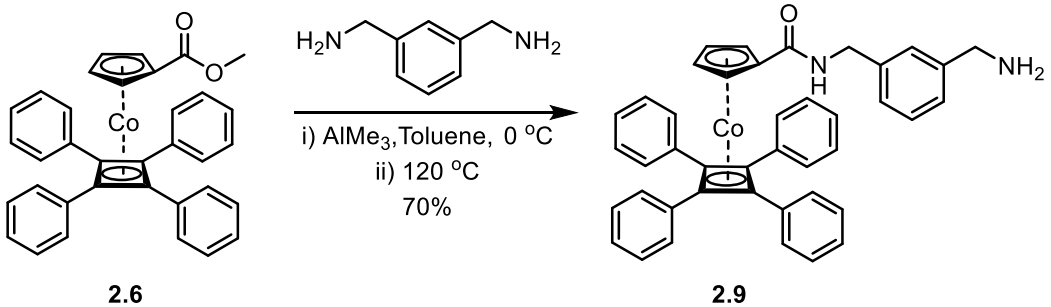

2.6 **2.9**

Scheme 2.18: Ester to amide conversion with the more sterically constrained m-xylylene diamine.

proved to be the case, as the reaction of **2.6** with *m*-xylylene diamine successfully converted the ester into the amino amide derivative **2.9**, Scheme 2.18.

Applying these same conditions to **2.4** gave the redesigned rotary system **2.10** in a 68% yield, Scheme 2.19. Furthermore, substituting silica gel with neutral alumina as the column stationary phase allowed for a relatively straightforward purification using milder eluent conditions of 97:3 DCM:methanol. The desired compound eluted second from the column as a yellow band following the minimal amount of unreacted **2.4** and was further purified by HPLC to remove some trace impurities.

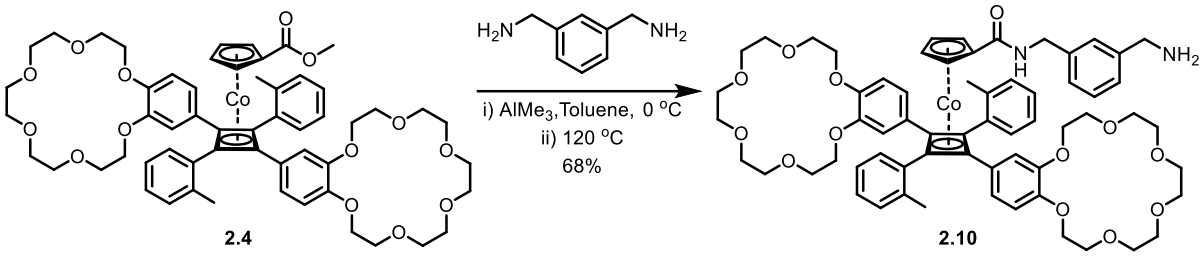

Scheme 2.19: Synthesis of the redesigned rotary system. 2.10 was purified by an alumina column using a 3% methanol in DCM eluent. The sandwich complex was subsequently purified by HPLC using a C18 column and a gradient eluent system starting in 2:8 acetonitrile:water, increasing to 100% acetonitrile over 30 min.

2.4.4. Synthesis of Control Compounds

With the headline rotary system synthesised and purified, attention turned towards populating a library of control compounds to assist with the variable temperature NMR experiments in probing the molecular motion. The four control compounds synthesised are shown below in Figure 2.10.

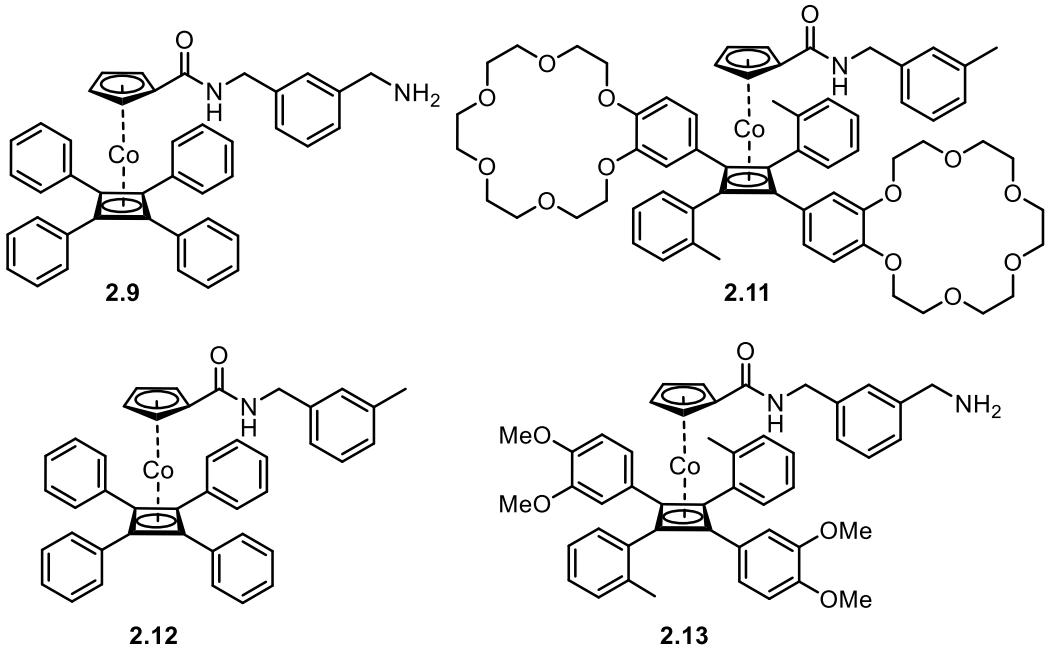

Figure 2.10: The library of control compounds.

The first two compounds each remove one of the two key interacting groups of the rotary system. The previously synthesised **2.9** conveniently has an unsubstituted η^4-tetraphenylcyclobutadiene ring, allowing for the behaviour of the primary amine in the absence of hydrogen bond-accepting crown ether units to be assessed, whilst **2.11** still possesses the crown ethers but not the hydrogen bond donor. Compound **2.11** was synthesised in almost exactly the same way as **2.10**, with 3-methyl benzylamine taking the place of *m*-xylylene diamine in the final step to give the Cp arm the same linker composition but ending at the carbon prior to the primary amine, Scheme 2.21.

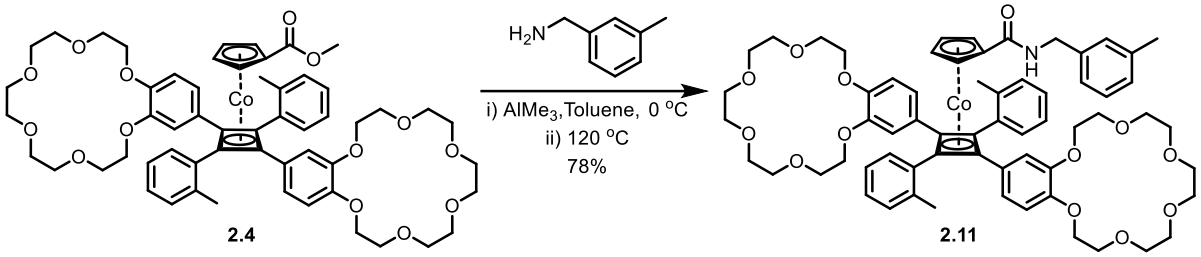

Scheme 2.21: Synthesis of control compound 2.11.

To complement these two compounds, the double negative control **2.12** was made. Like **2.9**, it was synthesised from metallocene **2.6** but using 3-methyl benzylamine as an alternative to *m*-xylylene diamine, as shown in Scheme 2.20.

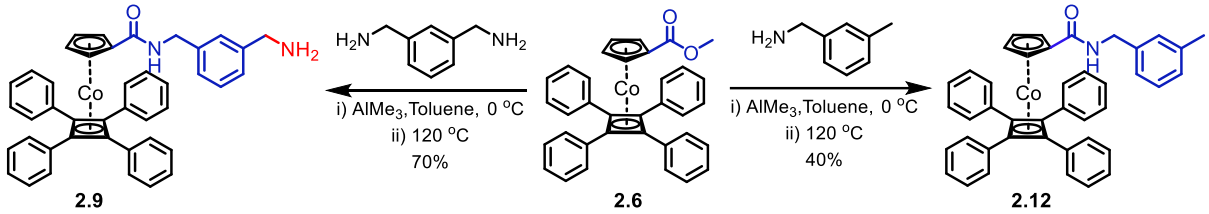

Scheme 2.20: Synthesis of control compounds with an unsubstituted η⁴-tetraphenylcyclobutadiene ring.

The final control compound **2.13** replaces each crown ether with two methoxy units. This compound was envisaged as acting as an intermediary between **2.9** and **2.10**; whilst the methoxy groups were not expected to interact with the protonated amine at low pH and therefore have a negligible effect on the rate of rotation about the ball-bearing axis, the electron density of the system would more closely match that of the crown ether derivative. Furthermore, studies on this compound would demonstrate unambiguously that the binding capabilities of the crown ethers are crucial the rotary behaviour of the system.

Control **2.13** was synthesised *via* an analogous pathway to the benzocrown organometallic derivative **2.10**, as shown in Scheme 2.22. The structural deviation was implemented early in the synthesis, with ethynyl-2-methylbenzene **2.2** being coupled to 4-bromoveratrole under

Sonogashira conditions to give alkyne **2.14** in good yield. From this, the cobalt sandwich complex **2.15** was formed. Purification of the reaction mixture was far simpler than for **2.4**, due to the absence of the crown ether units, and the desired *trans* isomer was obtained using milder column eluent conditions of 7:3 hexane:ethyl acetate in a yield of 28%. As observed previously, the ratio of stereoisomers in the crude mixture was approximately 2.5:1 *trans*:*cis*.

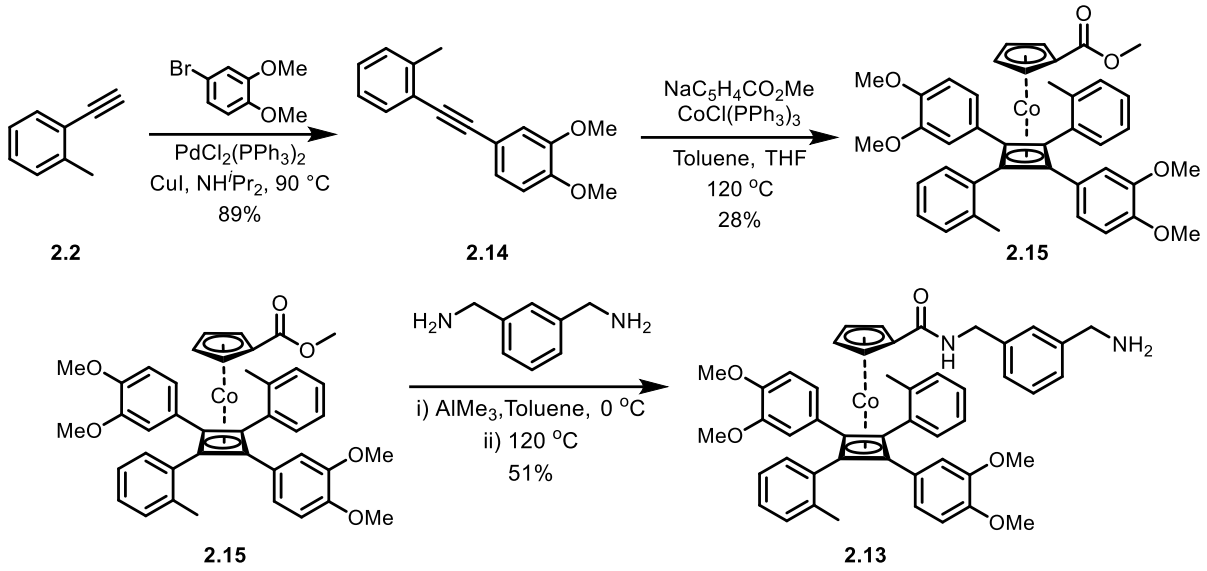

Scheme 2.22: Synthesis of control compound 2.13.

Single crystals of **2.15** were grown in the freezer from an NMR sample (solution in deuterated chloroform) and the crystal structure is displayed in Figure 2.11. It shows the aromatic rings about the cyclobutadiene ring adopting a conformation where neighbouring rings are rotated approximately 90° to each other to minimise unfavourable steric clashes. The prevalence of such an orientation in solution would help to explain why the presence of *meta* and *para* substituents have little effect on the distribution of stereoisomers. Note that the two *o*-methyl groups point down, away from the metallocene core. Another observation is that in the solid state, the amide unit prefers to sit in the same plane as the cyclopentadiene ring. This complements previous crystal structures obtained by Richards and co-workers.[48] It was

thought that such conformational preferences would become factors to consider upon subjecting the rotary system to low temperatures when probing the molecular motion.

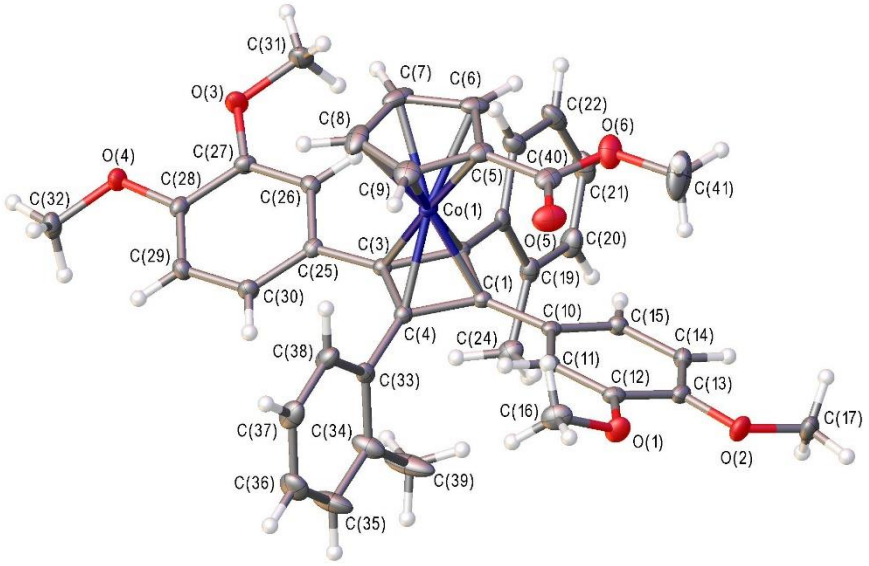

Figure 2.11: Crystal structure of methoxy cobalt sandwich complex ester 2.15 with ellipsoids drawn at the 50 % probability level. The structure occupies a centrosymmetric space group. All hydrogen atoms were fixed as riding models.

Reacting **2.15** with *m*-xylylene diamine gave the final control compound **2.13**. All control compounds were purified by HPLC using a C18 column and acetonitrile:water eluent system to ensure their purity in advance of the variable temperature NMR experiments (full purification methods outlined in *Chapter 5: Experimental*).

2.5. NMR Experiments

2.5.1. Protonation of the Primary Amine Tether

Attention turned to the suitability of the primary amine at performing its role as the switchable tether within compound **2.10**. The success of the system depended on the effect of its protonation on its intramolecular binding properties. The hypothesis was that a tripodal H-bonding interaction between the protonated tether and the benzocrown ethers would reduce the rate of rotation about the ball-bearing axis, as shown in Scheme 2.23. Due to its solubility in organic solvents, trifluoroacetic acid (TFA) is a popular choice amongst supramolecular chemists to lower the pH of solutions containing dynamic molecular systems, whilst pyridine is often employed as the base to return to neutral pH.[11]

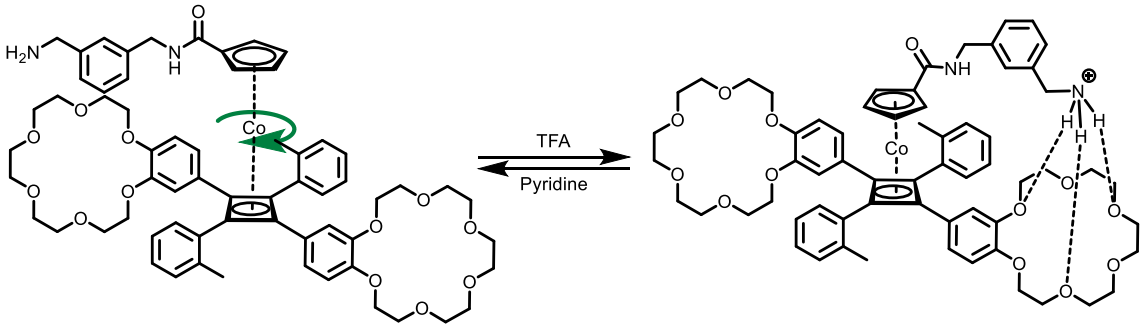

Scheme 2.23: The rotary system in action: at neutral pH (left) there is free rotation about the ball-bearing axis and it is in a state of faster exchange. In acidic conditions (right) the rate of rotation is slower due to stronger non-covalent interactions.

After stability studies with the benzocrown metallocene side product **2.4b** indicated that these two external chemical inputs could work in tandem with the benzocrown sandwich complex, ^{1}H NMR experiments of control compound **2.9** in CD_3CN were performed before and after the addition of a slight excess of TFA, Figure 2.12. Upon addition of 1.2 molar equivalents of TFA, H_1 is shifted downfield beyond H_2 and the splitting pattern changes from a singlet to a quartet, indicating the successful formation of the desired ammonium cation.

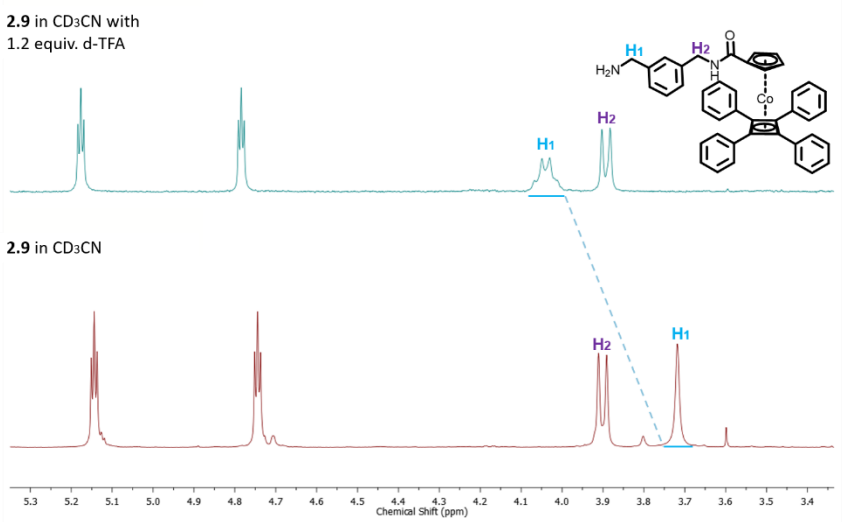

Figure 2.12: Overlaid partial ^{1}H NMR spectra of control compound 2.9 in deuterated acetonitrile (bottom) and upon addition of 1.2 equiv. of TFA to the solution (top).

2.5.2. Solvent Effects: Protic *vs* Aprotic

The formation of compound **2.10** led to some interesting observations. After dissolving the sample in deuterated chloroform (*ca.* 10 mM) to record its NMR spectrum, the sample set to a gel within five minutes. The same result was observed for deuterated DCM but not with deuterated acetonitrile and methanol. Clearly some form of aggregation was occurring in these chlorinated solvents, perhaps driven by ionic interactions resulting from their low dielectric constants. Interestingly, it was unique to this molecule; the phenomenon was not observed for the methyl ester **2.4** precursor nor any of the four control compounds, suggesting that the unique blend of HBD and HBA groups in **2.10** was responsible.

Exploring a range of solvents revealed further interesting phenomena in the NMR spectrum at room temperature. For example, certain hydrogen environments exhibited broadening when the proton NMR spectrum of **2.10** was recorded in deuterated acetonitrile, Figure 2.13.

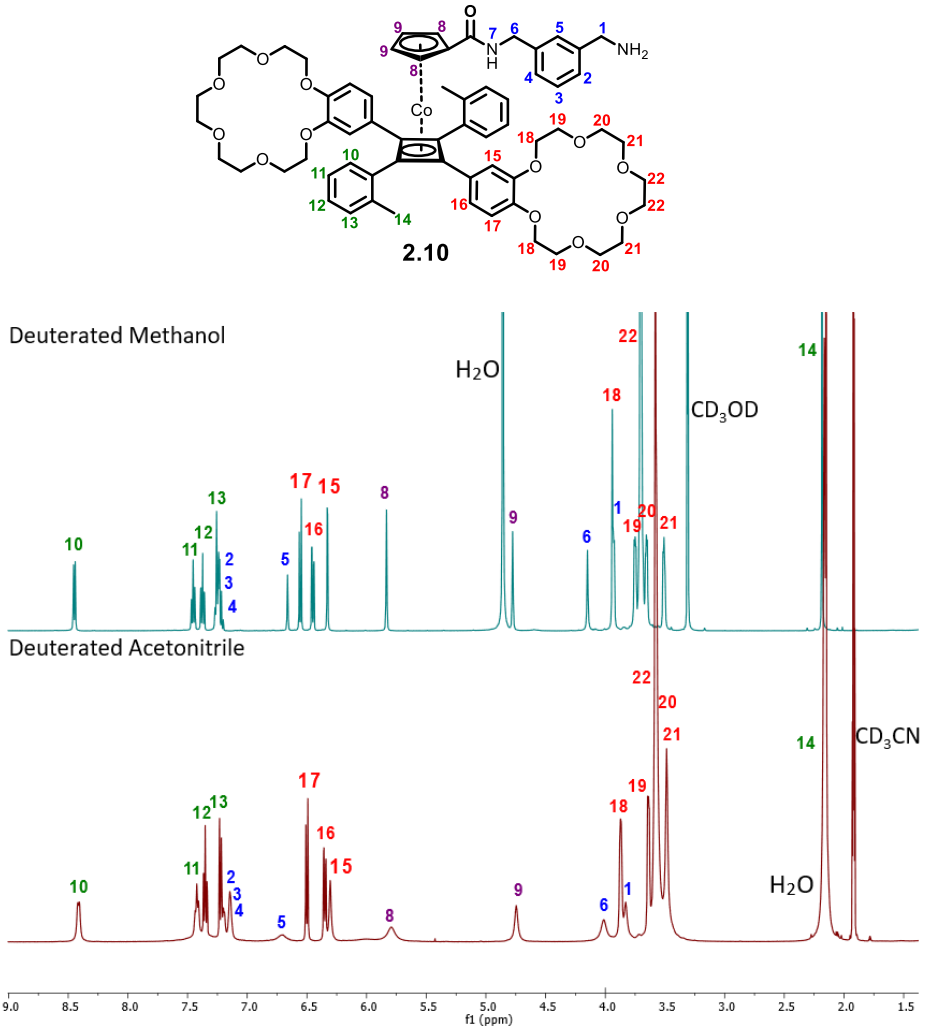

*Figure 2.13: The benzocrown metallocene rotary system. Proton environments are numbered (top). An overlay of the ^{1}H NMR spectra of compound **2.10** in deuterated methanol and acetonitrile. Spectra recorded at ambient temperature (bottom).*

Broadening of signals can be due to the self-aggregation of molecules in solution but in this case the observed phenomenon is likely to result from weak interactions between the unprotonated primary amine tether of the cyclopentadienyl ring and the benzocrown ethers of the cyclobutadiene ring which hinder free rotation about the ball-bearing axis. In support of this, the corresponding signals in the NMR spectrum of control compounds **2.9** and **2.11**, where the crown ether units or the amine tether have been removed, did not exhibit any broadening, Figure 2.14. The same lack of broadening was also observed for the cyclopentadienyl protons signals in the methyl ester precursor **2.4**.

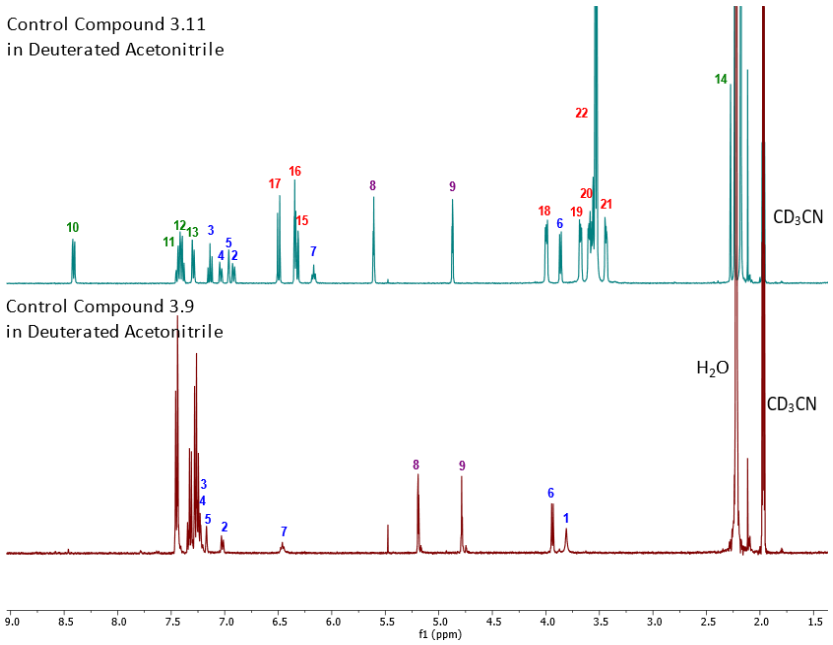

*Figure 2.14: An overlay of the ^{1}H NMR spectra of control compounds **2.9** (no crown ethers) (bottom) and **2.11** (no amine tether) in acetonitrile (top). The proton environments numbered are those shared with parent compound **2.10** in Figure 2.13. Spectra recorded in deuterated acetonitrile at ambient temperature.*

Replacing the aprotic NMR solvent acetonitrile with deuterated methanol resulted in the sharpening of these broadened peaks alongside some minor shifts in certain peak positions, Figure 2.13 above. Clearly the hydrogen bonding ability of the solvent is important, with the polar protic properties of methanol capable of disrupting weak intramolecular non-covalent interactions, leading to sharper signals.

The NMR experiments described above provide evidence that the moieties on each metallocene ring interact with one another, which is crucial to the success of the system. They also indicate that the choice of NMR solvent for the variable temperature NMR experiments is important. Given that it was possible that a protic solvent such as methanol could interfere with the desired intramolecular interactions, it was decided to explore both acetonitrile and methanol as solvents in initial low temperature studies, detailed in the next section.

2.6. Variable Temperature NMR Experiments

Variable temperature NMR experiments were to provide the evidence for controlled, variable rates of rotation about the ball-bearing axis of the rotary system, as shown in Scheme 2.24. As described earlier, it was anticipated that at neutral pH, where there is relatively free rotation about the cobalt core, cooling the rotary system would result in the broadening of certain signals in the NMR spectrum as the rate of rotation slows. However, under low pH conditions where tripodal H-bonding is possible due to protonation, the rotation was expected to be slower, with certain signals broadening to a far greater extent as the temperature is lowered.

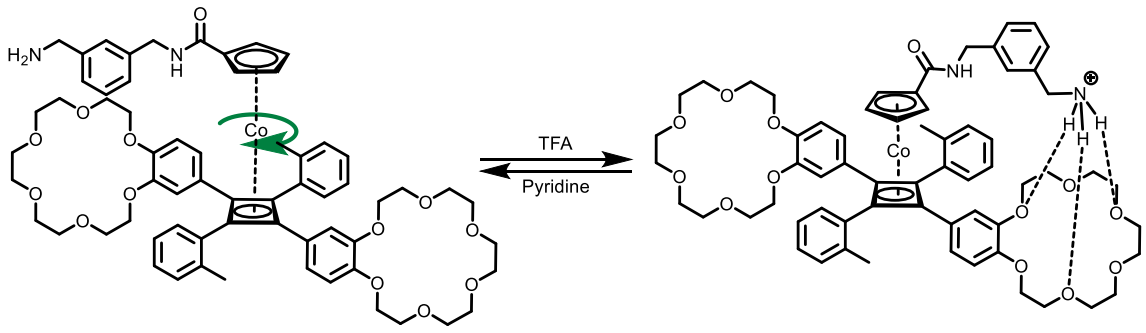

Scheme 2.24: The rotary system in action: at neutral pH (left) there is free rotation about the ball-bearing axis and it is in a state of faster exchange. In acidic conditions (right) the rate of rotation is slower due to stronger non-covalent interactions.

An important consideration was the choice of NMR solvent. As well as the previously discussed protic/aprotic properties, it was vital that the freezing point of the solvent was well below the lowest temperature investigated. As the experimental set up allowed for cooling to 238 K (-35 °C), the previously investigated solvents acetonitrile and methanol appeared to be suitable choices with freezing points of 228 K and 176 K, respectively.

2.6.1. Initial VT Studies on the Rotary System 2.10

2.6.1.1. Acetonitrile at Neutral pH

A solution of rotary system **2.10** in deuterated acetonitrile was cooled from 298 K to 238 K with NMR spectra recorded in ten-degree decrements. Figure 2.15, below, shows overlaid spectra, which enables changes in each signal to be readily tracked. The signals corresponding to environments 1, 5, 6, 8 and 9, already partially broadened at RT, broadened further upon cooling, with Cp ring proton 9 near coalescence at 238 K. Proton 5 shifted upfield into the

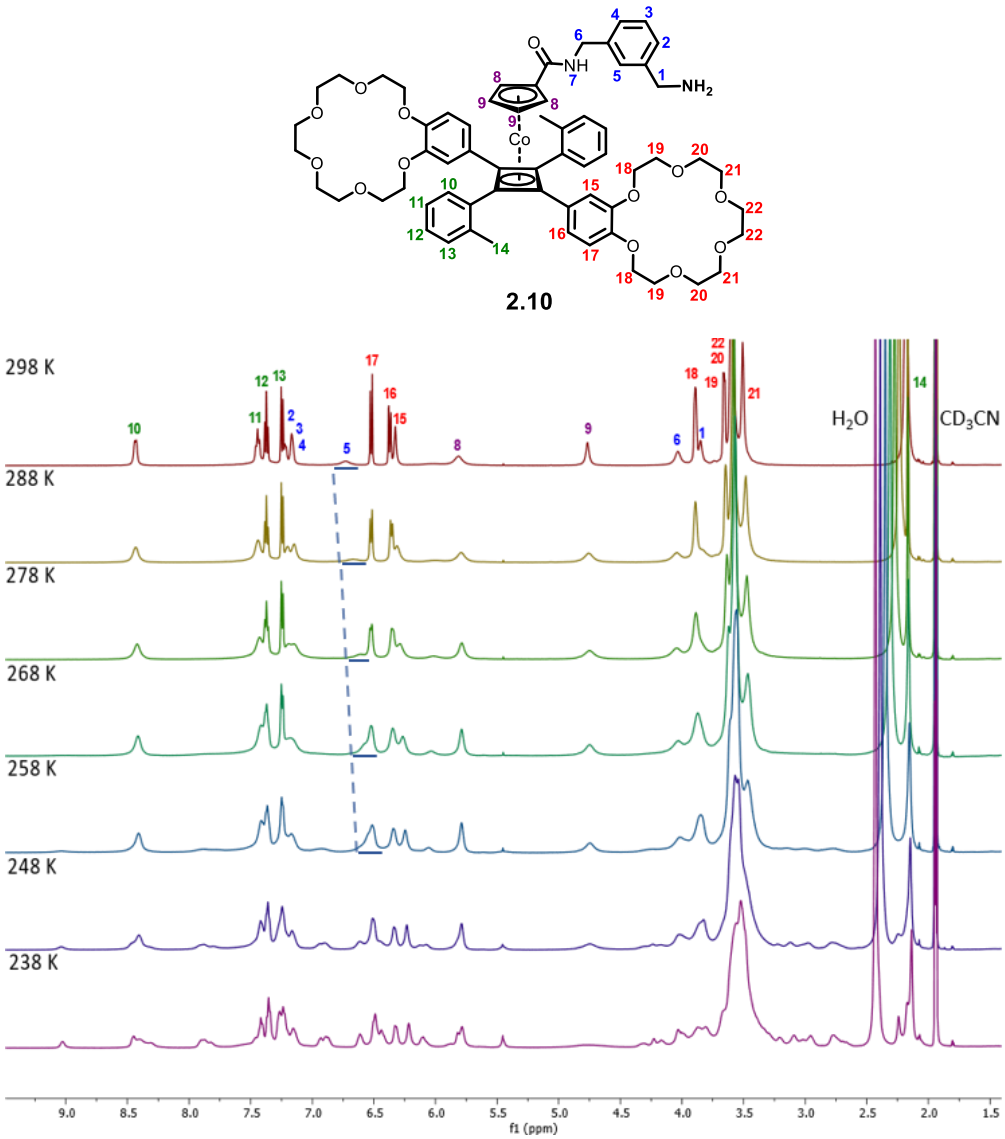

*Figure 2.15: (Top) Rotary system **2.10** with its proton environments numbered. (Bottom) Overlaid VT ^{1}H NMR spectra of rotary system **2.10** in deuterated acetonitrile at neutral pH. Concentration of **2.10** is 9.38 x 10^{-3} mol dm^{-3}.*

cluster of aromatic benzocrown proton signals 15, 16 and 17, which themselves broadened and shifted apart as the temperature decreased. The signals corresponding to the remaining crown ether environments 18-22 lost all their original resolution and merged upon cooling. Signal 10 also lost its original structure, whilst new peaks either side of it appeared. The remaining *ortho*-tolyl proton signals 11-14 began to lose their resolution but were relatively unaffected.

2.6.1.2. Acetonitrile at Acidic pH

Next, 1.2 molar equivalents of deuterated trifluoracetic acid were added to the NMR sample and the variable temperature studies were repeated, with the overlaid NMR spectra shown in Figure 2.16. Initially, the move to a low pH sharpened peaks that were broadened at 298 K at neutral pH, possibly due to the protic properties of TFA.

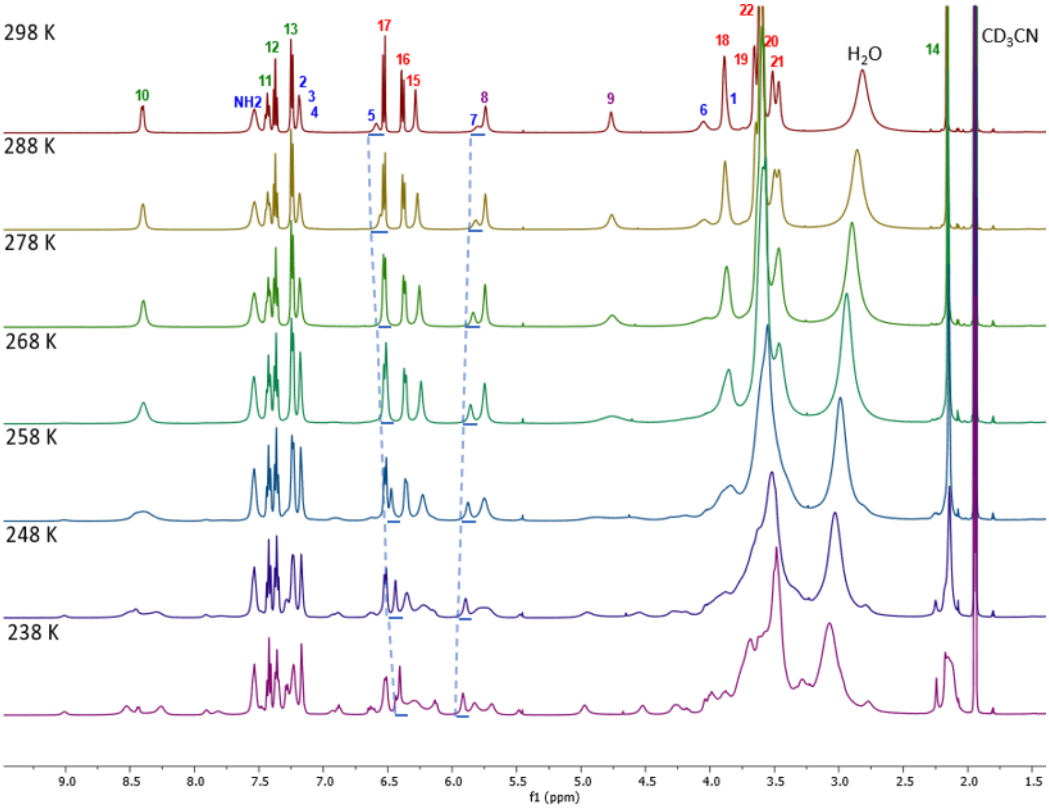

*Figure 2.16: Overlaid VT ^{1}H NMR spectra of rotary system **2.10** in deuterated acetonitrile with 1.2 equiv. of deuterated TFA. Signal numbering corresponds to the proton environments in Figure 2.15. The shifts of signals **5** and **7** are highlighted. Addition of TFA has revealed the amine and amide proton environments. Concentration of **2.10** is 9.38 x 10^{-3} mol dm^{-3}.*

A comparison of the appearance of the NMR spectra at 238 K before and after acidification is shown in Figure 2.17 below. At 298 K, whether the amine is protonated or not, there are only three benzocrown signals observed, which indicates fast rotation on the NMR timescale. In the case of the protonated system, such a process would involve exchange of the protonated arm between the two crown ether sites to make them equivalent. Upon cooling to 238 K, both spectra broaden significantly. The clear increase in broadening upon cooling, whether the system is protonated or not, indicates that dynamic processes within the rotary system are significantly affected by temperature, with two different environments now observed for the crown ether groups at 238 K in both cases. However on closer inspection of the spectra, there are still some notable differences between the protonated and unprotonated spectra at 238 K.

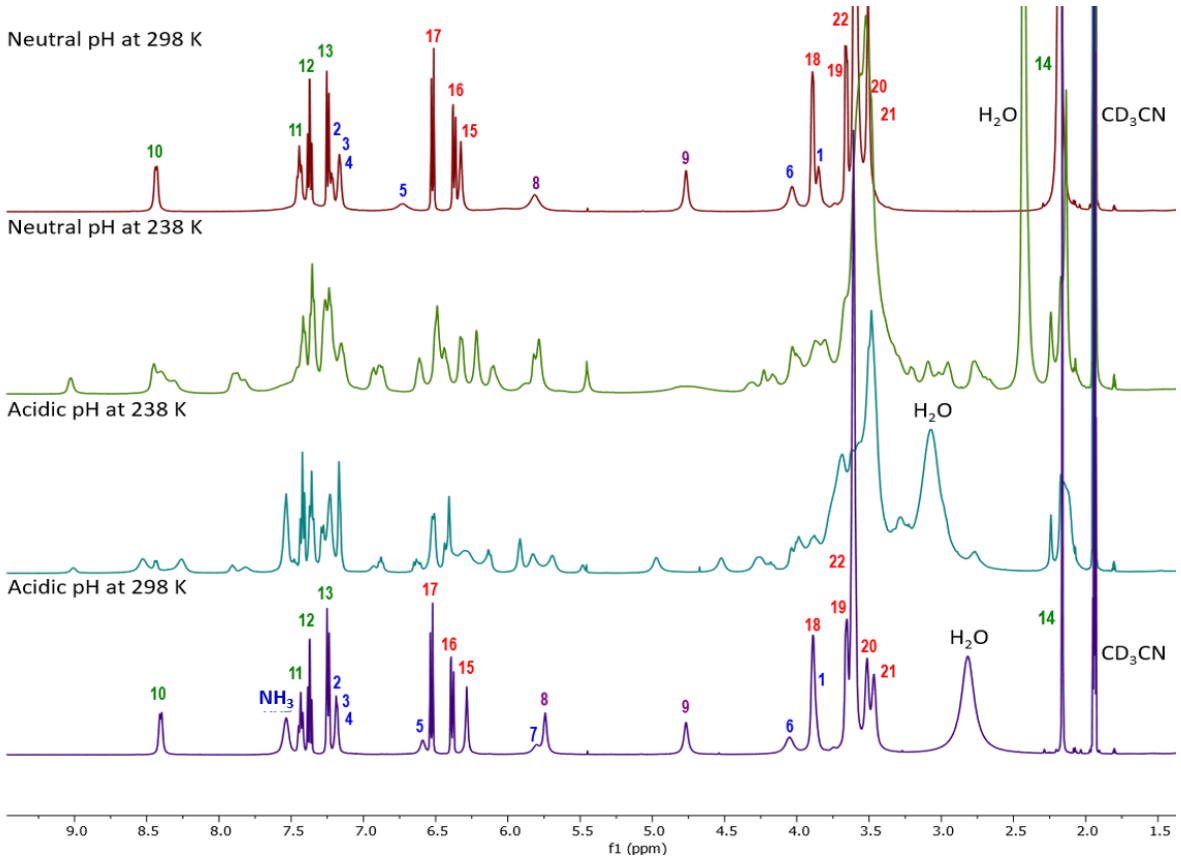

*Figure 2.17: Overlaid VT ^{1}H NMR spectra of rotary system **2.10** in deuterated acetonitrile at neutral pH 298 K (top), 238K (second), acidic pH 238 K (third) and 298 K (bottom). Signal numbering corresponds to the highlighted proton environments in Figure 2.15. Concentration of **2.10** is 9.38 x 10^{-3} mol dm^{-3}.*

For example, the signals for the Cp ring environments 8 and 9, as well as *ortho*-tolyl proton signal 10, are each split into two resonances by 238 K for the protonated system only. These differences are used later in this chapter to obtain quantitative information regarding the dynamic processes at play in this system. In addition, the aromatic benzocrown proton signals 15-17 are broadened more, whilst there are some subtle differences in signals representing environments in the linker arm 1 to 6, methyl group 14 and crown ether regions 18-22 were all heavily impacted.

Examining the conformation that rotary system **2.10** is likely to adopt upon protonation of the amine tether provides some insight into why certain signals in the NMR spectrum are affected more than others as the temperature is lowered, Figure 2.18.

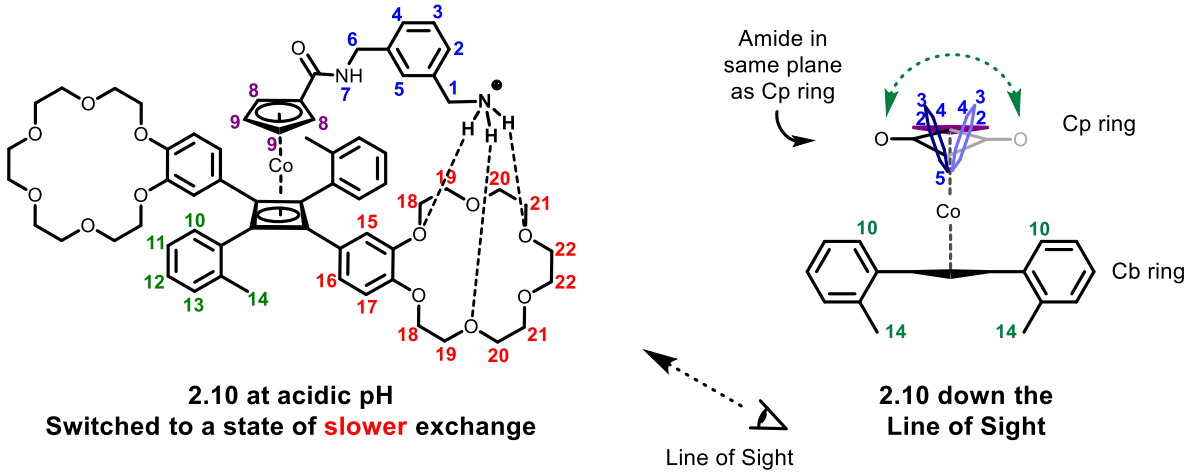

*Figure 2.18: (Left) The suspected conformation adopted by rotary system **2.10** at low pH. Proton environments are numbered. (Right) Side-on view looking at **2.10** directly down the benzocrown ether-cyclobutadiene C-C bond. View shows the desire of the amide unit to sit in the plane of the Cp ring and the effect this arrangement has on the position adopted by the aromatic linker of the amine arm.*

As mentioned above, the singlet corresponding to proton 10 broadened significantly upon cooling at neutral pH and split into two peaks for the protonated system. However interestingly, the signals for its neighbours on the ring (protons 11-13) were relatively unaffected. Whilst unaffected at neutral pH, the signal representing methyl group 14 was also significantly broadened upon cooling under acidic conditions. The crystal structure presented

in Figure 2.11, page 65, shows that the preferential conformation adopted by the *ortho*-tolyl group has the methyl group pointing down, away from the sandwich complex core. This in turn positions proton environment 10 upwards, in closer proximity to the binding site between the ammonium cation and either of the two benzocrown ethers. Such a conformation may explain the larger differences in the signal for 10 under slow exchange conditions compared to the other aromatic protons.

Finally, aromatic benzocrown signals 15-17 and crown ether environments 18-22 all experienced greater broadening and shifts when cooled under acidic conditions compared to neutral pH. Again, these observations indicate that the natural symmetry of the molecule is lost as the amine arm spends a greater amount of time in the vicinity of each crown, and that these proton environments are under conditions of slow exchange.

That the significantly affected signals in the NMR spectrum correspond to those proton environments that are in proximity to the binding site is telling of the increased non-covalent interactions between the benzocrown ether and the ammonium cation under acidic conditions. Whilst it cannot be stated that the rotation about the ball-bearing axis has completely stopped at 238 K at low pH, these initial VT NMR studies indicate that the rate of rotation about the ball-bearing axis has significantly decreased and is under switchable control.

2.6.1.3. Methanol at Neutral pH

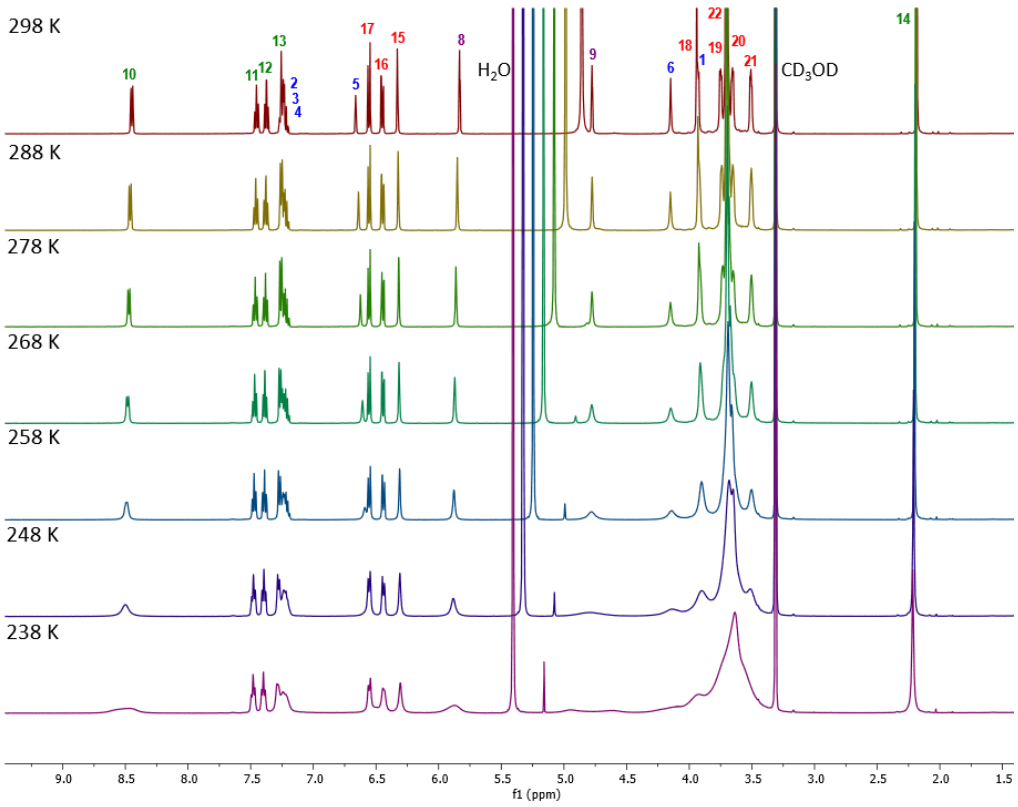

*Figure 2.19: Overlaid VT ^{1}H NMR spectra of rotary system **2.10** in deuterated methanol recorded at 10-degree increments. Signal numbering corresponds to the highlighted proton environments in Figure 2.15. Concentration of **2.10** is 8.93 x 10^{-3} mol dm^{-3}.*

Figure 2.19 shows that gradual cooling of rotary system **2.10** in deuterated methanol led to certain signals broadening, whilst others remained relatively unchanged. These affected signals complement those affected by changing between protic and aprotic solvents in section 2.5.2. At 238 K, many of the signals are broadened to a greater extent than in acetonitrile, with the signal corresponding to Cp ring proton 9 starting to split into two peaks. Signal 10 is also heavily broadened to the point of coalescence and crown ether proton environments 18-22 change from having sharp, well defined structures to merging and adopting a melted appearance. Whilst these signals appear to be more affected, the unaffected signals still have a relatively well-defined structure.

2.6.1.4. Methanol at Acidic pH

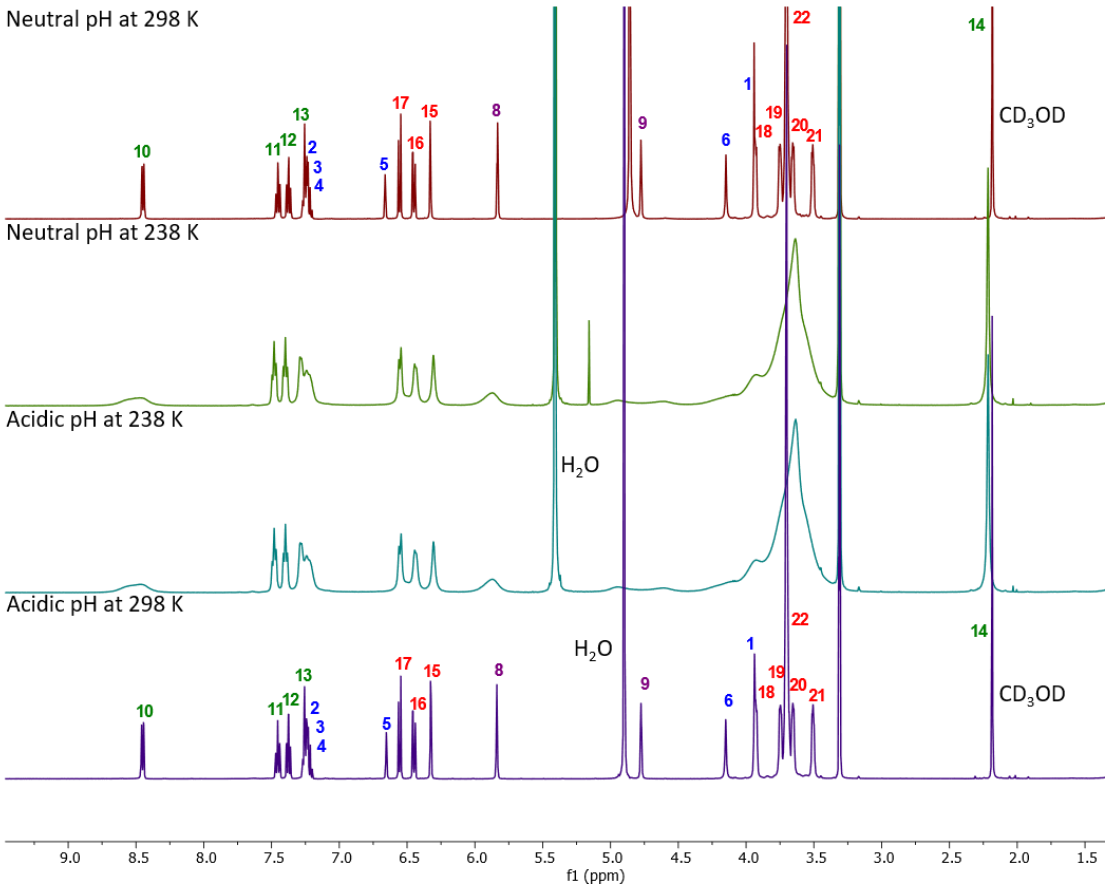

*Figure 2.20: Overlaid VT ^{1}H NMR spectra of rotary system **2.10** in deuterated methanol at neutral pH 298 K (top), 238K (second), acidic pH 238 K (third) and 298 K (bottom). Signal numbering corresponds to the highlighted proton environments in Figure 2.15. Concentration of **2.10** is 8.93 x 10^{-3} mol dm^{-3}.*

Acidifying the methanol solvent system with the addition of 1.2 molar equivalents of TFA appears to have had little effect on the spectra at 298 K or 238 K, Figure 2.20. Indeed, apart from the minor shifts in the water peak, the spectra at each temperature look almost identical in comparison to the changes in acetonitrile, where more changes were observed. The most likely explanation for this is that there is little or no intramolecular binding between the tether and the crown ether in this solvent because methanol is a more competitive solvent.

2.6.1.5. Summary

Initial NMR studies on rotary system **2.10** showed that the rate of rotation about the ball-bearing axis was dramatically affected by lowering the temperature. Cooling the system led to certain proton environments broadening and indicated that even at neutral pH there are weak interactions between the primary amine tether and the crown ethers, strong enough to affect the rotation about the ball-bearing axis at low temperatures. Cooling in the presence of a slight excess of acid enhanced these effects slightly, as the design intended, suggesting that complexation further slowed rotation about the core ball-bearing axis. These initial experiments indicated that the less competitive acetonitrile was a more appropriate solvent than methanol and was therefore chosen for use in further experiments.

One of the key questions that remained was the exact nature of the dynamic process; *i.e.* the extent to which the observed effects were due to the effect of binding on the rate of interconversion about the ball-bearing axis between two binding sites, compared to other dynamic processes within the system (*e.g.* related to steric effects alone) that might also become apparent upon cooling the system. It was anticipated that VT studies using the library of control compounds would help to clarify this aspect. In addition, determining the temperature of coalescence of certain signals in the NMR spectrum would allow for the calculation of kinetic information, whilst the reversibility of the switchable system and the effect of adding metal cations also need to be assessed.

2.6.2. Variable Temperature NMR Studies with the Control Compounds

Following the success of the variable temperature NMR experiments with rotary system **2.10**, samples of all four control compounds in deuterated acetonitrile were cooled from 298 K to 238 K in ten-degree decrements. As each control compound has at least one of the two key interactive units removed, it was expected that the VT and binding studies would reveal only minor changes in appearance to the NMR spectra, as rotation about the ball-bearing axis should not be impacted by non-covalent interactions.

2.6.2.1. Absence of the Amine Tether

Cooling of a CD_3CN solution of control compound **2.11** had little to no effect on the appearance of the ^1H NMR spectrum at either neutral or acidic pH. Most signals retained their sharpness and resolution, with only the signals corresponding to water and the amide proton 7 seeing notable shifts, with the latter also losing its triplet splitting pattern due to broadening.

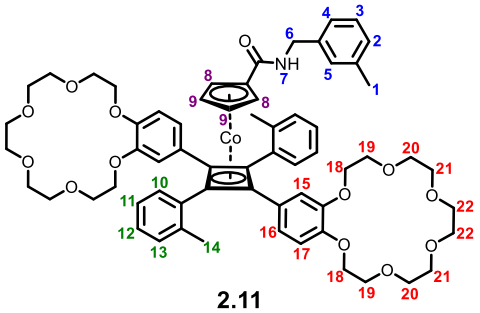

*Figure 2.21: Control compound **2.11**. Proton environments have been numbered.*

The absence of any changes in the NMR spectra of **2.11** is good evidence that the phenomena observed when cooling rotary system **2.10**, which has similar bulky groups, is a result of non-covalent interactions between the amine/ammonium ion and benzocrown ether. In other

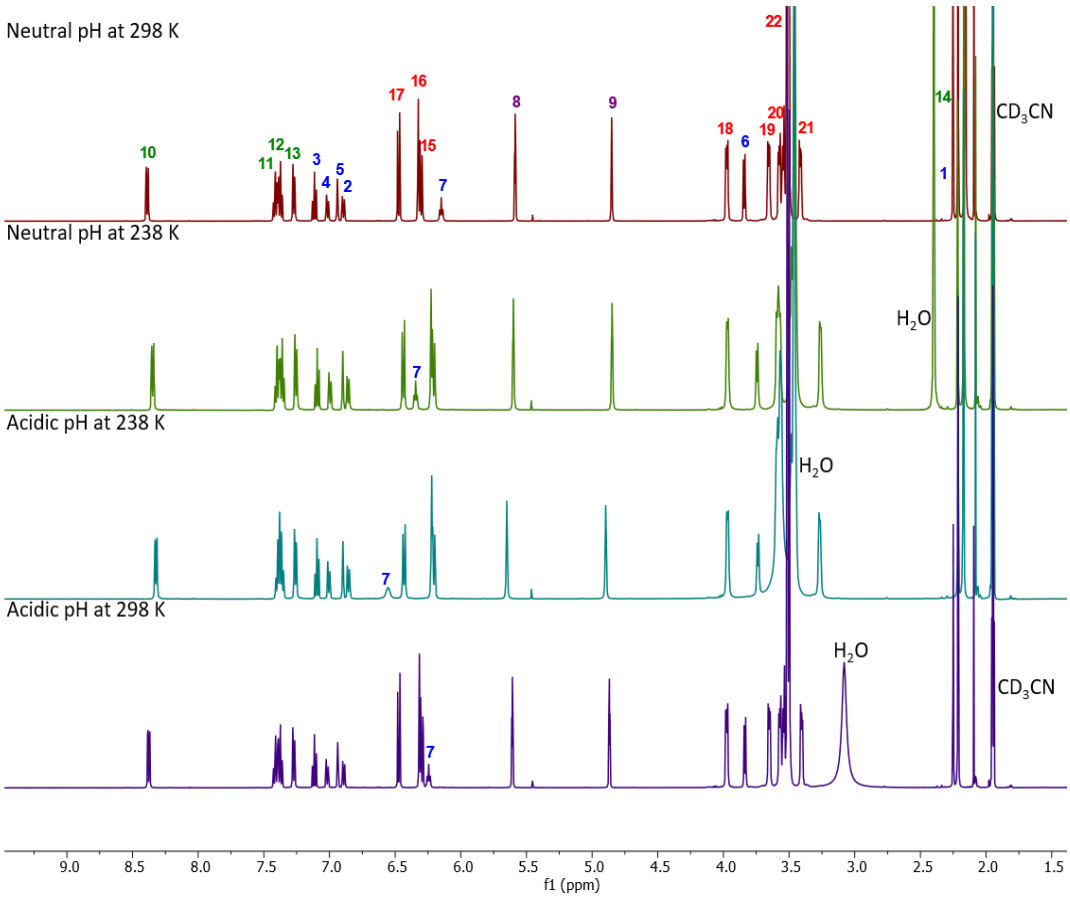

*Figure 2.22: Overlaid VT NMR spectra of control compound **2.11** in deuterated acetonitrile. Signals are numbered in relation to the proton environments outlined in Figure 2.21. Concentration = 6.765 x 10^{-3} mol dm^{-3}*

words, these studies on compound **2.11** lessen the possibility that the broadening effects observed at low temperature or at acidic pH are due to the slowing of rotation about various individual bonds in the molecule.

2.6.2.2. Absence of the Crown Ethers

As expected, studies on the control compound **2.9** containing no benzocrown ethers resulted in very minor changes being observed in the NMR spectrum upon cooling at neutral pH, Figure 2.23. The signals corresponding to aromatic protons 2-5 spread out slightly, whilst amide proton 7 experienced a downfield shift, as expected. Signal 1 sharpened as the system was cooled. Upon acidification, 1 shifted downfield and split into a quartet as its amine neighbour

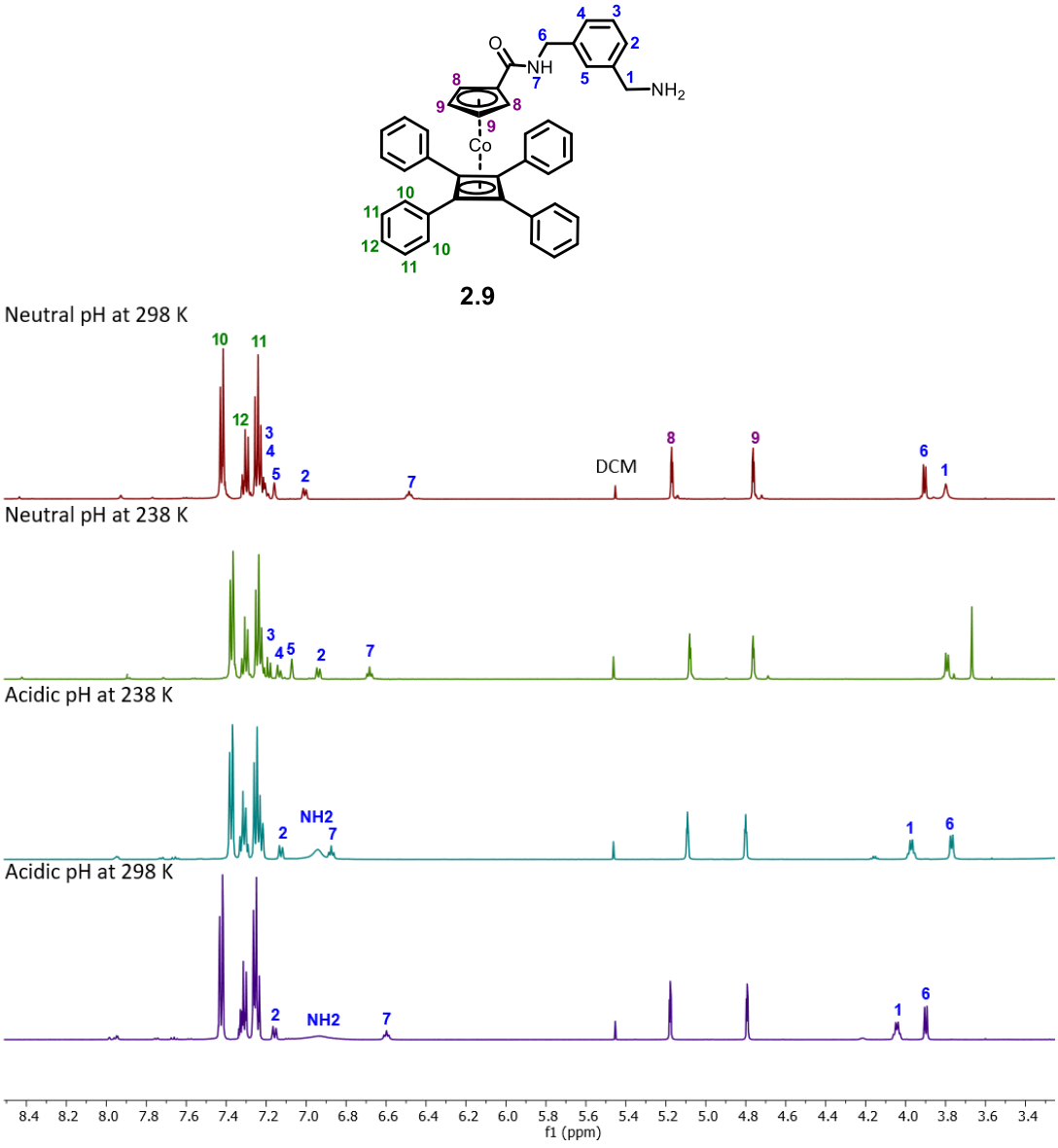

*Figure 2.23: (Top) Control compound **2.9**. Proton environments have been numbered. (Bottom) Overlaid VT NMR spectra of control compound **2.9** in deuterated acetonitrile. Concentration = 9.498 x 10^{-3} mol dm^{-3}.*

was protonated, as discussed in section 2.5.1 on page 66. Once again, signal 7 was shifted downfield on cooling, whilst the addition of TFA revealed the amine proton environment, which sharpened upon cooling.

2.6.2.3. Absence of the Amine Tether and the Crown Ethers

A similar trend was found for the double negative control compound **2.12**, with its NMR spectra appearing almost identical bar the predictable shifts observed in the signals relating to the amide proton 7 and residual water, Figure 2.24. Interestingly, the signals representing the aromatic linker protons 2-5 were spread out at room temperature. In compound **2.9**, a

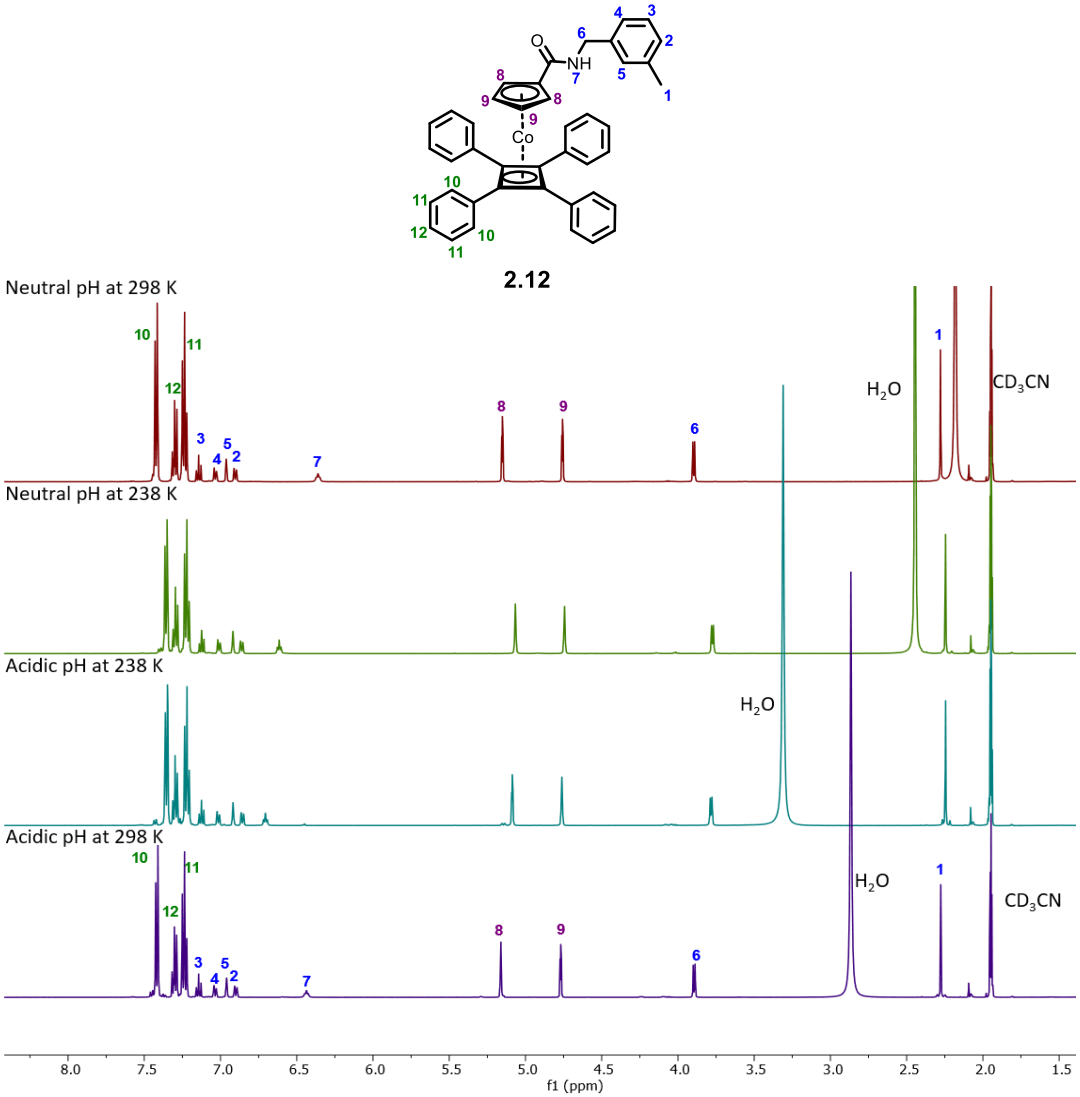

*Figure 2.24: (Top) The double negative control compound 2.12. Proton environments have been numbered. (Bottom) Overlaid VT NMR spectra of control compound **2.12** in deuterated acetonitrile. Concentration = 10.36 x 10^{-3} mol dm^{-3}.*

structure that only differs from **2.12** in possessing a primary amine, these signals are bunched together before separating upon cooling, Figure 2.23. The shifts are likely to be induced by changes in the degree of hydrogen bonding with temperature.

2.6.2.4. Crown Ethers replaced with Methoxy Units

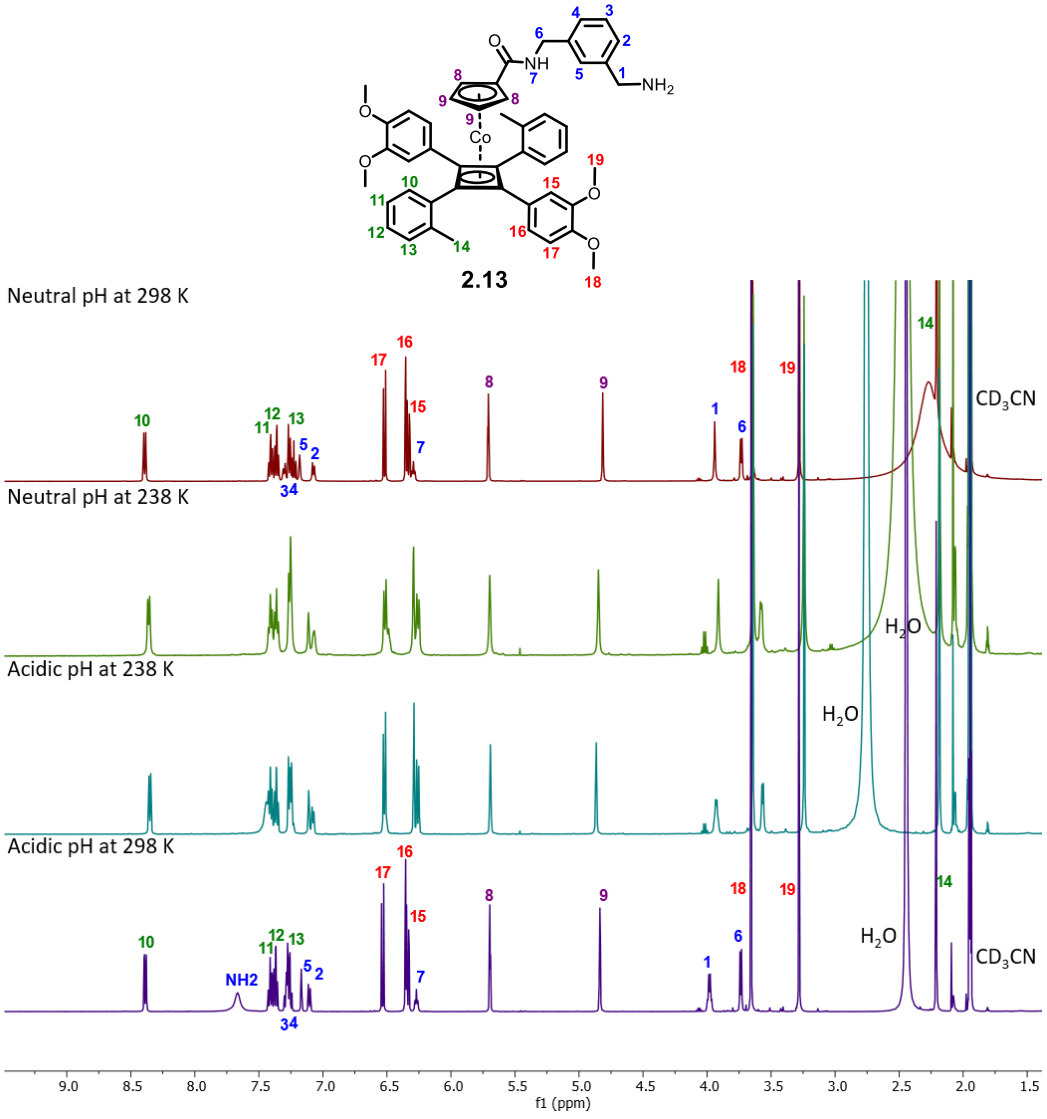

*Figure 2.25: (Top) Control compound 2.13 replaced the crown ethers with methoxy units. Proton environments have been numbered. (Bottom) Overlaid VT NMR spectra of control compound **2.13** in deuterated acetonitrile. Concentration = 7.592 x 10^{-3} mol dm^{-3}.*

Finally, VT NMR studies with **2.13** revealed a similar trend once again, with only small changes observed upon cooling the neutral and protonated forms. The expected shifts of signals relating to NH protons and residual water were observed, as well as minor shifts in signals 2-

5 upon cooling, Figure 2.25. The signal corresponding to proton environment 1 changed its splitting pattern to a quartet upon acidification as expected, but it unusually remained downfield of 6, even at neutral pH. Cooling resulted in a poorer signal resolution but these changes were clearly minor.

2.6.2.5. Control Compounds Summary

The variable temperature NMR experiments with the four control compounds support the hypothesis that the substantial broadening and splitting of certain signals observed in the ^{1}H NMR spectra of **2.10** are indicative of non-covalent interactions between the primary amine tether and benzocrown units, which affect the rate of rotation about the ball-bearing axis. The control experiments show that in the absence of one of these two interactive moieties, dynamic processes are uniformly fast on the NMR timescale, even at low temperatures and if two bulky groups are present, as is the case for compound 2.11. It is clear that only in the presence of both the amine tether group and the benzocrown ethers are broadened spectra and slower dynamic processes observed for these cobalt complexes.

2.6.3. Reversibility

Whilst the studies conducted in sections 2.6.1 and 2.6.2 provide good evidence that the exchange dynamics in the form of ball-bearing rotation can be affected by protonation, it was important to assess whether the process could be reversed if the system were to be regarded as truly switchable, as depicted in Scheme 2.25.

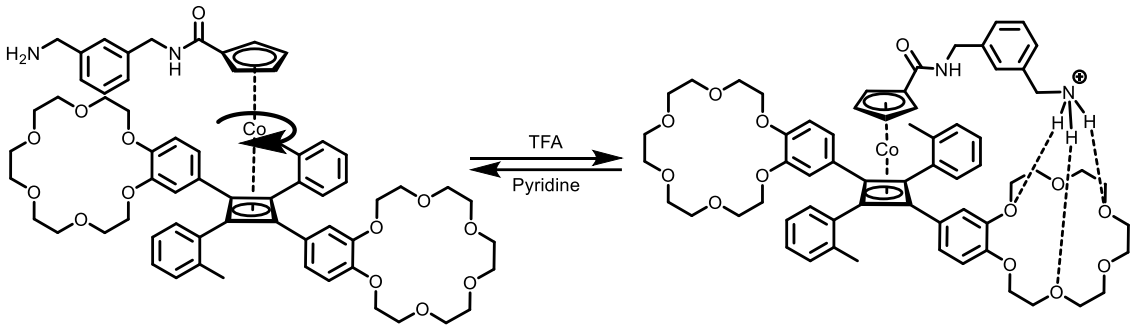

Scheme 2.25: The rotary system in action: at neutral pH (left) there is free rotation about the ball-bearing axis. Addition of TFA moves the system to a low pH and a state of slower exchange on the NMR timescale (right). Treatment with pyridine neutralises the system, switching it back to the free rotation state (left).

Therefore, following the completion of the variable temperature NMR studies on **2.10** at low pH, the sample was neutralised by adding 1.5 molar equivalents of deuterated pyridine. Following a ten-minute equilibration time, ^{1}H NMR spectra were recorded at 238 K and 298 K and compared to previous neutral and acidic pH spectra at the corresponding temperature, as shown in Figure 2.26. The change in appearance of signals 8, 9 and 10, which were split at low pH but coalesced and returned to a single signal following neutralisation, indicated that the system can transition back and forth between states of faster and slower exchange upon application of the appropriate chemical input, as the design intended.

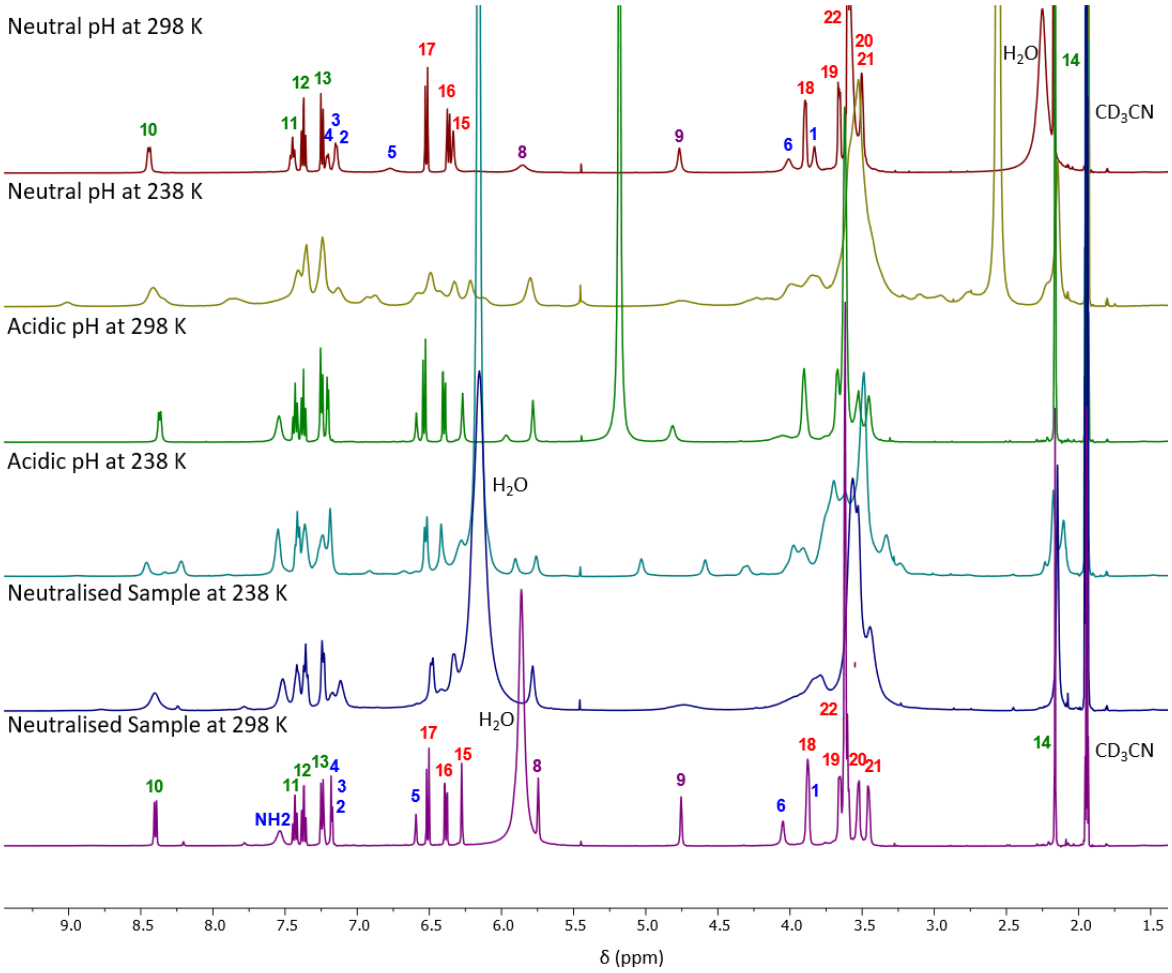

*Figure 2.26: Overlaid VT ^{1}H NMR spectra of rotary system **2.10** in deuterated acetonitrile under various conditions: neutral pH at 298 K (top) and 238 K (second from top), low pH following addition of 1.2 equiv. of TFA at 298 K (third from top) and 238 K (fourth from top), and finally returned to neutral pH following addition of 1.5 equiv. of pyridine at 238 k (second bottom) and 298 K (bottom). Concentration of **2.10** is 14.66 x 10^{-3} mol dm^{-3}.*

The spectrum of the neutralised sample at 298 K bears closer resemblance to the one recorded in deuterated methanol rather than acetonitrile, with all peaks exhibiting greater resolution and sharpness, Figure 2.27. TFA is a protic solvent, capable of acting as a hydrogen bond donor whilst pyridine acts as a hydrogen bond acceptor. The presence of these two species in the NMR solution leads to solvent effects that enhance the appearance of the spectrum, as previously discussed in section 2.5.2.

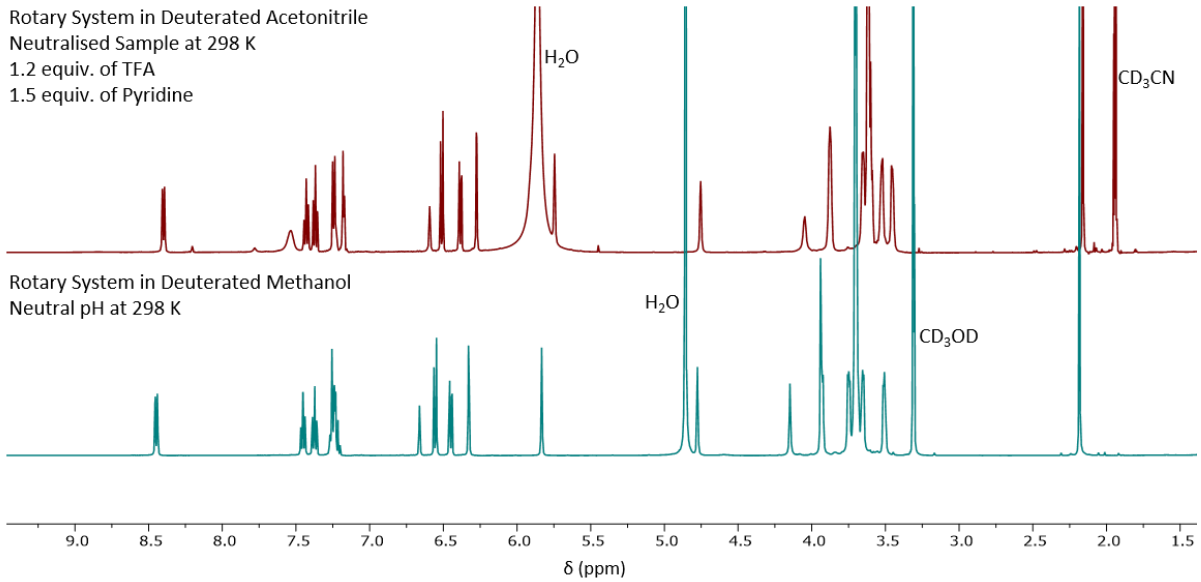

*Figure 2.27: Overlaid ^{1}H NMR spectra of rotary system **2.10** in deuterated acetonitrile following neutralisation compared with the system in deuterated methanol at neutral pH. Solvent effects due to pyridine and TFA leads to signals in the neutralised sample adopting a sharper, well resolved appearance previously unseen in acetonitrile.*

2.6.4. Calculation of Activation Parameters

After the initial studies gave an indication of the temperature of coalescence (T_c) of certain signals, further VT NMR experiments enabled the accurate determination of T_c and the subsequent calculation of activation parameters using Equations 2.1 and 2.2, page 48. Comparison of the values calculated for each signal informed whether the changes in appearance were associated with the same exchange process or were independent.

A fresh sample of rotary system **2.10** in deuterated acetonitrile in the presence of deuterated trifluoroacetic acid (TFA) was cooled from 298 K to 238 K with NMR spectra recorded at ten-degree intervals and additional measurements taken around the point of coalescence for the signals corresponding to protons 9 and 10. Partial NMR spectra showing the changes

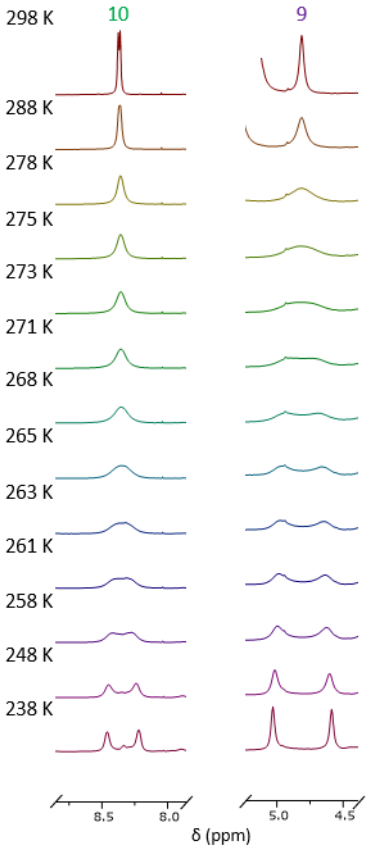

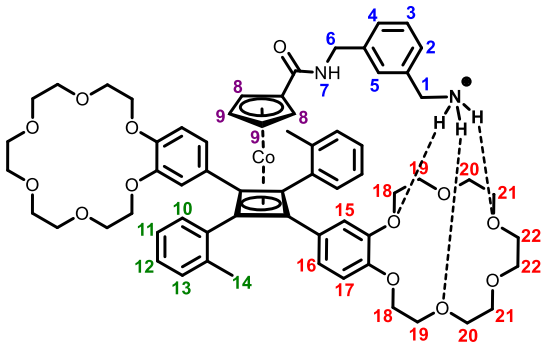

*Figure 2.28: (Right) The suspected conformation adopted by rotary system **2.10** at low pH. Proton environments are numbered. (Left) Overlaid partial VT ^{1}H NMR spectra of the rotary system **2.10** in in deuterated acetonitrile at acidic pH, mapping the coalescence of signals 9 and 10. The concentration of **2.10** is 14.7 x 10^{-3} mol dm^{-3}. 1.2 equiv. of TFA was added.*

observed for these two signals are presented in Figure 2.28. A signal assigned to Cp ring protons 8, that was also found to change under these conditions, was unfortunately masked by a peak for residual water present in the sample.

The signal for Cp ring environment 9 was found to broaden significantly upon cooling by twenty degrees, with two resonances clearly observed at 268 K, which were almost fully sharpened by 238 K. The studies indicated that the temperature of coalescence (T_c) for this signal was 273 K (± 2 K), with the peak just splitting into two by 271 K. The signal for the *ortho*-tolyl protons 10 meanwhile had a temperature of coalescence of 263 K (± 2 K). The NMR spectrum recorded at 238 K was used to determine the frequency of separation, $\Delta\nu$, of each signal under slow exchange conditions, Table 2.1. As the signal for protons 10 broadened at a lower temperature, the two resonances had not fully sharpened by 238 K and so the value of $\Delta\nu$ calculated is likely to be slightly lower than the actual value.

The rate constant, k_{ex}, for the environmental exchange at the coalescence temperature and the free energy of activation, $\Delta G^{\ddagger}$, for this process were calculated according to Equation 2.1 and Equation 2.2, respectively and are displayed in Table 2.1.

Table 2.1: The calculated kinetic parameters for signals 9 and 10 of rotary system ***2.10****. Temperature of coalescence determined from the VT NMR spectra displayed in Figure 2.28. The NMR sample had a concentration of 14.7 x 10^{-3} mol dm^{-3} in deuterated acetonitrile with 1.2 equiv. of TFA. NMR experiments performed using a 500 MHz spectrometer.*

Signal	T_c / K	$\Delta\nu$ / *Hz*	k_{ex} / s^{-1}	$\Delta G^{\ddagger}$ / kJ mol^{-1}
10	263 ± 2	120	266.6	52.0 ± 0.4
9	273 ± 2	220	488.7	52.7 ± 0.4

Whereas the different rate constants at coalescence reflect the different Δν values, it is interesting to note that the $\Delta G^{\ddagger}$ values for 9 and 10 are approximately the same (i.e. within error of one another), with values of 52.7 ± 0.4 kJ mol^{-1} and 52.0 ± 0.4 kJ mol^{-1}, respectively (note that the significance of these values is discussed further in Section 2.7). This suggests that the exchange process responsible for the observed effects is the same, even though the protons are located in different parts of the molecule. This finding is consistent with rotation about the ball bearing axis of the metallocene core of **2.10** being the primary cause of the peak broadening: slow interconversion on the NMR timescale of the protonated tether between the identical two benzocrown binding sites would make the two protons assigned to each of positions 8 and 9 non-equivalent, as illustrated in Figure 2.29.

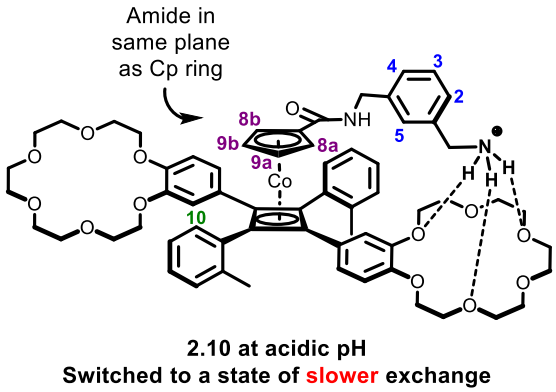

Figure 2.29: The conformation adopted by 2.10 at acidic pH is thought to have the amide unit in the same plane as the cp ring, making the cp protons non-equivalent.

As already noted, the unprotonated form of **2.10** also gave broadened spectra upon cooling but with changes that were slightly different and less marked than for the protonated form. This can be conveniently illustrated by comparing the changes observed for the signals for proton position 9 under acidic and neutral conditions, as displayed in Figure 2.30.

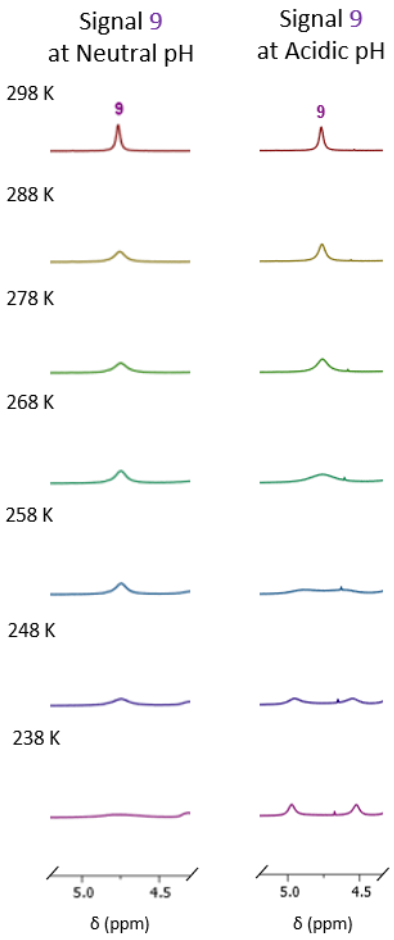

*Figure 2.30: Overlaid partial VT ^{1}H NMR spectra of **2.10** signal 9 in acetonitrile at neutral pH (left) and acidic pH (right). Concentration = 9.38 x 10^{-3} mol dm^{-3}.*

Upon cooling to 238 K at acidic pH signal 9 split into two peaks, whilst at neutral pH it only broadened, indicating that a lower temperature must be reached to observe coalescence. As the neutral form exhibited broadening it is likely that the amine tether, although not protonated, still H-bonded with the benzocrown units. However, this is a weaker interaction than at acidic pH as fewer H-bonds can be formed and it is not charged. It should be noted that it is assumed that the ppm values for slow exchange at neutral pH are the same as they are for the acidic ppm values.

2.6.5. Probing the Nature of the Non-covalent Interactions

A further challenge was to gauge whether the non-covalent interactions responsible for slowing the rotation rates were exclusively intramolecular, or whether there were also some intermolecular interactions between neighbouring molecules in solution. An experiment was designed to probe the nature of the interactions using the temperature of coalescence. The NMR sample of **2.10** used to determine T_c was almost double the concentration of the sample used in the initial VT studies in section 2.6.1. The rationale followed that if the broadening and splitting of peaks occurred at a similar temperature, their origin would be intramolecular interactions. If intermolecular, the increased concentration would lead to the occurrence of coalescence at a higher temperature than before.

Tracking the progress of the signals corresponding to proton environments signals 8, 9 and 10 allowed for a clear assessment of the rate of broadening and splitting in the higher and lower concentration samples. Partial NMR spectra showing the changes observed for these three signals are presented in Figure 2.31 below. Whilst the initial data collected at the lower concentration narrowly missed the exact point of coalescence for peaks 9 and 10, comparisons can be drawn with the spectra for the concentrated sample to determine the progress of the splitting process.

At the lower concentration, signal 9 was significantly broadened and close to coalescence at 268 K, before splitting into two by 258 K. Coalescence occurred at 273 K (± 2 K) in the higher concentration sample, several degrees higher. The extent of the splitting of 9 observed at 258 K in the lower concentration sample is comparable to that displayed between 268 K and 265 K at higher concentration, indicating some dependence on concentration.

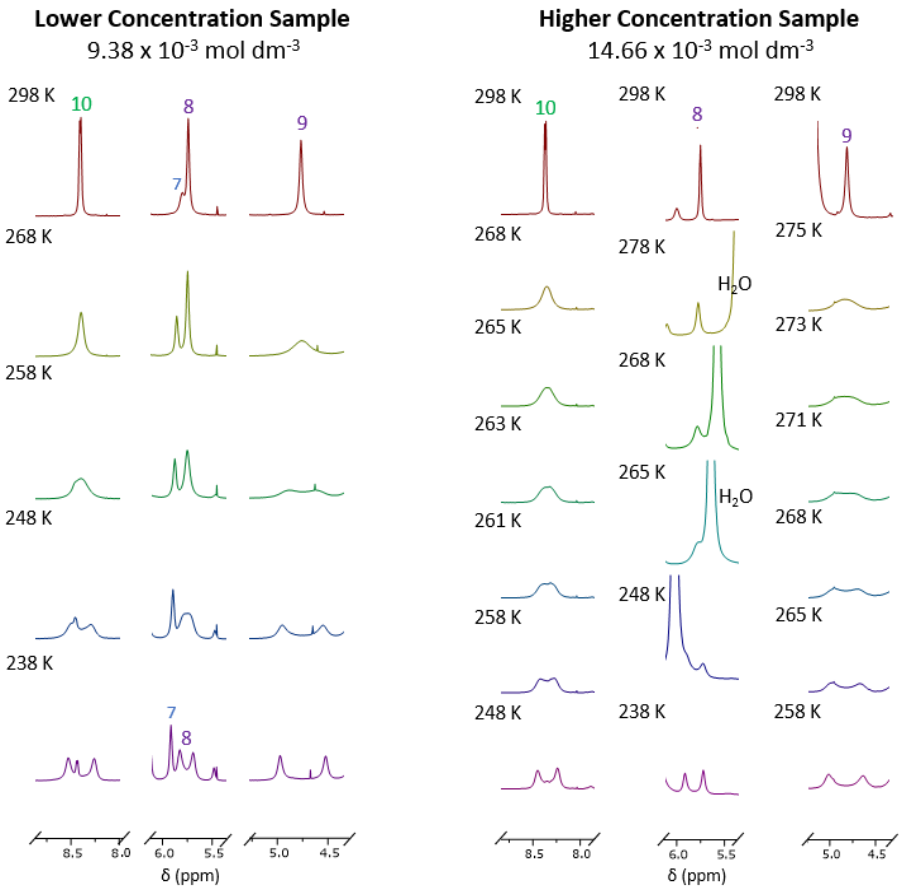

*Figure 2.31: Overlaid partial VT ^{1}H NMR spectra of **2.10** at acidic pH showing signals 8, 9 and 10 for the lower concentration sample (left) and the higher concentration sample (right).*

Signal 10 coalesced at 263 K (± 2 K) in the concentrated sample whilst the same point was reached at approximately 258 K at the lower concentration. The difference of five degrees is comparable to the approximate four-degree instrumental error present when comparing temperature readings. The extent of the splitting of 10 at 248 K in the NMR spectra of the higher concentration sample appears greater than at the same temperature at the lower concentration. However, it is possible that this may also fall within error.

Although the residual water peak limits the tracking of 8 in the NMR spectra of the higher concentration sample, conclusions can still be drawn. The lower concentration NMR experiment at 248 K captured the coalescence of 8. Whilst the signal in the equivalent experiment at the higher concentration was masked by the water peak, it is apparent that

signal 8 had already split by 248 K. The extent of splitting at 238 K was greater at higher concentration, but the difference was marginal and possibly only 3 or 4 degrees apart.

Overall, the study showed that increasing the concentration of **2.10** led to coalescence at a higher temperature. However, in several instances the difference in temperature were not far outside of the instrumental error range of the temperature reading. An improvement to this experiment would be to use samples with concentrations that differ by orders of magnitude, notwithstanding that very dilute samples would give weak signals and highly concentrated samples might lead to precipitation. It is also worth noting the aggregations observed when dissolving **2.10** in certain NMR solvents, discussed in section 2.5.2. Whilst not definitive, it is reasonable to conclude that there is an intermolecular element to the non-covalent interactions between the amine tether and crown ethers, working in tandem with intramolecular interactions to slow the rotation about the ball-bearing axis.

2.7. Exploring Alkali Metal Cations as a Switch

With the metal binding capabilities of crown ethers already detailed in this thesis, it would have been odd not to have explored the impact on this rotary system of adding a inorganic cation. As 18-crown-6 ethers feature in infrastructure of the rotary system, the most appropriate alkali metal cation to study was potassium due to its size being the optimum fit for the crown's cavity.

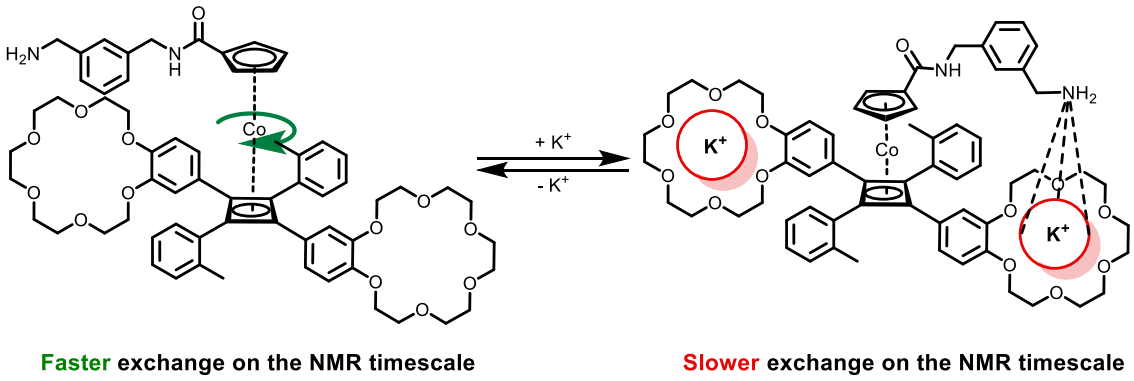

Scheme 2.26: Addition of a potassium cation to the rotary system will result in a reduced rate of rotation about the ball-bearing axis.

The addition of an excess amount of potassium to the system would result in it being bound by both crown ethers. In this situation, it was expected that the molecular dynamics of the system would be affected, for example as a result of a binding interaction from the tether in its neutral form action, as depicted in Scheme 2.26.

2.7.1. Potassium Titrations

Potassium hexafluorophosphate was deemed a suitable salt for acetonitrile and, by titrating aliquots of the salt into an NMR sample of control compound **2.11**, it was determined that two equivalents of salt could saturate the crown ether units at a host concentration of 6 mM. The complexation was monitored by tracking the small changes in appearance of the signals for the -CH_2O- protons of the benzocrown 18-22 in the overlaid NMR spectra of Figure 2.32.

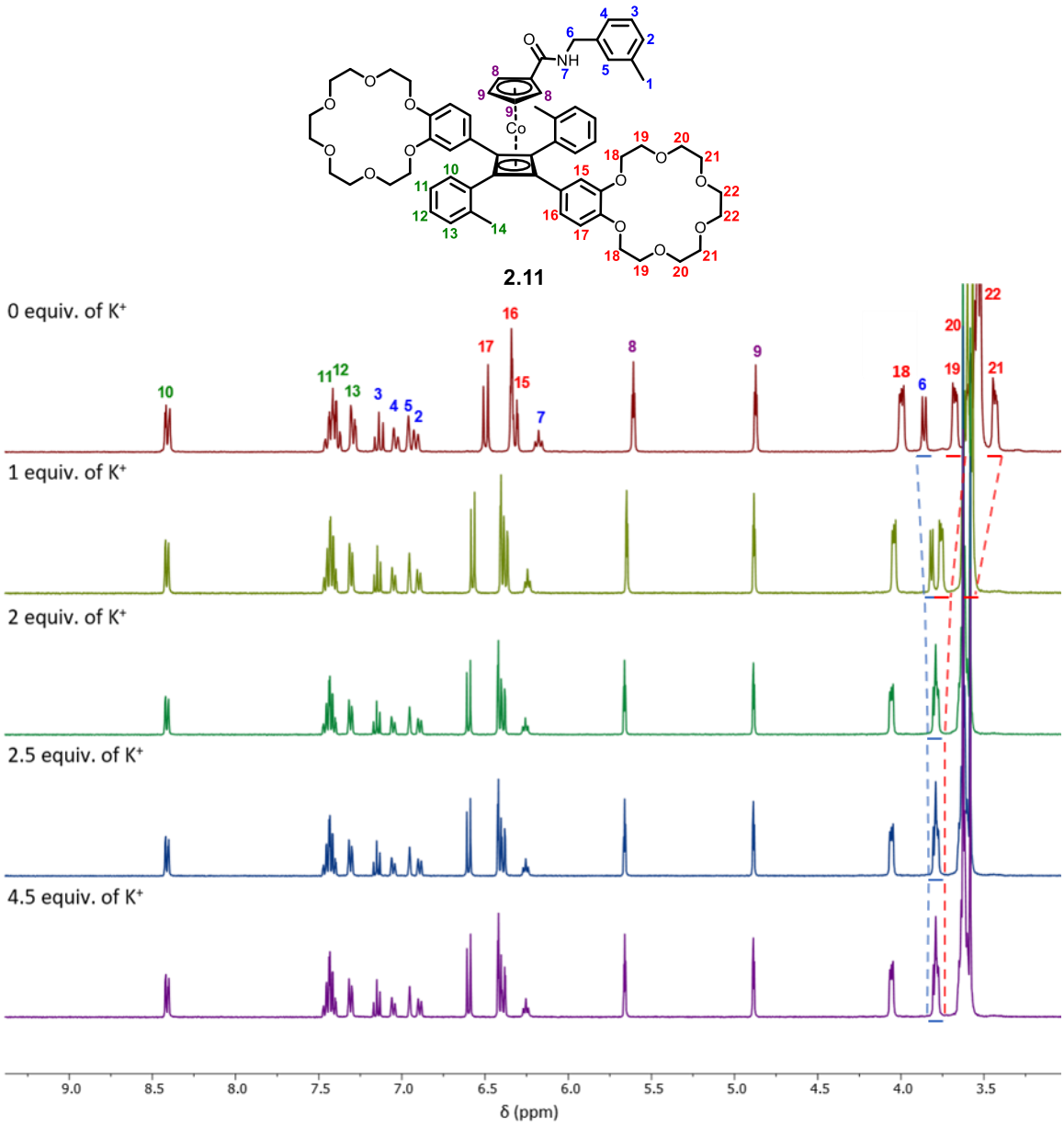

*Figure 2.32: (Top) Control compound 2.11 with proton environments numbered. (Bottom) Overlaid partial ^{1}H NMR spectra of control compound **2.11** in deuterated acetonitrile with increasing amounts of KPF_6 being added to the NMR sample. Spectra recorded at RT. Concentration of **2.11** is 6.08 x 10^{-3} mol dm^{-3}.*

The addition of 2.5 molar equivalents of the salt to rotary system **2.10** containing the amine tether resulted in fairly similar changes to crown ether proton signals, alongside some changes to signals representing environments in the amine arm. Figure 2.33 compares the NMR spectra of **2.10** at room temperature before and after the addition of potassium. Alongside the aforementioned changes to the signals for the -CH_2O- protons, 18-22, the signals representing the aromatic protons of the benzocrown units 15 and 17 broadened,

changes that were not seen in the spectra of **2.11**. Signals 1 and 6 were also significantly broadened and shifted, changes which suggested that the amine arm was interacting with the cation, which was affecting the rotary dynamics of the system in the desired way (Scheme 2.26). Environments 15 and 17 neighbour the crown ether macrocycle and feel the effects of their proximity to the crown-potassium complex and any binding event with the amine tether.

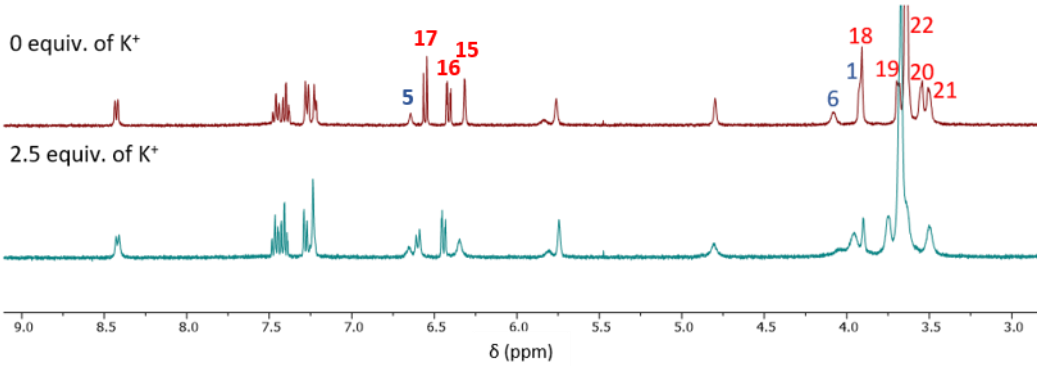

*Figure 2.33: Overlaid ^{1}H NMR spectra of rotary system **2.10** in deuterated acetonitrile before and after the addition of 2.5 equiv. of KPF_6 at ambient temperature. Concentration of **2.10** is 6.60 x 10^{-3} mol dm^{-3}.*

2.7.2. Variable Temperature NMR Studies

2.7.2.1. Rotary System 2.10

In order to probe the system further, it was decided to carry out some VT studies in the presence of potassium. Compound **2.10** was dissolved in deuterated acetonitrile and 2.5 molar equivalents of potassium hexafluorophosphate were added to saturate the benzocrown ether cavities. The sample was then cooled from 298 K to 238 K in ten-degree stages, with measurements at additional temperatures to determine coalescence temperatures of signals 8, 9 and 10, Figure 2.34.

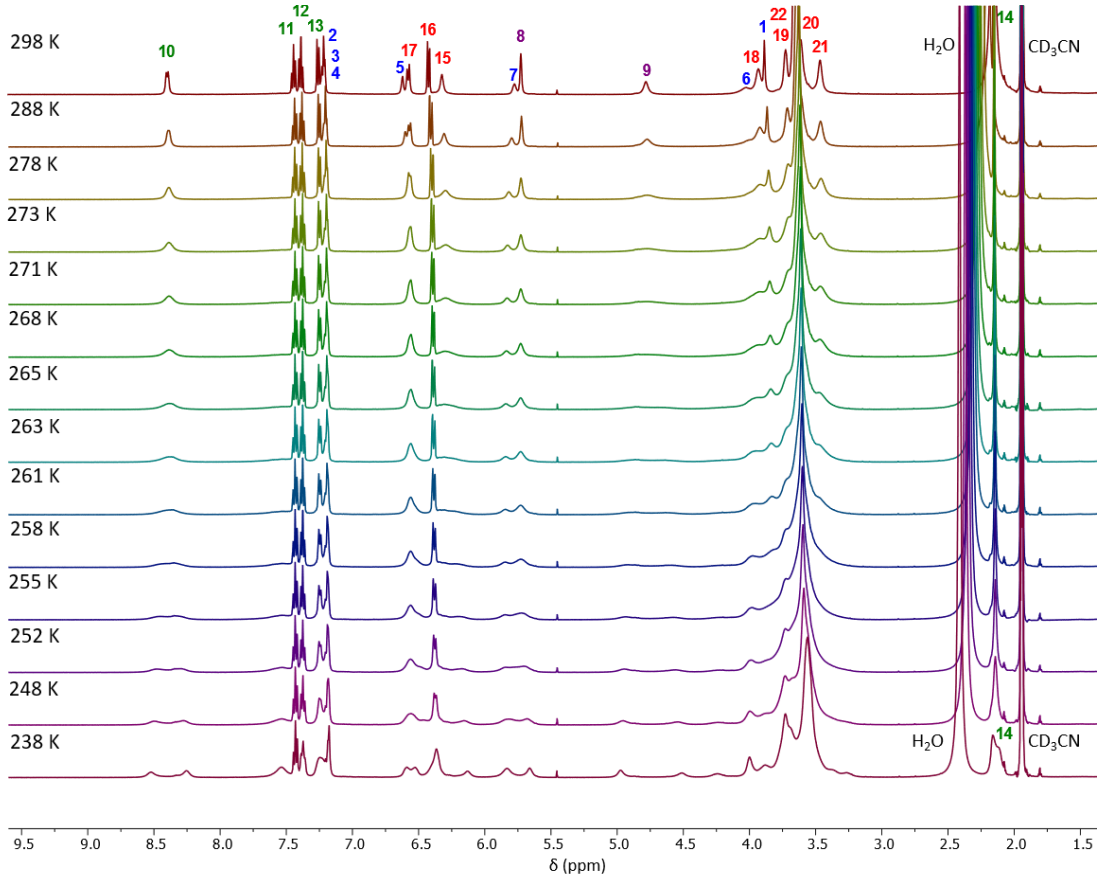

*Figure 2.34: Overlaid VT ^{1}H NMR spectra of rotary system **2.10** in deuterated acetonitrile with 2.5 equiv. of KPF_6. Concentration of **2.10** is 6.60 x 10^{-3} mol dm^{-3}.*

Cooling the system led to broadening of the same signals (8, 9 and 10) that were affected previously when pH changes were employed as the switch. This is to be expected in that

although the external chemical stimulus has changed, according to Scheme 2.26, the rotation about the ball-bearing axis would be affected in the same way. These changes provide good evidence that the addition of potassium has indeed affected the rotary motion about the ball-bearing axis and the system is under slow exchange conditions, as anticipated.

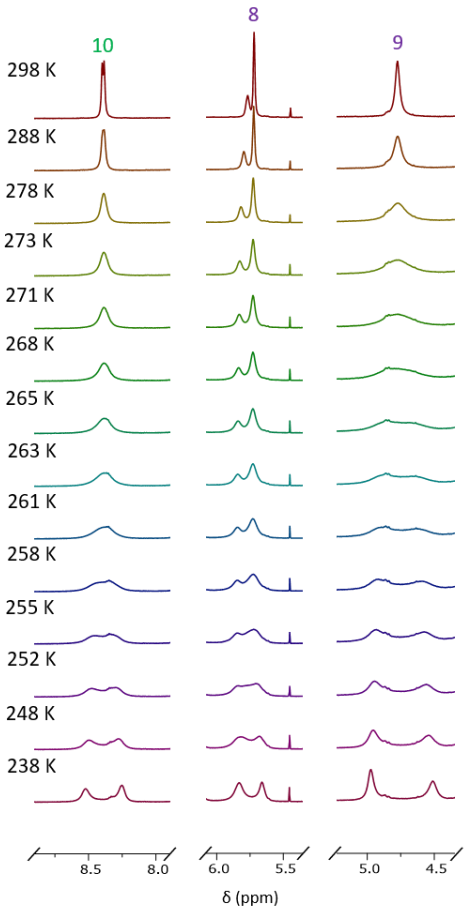

*Figure 2.35: Overlaid partial VT ^{1}H NMR spectra of rotary system **2.10** in deuterated acetonitrile with 2.5 equiv. of KPF_6 added, focusing on signals 8, 9 and 10. Concentration of **2.10** is 6.60 x 10^{-3} mol dm^{-3}.*

As previously observed, three signals corresponding to proton environments display fluxional behaviour: the cyclopentadiene ring protons 8 and 9, and the aromatic *ortho*-tolyl proton 10. As seen in Figure 2.35, signal 9 was the first to split, with a coalescence temperature of 268 K (± 2 K), whilst signal 10 coalesced at 261 K (± 2 K). Although the signal for protons 8 was easier to follow for the potassium system compared to the TFA system, tracking 8 was still complicated by the presence of an overlapping signal for the amide proton 7. However, the

signal was adjudged to have split between 255 K and 252 K, with the two resonances continuing to widen and sharpen down to 238 K. Signal 8 in particular had not fully separated by 238 K and, whilst not possible with the experimental set up, would ideally have been cooled further to reach the lower limit of exchange.

*Table 2.2: Temperature of coalescence T_c, the rate constant, k_{ex}, for the exchange at coalescence T_c and the free energy of activation $\Delta G^{\ddagger}$ for the rotary system **2.10** in the presence of TFA (1.2 equiv.) or KPF_6 (2.5 equiv.) in deuterated acetonitrile. *values for signal 8 have greater error values due to the difficulties in determining its T_c.*

Switch: *Sample Conc.:*	TFA 14.7×10^{-3}mol dm^{-3}			KPF_6 6.60×10^{-3}mol dm^{-3}		
Signal:	T_c / K	k_{ex} / s^{-1}	$\Delta G^{\ddagger}$ / kJ mol^{-1}	T_c / K	k_{ex} / s^{-1}	$\Delta G^{\ddagger}$ / kJ mol^{-1}
10	263 ± 2	266.6	52.0 ± 0.4	261 ± 2	311.0	51.2 ± 0.4
9	273 ± 2	488.7	52.7 ± 0.4	268 ± 2	510.9	51.6 ± 0.4
8*	-	-	-	253 ± 3	199.9	50.5 ± 0.6

The data presented in Table 2.2 lists the coalescence temperatures, the exchange rate constants and the free energies of activation for the protons 8, 9 and 10 in receptor system **2.10** in the presence of either potassium or TFA. The similarity of the $\Delta G^{\ddagger}$ values in the presence of potassium for three different sets of protons is again consistent with the hypothesis that it is rotation about the ball-bearing axis that is being slowed down by complexation.

It is interesting to note that the $\Delta G^{\ddagger}$ values for the two different inputs, TFA or KPF_6, are similar. This complements the hypothesis that both inputs lead to a complexation event that clamps the upper and lower components of the sandwich compound together and consequently reduces the rate of rotation about the metallocene axis. In each case, a

dissociative hydrogen bond-breaking step would be required to allow rotation and subsequent binding at the second benzocrown. It would certainly be in keeping with the design of the system that the energy barrier to rotation would approximate to the strength of the supramolecular interactions that clamp the upper and lower components together. Here the similar values suggest that these two interactions are of a comparable strength and in this respect it is interesting to note that Δ*H* values recorded for an ammonium ion binding to a crown ether in organic solvents that include acetonitrile are also of the order of 40 to 50 kJ mol^{-1}.[60, 61]

2.7.2.2. Control Compound 2.11

Control compound **2.11**, which possesses the benzocrown ether units but not the amine tether, was cooled to 238 K in the presence of excess potassium hexafluorophosphate. These

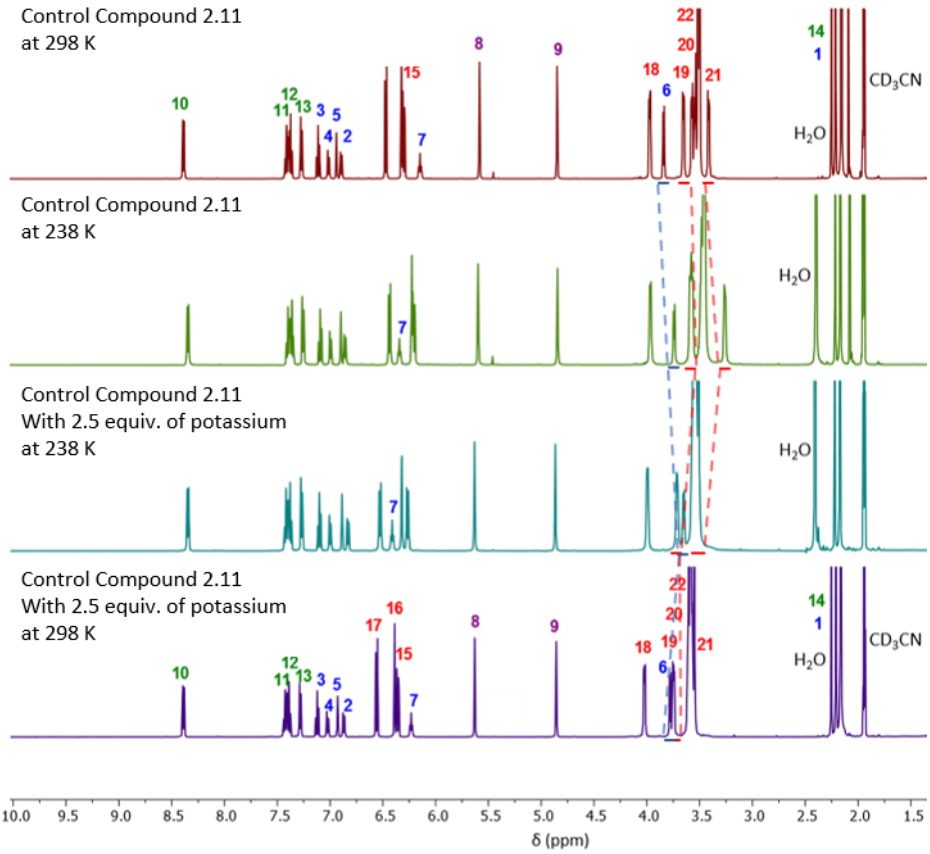

*Figure 2.36: Overlaid VT ^{1}H NMR spectra of control compound **2.11** in deuterated acetonitrile before and after the addition of 2.5 equiv. of KPF_6. Concentration of **2.10** is 2.97 x 10^{-3} mol dm^{-3}.*

signals experienced slight changes upon cooling to 238 K, as shown in Figure 2.36. The other signals affected included amide 7 which exhibited its familiar downfield shift upon cooling, and signal 6 which experienced minor shifts in position. However overall, no broadening was observed, again supporting the premise that the phenomena observed in the spectra of **2.10** are due to the rate of rotation about the ball-bearing axis being significantly slowed by complexation.

2.7.3. Reversibility Studies

The system was successfully returned to a state of free rotation, albeit through a rather long-winded method that drew on the previous work using pH as a switch, outlined below in Scheme 2.27.

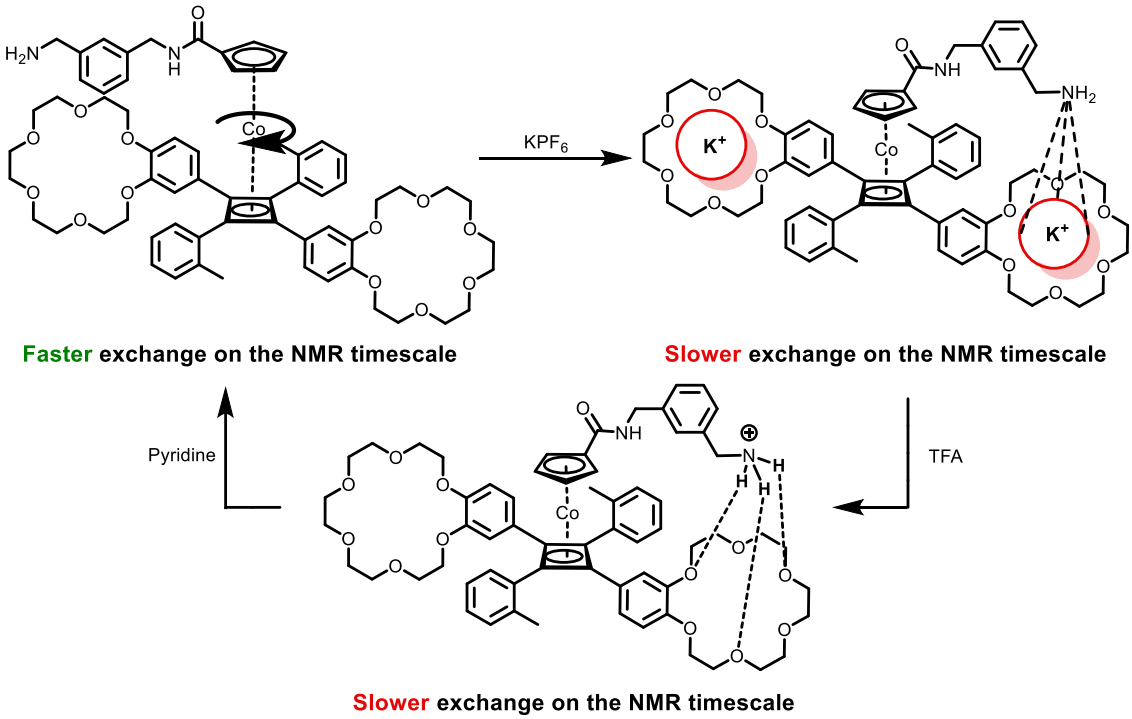

Scheme 2.27: The reversibility pathway for the rotary system.

Interestingly, the addition of 2.5 molar equivalents of TFA proved sufficient not only to protonate the amine tether but also displace the potassium cation from the cavity of the crown ethers, as evidenced by changes in the NMR spectrum in Figure 2.37. Comparing the

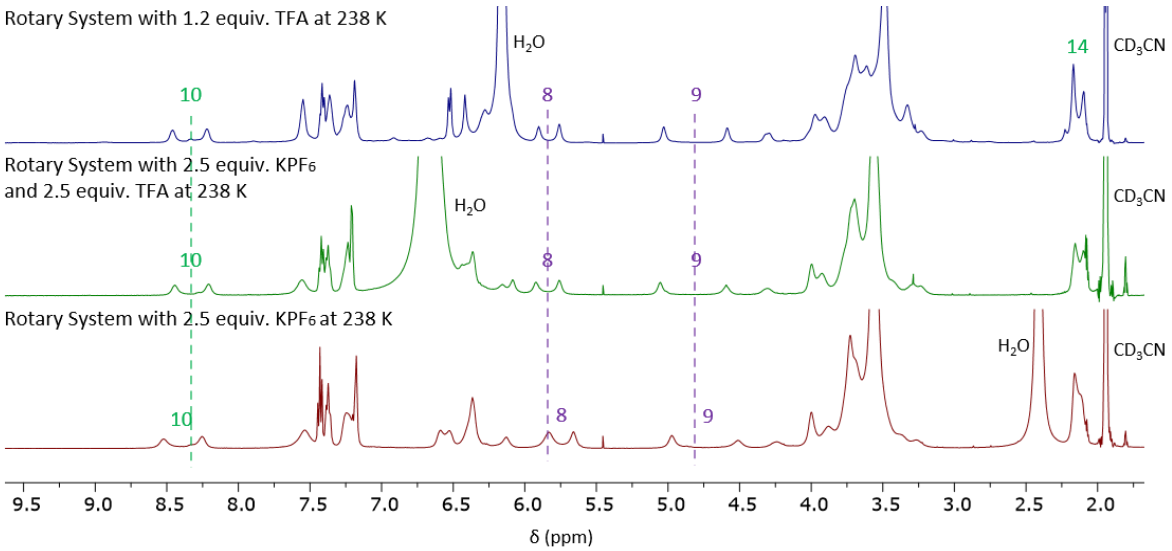

*Figure 2.37: Overlaid NMR spectra of **2.10** with 1.2 equiv. of TFA at 238 K (top), 2.5 equiv. of KPF_6 at 238 K (bottom) and 2.5 equiv of TFA and 2.5 equiv. KPF_6 238 K (middle).*

spectrum of **2.10** recorded in the presence of acid alone (top) with the corresponding spectrum with solely KPF_6 added (bottom) highlights subtle shifts in position of certain resonances including 8, 9 and 10. Comparing these to the spectrum of **2.10** with both acid and potassium salt present (middle) shows the signal positions of 8, 9 and 10 most resemble those under acidic conditions (top), which suggests that potassium is displaced upon the addition of acid. Certainly, the proximity of the metal cation to the positively charged ammonium species would be electrostatically unfavourable and disfavour binding of both guest species at the same time. Whilst the binding constants reported in the literature indicate that the complexation of a potassium cation is marginally preferred over an ammonium cation for an 18-crown-6 ether, as the ammonium species in this instance is covalently attached to the crown ether, its complexation is thought to be entropically favoured.[61]

The partial NMR spectra presented in Figure 2.38 illustrates how the transition between complexation states can be followed by monitoring the changes in signals 9 and 10 as a

function of temperature. Addition of an excess of pyridine neutralised the sample, as before, but now with a reversion to an NMR spectrum with sharp peaks that indicated free rotation. It is possible that following neutralisation, the potassium cations were again bound by the benzocrown units, but the presence of pyridine, which could hydrogen bond to the amine tether as well as compete to coordinate the benzocrown-complexed potassium cation at the axial site, disrupts the intramolecular interactions. Consequently, faster exchange is observed on the NMR timescale.

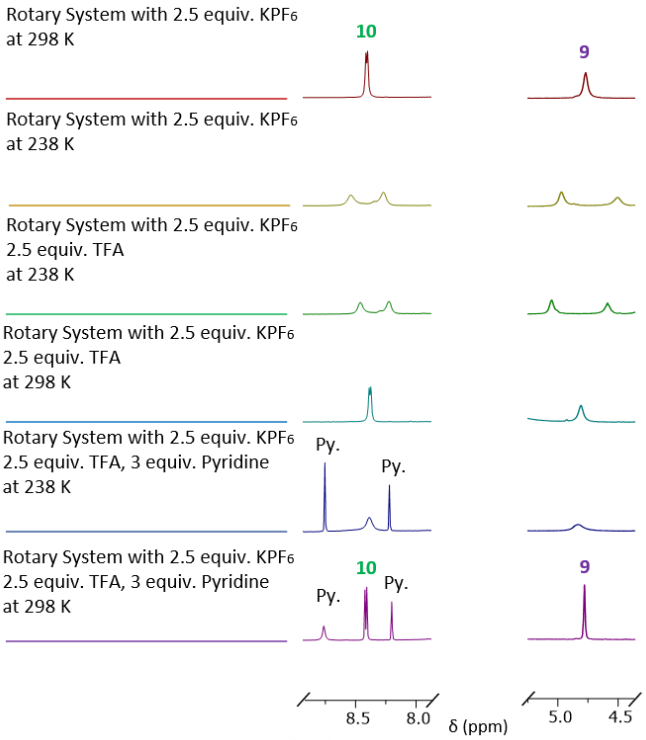

*Figure 2.38: Overlaid partial VT ^{1}H NMR spectra of **2.10** in deuterated acetonitrile under various conditions. The progress of signals 9 and 10 are highlighted, their splitting at 238 K clearly showing the switch between conditions of fast/slow exchange on the NMR timescale as the rate of rotation is varied. Concentration of **2.10** is 6.60 x 10^{-3} mol dm^{-3}.*

A final observation from these reversibility studies is that the rotary system is behaving as an OR molecular logic gate.[62] As outlined in the truth table shown in Table 2.3, it is capable of a single binary output, fast rotation about the ball-bearing axis, and this rotation is slowed by the presence of either or both inputs (acid or alkali metal cation). If neither are present, or

the sample has been neutralised, the system returns to its initial state where rotation can proceed freely. As noted in *Chapter 1*, complex logic gates, which require two inputs, are important nanotechnologies that are key building blocks in digital devices due to their ability to quickly solve complex problems.

Table 2.3: Truth table depicting the alternative and joint slowing of rotation about the ball-bearing axis by the inputs (change to an acidic pH and addition of potassium(I) cations). This behaviour by the rotary system resembles an OR logic gate.

Input		Output
H^+	K^+	*Fast Rotation*
0	0	1
1	0	0
0	1	0
1	1	0

2.8. Conclusions

A novel rotary system, comprising a cobalt sandwich complex with a pendant tether arm and two benzocrown ether units, has been synthesised and characterised. The system can respond to external chemical inputs that alter the rate of rotation about its ball-bearing axis. Variable temperature NMR experiments provide evidence for the system's switching between states of faster and slower exchange on the NMR timescale upon changes in pH and the addition of potassium ions. The calculation of kinetic parameters such as the free energy of activation, alongside VT NMR studies conducted with a library of newly synthesised control compounds, suggest that non-covalent intramolecular interactions are responsible for

changes in molecular dynamics, with guest decomplexation required for exchange between crown ether binding sites.

2.9. Future Work

This foray into controlled molecular motion has demonstrated that two separate entities of a sandwich complex, the functionalised arm of the cyclopentadiene ring and the crown ethers of the cyclobutadiene ring, can work in tandem to perform a greater task. The versatility of the components of the Cp ring could allow future generations of this system to be developed for other applications. For example, the functionalised Cp arm could exert other forms of control over the binding properties of the crowns, as Cram demonstrated by positioning a carboxylic acid arm in the proximity of a crown ether.[63]

Aside from supramolecular exchange processes, another avenue for exploration is the use of the sandwich system in asymmetric catalysis. Richards and Arthur have synthesised the (η^4-tetraarylcyclobutadiene) (η^5-cyclopentadienyl) cobalt analogues of a range of asymmetric ferrocene systems and assessing their capabilities in asymmetric catalysis, Scheme 2.28.[42, 64]

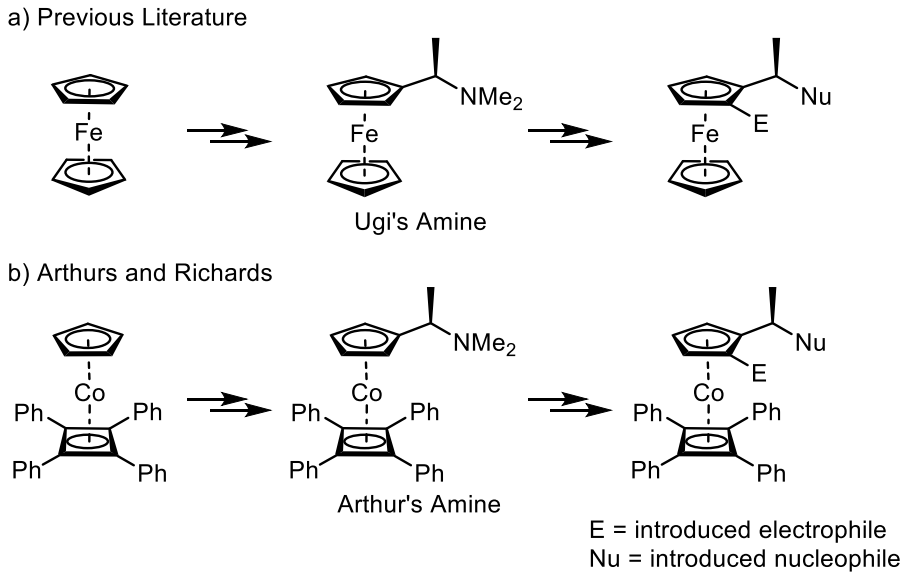

Scheme 2.28: Known (a) and recently published (b) methods for asymmetric synthesis of sandwich complexes displaying central and planar chirality.

These sandwich complexes often aid the catalytic process through utilising the directing effects of certain metals, including palladium and iridium.[42, 65] Initial, unpublished studies are promising, suggesting that catalysts possessing the cobalt sandwich complex core offer greater enantiomeric selectivities and reduced reaction times over the ferrocene equivalents.

A key intermediate in the formation of these asymmetric metallocenes is Arthur's amine, the cobalt sandwich complex analogue of Ugi's amine, from which a range of functionalities can be introduced. The chirality is implemented into the arm of the cyclopentadiene ring in the prior step through the asymmetric reduction of a ketone using a CBS catalyst. The amine is then formed in two steps *via* the installation of an acetyl group on the alcohol.[42]

It is envisaged that the benzocrown system could offer a further advance on such catalysts, utilising the crowns about the cyclobutadiene ring to bind an additional metal cation to provide additional directing effects. The *cis*-benzocrown system could allow the two crowns to work in unison to bind larger cations, whilst the design of the arm may allow for switchable binding.

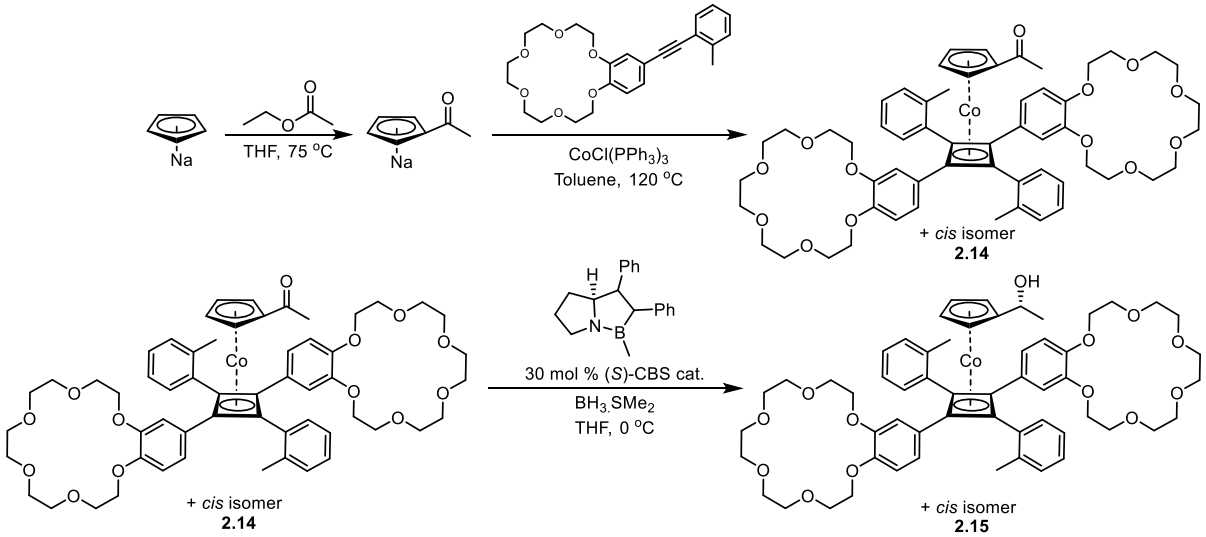

*Scheme 2.29: Synthesis and subsequent asymmetric reduction of (η^4-1,3-o-Tolyl-2,4-benzo-18-crown-6-ether-cyclobutadiene) (η^5-cyclopentadienylethanone) cobalt **2.14**.*

The viability of the synthetic pathway towards Arthur's amine was investigated with the benzocrown system through the formation of ketone **2.14** and subsequent asymmetric reduction to give **2.15**, Scheme 2.29. The successful reduction of the ketone whilst preserving the benzocrown units means the system has withstood one of the most challenging synthetic steps. This pathway now looks promising on synthetic grounds to progress to the Arthur's amine analogue and explore the benzocrown sandwich complex as a scaffold for future catalysts.

2.10. References

1. S. Erbas-Cakmak, D. A. Leigh, C. T. McTernan and A. L. Nussbaumer, *Chem. Rev.*, 2015, **115**, 10081.
2. R. P. Feynman, *Eng. Sci.*, 1960, **23**, 22.
3. K. Kinbara and T. Aida, *Chem. Rev.*, 2005, **105**, 1377.
4. V. Mermall, P. L. Post and M. S. Mooseker, *Science*, 1998, **279**, 527.
5. A. S. Spirin, *FEBS Lett.*, 2002, **514**, 2.
6. T. R. Kelly, M. C. Bowyer, K. V. Bhaskar, D. Bebbington, A. Garcia, F. Lang, M. H. Kim and M. P. Jette, *J. Am. Chem. Soc*, 1993, **116**, 3657.
7. K. Sanada, H. Ube and M. Shionoya, *J. Am. Chem. Soc*, 2016, **138**, 2945.
8. T. Muraoka, K. Kinbara and T. Aida, *Nature*, 2006, **440**, 512.
9. S. Paliwal, S. Geib and C. S. Wilcox, *J. Am. Chem. Soc*, 1994, **116**, 4497.
10. C. O. Dietrich-Buchecker, J.-P. Sauvage and J. P. Kintzinger, *Tetrahedron Lett.*, 1983, **24**, 5095.
11. R. A. Bissell, E. Cordova, A. E. Kaifer and J. F. Stoddart, *Nature*, 1994, **369**, 133.
12. N. Koumura, R. W. J. Zijlstra, R. A. van Delden, N. Harada and B. L. Feringa, *Nature*, 1999, **401**, 152.
13. T. R. Kelly, H. D. Silva and R. A. Silva, *Nature*, 1999, **401**, 150.
14. T. R. Kelly, *Acc. Chem. Res.*, 2001, **34**, 514.
15. A. S. Lane, D. A. Leigh and A. Murphy, *J. Am. Chem. Soc*, 1997, **119**, 11092.
16. D. A. Leigh, J. K. Y. Wong, F. Dehez and F. Zerbetto, *Nature*, 2003, **424**, 174.
17. V. Serreli, C.-F. Lee, E. R. Kay and D. A. Leigh, *Nature*, 2007, **445**, 523.
18. J. Berna, D. A. Leigh, M. Lubomska, S. M. Mendoza, E. M. Perez, P. Rudolf, G. Teobaldi and F. Zerbetto, *Nat. Mater.*, 2005, **4**, 704.
19. M. v. Delius, E. M. Geertsema and D. A. Leigh, *Nat. Chem.*, 2010, **2**, 96.
20. P. Yin, H. Yan, X. G. Daniell, A. J. Turberfield and J. H. Reif, *Angew. Chem. Int. Ed.*, 2004, **43**, 4906.
21. S. Kassem, A. T. L. Lee, D. A. Leigh, A. Markevicius and J. Solà, *Nat. Chem.*, 2016, **8**, 138.
22. T. J. Kealy and P. L. Pauson, *Nature*, 1951, **168**, 1039.
23. S. A. Miller, J. A. Tebboth and J. F. Tremaine, *J. Chem. Soc*, 1952, 632.
24. G. Wilkinson, M. Rosenblum, M. C. Whiting and R. B. Woodward, *J. Am. Chem. Soc*, 1952, **74**, 6148.
25. O. E. Fischer and W. Pfab, *Z. Naturforsch. B.*, 1952, **7**, 377.
26. A. E. G. Cass, G. Davis, G. D. Francis, H. A. O. Hill, W. J. Aston, I. J. Higgins, E. V. Plotkin, L. D. L. Scott and A. P. F. Turner, *Anal. Chem.* , 1984, **56**, 667.
27. P. D. Beer, H. Sikanyika, C. Blackburn, J. F. McAleer and M. G. B. Drew, *J. Chem. Soc., Dalton Tans.* , 1990, 3295.
28. P. D. Beer, A. D. Keefe, H. Sikanyika, C. Blackburn and J. F. McAleer, *J. Chem. Soc., Dalton Trans.*, 1990, 3289.
29. H. V. Nguyen, A. Sallustrau, J. Balzarini, M. R. Bedford, J. C. Eden, N. Georgousi, N. J. Hodges, J. Kedge, Y. Mehellou, C. Tselepis and J. H. R. Tucker, *J. Med. Chem.*, 2014, **57**, 5817.
30. J. L. Kedge, H. V. Nguyen, Z. Khan, L. Male, M. K. Ismail, H. V. Roberts, N. J. Hodges, S. L. Horswell, Y. Mehellou and J. H. R. Tucker, *Eur. J. Inorg. Chem.*, 2017, 466.
31. M. K. Ismail, K. A. Armstrong, S. L. Hodder, S. L. Horswell, L. Male, H. V. Nguyen, E. A. Wilkinson, N. J. Hodges and J. H. R. Tucker, *Dalton Trans.*, 2020, **49**, 1181.
32. M. K. Ismail, Z. Khan, M. Rana, S. L. Horswell, L. Male, H. V. Nguyen, A. Perotti, I. Romero-Canelón, E. A. Wilkinson, N. J. Hodges and J. H. R. Tucker, *ChemBioChem*, 2020, **21**, 1.
33. C. Biot, G. Glorian, L. A. Maciejewski and J. S. Brocard, *J. Med. Chem.*, 1997, **40**, 3715.
34. A. Haaland, *Acc. Chem. Res.*, 1979, **12**, 415.

35. J. D. Crowley, I. M. Steele and B. Bosnich, *Chem. Eur. J.*, 2006, **12**, 8935.
36. C. Li, J. C. Medina, G. E. M. Maguire, E. Abel, J. L. Atwood and G. W. Gokel, *J. Am. Chem. Soc*, 1997, **119**, 1609.
37. S. Ø. Scottwell, A. B. S. Elliott, K. J. Shaffer, A. Nafady, C. J. McAdam, K. C. Gordon and J. D. Crowley, *Chem. Commun.*, 2015, **51**, 8161.
38. S. Ø. Scottwell, J. E. Barnsley, C. J. McAdam, K. C. Gordon and J. D. Crowley, *Chem. Commun.*, 2017, **53**, 7628.
39. K. Kinbara, T. Muraoka and T. Aida, *Org. Biomol. Chem.*, 2008, **6**, 1871.
40. N. G. Connelly and W. E. Geiger, *Chem. Rev.*, 1996, **96**, 877.
41. F. X. Roca, M. Motevalli and C. J. Richards, *J. Am. Chem. Soc*, 2005, **127**, 2388.
42. R. A. Arthurs, P. N. Horton, S. J. Coles and C. J. Richards, *Chem. Eur. J.*, 2018, **24**, 4310.
43. A. M. Stevens and C. J. Richards, *Tetrahedron Lett.*, 1997, **38**, 7805.
44. X. Zheng, M. E. Mulcahy, D. Horinek, F. Galeotti, T. F. Magnera and J. Michl, *J. Am. Chem. Soc*, 2004, **126**, 4540.
45. G. Wilkinson, *Org. Synth.*, 1963, **4**, 473.
46. R. B. Woodward, M. Rosenblum and M. C. Whiting, *J. Am. Chem. Soc*, 1952, **74**, 3458.
47. G. D. Broadhead, J. M. Osgerby and P. L. Pauson, *Chem. and Ind.*, 1957, 209.
48. D. J. Cassar, E.Nagaradja, D. C. D. Butler, D. Villemin and C. J. Richards, *Org. Lett.*, 2012, **14**, 894.
49. A. M. Stevens and C. J. Richards, *Organometallics*, 1999, **18**, 1346.
50. D. H. Williams and I. Fleming, *Spectroscopic Methods In Organic Chemistry*, McGraw-Hill, 5 edn., 1998.
51. L. Giordano, C. T. Hoang, M. Shipman, J. H. R. Tucker and T. R. Walsh, *Angew. Chem. Int. Ed.*, 2011, **50**, 741.
52. M. W. Davies, M. Shipman, J. H. R. Tucker and T. R. Walsh, *J. Am. Chem. Soc*, 2006, **128**, 14260.
53. M. W. Davies, A. J. Clarke, G. J. Clarkson, M. Shipman and J. H. R. Tucker, *Chem. Commun.*, 2007, 5078.
54. A. Jutand, S. Négri and A. Principaud, *Eur. J. Inorg. Chem.*, 2005, 631.
55. Y. Wakatsuki and H. Yamazaki, *Inorg. Synth.*, 1989, **26**, 190.
56. A. Basha, M. Lipton and S. M. Weinreb, *Tetrahedron Lett.*, 1977, **48**, 4171.
57. J. Li, K. Subramaniam, D. Smith, J. X. Qiao, J. J. Li, J. Qian-Cutrone, J. F. Kadow, G. D. Vite and B.-C. Chen, *Org. Lett.*, 2012, **14**, 214.
58. K. H. Ahn, C.-W. Cho, H.-H. Baek, J. Park and S. Lee, *J. Org. Chem.*, 1996, **61**, 4937.
59. V. H. G. Rohde, P. Pommerening, H. F. T. Klare and M. Oestreich, *Organometallics*, 2014, **33**, 3618.
60. H.-J. Buschmann and E. Schollmeyer, *Supramolecular Science*, 1998, **5**, 139.
61. V. Rüdiger, H.-J. Schneider, V. P. Solovev, V. P. Kazachenko and O. A. Raevsky, *Eur. J. Org. Chem*, 1999, 1847.
62. S. Erbas-Cakmak, S. Kolemen, A. C. Sedgwick, T. Gunnlaugsson, T. D. James, J. Yoon and E. U. Akkaya, *Chem. Soc. Rev.*, 2018, **47**, 2221.
63. R. C. Helgeson, G. R. Weisman, J. L. Toner, T. L. Tarnowski, Y. Chao, J. M. Mayer and D. J. Cram, *J. Am. Chem. Soc*, 1979, **101**, 4928.
64. R. A. Arthurs, C. C. Prior, D. L. Hughes, V. S. Oganesyan and C. J. Richards, *Organometallics*, 2018, **37**, 4202.
65. R. A. Arthurs, C. C. Prior, D. L. Hughes, V. S. Oganesyan and C. J. Richards, *Organometallics*, 2018, **37**, 4204.

3. Metal-Modified Nucleic Acids

3.1. Introduction

3.1.1. Deoxyribonucleic Acid

The human genome, that extraordinary trove of information about human history, inheritance and evolution that has informed the development of medicines and the advancement of our understanding of physiology, consists of one truly remarkable molecule: deoxyribonucleic acid, more commonly referred to as DNA.[1, 2] DNA is part of a family of biopolymers called nucleic acids, which consist of repeating monomer units called nucleotides. These consist of a pentose sugar ring, an N-heterocyclic nucleobase and a phosphomonoester. The sugar is the central scaffold with the nucleobase attached to the 1' position (green) and the phosphomonoester to the 5' position (blue), as shown in Figure 3.1.

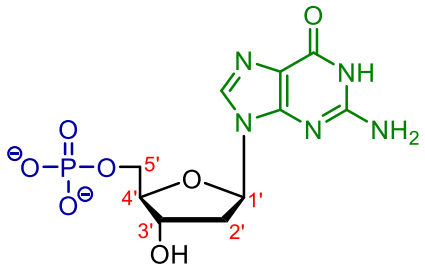

Figure 3.1: The nucleotide structure with a guanine nucleobase. The sugar in DNA is deoxyribose whereas fellow nucleic acid ribonucleic acid, RNA, has a ribose sugar, which has an additional hydroxyl unit in the 2' position. Under physiological conditions the phosphomonoester is deprotonated, giving nucleic acids their negative charge and acidity.

There are four naturally occurring nucleobases in DNA, adenine, cytosine, guanine and thymine, and they are split into two categories: the monocyclic pyrimidines and the bicyclic purines, depicted in Figure 3.2.

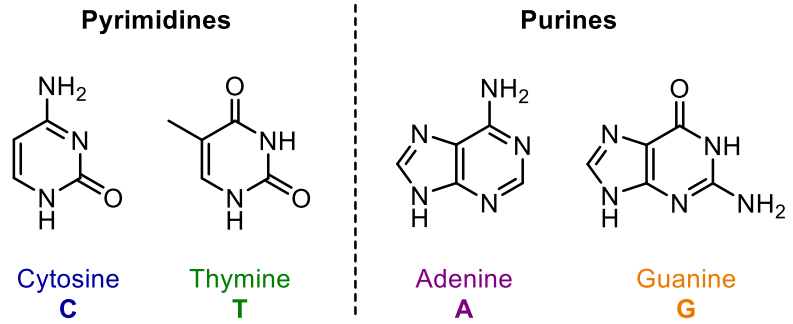

Figure 3.2: The structures of the four natural DNA nucleobases. The labelling of a nucleic acid sequence sees the first letter of each base represent the nucleobase in the sequence, hence A for adenine, C for cytosine, G for guanine and T for thymine. RNA also has four nucleobases, with pyrimidine uracil taking the place of thymine.

A condensation polymerisation links the nucleotides together *via* phosphodiester bonds to form oligonucleotides. The phosphate group in the 5' position of one nucleotide reacts with the 3' hydroxyl group of another, crafting a sugar phosphate backbone that runs along the length of the DNA strand with a specific 5' to 3' alignment, or directionality. Protruding from this scaffold are the nucleobases, allowing the strand to adopt secondary structures.

It is here that nature exhibits its true genius, demonstrating subtle design intricacies and delicate pre-programming that are unrivalled. In isolation the nucleotides and their nucleobases appear unremarkable, but when two oligonucleotides are drawn together, they adopt a helical structure that reveals the complementary nature of the nucleobases. Each nucleobase possesses a combination of hydrogen bond donor and acceptor groups which

allow it to form hydrogen bonds with its complementary base pair, Figure 3.3. Cytosine forms three hydrogen bonds with guanine whilst adenine forms two hydrogen bonds with thymine.

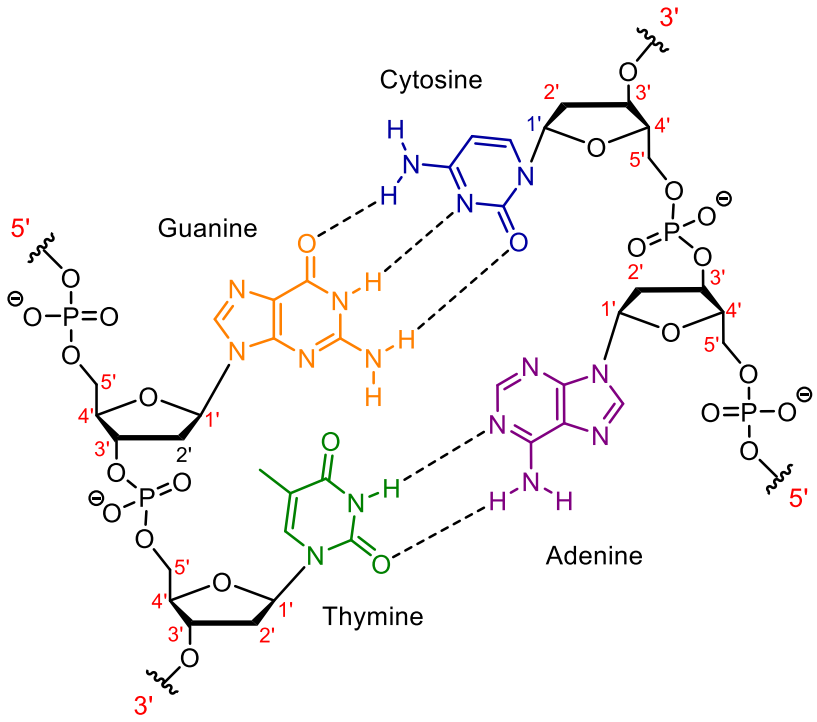

Figure 3.3: The complementary hydrogen bonding network between the nucleobases holds the duplex together. The strands are aligned antiparallel to one another, with the 3' end of one strand paired to the 5' end of the of the other. The directionality of the sugar phosphate backbone is shown.

James Watson and Francis Crick elucidated the double helix structure of DNA in 1953.[3] It is the structure that is readily adopted in biology, with two oligonucleotide strands with complementary nucleobases running antiparallel to one another and twisting into a right-handed coil. This twisted arrangement gives DNA its stability; the hydrophobic nucleobase interior is rich in π-stacking interactions whilst the more external sugar phosphate backbone is negatively charged, thus allowing the helical duplex to repel water and prevent it being hydrolysed under aqueous conditions.[4]

The double helix has been found to adopt three main conformations in aqueous solution, Figure 3.4, each with varying dimensions and arrangements. The most common form is B-DNA, the right-handed conformation adopted in the DNA of humans. It is 2 nm wide

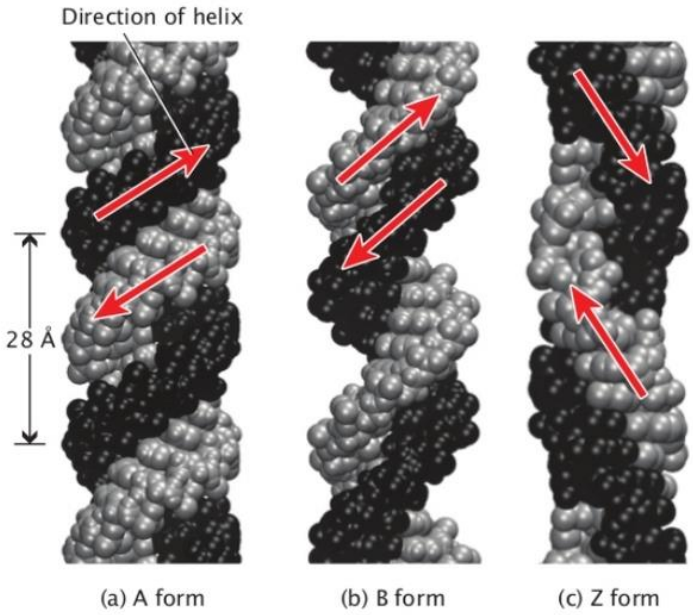

Figure 3.4: The three confirmations of the DNA double helix.[5]

throughout and has approximately 10 nucleobases per turn in the helix, with each turn measuring 34 nm long. The wider, shorter A-DNA is scarcely observed under physiological conditions whilst Z-DNA, a left-handed helix, is even rarer.[5]

3.1.2. DNA in the Human Genome

Much like the 26 letters of the alphabet are be used to communicate a large volume of information or binary code provides the foundations for computing, the 4 nucleobases of DNA communicate the instructions and foundations of life. The human genome contains over 3 billion nucleobase pairs, stored in 23 pairs of chromosomes which are found in the nucleus of cells. Within chromosomes are thousands of genes: long sections of DNA which can be split into three-letter nucleobase sets called codons, providing the instructions for tasks such as protein synthesis. These specific, linear sequences of nucleobases constitute the genetic code, Figure 3.5.

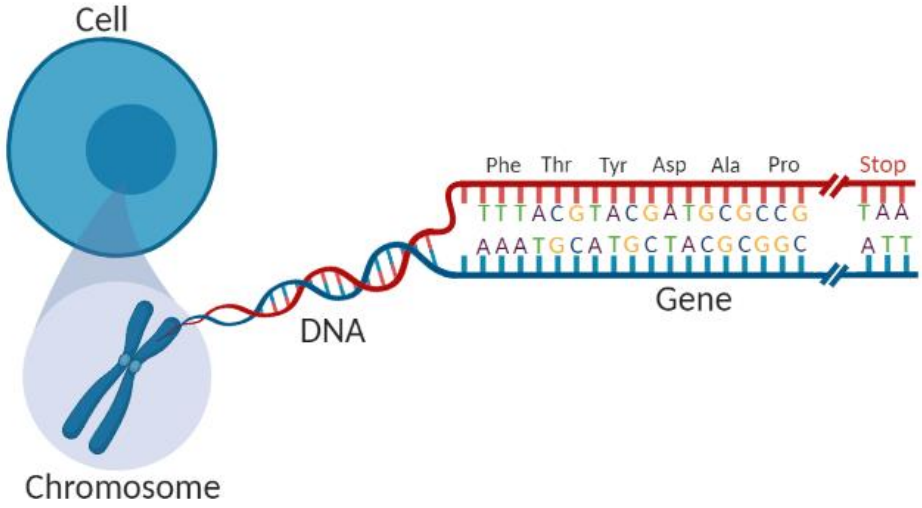

Figure 3.5: Chromosomes in the nucleus of the cell store the DNA. These sequences of nucleobases are split into genes, which in turn contain trinucleotide segments called codons, that code specific amino acids (labelled above the DNA strand) in protein synthesis. Start and stop codons help control the synthesis.

Alongside the protection of the genetic blueprint, the double helix structure of DNA allows it to effectively communicate the information it holds. One such method of dissemination is transcription, in which the double helix partially separates to allow a complementary strand of ribonucleic acid (RNA) to form against it *via* hydrogen bonds. The single-stranded DNA acts as a template, dictating the sequence of the RNA nucleobases and transmitting the genetic instructions. Gene expression governs this process. Start and stop codons regulate when and where transcription should occur whilst others inform the desired amino acid sequence. Each codon relates to a specific amino acid or stop signal, for instance the nucleobase triplet GCT corresponds to the amino acid alanine, whilst GTT is valine. The specifically synthesised complementary oligonucleotide is messenger RNA, whose function, as the name suggests, is to deliver the genetic instructions to the ribosome which subsequently uses this information to direct protein synthesis. This communication process is aptly termed translation.

The other key process is replication, the reproduction of cells. The DNA double helix is completely unravelled by the enzyme helicase, to allow the single oligonucleotide strands to

bind to free complementary nucleobases and build new strands under the direction of DNA polymerase. The result is two identical copies of the original DNA strand. This replication process allows for the cellular organism to grow.

3.1.3. Single Point Variants

Whilst the vast majority of the genetic code is consistent between humans, some variations are observed and the subtle differences give an insight into a person's ancestry.[1] These variations in nucleobase sequence can also be attributed to diseases that have a genetic element, including many cancers, and so are of great scientific and medical interest.[6] Some of these variations occur at the single base level, known a single point variants (SPV). These include single nucleotide polymorphisms (SNPs) and epigenetic changes.[7, 8]

3.1.3.1. Single Nucleotide Polymorphisms

The most common type of genetic variation is single nucleotide polymorphisms (SNPs), point variations at specific positions in the genome that see a single nucleobase in the wild type DNA replaced with one of the other three nucleobases, as in Figure 3.6. SNPs occur in >1% of the gene population and include somatic mutations, which occur in all cells except germ cells over the life-time of an individual, and germline mutations, which can be inherited from parents.[9, 10] Over 1.4 million polymorphisms have been identified in the genetic code of humans, with the majority of these occur in the regions of DNA between genes and account for the genetic diversity between any two humans, such as hair and eye colour.[1, 7] However, if the SNP occurs in DNA that resides either in protein encoding regions or regulatory regions then they can affect the DNA transcription process and the subsequent production of proteins. Whilst the initial changes to the genetic code may be small, they can catalyse a chain

of events that causes extensive genetic remodelling and protein malfunction, climaxing in the development of a variety of diseases including cancers.[1, 11, 12]

Figure 3.6: A single nucleotide polymorphism in the KRAS gene sees a guanine replaced with a thymine. SNP site is highlighted.

SNPs are therefore important biomarkers for a range of genetic diseases and recent advances in sequencing technology has allowed for many to be identified. Examples include the BRAF-V600E mutation which is associated with colorectal cancer[13] and melanoma.[14, 15] The SNP sees a thymine at position 1799 in the healthy, wild-type DNA of the BRAF gene substituted with an adenine, a nucleobase change that consequently results in the substitution of the amino acid valine with glutamic acid in the protein. The naming convention of SNPs is informative to the amino acid transformation caused by the variant; valine (V) at amino acid 600 is replaced with glutamic acid (E).[14, 16] The mutation results in the cell-signalling pathway repeatedly sending signals to the nucleus, leading to overexpression and uncontrolled cell growth.[15, 17]

The KRAS gene is the most frequently mutated in cancers, with SNPs associated with lung, colorectal and pancreatic cancers.[18, 19] Mutations in KRAS codon 12 in particular are associated with lower survival rates in patients with colorectal cancer. The associated SNPs include the KRAS G12V mutation which sees the wild-type guanine substituted with thymine,

and the KRAS G12D where the wild-type guanine changes to adenine.[18, 20] The PIK3CA mutation is another SNP associated with colorectal cancer as well as breast and ovarian cancers among others.[21]

With such a range of SNPs associated with so many cancers, identification is of vital importance. Whilst sequencing can be used to identify genetic variations or heritable diseases, the equipment is still relatively expensive and the process time-consuming as large amounts of DNA will have to sequenced to find the SNP. Cheaper, faster methods are required. The detection of SNPs can be used to identify hereditary diseases in family members before they develop, allowing them to be addressed early, increasing the odds of successful treatment. They also provide information about the illness that is specific to that patient, allowing treatment plans to be tailored from one individual to another. As a cancer develops, an increasing amount of wild-type DNA is converted to mutant DNA. Being able to quantify the ratio of healthy to mutant DNA (the allelic ratio) would inform the extent of a cancer's development, as well as how a patient is responding to treatment. Such a SNP sensor would be a valuable diagnostic tool for doctors.

3.1.3.2. Epigenetic Mutations

Unlike polymorphisms, epigenetic mutations do not involve changes to the DNA sequence; rather than the substitution, deletion or duplication of a nucleobase, more subtle alterations are observed. A common example is DNA methylation, an enzyme-driven process which adds a methyl group to the C^5 position of the cytosine nucleobase. It is a very specific event, only

occurring in regions where the cytosine has a guanine neighbour, known as CpG sites, Figure 3.7.[22]

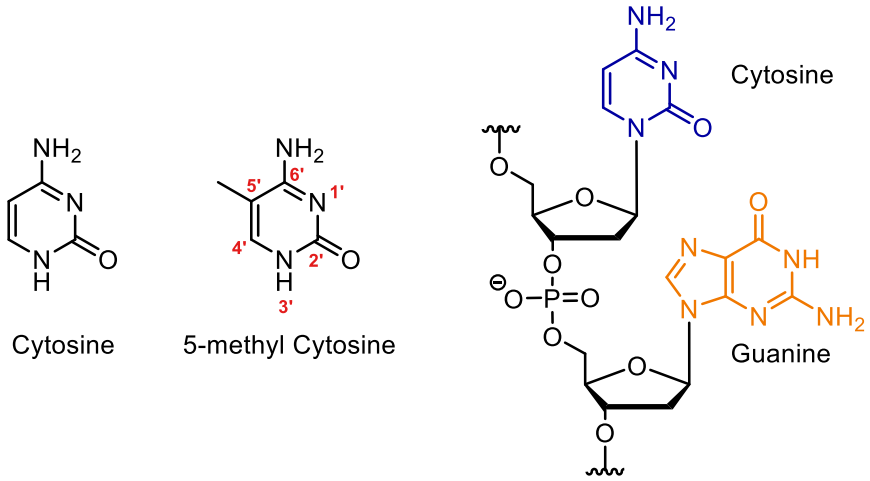

Figure 3.7: Cytosine (left) and the epigenetic mutant 5-methyl cytosine (centre). Methylation occurs at CpG sites (right) which are so named to represent the DNA sequence 5'-cytosine-phosphate-guanine-3'.

Methylation is a well-established mechanism for gene silencing, the presence of the methyl group protruding from the nucleobase preventing normal transcription from proceeding. Silencing prevents the gene from expressing and communicating effectively, which is problematic if the gene in question controls functions such as tumour suppression or cell growth, with the breakdown in cell communication resulting in the growth of cancerous tissue. Indeed, hypermethylation of the promoter regions of genes is a frequently observed feature of tumour and therapies have been developed that centre on reactivating cell expression through inhibiting methylation.[23, 24]

An interesting evolutionary response to methylation has been observed in human DNA. Evidence suggests that methylation did not occur in early genomes and that these genomes contained a spread of CpG dinucleotides that would be expected statistically. Over time, the presence of 5-methyl cytosine was increasingly observed, with isolated CpG sites proving to be particularly susceptible to methylation. 5-methyl cytosine is known to mutate to thymine

via deamination, resulting methylated CpG sites converting to TpG and depleting in the genetic code. To combat this, CpG-rich regions of DNA started to develop, known as CpG islands. These clusters appear to possess some immunity to methylation, having been conserved through human evolution. They are often situated in the promoter regions of genes, so when methylation does occur it has serious consequences.[23, 24]

3.1.4. Automated Solid-Phase DNA Synthesis

The development of automated DNA synthesis was a major milestone in nucleic acid research, enabling the chemical synthesis of tailor-made oligonucleotides with a specific nucleobase sequence and length, ranging from a handful of nucleotides long to approximately a hundred long, in relatively fast time and in high yields.[25, 26] The technique uses phosphoramidite chemistry to construct the strand one nucleobase at a time on a solid support. Controlled pore glass (CPG) is the most commonly used solid support due to its rigidity, chemical inertness and non-swellable properties. Performing DNA synthesis on a solid phase is advantageous as it allows a large excess of reagents to be employed to ensure the coupling reaction is pushed to completion. Any unreacted species and impurities can subsequently be washed from the support and removed after each coupling step. The strategic use of protecting groups and capping reagents control any unwanted branching of the oligonucleotide chain or deviations from the desired sequence, ensuring the strand is synthesised at a relatively high purity.[4]

3.1.4.1. Preparation of Nucleobase Phosphoramidites

Phosphoramidite chemistry employs specific protecting groups on the nucleoside monomer units to control the synthesis of the oligonucleotide strand. The 3' hydroxyl group of the sugar ring is phosphitylated with a phosphoramidite moiety which subsequently forms the phosphodiester of the DNA backbone when coupled to its neighbouring nucleoside. Whilst this protecting group becomes a key component in the DNA structure, the other nucleophilic sites of the nucleosides must be protected to prevent branching, degradation processes including depurination, and ensure the regiocontrol over each coupling step. Alongside the hydroxyl groups, the main nucleophilic sites are the primary amine units of the adenine, cytosine and guanine nucleobases. Acyl protecting groups are employed, as seen in Figure 3.8, with the benzoyl group routinely used to protect the adenine and cytosine amines, whilst isobutyryl is the protecting group of choice for guanine. They remain in place for the entirety of the automated synthesis process and are removed upon completion.[4, 27]

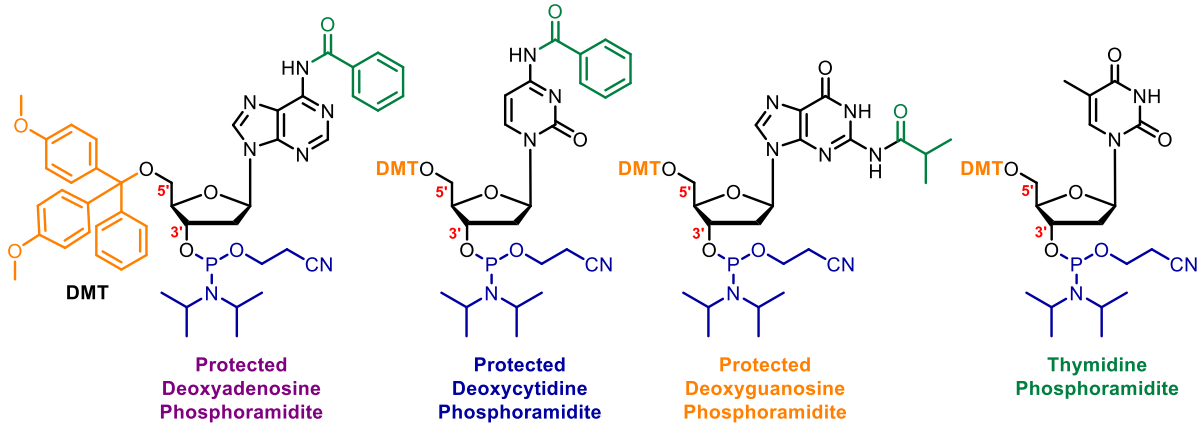

Figure 3.8: The protecting groups employed on each nucleoside include phosphoramidites on the 3' hydroxyl (blue), dimethoxytrityl (DMT) on the 5' hydroxyl (orange) and acyl groups on the primary amine units of the adenine, cytosine and guanine bases (green).

The 5' hydroxyl group of the end nucleotide of the partially constructed strand reacts with the 3' phosphoramidite unit of the latest nucleoside to couple the next monomer unit in the sequence, extending the strand. The 3' hydroxyl group is phosphitylated as the primary

hydroxyl group in the 5’ position is more nucleophilic and better suited to attack the phosphorous atom of the phosphoramidite. Consequently, the strand is built in a 3’ to 5’ direction, the opposite to natural DNA synthesis. The 5’ hydroxyl group is protected with a dimethoxytrityl (DMT) unit which is removed at the appropriate stage of the DNA synthesis cycle to ensure the correct coupling reaction occurs. The cationic DMT species that is generated in the deprotection step possesses a strong orange colour and its absorption profile is monitored to gauge the success of the coupling step. This is reported in the form of a trityl yield.[4]

The first nucleoside at the 3’ terminal of the sequence is readily attached to the CPG solid support and provides the foundation upon which the strand is built. A succinate linker takes the place of the phosphoramidite moiety on the 3’ hydroxyl group but retains the DMT group and the acyl protecting groups. The carboxylic acid of the succinyl chain reacts with the amine unit of the CPG support to form an amide linkage that is stable throughout the DNA synthesis cycle, before being cleaved post-synthetically in ammonia to afford the freshly made oligonucleotide.[27]

3.1.4.2. The DNA Synthesis Cycle

The stages of automated solid-phase DNA synthesis are depicted below in Scheme 3.1 and are repeated for the coupling of each nucleoside until the strand is completed.

Start: With the first nucleoside in the sequence loaded onto the CPG solid support, it must first be prepared for coupling with the next nucleoside in the sequence. The DMT group is removed from the 5’ hydroxyl group upon addition of trichloroacetic acid (TCA) in DCM. DMT

is the only protecting group used that is sensitive to mildly acidic conditions, allowing it to be selectively removed in this step whilst keeping the other protecting groups in place.

Step 1: The phosphoramidite of the second nucleoside in the sequence is then added in a 0.1 M acetonitrile solution, activated with tetrazole in acetonitrile, and subsequently coupled to the first nucleoside on the CPG support, forming a phosphite triester.

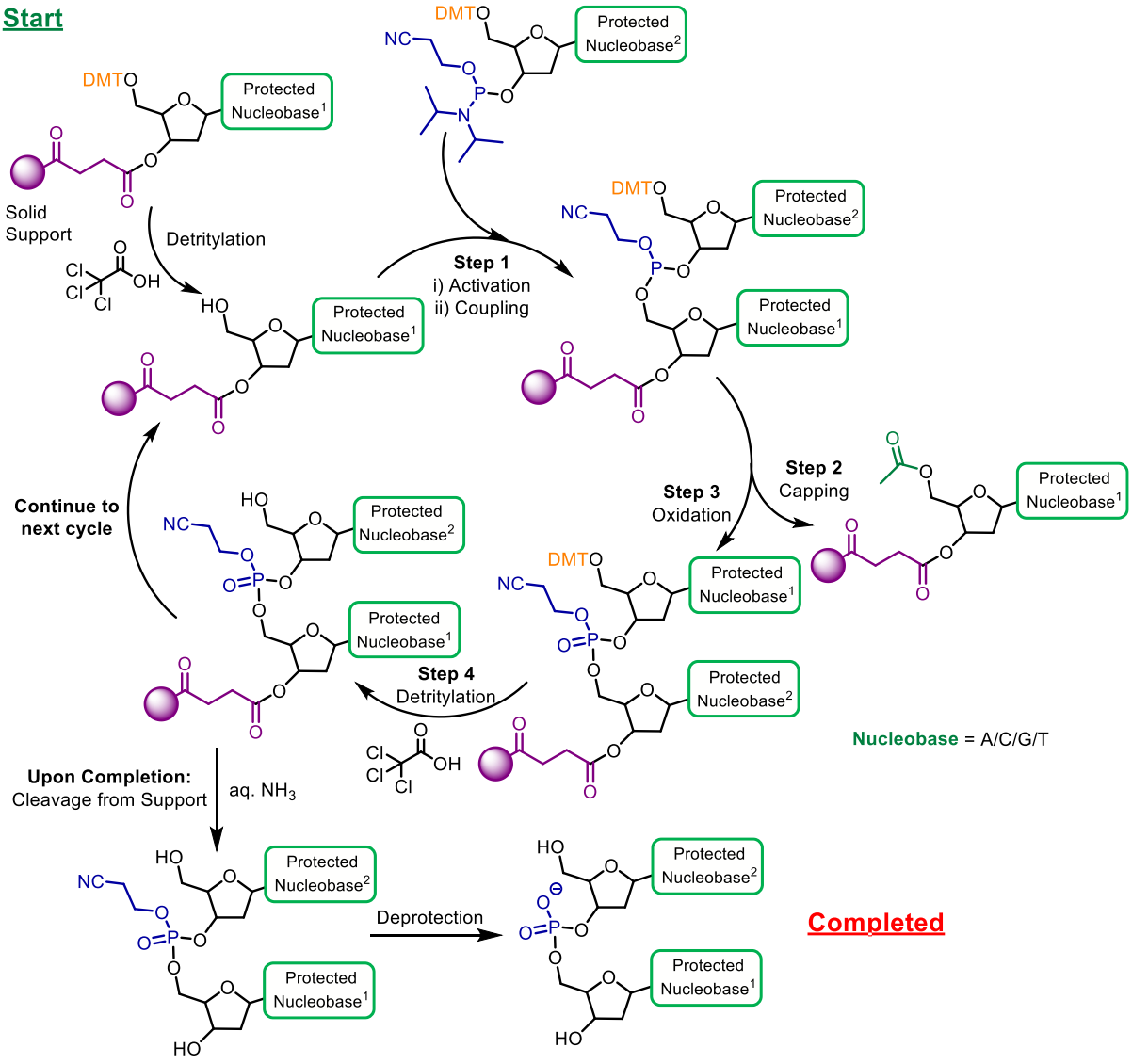

Scheme 3.1: The DNA Synthesis Cycle.

Step 2: Any unreacted 3' hydroxyl groups of the CPG-appended nucleoside are capped using N-methylimidazole and acetic anhydride, ensuring they do not react with subsequent

nucleoside phosphoramidites to produce sequences with nucleoside deletions. Any excess phosphoramidite is washed away.

Step 3: The freshly formed phosphite triester linking the two recently coupled nucleosides is oxidised to a phosphate triester using a solution of iodine in water. Pyridine is also present in the solution to neutralise the hydrogen iodide by-product.

Step 4: The final step of the cycle removes the 5' DMT group of the newly installed nucleoside, revealing the 5' hydroxyl group ready to couple the next nucleoside phosphoramidite. The trityl yield is recorded by monitoring the absorbance of the DMT cation at 495 nm.

Completion: The cycle is subsequently repeated until the desired sequence has been constructed. The strand is cleaved from the solid support using aqueous ammonia and the solution is then heated at 60 °C for 6 hours to remove the cyanoethyl unit of the phosphate triester alongside the acyl protecting groups of the nucleobases. The ammonia is removed by evaporation and the crude mixture is subsequently purified by HPLC and characterised by mass spectrometry.[27, 28]

3.1.4.3. Ultra-mild DNA Synthesis Conditions

The development of automated solid-phase DNA synthesis sparked an interest in synthetically modified DNA, a topic that is discussed below. Whilst the technique could allow the incorporation of synthetic alternatives to the standard nucleotides and nucleobases into DNA, not all modifications were robust enough to withstand the relatively harsh conditions of certain stages in the DNA synthesis cycle, such as heating in aqueous ammonia to cleave the strand from the solid support and deprotect each nucleobase.

Ultra-mild protecting groups were developed to overcome this challenge, Figure 3.9, enabling the use of milder deprotecting conditions such as a room temperature solution of potassium carbonate in methanol, alongside a weaker oxidising solution and milder activating agent.

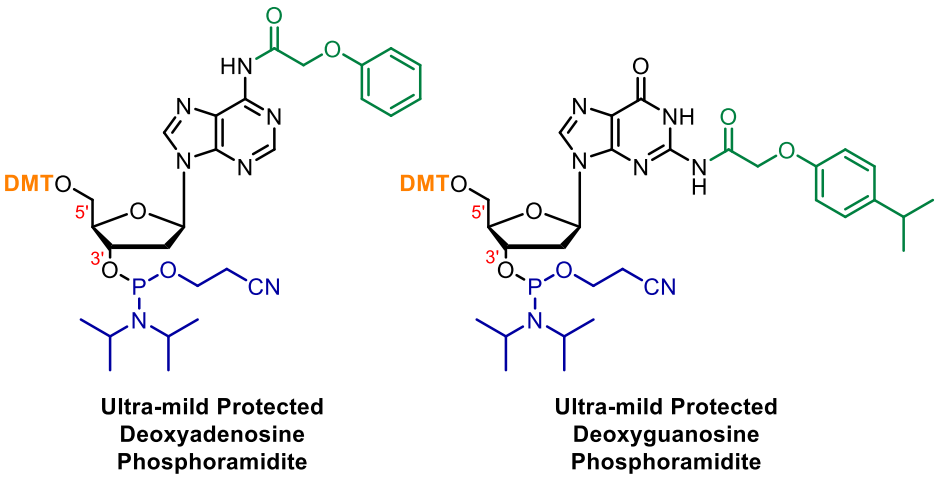

Figure 3.9: The protecting groups of adenine and guanine are adapted for ultra-mild DNA synthesis. The standard cytosine protecting groups are compatible with the conditions, whilst thymine does not require a protecting group.

The drawback of employing ultra-mild conditions is a partially reduced yield of the final oligonucleotide product, which is in part because the milder conditions do not always drive each coupling step to absolute completion. The labile protecting groups used also lead to greater difficulty in synthesising the phosphoramidites, resulting in their being more expensive than the traditional alternative.

3.1.5. Modified DNA

As scientists' understanding of DNA increased and automated synthesis progressed, investigations began into utilising it as an effective element of a chemist's toolkit. Over time, DNA has been synthetically altered in numerous ways, allowing it to be successfully employed in areas including biosensing, drug delivery and in nano-electronics. Three main approaches are used for DNA strand modification. These include altering the nucleobase structure, the sugar-ring, which often also involves replacing the nucleobase as well, and finally modifying the phosphate within the backbone.

3.1.5.1. Nucleobase Modifications

Nucleobases are often tagged or modified to introduce fluorescent properties to DNA, a quality that is particularly useful for sensing applications.[29] With the nucleobase playing a key role in the DNA helical structure, it is desirable that any modifications do not distort and destabilise the duplex.

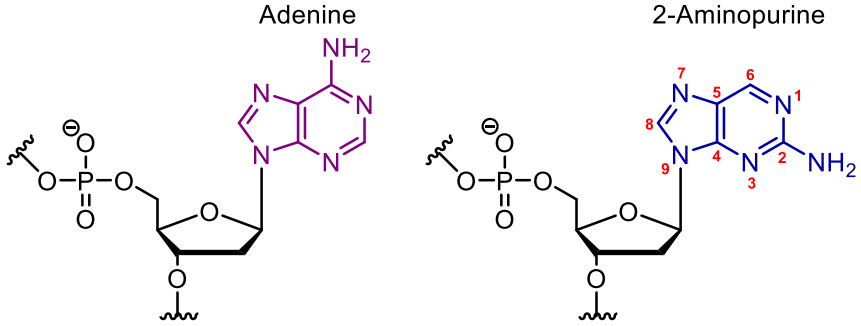

Figure 3.10: Nucleobase modification: Adenine (left) and 2-aminopurine (right). The simple move of the amine unit from the 6 to the 2 position by Stryer et al. increases the fluorescence of the nucleobase.

Early research investigated minor structural changes: the synthetic nucleobase 2-aminopurine simply alters the position of the amine unit of adenine, moving it to the two position of the purine ring, as shown in Figure 3.10.[30] This small deviation retains the hydrogen bond donor and π-stacking ability of the nucleobase whilst enhancing the fluorescent properties of the molecule. Functionalising DNA with reporter groups enables

information to be obtained *via* a readout signal, something that can greatly benefit the field of biosensing.

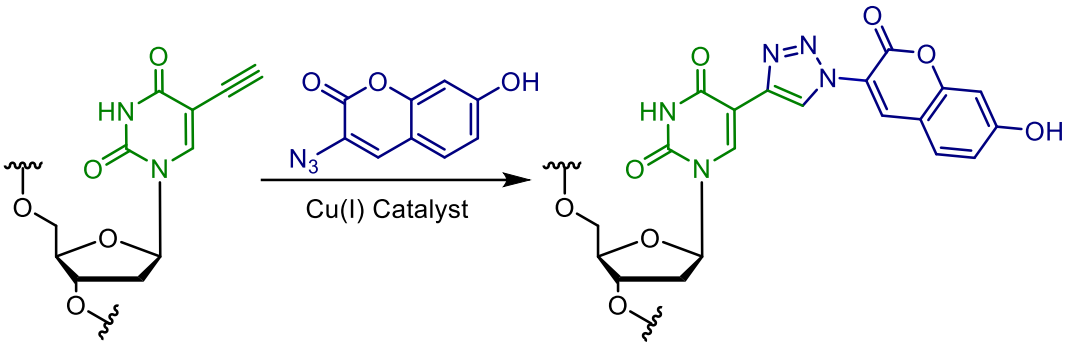

Scheme 3.2: An alkyne-modified thymine nucleobase can be coupled to an azide-functionalised coumarin derivative via azide-alkyne click chemistry to introduce a fluorescent reporter group.

Attaching a terminal alkyne group to the nucleobase and utilizing azide-alkyne click chemistry is another popular method for introducing functionality to the DNA strand, for example the fluorophore coumarin in Scheme 3.2. The DNA-alkyne reacts with an azide-modified reporter group in the presence of a copper catalyst to form a cyclic 1,4-triazole unit, offering a relatively simple and rapid coupling pathway.[31, 32] The approach enables a vast substrate scope; any azide-functionalised unit could in theory react with the DNA-alkyne and so it is unsurprising that azide-alkyne click chemistry has been used to introduce a variety of fluorophores into DNA for sensing applications. This includes labelling DNA for high-throughput sequencing and genomic analysis, as well as forming DNA-peptide conjugates.[32]

Functionality may also be introduced to the DNA strand by directly replacing the nucleobase with a reporter group. The unit taking the place of the base on the deoxyribose sugar of the nucleotide must be of an appropriate size and configuration so not to destabilise the DNA duplex. Many of the chosen moieties are planar aromatic molecules like pyrene that, although they cannot hydrogen bond with neighbouring nucleobases, are capable of intercalating into the duplex and providing stability through π-stacking interactions. The pyrene nucleotide in

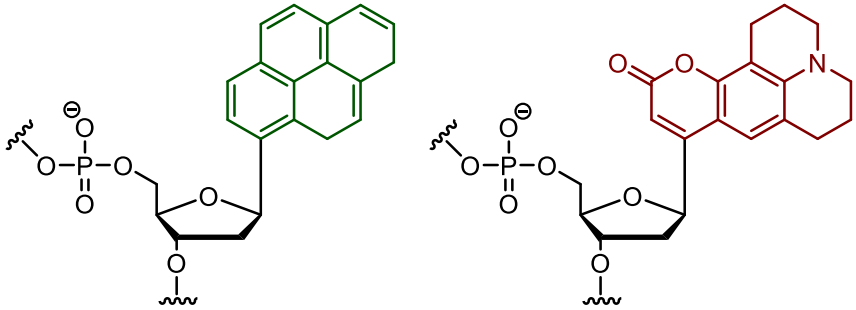

Figure 3.11: Nucleobase substitutions: a pyrene nucleotide (left) and a coumarin derivative (right).

Figure 3.11 was the first example to stabilise its surroundings and form a base pair in the absence of hydrogen bonding and also demonstrated that hydrogen bonding is not essential for DNA replication.[33, 34] Pyrene is also fluorescent and is one of numerous fluorophores including cyanine dyes and coumarin derivatives that have been appended to the sugar ring of the nucleotide.[35, 36]

3.1.5.2. Sugar Ring Modifications

In addition to altering the groups attached to the deoxyribose sugar of the nucleotide, the sugar unit itself can be substituted with an appropriate linkage. An example of such a linkage is threoninol, a chiral molecule that has three carbons between its two alcohol groups, identical to the nucleotide sugar ring, Figure 3.12. As well as possessing a suitable structure, the molecule is well suited to incorporation into DNA *via* automated solid-phase DNA synthesis as the two alcohol units can be functionalised for phosphoramidite chemistry.

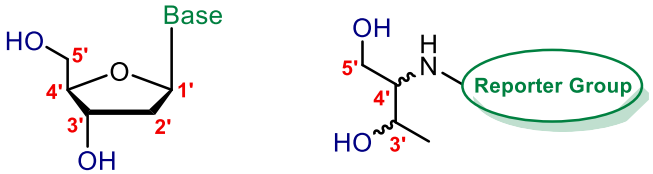

Figure 3.12: Linkages with three carbons between the two hydroxyl groups have been used to tag molecules to the phosphate backbone in place of the sugar ring. An example of an appropriate linker is threoninol (right). This is the optimum linker length and compares to the distance found in natural nucleotides (left).

Closely mimicking the structure of the sugar unit with similar linker groups allows reporter groups to be incorporated into the phosphate backbone whilst minimising any potential

destabilisation to the structure, as evidenced by thermal melting studies.[37, 38] Using this methodology, Tucker and co-workers tagged the fluorescent polyaromatic anthracene to the DNA backbone and could use the probe to discriminate between nucleobases, with changes in its readout signal allowing the detection of point variants. Its structure and geometry, alongside the chirality of the threoninol linker, enabled the anthracene unit to intercalate into the duplex and π-stack with neighbouring bases.[37, 38]

3.1.5.3. Backbone Modifications

One of the early DNA backbone modifications was centred on the phosphate unit of the nucleotide, replacing one of the oxygen atoms with a sulfur atom to give a phosphorothioate group whilst leaving the sugar ring and nucleobase unaffected.[39] The substitution of oxygen with sulfur conserves the negative charge of the DNA backbone whilst increasing the stability of the strand in the body, with enzymes including nuclease less likely to cleave it.[40]

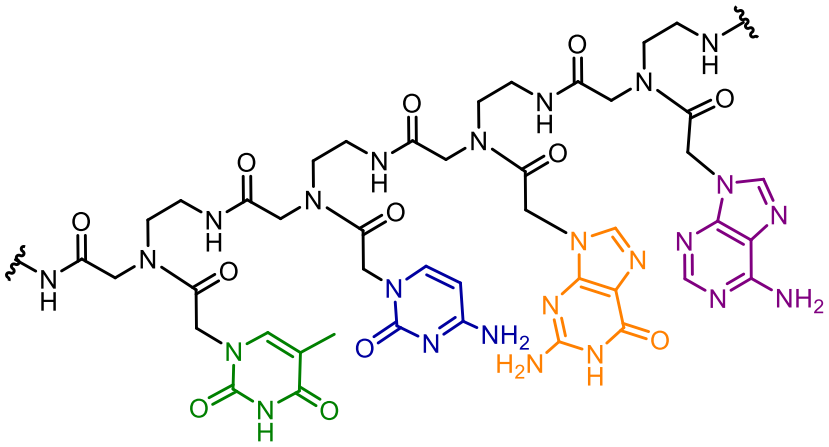

Figure 3.13: Peptide nucleic acid (PNA).

The development of peptide nucleic acid, PNA, removed the sugar phosphate backbone entirely and replaced it with polyamide spine consisting of *N*-(2-aminoethyl) glycine linkages, as depicted in Figure 3.13.[41] Retaining the nucleobases and positioning them the same distance away from the backbone enables inter-strand recognition between PNA and DNA

and hybridisation. The removal of the negatively charged phosphate backbone means the strand has no charge and consequently no repulsive electrostatic interactions are present when two strands come together. This, alongside the added flexibility of the polyamide linkages, results in the PNA duplex possessing greater stability than their natural nucleic acid counterparts, reflected in higher thermal melting values for the PNA-DNA duplexes.[41-43]

The ability to mimic and interact with DNA has led to PNA being a valuable biological tool. It has found applications in gene therapy drug design, demonstrating an ability to inhibit transcription and translation, with its high binding efficiency capable of blocking key DNA segments and disrupting the process.[42] PNA has also found uses in cellular delivery, biosensing and as a scaffold for supramolecular drugs.[42, 44]

Phosphoramidite chemistry and solid-phase DNA synthesis is employed to introduce functional groups to the 3' and 5' terminals of the phosphate backbone or at an internal position. Modifying the desired functional unit with a hydroxyl group and subjecting it to either phosphitylation or DMT protection, depending on which end of the DNA is to be modified, equips it for use in solid-phase synthesis, Figure 3.14.

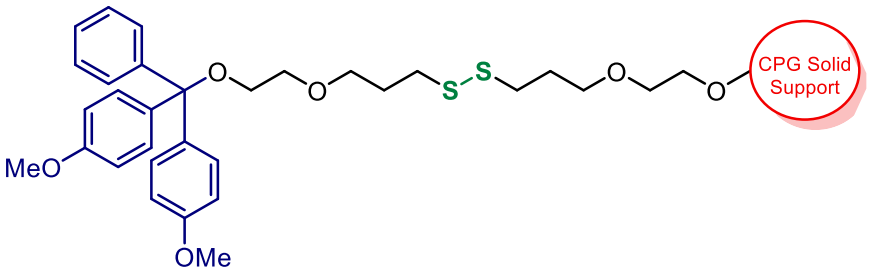

Figure 3.14: A commercially available 3' thiol modification. The central disulfide (green) is reduced after DNA synthesis to give a thiol moiety. The thiol is connected via an alkyl linker chain to a hydroxyl group which has been protected by a 4,4'-dimethoxytrityl unit (blue) which will be coupled to the 3' alcohol of the next nucleotide in solid-phase DNA synthesis.

The addition of thiol units to the termini of the DNA strand is a popular modification as it allows the DNA to be anchored to a surface. Sulfur can form a covalent bond with gold that is very robust and the formation of self-assembled monolayers on a gold surface is of particular

importance in the fabrication of nano-scale devices.[45] It has also enabled DNA to be analysed by surface techniques including atomic force microscopy (AFM)[46] and X-ray photoelectron spectroscopy (XPS).[47]

Thiols can also be reacted with groups such as maleimide to attach DNA to surfaces other than gold. A maleimide tether can first be fixed to the surface, which can range from a glass slide or coverslip to silicon-based materials, before subsequent reaction of the maleimide with the thiol group binds the DNA.[48] Incorporating an alkyne unit at the terminals of the phosphate backbone, azide-alkyne click chemistry offers an alternative method for immobilising DNA to a surface.[32]

3.1.6. Incorporating Metals into DNA for Electrochemical Applications

Functionalising DNA with metals introduces a wealth of properties that are beneficial in nanotechnology, including an increased stability, catalytic and magnetic properties. Combining the redox activity of transition metals with the recognition ability of DNA has led to electrochemical sensors that rival fluorescent probes,[49] whilst the charge transfer ability of metals can enhance the conductivity of DNA and make it suitable for use in nanoelectronics and as molecular wires.[50-53] The ability to form programmable nanoarchitectures such as nanotubes makes DNA the ideal scaffold for discrete, well-defined transition metal structures that are difficult to fabricate or simply unattainable by conventional supramolecular methods.[54] Such metal-organic frameworks have application in future nanoscale technologies including nano-electronic circuits, data storage and catalytic devices.

The process of functionalising DNA with metals is more complicated than incorporating many of the fluorophores mentioned above as metals cannot be covalently bonded directly to a

nucleobase or the sugar-phosphate backbone. Consequently, the stability of the metal coordination complex is of great importance. Many complexes are not robust enough to withstand the harsh conditions of solid-phase DNA synthesis, with decomplexation occurring and post-synthetic reintroduction of the cation required. As well as adding an extra synthetic step, having free metal cations in the vicinity of DNA is cause for concern as they are associated with inducing DNA damage such as double strand breaks.[55, 56] Though the benefits of combining metals with DNA are large, in practice it proves a challenge. Nevertheless, a variety of metals have been incorporated into DNA through several different methods.

3.1.6.1. Metal-Base Pairs

An interesting discovery was that certain nucleobases are capable of selectively complexing metals to form metal-base pairs. Katz reported that two thymine units stationed opposite each other in the duplex, a mismatch that would otherwise destabilise the double helix, could coordinate a Hg^{2+} cation and subsequently stabilise the duplex.[57] A similar effect was observed by Ono *et al.* with a cytosine mismatch and a Ag^{+} cation, shown in Figure 3.15.[58] Metal-base pairs offer a less disruptive route for incorporating metals into DNA which only requires programming of the nucleobase sequence, rather than the more elaborate synthetic

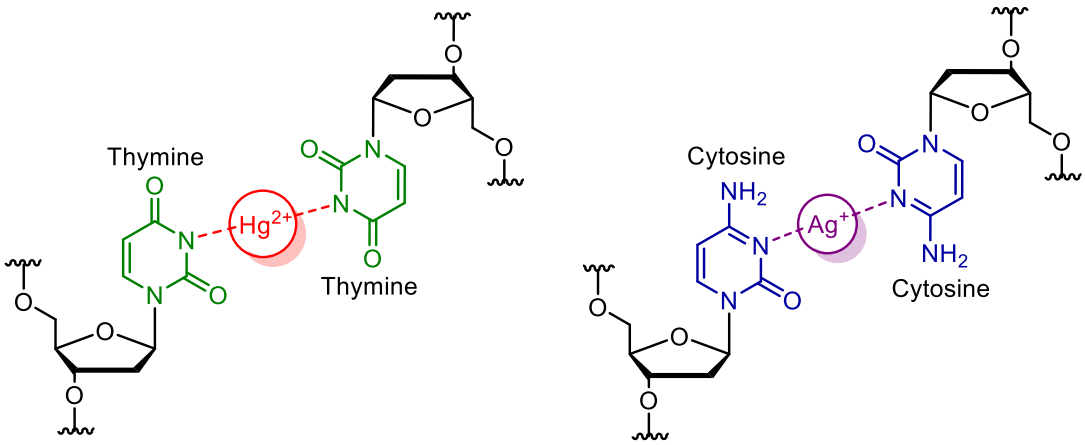

Figure 3.15: The thymine-Hg^{2+}-thymine (left) and cytosine-Ag^{+}-cytosine (right) metal base pairs.

modifications described previously. However, the selectivity of the bases means that the range of metals that can be introduced is extremely limited.

Shionoya replaced the natural nucleobases on the sugar ring with chelating ligands to widen the scope of metals that could be bound. Positioning two phenylenediamine units opposite each other in the duplex allowed a Pd^{2+} cation to be bound with a square planar geometry,[59] whilst pyridine moieties formed a linear pair with a Ag^{+} cation, Figure 3.16.[60]

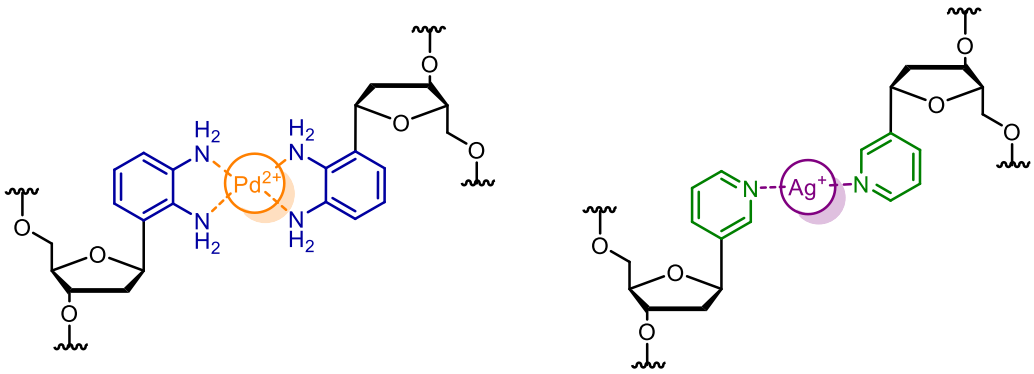

Figure 3.16: Shionoya's phenylenediamine-Pd^{2+}-phenylenediamine (left) and pyridine-Ag^{+}-pyridine (right) chelator-type pairs.

The ability to bind a variety of metals and dictate their positions in the DNA strand is of particular interest in nano-electronic devices including molecular wires, offering potential methods for improving properties such as conductivity.[61] Shionoya *et al.* demonstrated the potential of the metal-base pair to fabricate such nanotechnology through combining the

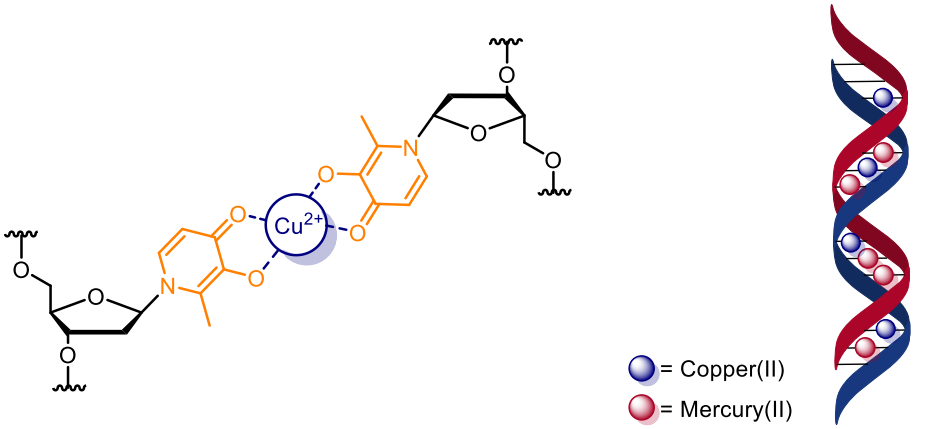

Figure 3.17: Shionoya designed a hydroxypyridone-Cu^{2+}-hydroxypyridone chelator-type pair (left) and combined it with the thymine-Hg^{2+}-thymine metal base pair to precisely build a backbone of metal atoms along a DNA duplex.

thymine-Hg^{2+}-thymine metal base pair with a synthetic chelator-type pair, hydroxypyridone-Cu^{2+}-hydroxypyridone,[62, 63] to program the position of heterogenous metals along the backbone of a single DNA duplex, Figure 3.17.[64] The number and the sequence of the metal cations can be precisely controlled and varied at will, demonstrating the potential for the preparation of a range of well-defined molecular architectures.[64]

3.1.6.2. Ligand-Metal Coordination Complexes

Others have transferred well known coordination complexes to DNA, fixing ligands to the backbone and using them to then bind metal atoms. Sleiman *et al.* used phosphoramidite chemistry and automated synthesis to incorporate terpyridine (tpy) and diphenylphenanthroline (dpp) ligands at the 5' and 3' termini of complementary DNA strands to allow for the formation of three coordination spheres, each capable of selectively binding different metal cations, Scheme 3.3. A DNA duplex with two tpy ligands could bind Co^{2+}, Zn^{2+}, Ag^{+} and Cu^{2+} readily, with a particular high binding affinity for Fe^{2+}. A coordination sphere containing two dpp ligands demonstrated a high stability when complexing Cu^{+}, the four-coordinate binding site selectively binding Cu^{+} over Cu^{2+}. Combining the ligands in a dpp:tpy site led to a preference for Cu^{2+}, as well as binding the other metal cations.[65, 66]

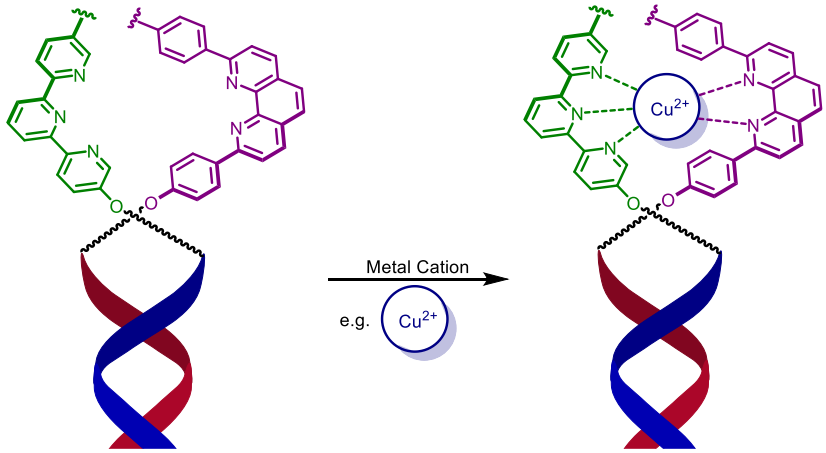

Scheme 3.3: Sleiman and co-workers incorporated tpy (purple) and dpp (green) ligands into DNA to bind a range of metals. A tpy:dpp coordination sphere had a preference for Cu^{2+} cations.

With guest-host chemistry unaffected by using oligonucleotides as a scaffold for the ligands, a natural progression is to use macrocyclic complexes and their rich coordination chemistry to introduce metals into DNA. Porphyrins have been popular choices for incorporation, fixed to the terminals of the phosphate backbone[67] and replacing the nucleobase on the sugar ring.[35] Stulz *et al.* attached a porphyrin unit to a thymine, Figure 3.18, and with it have bound Co^{2+}, Cu^{2+} and Zn^{2+} cations. The metals are added after automated DNA synthesis as the complexes are not robust enough to withstand the harsh conditions employed during DNA synthesis. Even when formed post-synthetically, the zinc complex survived for only a matter of minutes before decomplexation.[68] The central location of the complex in the duplex is important in its successful application as an electrochemical sensor with a femtomolar detection limit.[49, 69]

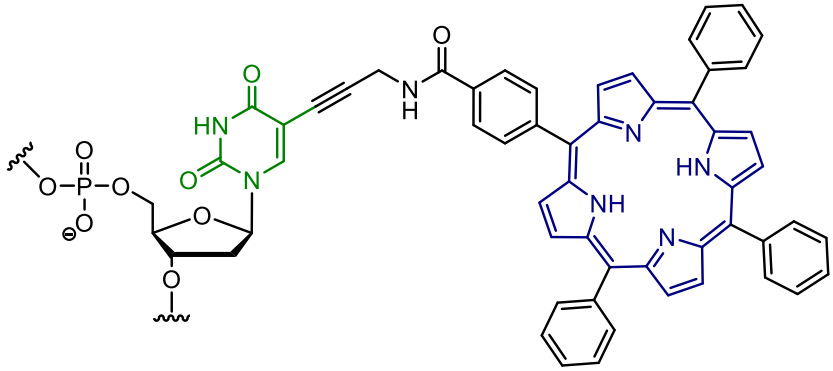

Figure 3.18: Stulz and co-workers attached a porphyrin ring to a thymine and incorporated it into DNA.

A similar porphyrin derivative binding a Mn^{3+} cation was tagged to the end of a PNA strand and mimicked the behaviour of DNA recognition proteins which are vital in biological processes such as DNA replication. The metal-PNA conjugate combines the ability of PNA to target DNA with the capability of the manganese complex to facilitate the oxidative cleavage of double strands of DNA to create irreversible damages efficiently and selectively to DNA, an important tool in gene therapy. The presence of the metal complex also enhances the DNA

binding ability of the PNA strand, with the porphyrin known to have a high affinity for the minor groove of the duplex.[70]

3.1.6.3. Metallocenes

The metallocene complex ferrocene has proved a reliable source of iron atoms for DNA incorporation. The high stability of the complex ensures the iron cation can withstand the harsh conditions of automated solid-phase DNA synthesis, allowing phosphoramidite chemistry to be used to attach ferrocene to the phosphate sugar backbone. Unlike many of the fluorescent modifications mentioned earlier, at first glance, the structure of the metallocene does not appear suitable for DNA incorporation. As they are not planar, they are incapable of contributing to the stability of the duplex through intercalation and π-stacking interactions.

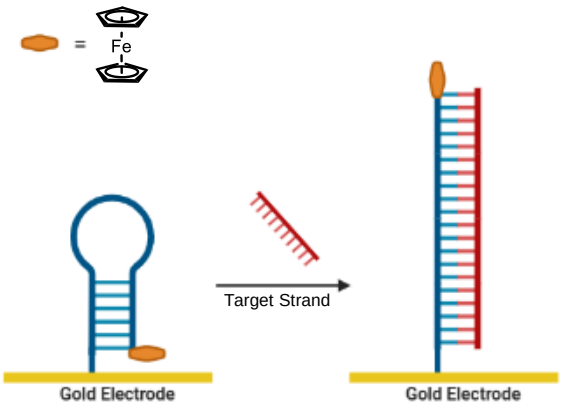

Scheme 3.4: Plaxco's electrochemical sensor used a hairpin strand that underwent a significant conformation change upon binding its nucleic acid target. The binding event moves the ferrocene tag away from the electrode surface, decreasing the signal intensity.

Nevertheless, attaching a ferrocene tag to the 3' or 5' terminal of a strand has proved a successful modification that does not destabilise the DNA or the duplex.[71, 72] The well-characterised iron (II/III) redox couple has led to the use of these termini tagged ferrocenes in electrochemical DNA sensors, including the hairpin-like probe designed by Plaxco and co-workers pictured in Scheme 3.4.[72-74]

3.1.6.4. Direct Incorporation of Metals into the DNA Backbone

Tucker and co-workers employ phosphoramidite chemistry and automated solid-phase DNA synthesis to incorporate molecules directly into the sugar-phosphate backbone of DNA in place of an entire nucleotide unit. This can be done by mimicking the structure of the sugar ring and functionalising the desired modification with two hydroxyl groups. Strategically protecting the diol with DMT, followed by phosphitylation, Scheme 3.5, allows the reporter group to be incorporated into the DNA backbone during oligonucleotide synthesis in a controlled fashion with the desired geometry.

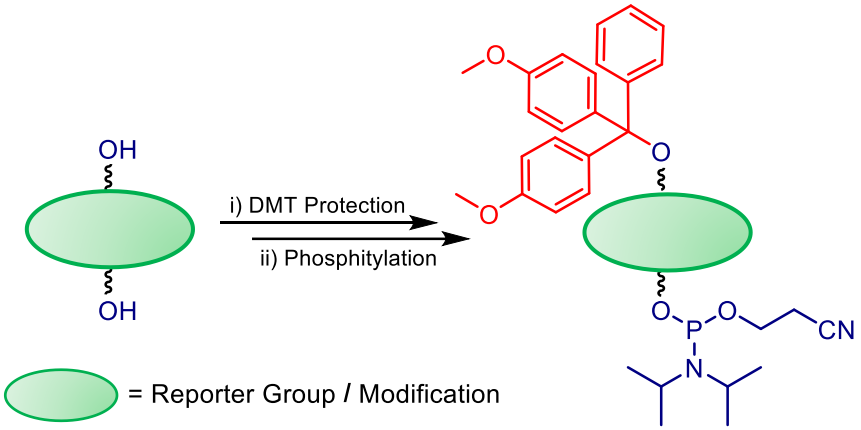

Scheme 3.5: The strategic protection of the hydroxyl groups is key to using phosphoramidite chemistry in oligonucleotide synthesis.

Ferrocene is an ideal candidate for such backbone modifications as it has formed a scaffold of organometallic nucleotide analogues, with nucleobases having been attached to the cyclopentadiene (Cp) rings of the metallocene and proving capable of forming hydrogen-bonding arrays,[75] as well as its compatibility with phosphoramidite chemistry and automated DNA synthesis. Most importantly, Tucker and co-workers noted that the distance between the two Cp rings (3.3 Å) compares favourably with that between two adjacent nucleobases in a strand of B-DNA (3.4 Å).[76] This structural similarity enabled the construction of ferrocene nucleic acid, FcNA, the first structural organometallic nucleic acid analogue, where ferrocene

directly replaced multiple sugar-phosphate-sugar units along the backbone of the strand, depicted in Figure 3.19.

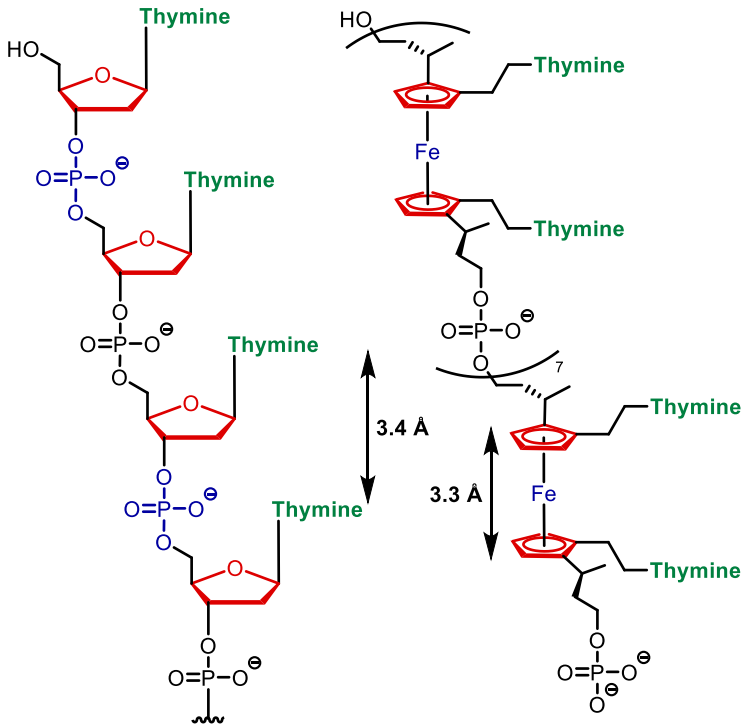

Figure 3.19: Tucker and co-workers constructed the first organometallic structural mimic of DNA, ferrocene nucleic acid (FcNA). The FcNA backbone comprised entirely of ferrocene-phosphate units but still contained nucleobases in the correct position.

With each Cp ring was functionalised with a thymine unit, the UV-vis spectrum of FcNA contained a strong absorbance band at 260 nm, characteristic of DNA. The retention of the phosphate units bestowed water solubility, whilst the iron atoms made the strand redox-active. Remarkably, oxidation of the ferrocene units did not lead to any degradation of the strand, with the redox event being quasi-reversible as seen in similar mono-ferrocene units.[76] FcNA and its electrochemical properties is an exciting creation for nano-technologies such as molecular wires,[77, 78] whilst the complete replacement of nucleotide units could lead to advancements in existing DNA technologies in sensing.[10]

Whilst FcNA pushed backbone modifications to an extreme, mono-substitutions of nucleotides for reporter groups can greatly improve the suitability of a DNA strand for a given

application, as discussed earlier in section 3.1.5.2 on page 128. It was using this methodology that the macrocyclic ligand cyclidene and its Cu^{2+} and Ni^{2+} complexes were incorporated into the DNA backbone by Tucker and co-workers.[79] Cyclidene complexes possess several appealing properties that make them suitable for DNA incorporation. Their neutral charge and square planar geometry facilitates intercalation between neighbouring nucleobases,[80] whilst their shape and size are similar to a number of fluorophore tags, none more so than pyrene, whose successful integration into DNA was described on page 128. The presence of the redox-active transition metal enables the generation of an electrochemical readout signal. Crucially, these complexes are remarkably stable and were found to withstand the automated DNA synthesis process, including the transition metal cations remaining coordinated, something not observed in other metal complexes.[79]

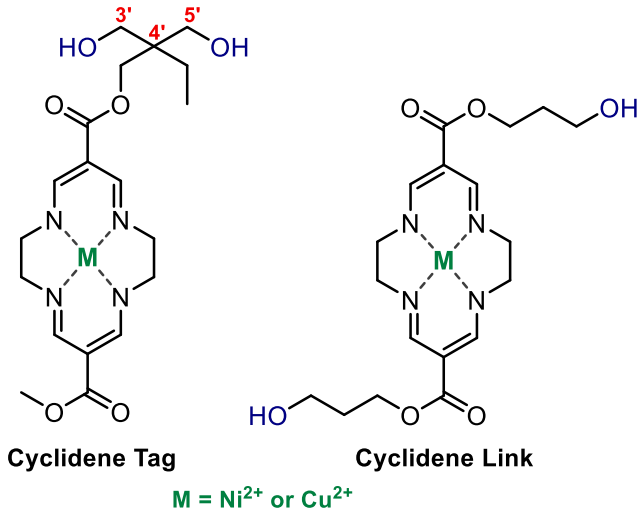

Figure 3.20: The Cu^{2+} and Ni^{2+}cyclidene complexes were incorporated into the DNA backbone in two different orientations by Tucker: as a tag (left) and as a linker (right).

Using the ester units at either end of the molecule as a synthetic pathway, two different structures were explored for backbone incorporation, Figure 3.20. The tag system follows the design rationale outlined in Figure 3.12, with tris(hydroxymethyl)propane providing the three-carbon linker chain between the two hydroxyl groups. Tethering the macrocycle at only

one end allows it to take advantage of its intercalating abilities and insert into the DNA duplex. This tag system was found to be particularly beneficial for sensing applications, with the copper complex capable of distinguishing between all four natural nucleobases at a specific position in a target strand through changes in the electrochemical current signal. The base-discriminating ability of the system could be of particular use in detecting point variants and identifying critical disease biomarkers.[79]

The link system drew inspiration from FcNA, attaching a three-carbon linker to each end of the molecule to form a metal bridge along the backbone. This arrangement restricts the intercalating ability of the cyclidene complex and consequently the cyclidene-link does not possess the same nucleobase sensing capabilities as the tag. However, the system could still be of use as an internal reference signal in a sensing system, in molecular wires[77] or in other supramolecular DNA assemblies, for example, as an abiotic oligomer similar to the pyrene-based oligonucleotides developed by Häner and co-workers.[81] Interestingly, the redox signal of the nickel complexes was unable to be observed within the accessible potential window, with the redox peak likely to occur at a more positive potential, because the oxidation of the d^8 Ni^{2+} centre is less thermodynamically favourable than that of the d^9 Cu^{2+} cation.[79] Overall, the cyclidene systems were a promising development, as the ability to line the backbone with different metals at any desired position is a valuable tool for a variety of nanotechnologies.

3.1.7. Electrochemistry

The ability to bind transition metal cations gives macrocyclic complexes a rich redox chemistry that has been harnessed in a variety of applications, from being the detectable signal in a sensor to being the driving force for a switchable system. In many instances, the M^{2+} cation undergoes a single-electron oxidation to the M^{3+} cation, a reversible process that sees the M^{3+} cation reduced back to the M^{2+} species. The transfer of the electrons can be measured as an electrochemical current.

3.1.7.1. Electrochemical Set Up

The electrochemistry detailed in this thesis was performed using a three-electrode set-up, comprising a working electrode (WE), a platinum wire counter electrode (CE) and a Ag/AgCl reference electrode (RE). The electrodes are immersed in an electrolyte solution in a sealed glass cell under an inert atmosphere and connected to a potentiostat, pictured in Figure 3.21.

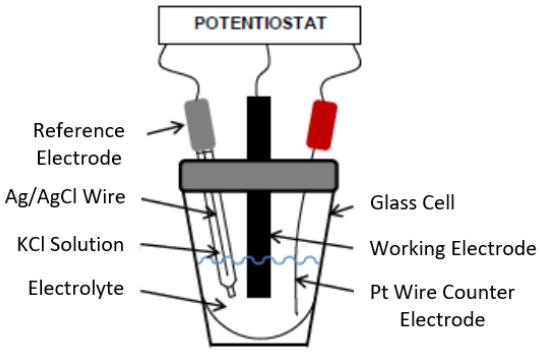

Figure 3.21: The experimental set up of the electrochemical cell.

The electrochemical event of interest, in this case the oxidation and reduction of the macrocycle complex, occurs at the WE surface. A voltage is applied and a current flows between the WE and the CE. This current is recorded as a function of the applied voltage relative to the RE, allowing the voltage (also called the potential difference) to be reported relative to a stable reference reaction. As the redox event occurs at the electrode surface, it

is imperative that the surface is clean, which is routinely achieved through a combination of mechanical polishing and electrochemical cycling, and that its surface area has been characterised.[82]

3.1.7.2. Cyclic Voltammetry

Cyclic voltammetry is one of the most widespread electrochemical techniques because of its versatility, ease of measurement and its ability to rapidly observe redox behaviour over a wide potential range. As the name suggests, it involves cycling the applied potential at the WE between two limits, in this case from a negative potential limit to a positive potential limit to oxidise the analyte, before returning to a negative potential and reducing the redox active species to its initial state, Figure 3.22a. The resulting current signal is plotted against the potential to produce a cyclic voltammogram (CV), Figure 3.22b.[82, 83]

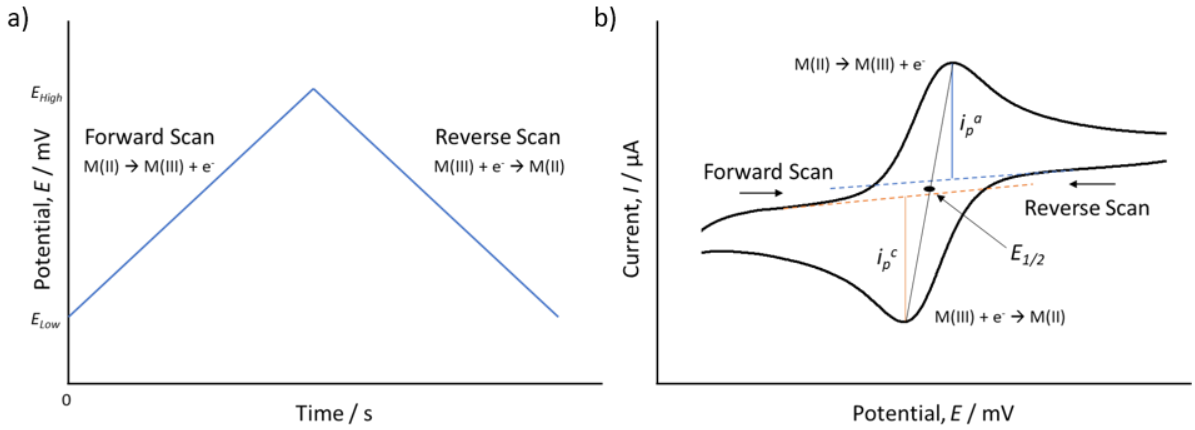

Figure 3.22: a) The triangular waveform employed in cyclic voltammetry. b) The resulting cyclic voltammogram showing oxidation and reduction peaks for the redox active species M, which have anodic and cathodic currents, i_p^a and i_p^c, respectively. The midpoint between the anodic and cathodic peaks is the half-wave potential, $E_{1/2}$.

Whilst the initial potentials applied are not capable of inducing electron transfer, eventually the potential is positive enough to oxidise the redox centre. This results in a peak in the CV as the electrons lost by the metal centre are transferred to the WE, producing a current. As more of the analyte is oxidised the peak reaches a maximum current, i_p^a, before decreasing as the

species at the electrode surface is consumed and only partially replaced with fresh material from the solution. The process is then reversed, with the oxidised species returned to its initial state as the potential becomes more negative. As before, a peak is observed for the reduction of the analyte, with a maximum current i_p^c.[82, 83]

The experiment is often repeated at a range of scan rates to allow for a wealth of information to be garnered from the CV. The half-wave potential, $E_{1/2}$, the midpoint between the anodic and cathodic peak potentials can be calculated using Equation 1.1 and is often used to compare the electrochemical behaviour of different species.

Equation 1.1 $$E_{1/2} = \frac{E_p{}^a + E_p{}^c}{2}$$

The appearance and relationship between the two peaks can be informative about the reversibility of the redox process. There are three main diagnostic tests for a reaction to be deemed electrochemically reversible.[82, 84] The first is that the separation of the anodic and cathodic peaks, ΔE_p, is approximately $59/n$ mV at 25 °C, where n is the number of electrons transferred, as in Equation 1.2.

Equation 1.2 $$\Delta E_p = E_p{}^a - E_p{}^c \approx 59/n\, mV$$

Secondly, the two peak currents must be the of same magnitude, Equation 1.3.

Equation 1.3 $$\frac{i_p{}^a}{i_p{}^c} = 1$$

This criterion assumes similar diffusion coefficients for the oxidised and reduced forms of the analyte. Finally, the peak current and the square root of the scan rate should be proportional, as seen in Figure 3.23a. Larger peak currents are observed at higher scan rates. Figure 3.23b.[82-84]

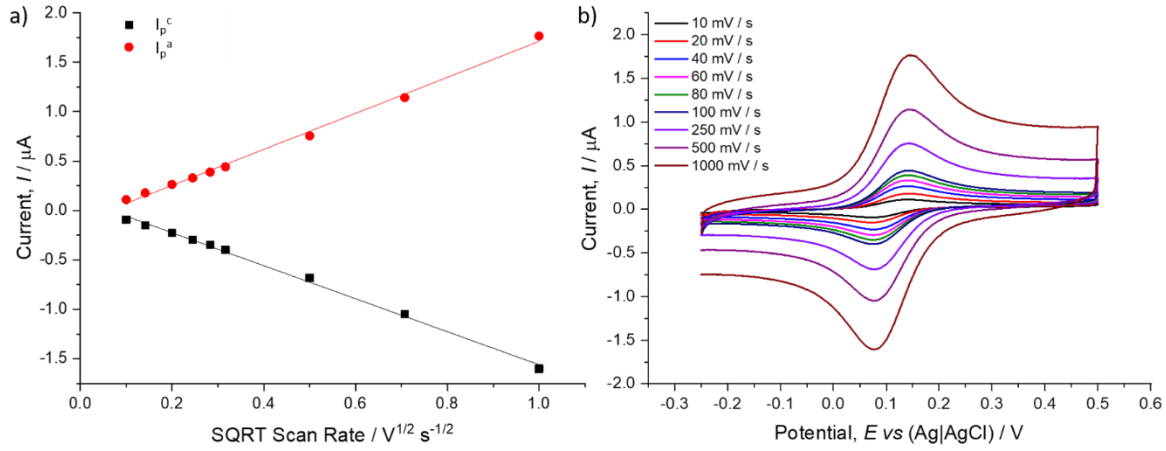

Figure 3.23: a) Plot of the peak current vs the square route of the scan rate in a solution-based ferrocene species. b) Overlaid CVs recorded for a range of scan rates of a Ferrocene-DNA conjugate.

The diffusion coefficient, *D*, of the redox-active species can be calculated using the gradient of the plot in Figure 3.23a and the Randles-Sevčik equation, **Equation 1.4**. A species moving faster through the electrolyte solution to and from the WE surface would possess a higher diffusion coefficient.[82]

Equation 1.4 $$i_{\mathrm{p}} = 0.4463\, nFAC\left(\frac{nFvD}{RT}\right)^{\frac{1}{2}}$$

where:

i_p = peak current (A)

n = no. of electrons transferred per molecule

F = Faraday's constant (C mol^{-1})

A = geometric working electrode surface area (cm^2)

T = temperature (K)

C = bulk concentration of solution (mol cm^{-3})

v = scan rate (V s^{-1})

D = diffusion coefficient

R = Molar Gas constant (V C K^{-1} mol^{-1})

This can be simplified to **Equation 1.5** for a single electron transfer process at 25 °C.

Equation 1.5 $$i_{\mathrm{p}} = 268600\, A D^{\frac{1}{2}}\, C v^{\frac{1}{2}}$$

This can be re-written in terms of the gradient, *m*, of the plot of i_{p} vs $v^{1/2}$ in Figure 3.23a to allow the diffusion coefficient, *D*, to be calculated from **Equation 1.6**.

Equation 1.6 $$D = \left(\frac{m}{268600\, A\, C}\right)^2$$

Electrochemical reactions with slower electron transfer kinetics, termed irreversible processes, exhibit a larger peak separation than 59/*n* mV and smaller peak heights but similar peak heights in each direction. The oxidation peak takes place at more positive potentials and the reduction peak at more negative potentials because a greater driving force is needed for electron transfer, to overcome the larger activation barrier; consequently the diffusion limitations become significant only at more positive/negative potentials (for oxidation/reduction processes, respectively). For electrochemical reactions where the redox centre is bound to the surface, diffusion does not play a role and, for fast reaction kinetics, the anodic and cathodic peaks have the same size and position. A wider peak separation would indicate a slower electron transfer process.

3.2. Aims and Objectives

This work aims to build on the cyclidene-DNA conjugates reported by Tucker and co-workers above.[79] Establishing the synthesis of the cyclidene complexes and the tag and link systems in the research group is vital for the success of the project and the primary objective of this Chapter. The synthesis of these molecules had previously been conducted by collaborator Jarosław Kowalski, whose work with Bohdan Korybut-Daszkiewicz and colleagues at the Institute of Organic Chemistry in Warsaw, Poland has developed a range of uses for these remarkable macrocycles.[80, 85, 86]

Kowalski and co-workers employed Takamura's condensation conditions to react methyl diformylacetate, developed by Knutson, with excess ethylene diamine to give a cyclidene unit functionalised with two methyl ester units, pictured in Figure 3.24.[87-89] The desired metal cation can subsequently be complexed and the esters functionalised to yield the tag and link systems, before DMT protection and phosphitylation steps equip the complex for automated DNA synthesis.[79]

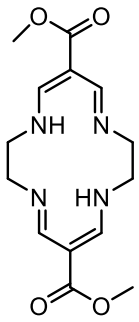

Figure 3.24: The cyclidene derivative explored in this work is constructed with two ester units at either end of the molecule.

Following the synthesis of the macrocyclic systems, this chapter will explore the incorporation of the Nickel link cyclidene into a variety of DNA strands, aiming to build a library of metal-functionalised oligonucleotides. The chapter will conclude by addressing the electrochemical issues encountered with the Ni^{2+} cyclidene complexes explained on page 139, enabling the

redox properties of these metal-functionalised oligonucleotides to be utilised. *Chapter 4* will explore the development of the copper-tag system as a surface-bound nucleic acid electrochemical sensor capable of detecting disease biomarkers such as point variants.

3.3. Monomer Synthesis

3.3.1. Synthesis of Cyclidene Macrocycle

The conjugated framework and methyl ester units of the cyclidene macrocycle were provided by methyl diformylacetate **3.1**, which was synthesised and used in tandem with ethylene diamine to construct the cyclidene ligand **3.2** in two synthetic steps, shown in Scheme 3.6.

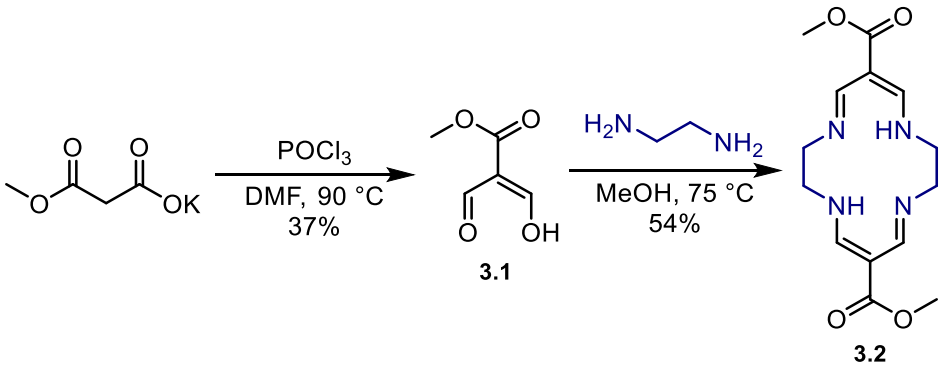

Scheme 3.6: The two-step synthesis of the cyclidene macrocycle. The atoms and bonds coloured in blue in cyclidene 3.2 highlight those contributed by ethylene diamine, whilst those in black originate from 3.1.

Methyl diformylacetate **3.2** was synthesised as detailed by Knutson.[87, 90] The tricky synthesis started by reacting phosphorous oxychloride and dimethyl formamide (DMF) to give the Vilsmeier reagent, Scheme 3.7. This is usually employed in a Vilsmeier-Haack reaction to formylate aromatics *via* electrophilic aromatic substitution and subsequent hydrolysis.

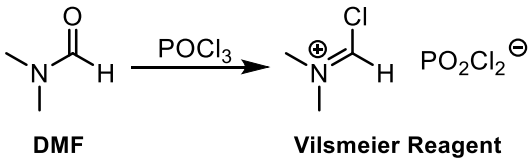

Scheme 3.7: Formation of the Vilsmeier Reagent.

In this instance however, the loss of carbon dioxide gas from potassium monomethyl malonate drove an addition to the Vilsmeier reagent, an unusual turn of events that started to build the basic conjugated methyl ester scaffold, intermediate **3.1a** in Scheme 3.8. Reaction with a further molecule of Vilsmeier reagent gave intermediate **3.1c** *via* **b** before hydrolysis conditions induced a formylation event much like a traditional Vilsmeier-Haack to give intermediate **3.1d**. Finally, an acidic work-up yielded **3.1**, which was collected by vacuum distillation. Due to the volatility of the product, the collection flask must be cooled in an acetone-dry ice bath to encourage the condensation of **3.1**. The formation of the Vilsmeier reagent is important and fresh (or freshly distilled) phosphorous oxychloride must be used. The crude material is also unstable to small amounts of acid over long periods of time, so the acid work-up must be performed quickly to minimise degradation of the product. These factors contributed to the low yield of 37%.

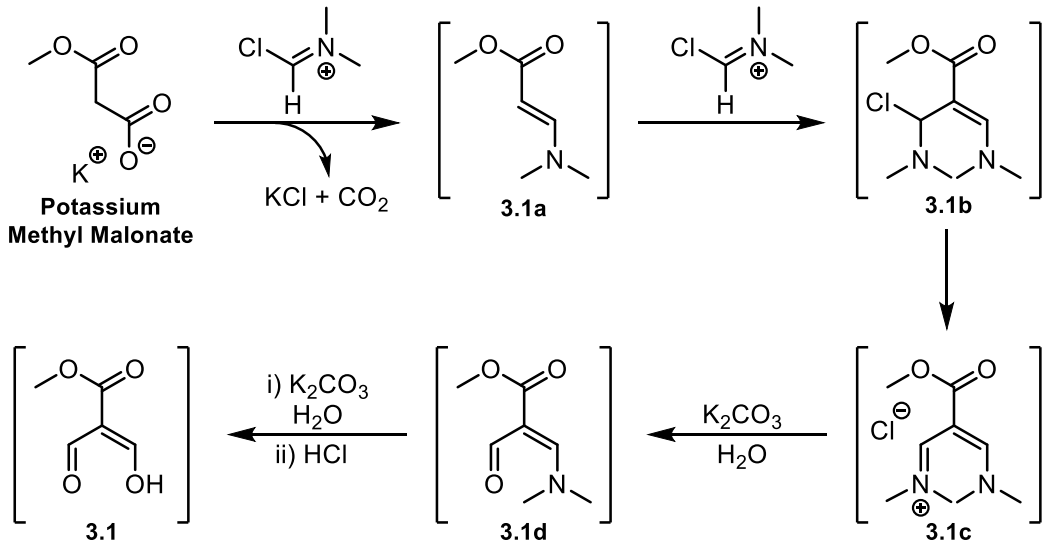

Scheme 3.8: Key mechanistic intermediates in the formation of methyl diformylacetate.

Cyclidene macrocycle **3.2** was prepared through a condensation reaction between two molecules of **3.1** and two molecules of ethylene diamine in dry methanol. The diamine was diluted in the solvent before dropwise addition.[88, 89] The conditions are similar to high dilution

methods of macrocycle synthesis and yield the 14-membered cyclidene. The larger 15- and 16-membered derivatives cannot be prepared under these conditions, instead requiring a templating metal cation to preorganise the longer alkyl-chained diamine and induce formation.[89]

Macrocycle formation with high dilution conditions is a delicate procedure, with competing reactions threatening the return of product. Although the yield of 54% betters some early high dilution methods, it is significantly lower than the best effort Takamura *et al.* reported. One source of discrepancy was that the reaction mixture had a concentration of 0.4 M, higher than the 0.1 M solution in the literature.[88] However, diluting the reaction mixture had a negative impact on the yield. In the future, cooling the solution before diamine addition could slow the reaction and possibly favour macrocycle formation.

3.3.2. Metal Complexation

The metal cation was introduced by refluxing the macrocycle with the appropriate metal acetate salt. Upon heating, the complexation event was rapid and could be witnessed *via* a colour change. Heating the solution of **3.2** and the blue-green copper acetate monohydrate salt caused it to turn a pink-red colour within a few minutes. Likewise, **3.2** and nickel acetate

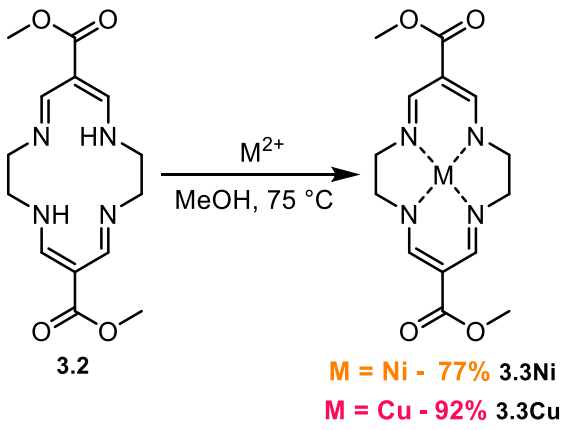

Scheme 3.9: Formation of the Cu^{2+} and Ni^{2+}cyclidene complexes.

tetrahydrate gave an orange solution from the initial green colouring as the nickel cation became bound. The 92% yield for **3.3Cu** improved on the reported literature value,[89] which likely stemmed from increasing the concentration of the reaction mixture through reducing the volume of solvent used. The lower yield for **3.3Ni** was in part due to the reaction only being conducted once. Applying the adjustments to the conditions used for the copper complexation is likely to improve the yield.

Owing to a d^8 electron configuration, Ni^{2+} cations are perfectly suited to sitting in the square-planar cyclidene cavity. This stability was reflected in the nickel complexes showcasing a better reactivity than their d^9 copper counterparts, evidenced by higher yields. The d^9 electron configuration of the Cu^{2+} cation proved problematic for the synthesis and characterisation of its complexes as its extra electron rendered them paramagnetic, resulting in broad NMR spectra. As seen in the literature, the characterisation of the copper complexes relied heavily on mass spectrometry, infrared spectroscopy, and chromatography in the absence of NMR spectroscopy.[79, 80, 85, 86, 89] Fortunately, the pathway for the tag and link phosphoramidite systems are identical regardless of the metal centre,[79] allowing the nickel complexes, which could be fully characterised, to act as a test for the reaction conditions before forming the copper analogue.

3.3.3. Synthesis of Cyclidene Link System

3.3.3.1. Synthesis of Link Diol

The ester units of **3.3** underwent an alkaline transesterification with propanediol to give the link system **3.4**, Scheme 3.10. Due to the stability afforded to the cyclidene core by the conjugated system, harsh conditions, including high temperatures, long reaction times and the use of a sodium metal catalyst, must be employed to drive the reaction.[79]

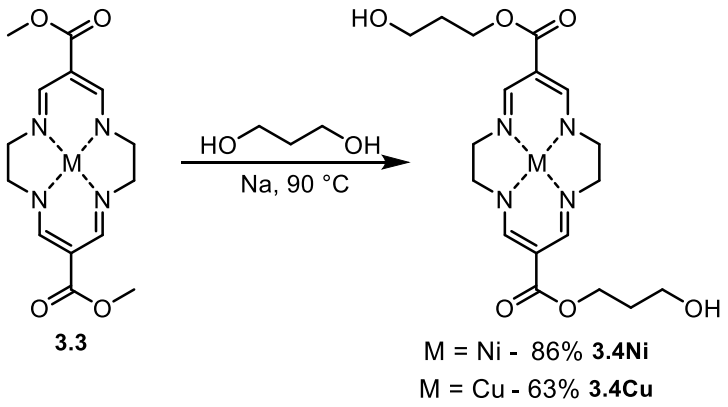

Scheme 3.10: Formation of the Cu^{2+} and Ni^{2+} cyclidene link systems.

Whilst the reaction conditions see little deviation from the literature methods,[79] the work-up and purification of **3.4** was adjusted. The protocol involved pouring the reaction mixture into ice-water to induce precipitation of the cyclidene species which would be collected by filtration. However, the remaining filtrate would often contain further cyclidene species which were extracted through washing with dichloromethane. TLC analysis of the precipitate and washings confirmed they were of the same composition and could be combined, but also identified the presence of trace amounts of unreacted **3.3** and the mono-substituted side product as well as the desired bis-substituted **3.4**. The recrystallisation conditions in the literature are unable to separate these cyclidene species and so column chromatography was employed to acquire the pure product. As the Ni^{2+} complex was found to be sensitive to the

slightly acidic silica gel of the column, triethylamine (1 %) was added to the eluent mixture to neutralise the stationary phase and prevent any decomposition.

3.3.3.2. Preparation for DNA Synthesis: DMT Protection

The challenge in protecting diol **3.4** with a DMT group was achieving the solely mono-protected product **3.5** from two equivalent hydroxyl groups, Scheme 3.11.

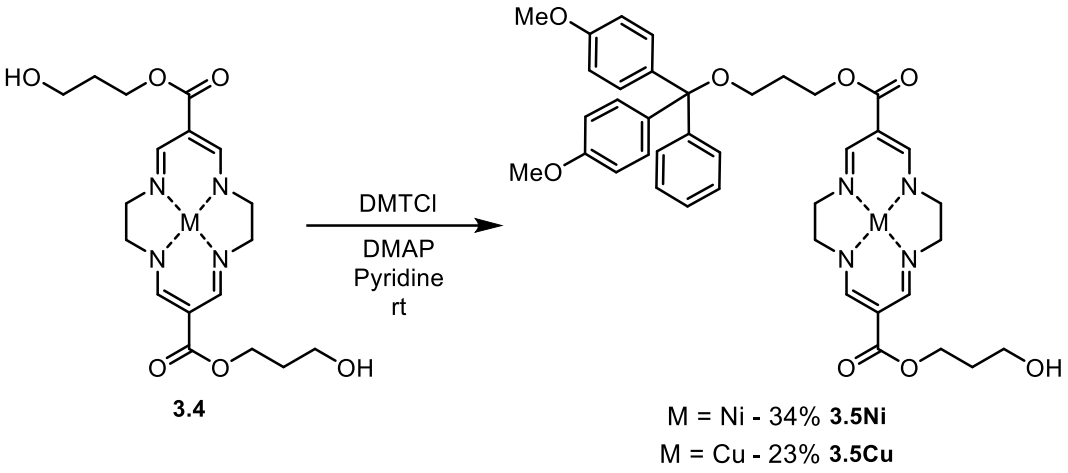

Scheme 3.11: The mono-protection of alcohol groups in the cyclidene link system with dimethoxytrityl units.

Whilst over-substitution was managed by controlling the molar equivalents of 4,4'-dimethoxytrityl chloride (DMTCl) used in relation to **3.4**, a significant amount of starting material remained unreacted. DMTCl is prone to reacting with trace amounts of moisture to form DMTOH. Simply including a large excess of DMTCl to legislate for this side reaction was not viable, as this would encourage over-substitution of **3.4**. Therefore, the reaction conditions employed were a trade-off between reacting as much of **3.4** as possible whilst minimising the bis-substituted side product. Adding between 1 and 1.2 equivalents of DMTCl, as a solid rather than in solution with pyridine, per 1 molar equivalent of diol **3.4** was found to be the optimum conditions. Unreacted starting material could be recovered during purification by column chromatography and reacted again. Including a catalytic amount of DMAP in the reaction was also found to minimise over-substitution.

The DMT protecting group is very acid-sensitive, which is what makes it suitable for its role in DNA synthesis, but this is problematic during purification. Therefore, a small percentage of triethylamine must be added to the eluent system to neutralise the slightly acidic silica gel stationary phase and prevent the deprotection of the freshly made product. If the bis-protected side product was formed, it was found that treatment with trifluoroacetic acid could regenerate **3.4**.

3.3.3.3. Preparation for DNA Synthesis: Phosphitylation

Cyclidene link phosphoramidite **3.6** was synthesised as described by Tucker and co-workers, Scheme 3.12.[79] The phosphorous centre of **3.6** is prone to oxidation from a phosphorous(III) species to phosphorous(V), an undesirable event that inhibits the coupling of the phosphoramidite to the manufactured strand in DNA synthesis. In addition to employing dry reaction conditions, the unusual step of deoxygenating all solutions, including aqueous solutions and eluents used in the work-up and purification steps, was taken to minimise oxidation of the product. The result was the formation of link phosphoramidite **3.6** with both metal centres in good yields, ready for use in automated DNA synthesis.

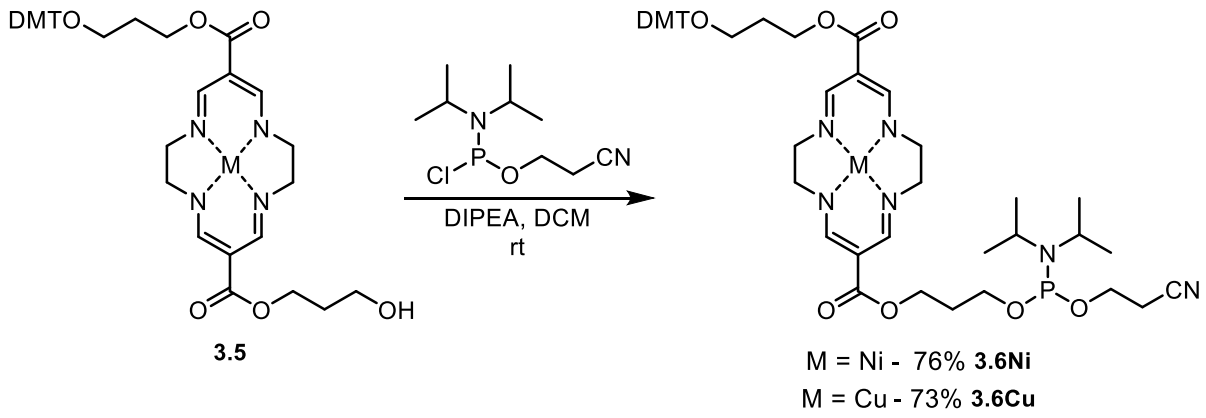

Scheme 3.12: Phosphitylation of DMT protected cyclidene link.

3.3.4. Synthesis of Cyclidene Tag System

3.3.4.1. Synthesis of Tag Diol

As with the link system, the formation of the tag system required forcing conditions to functionalise the ester units, as shown in Scheme 3.13.[79] The reaction struck a balance between achieving a reasonable yield of the desired mono-product **3.7Cu** whilst minimising the bis-tag side product.

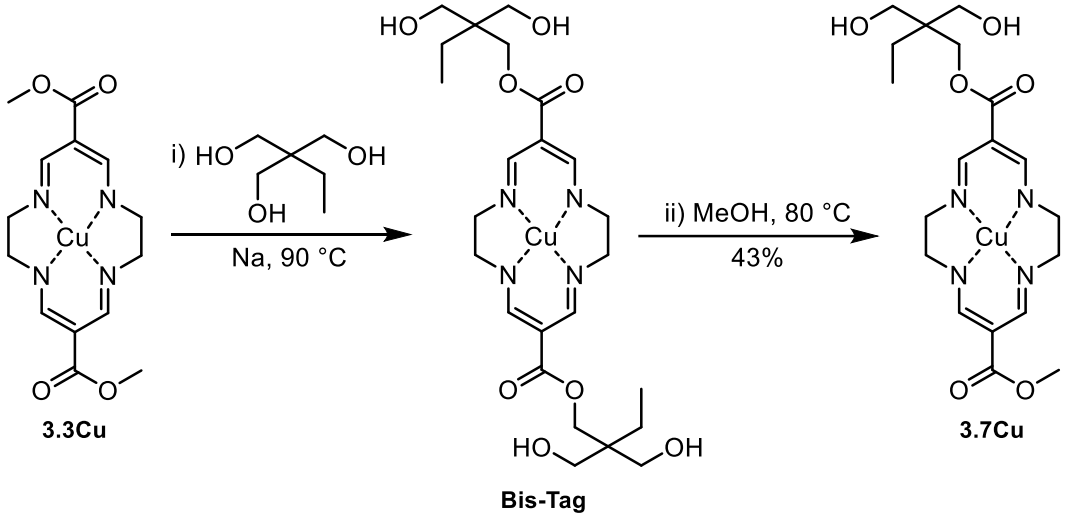

Scheme 3.13: Formation of the cyclidene tag diol. Reaction proceeds via the over-substituted bis tag system.

The reaction converted **3.3Cu** to the over-substituted bis-tag, before gradual conversion back to the desired mono-product. The structure of tris(hydroxymethyl)propane is crucial to installing the tag framework but upon heating the three hydroxyl units formed a strong hydrogen bonding network that gave the reaction mixture a viscid nature that resembled a thick syrup rather than a solution. Consequently, it was a challenge just to get the magnetic stirrer bar to uniformly stir the mixture and so the reaction proceeds at different rates, affording limited control over the selectivity.

Upon complete conversion of **3.3Cu** to the bis-tag, methanol was added to the mixture to aid mixing as well as allowing a second transesterification to form the desired mono-tag **3.7Cu**. A

minor variation to the literature conditions found that only adding methanol and allowing the sodium metal already present in the reaction mixture to facilitate the conversion, as opposed to adding fresh sodium metal, provided a boost to the yield. These conditions allowed conversion to the desired mono-tag product, whilst minimising the conversion of mono-tag back to starting material **3.3Cu**. When this optimum point was reached, the reaction was stopped and the desired product isolated by column chromatography. Any starting material or bis-tag was recovered and rereacted. To maximise material for use in developing the electrochemical sensing capabilities of the cyclidene tag, only the Cu^{2+} complex was synthesised at a significant scale.

3.3.4.2. Preparation for DNA Synthesis: DMT Protection

The formation of mono-DMT protected tag **3.8Cu** was achieved using similar conditions to those used with the link system, Scheme 3.14. The selectivity was aided by the proximity of the two hydroxyl groups to one another, with the formation of any bis-protected side-products sterically unfavourable. The molar equivalent amounts of DMTCl to cyclidene tag diol **3.7Cu** were still controlled but DMAP was not used and only on rare occasions were

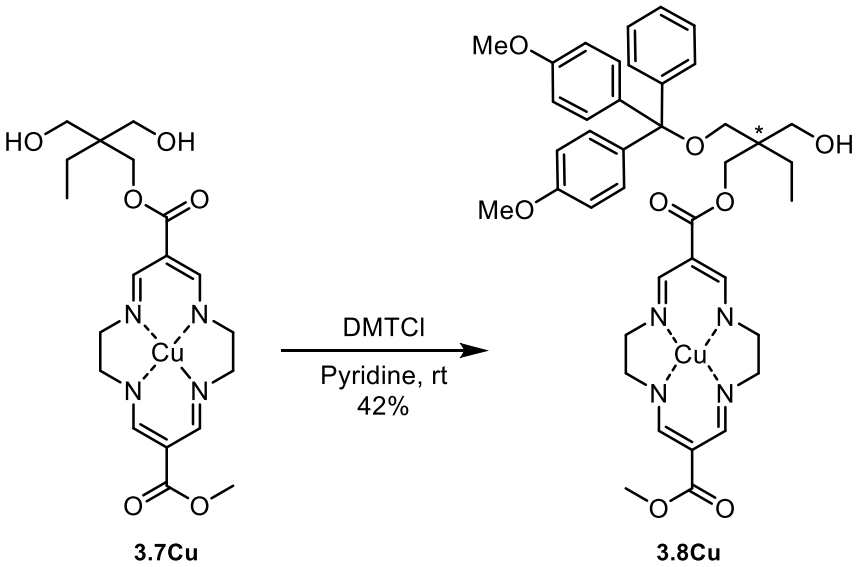

3.7Cu **3.8Cu**

*Scheme 3.14: Tritylation of cyclidene tag diol. The stereogenic centre is designated by *.*

minimal amounts of side-product formed. This resulted in a higher yield observed for the tag system over the link system, although a significant amount of the diol remained unreacted as previously observed.

It is important to note that the protection of one of the alcohol units of the tag moiety created a stereogenic centre, with both configurations retained following incorporated into DNA.[79]

3.3.4.3. Preparation for DNA Synthesis: Phosphitylation

Phosphoramidite **3.9Cu** was formed as detailed in the literature along with the adjustments to the work-up and purification outlined for the link system. Implementation of these tweaks alongside employing a reduced polarity eluent system during column chromatography afforded the product in an improved yield, Scheme 3.15.[79]

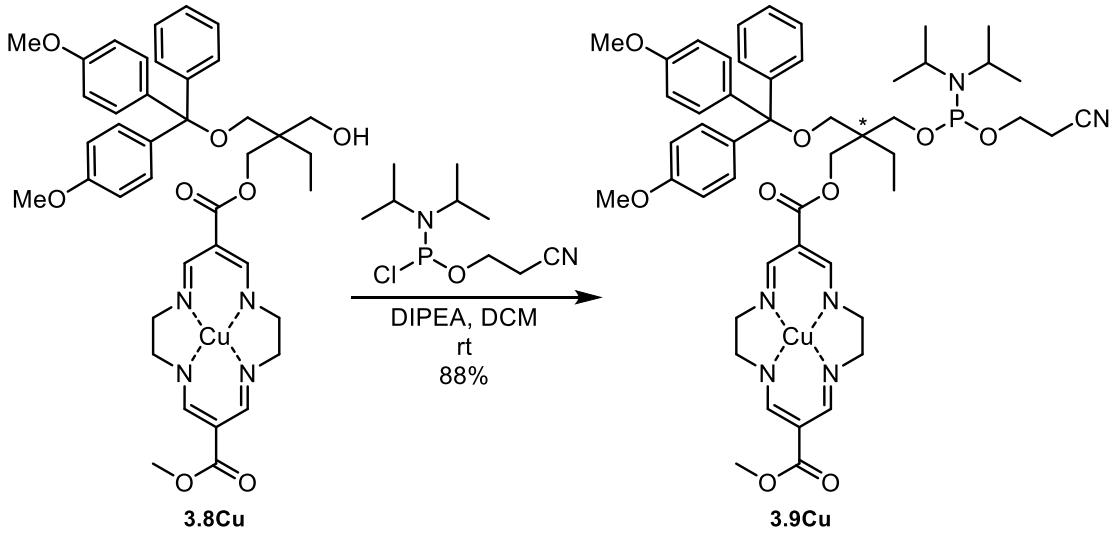

Scheme 3.15: Phosphitylation of cyclidene tag system.

Following careful storage under argon and in the freezer at -18 °C, all cyclidene phosphoramidites were dissolved in anhydrous acetonitrile at a concentration of 0.1 M immediately before attachment to the DNA synthesiser for automated solid-phase synthesis.

3.4. Incorporation into DNA

3.4.1. DNA Synthesis

After synthesising cyclidene-oligonucleotides under a variety of standard and mild conditions, the cyclidene complexes were found to be susceptible to oxidation when using oxidiser solution at a higher concentration (0.1 M iodine, as used in the standard automated synthesis process). Mass spectrometry studies identified the problem, with modified cyclidene strands possessing a mass 15 m/z higher than expected. The extra mass units were attributed to the presence of an oxygen atom associated with the oxidised cyclidene complex. Consequently, all incorporations of cyclidene moieties into DNA had to be performed using the milder 0.02 M iodine oxidising solution, which shows no trace of oxidising the cyclidene unit. All cyclidene-modified strands detailed in this thesis were synthesised using ultra-mild conditions.

3.4.2. Purification and Characterisation

The crude oligonucleotide sample contains a mixture of truncated strands, impurities and by-products from the deprotection/capping steps alongside the desired DNA strand. Reverse-phase HPLC using an acetonitrile/triethylammonium acetate buffer gradient eluent system is employed to purify the crude mixture before characterisation with mass spectrometry. The exact eluent system depends on the oligonucleotide length and modification, with cyclidene-modified strands having a greater retention time through the column compared to their unmodified counterparts due to their enhanced lipophilicity and hydrophobicity. The exact solvent conditions used for each strand are detailed in *Chapter 5: Experimental, section 5.5.2* alongside the full characterisation by mass spectrometry and analytical HPLC in *Chapter 6: Appendix*.

The oligonucleotide strands subsequently discussed in this chapter contain the nickel cyclidene link system and have been studied with a view to improving the electrochemical detection and characterisation of the Ni^{2+} complex, alongside exploring multiple incorporations of cyclidene units into DNA. Both features are crucial for the application of cyclidene-DNA conjugates in nanotechnologies such as molecular wires. *Chapter 4* focuses on the copper tag system and its development as a biosensor.

3.5. Electrochemical Detection of Nickel Cyclidene Strands

3.5.1. Introduction

3.5.1.1. Redox Activity of Cyclidene Complexes

The electrochemistry of the Ni^{2+} and Cu^{2+} cyclidene macrocycles, **3.3Ni** and **3.3Cu**, respectively, has been well documented by Kowalski, Korybut-Daszkiewicz and colleagues.[89, 91] A reported cyclic voltammogram (CV) of **3.3Cu** possesses a redox peak with a half-wave potential ($E_{1/2}$) of 566 mV *vs* Ag/AgCl in acetonitrile, whereas the $E_{1/2}$ of **3.3Ni** is more positive at 783 mV. Both these processes are near-reversible and show no signs of chemical adsorption or instability.[89]

The significant shift to a more positive potential for the nickel complex reflects the different electron configurations of the two cations and their preferred geometries. Oxidation of the d^9 Cu^{2+} cation to the d^8 Cu^{3+} makes it more suitable for a square planar geometry, ideal for the cyclidene complex. The Ni^{2+} cation however, already possesses the square planar geometry preferred by its d^8 electron configuration, which makes oxidation more unfavourable.

A similar effect was observed when electrochemically probing the larger 15- and 16-membered copper cyclidene analogues.[89] As the ring size increased, the $E_{1/2}$ values were found to shift to more positive potentials. The larger ring systems are more flexible and can deviate from the ideal planar environment desired by the oxidised cation, which means that the structural benefit acquired by oxidising the Cu^{2+} cation is less apparent. Conversely, the nickel complexes with the larger macrocycles exhibit only minor shifts as the deviation from planarity is of little consequence to the d^7 Ni^{3+} centre.

3.5.1.2. Redox Activity in DNA

Inserting reporter groups into DNA can lead to changes to their output signals as they enter a more hydrophobic environment. These changes often take the form of shifts in wavelength or potential for fluorescent or redox signals, respectively. In the case of the copper cyclidene systems, incorporation into DNA shifted the redox potentials to more negative values, the tag systems possessing an $E_{1/2}$ of *ca.* 440 mV *vs* Ag/AgCl, and the link systems *ca.* 429 mV, a shift of over -100 mV compared to **3.3Cu** (566 mV).[79]

One of the main challenges in taking electrochemical measurements of DNA samples in comparison to small synthetic compounds is the need to use aqueous buffers rather than organic solvents. This is an issue because salts in the buffers can partake in electrochemical process and absorb onto the electrode surface, leading to strong peaks and background currents in the CV. This limits the accessible potential window that redox active species can be observed in. Alongside the buffer conditions, this window is influenced by the composition of the working electrode.[82] The redox processes of the copper cyclidene-oligonucleotides

could be observed in this window using a glassy carbon working electrode, however the nickel analogues could not. Neither could be observed using a gold electrode.[79]

3.5.2. Synthesised DNA Strands

Two DNA strands containing the Ni^{2+} cyclidene link at their centre were synthesised and investigated electrochemically. The sequences of the strands are outlined in Table 3.1 and include a 40mer with twenty nucleobases either side of the metal complex, and a 10mer. The characterisation of the strands by mass spectrometry and analytical HPLC is detailed in *Appendix section 6.2.1.*

Table 3.1: The two cyclidene-DNA conjugates synthesised for electrochemical studies. X = the nickel cyclidene link system.

Name	*Sequence*
NiLink10mer	5' - CC GGG **X** CCC GG - 3'
NiLink40mer	5' – GCA ATA CTA TTT CGA TCT GG **X** AC ATG GTA GAA GGA GGA AAG – 3'

NiLink10mer was to be the focus of the initial investigations. Along with its shorter length, which could be beneficial for detecting the redox signal, the strand is palindromic and therefore capable of self-dimerising. This was thought to be advantageous in the analysis of duplexes as both strands would contain a complex, which should increase the current signal intensity. If the redox signal of the 10mer could be successfully detected, **NiLink40mer** would offer the challenge of detecting the nickel redox couple in a longer strand which was more susceptible to forming secondary structures.

3.5.3. Visualising the Nickel Redox Signal

The inability to visualise the nickel(II/III) redox couple in previous work[92] may result from two things: it could have either been lost in the background current, or occurred outside of the potential window that could be accessed by the working electrode. One way to enhance the signal is to simply use a higher concentration of the modified strand. However, even at a 50 µM concentration used for solution-based electrochemical studies (a relatively low concentration for conventional cyclic voltammetry), the amount of synthetic DNA required for each experiment is large. Using even more material is impractical and not a viable way forward.

3.5.3.1. Varying the Buffer Conditions

A simple way that the accessible potential window could potentially be extended is by varying the buffer conditions in order to minimise any background current. The initial published work was conducted using a glassy carbon working electrode in a 10 mM tris HCl buffer at pH 7.0 with 100 mM NaCl salt.[92] The onset of surface oxidation, caused by different species and

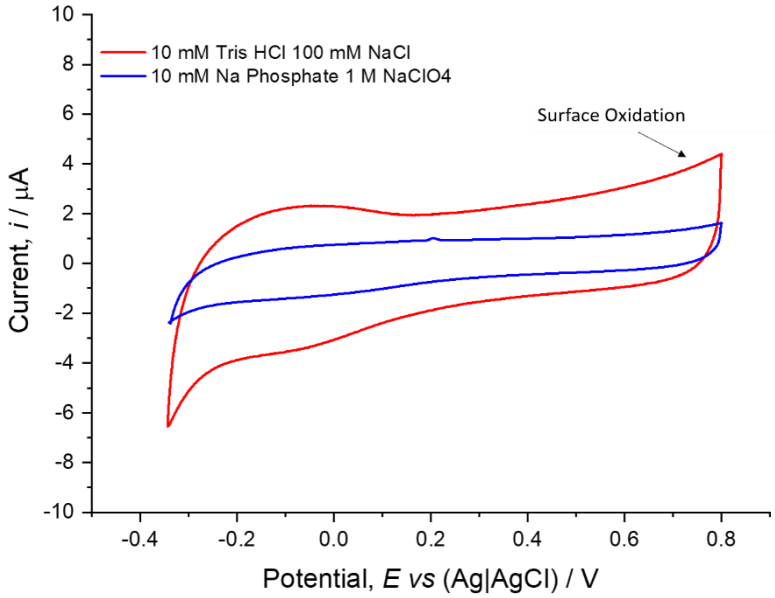

Figure 3.25: Overlaid cyclic voltammograms comparing 10 mM tris HCl buffer (pH 7.0), 100 mM NaCl with 10 mM sodium phosphate buffer pH 7.0, 1 M $NaClO_4$ on a glassy carbon working electrode. Scan rate: 100 mV s^{-1}.

adsorbing anions in the buffer solution, led to a peak in the CV around 0.75 to 1 V which limited the visibility in that potential range. In recent years, work within the group has found that a 10 mM sodium phosphate buffer (pH 7.0), 1 M $NaClO_4$ has been a suitable electrolyte for sensing experiments involving ferrocene-modified nucleic acids. Importantly, when compared to 10 mM tris HCl buffer (pH 7.0), 100 mM NaCl, as shown in Figure 3.25, it was found to have a significantly smaller surface oxidation peak and background current, allowing a marginally wider potential window.

Interestingly, the presence of **NiLink10mer** could be detected in both buffers as shown in Figure 3.26. Whilst both CVs clearly display the nickel (II/III) redox couple, the signals are fairly faint against the background buffer signal. This suggests that previous attempts to visualise the nickel cyclidene systems were thwarted by the background current, rather than by the signal occurring outside of the accessible potential window. However, it is possible that the palindromic design of the 10mer, alongside its shorter length, has helped to sufficiently enhance the signal intensity enough so that it can be detected.

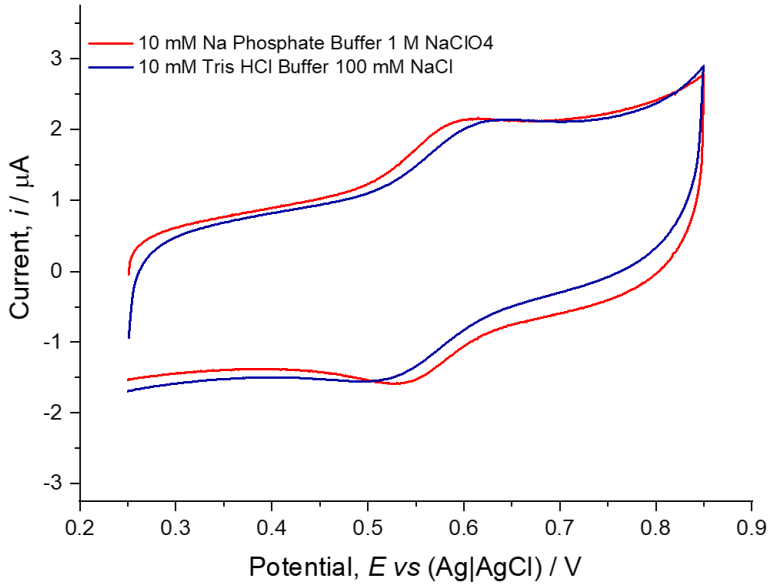

Figure 3.26: Cyclic voltammograms of the NiLink10mer (50 µM) in 10 mM sodium phosphate buffer (pH 7.0) 1 M $NaClO_4$ (red) and 10 mM tris HCl buffer (pH 7.0) 100 mM NaCl (blue). Measurements performed on a glassy carbon working electrode. Potential window: 250 to 850 mV Scan rate: 100 mV s^{-1}

Table 3.2: The oxidation E_{pa} and reduction E_{pc} potentials vs Ag/AgCl and the difference between them ΔE_p, along with the half-wave potential $E_{1/2}$ vs Ag/AgCl of the nickel cyclidene-modified 10mer in 10 mM tris HCl buffer (pH 7.0) 100 mM NaCl and 10 mM sodium phosphate buffer(pH 7.0) 1 M $NaClO_4$.

Buffer	E_p^a	E_p^c	ΔE_p	$E_{1/2}$ *Potential*
Sodium Phosph.	600 mV	532 mV	68 mV	566 mV
Tris HCl	629 mV	508 mV	121 mV	568 mV

Table 3.2 reports the redox potential data from the CVs in Figure 3.26. It is evident that the quality of the CV recorded in the sodium phosphate buffer is greater than that in the tris HCl buffer, which leads to a far wider peak separation, ΔE_p. This indicates that the nickel redox centre is not exhibiting electrochemically reversible behaviour in the tris buffer conditions. However, the half-wave potentials, $E_{1/2}$, in the two buffers are almost identical, as expected. At 566 mV, the half-wave potential of the nickel cation has been significantly shifted to a less-positive potential upon incorporation into DNA ($E_{1/2}$ for **3.3Ni** = 783 mV). This trend is similar to what was found for its copper counterpart and suggests that the surrounding nucleobases and negatively charged phosphate backbone of DNA impart additional stability to the oxidised nickel complex. The intercalating ability of the cyclidene and subsequent π-stacking interactions are also likely to contribute to this stability.

3.5.3.2. Varying the Working Electrode: Boron Doped Diamond

The type of working electrode surface can also affect the size of the accessible potential window as buffer species may interact with different surfaces to varying extents. Tucker and co-workers used a glassy carbon electrode for the initial studies.[79] The interface between glassy carbon and the solution has a high capacitance, which leads to a large capacitive current. However, studies using a gold working electrode were unable to detect even the copper cyclidene complex, let alone its more challenging nickel analogue, making it a poorer choice because many electrolyte anions adsorb on the gold surface.

An alternative working electrode material which has recently been developed is boron-doped diamond (BDD).[93, 94] It offers the widest accessible potential window of all electrodes, alongside a low background signal, resulting from lower capacitance and a greater resistance to surface fouling. These properties are demonstrated in Figure 3.27, which compares a BDD working electrode to glassy carbon and polycrystalline gold electrodes in a buffer solution. In

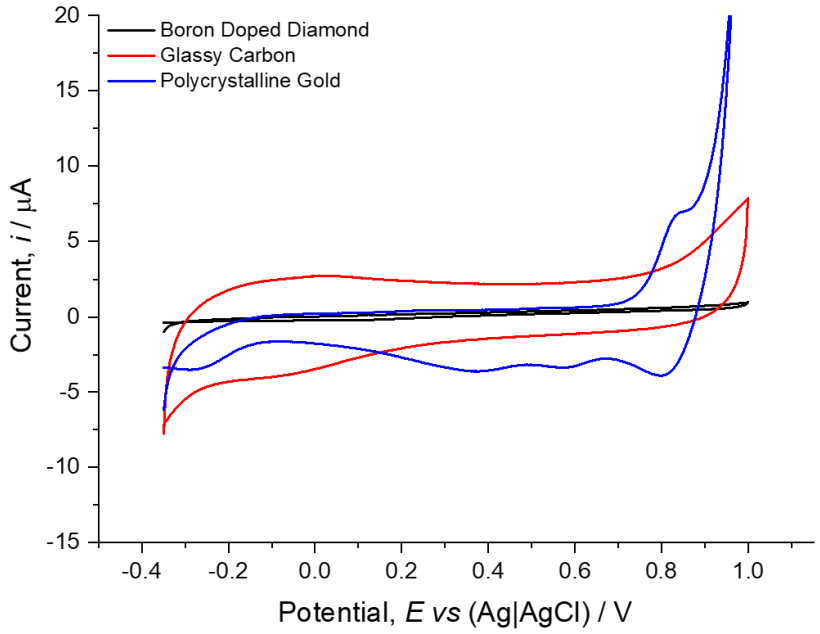

Figure 3.27: Overlaid cyclic voltammograms of three working electrodes (BDD (black), glassy carbon (red) and gold (blue)) in a blank 10 mM tris HCl buffer (pH 7.0) 100 mM NaCl solution. Potential window: -350 mV to 1000 mV. Scan rate: 100 mV s^{-1}

terms of width of the accessible potential window and minimising any background signal, the BDD electrode is clearly far superior.

Given these results, a CV of **NiLink10mer** was next recorded using the BDD electrode in phosphate buffer, as shown below in Figure 3.28. This successfully decreased the background signal and consequently increased the quality of the nickel redox signal. As expected, the $E_{1/2}$ potential of 566 mV was identical to the value obtained in the same buffer conditions using the glassy carbon electrode. The average peak difference ΔE_p of 67 mV along with the linear relationship in the scan rate dependence plots (*Appendix section 6.2.3*) indicates near-reversible electrochemical behaviour, as also observed for the nickel cyclidene monomer, as discussed above.[89] Finally, when subjected to repeated cycling, there was no evidence of strand degradation to the modified strand in the CV (Figure 3.28).

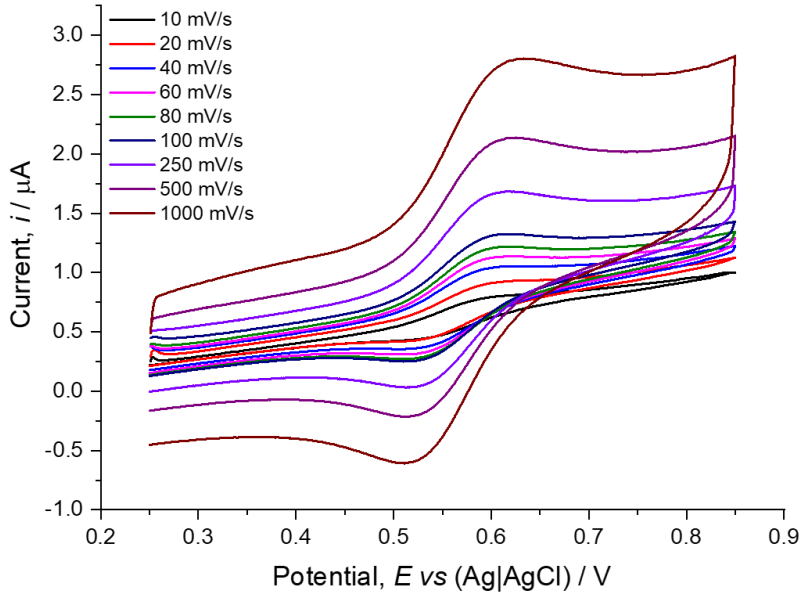

Figure 3.28: CVs of 50 µM NiLink10mer oligonucleotide in a 10 mM sodium phosphate buffer pH 7.0, 1 M $NaClO_4$ solution recorded using the boron-doped diamond working electrode. Potential window: 250 mV to 850 mV.

Attention then turned to the longer **NiLink40mer**, which proved harder to detect than the shorter strand. Surprisingly, the sodium phosphate buffer conditions were unsuitable for detecting the nickel redox chemistry, while a tris buffer, which gave inferior quality data with the 10mer, was more successful. Crucially, lower scan rates had to be employed to capture the redox signal above the background current. Even though BDD electrodes offer a low background signal, the nickel redox signal is far weaker in the longer DNA strand. This is to be expected as a larger strand would lead to slower diffusion to and from the electrode surface. It is also possible that the greater amount of DNA limits the electron transfer from the redox centre to the electrode surface.

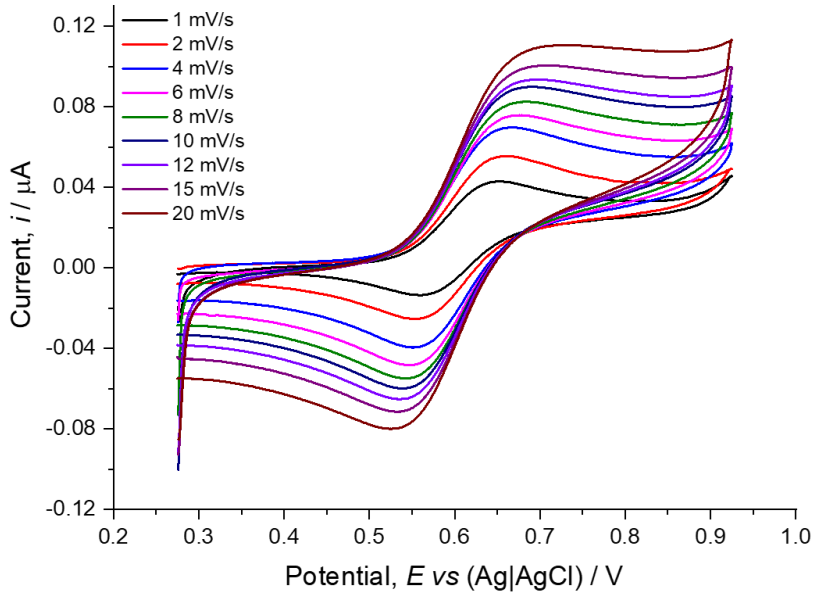

Figure 3.29: CVs of 25 µM NiLink40mer oligonucleotide in a 10 mM tris HCl buffer pH 7.0, 1 M NaCl solution recorded using the boron-doped diamond working electrode. Potential window: 275 mV to 925 mV.

Once the conditions had been fine-tuned, it was found that the redox signal could be detected using half the concentration (25 µM) of modified oligo normally used in the group for solution-based electrochemistry of DNA, Figure 3.29. The CV has a larger background signal than the 10mer, but still clearly shows the oxidation and reduction redox peaks. Halving the

amount of oligo required for the same signal is hugely advantageous due to the amount of material required to perform solution-based electrochemistry, as discussed above.

Table 3.3: The oxidation E_p^a and reduction E_p^c potentials and the difference between them ΔE_p, along with the half-wave potential $E_{1/2}$ of the nickel cyclidene monomer and modified 10mer and 40mer oligos recorded on the BDD electrode. CVs of oligos recorded in the conditions listed above, monomer 3.4Ni recorded dry DCM with $TBAPF_6$ electrolyte, [3.4Ni] = 1 mM.

Strand	E_{pa}	E_{pc}	ΔE_p	$E_{1/2}$ *Potential*
NiLink10mer	599 mV	532 mV	67 mV	566 mV
NiLink40mer	555 mV	658 mV	103 mV	607 mV
3.4Ni Monomer	779 mV	845 mV	59 mV	816 mV

Table 3.3 summarises the potentials of the CVs of the nickel cyclidene link oligos and the monomer **3.4Ni** recorded using the BDD electrode. The half-wave potential recorded for link diol **3.4Ni** was more positive than the literature value reported for **3.3Ni** (783 mV)[89] whilst the ΔE_p value was smaller, indicating a more electrochemically reversible behaviour.[89] Upon incorporation into DNA, $E_{1/2}$ shifted to a less positive half-wave potential as previously noted, with a larger shift observed for the **NiLink10mer**. **NiLink40mer** also had a far larger ΔE_p, which suggests quasi-reversible behaviour due to a slower electron transfer rate.

3.5.4. Conclusion

The challenge of studying the nickel cyclidene-DNA conjugates using electrochemistry has been overcome, largely through the use of a boron-doped diamond working electrode. The combination of a low background signal and a wide potential window has allowed informative cyclic voltammograms to be recorded of a superior quality to those using glassy carbon or gold electrodes. With the redox chemistry of these nickel complexes now accessible and

characterised, investigations can begin towards utilising them in more advanced DNA assemblies.

3.6. Multiple Cyclidene DNA-backbone Modifications

This section describes initial investigations into the feasibility of spacing multiple cyclidene link complexes along the phosphate backbone of DNA.

3.6.1. Previous Work

Within the initial investigations into cyclidene-DNA conjugates, Tucker and co-workers reported the synthesis of three DNA strands containing double incorporations of copper link and tag cyclidene systems, Table 3.4.[79]

Table 3.4: The double copper cyclidene incorporation strands made by Tucker and co-workers. X represents the cyclidene modification.

Modification, X	*Sequence*
Cu-Tag(S) - Cu-Tag(S)	5’ - TGG ACT C - **X** - **X** - C TCA ATG - 3’
Cu-Tag(R) - Cu-Tag(R)	5’ - TGG ACT C - **X** - **X** - C TCA ATG - 3’
Cu-Link - Cu-Link	5’ - TGG ACT C - **X** - **X** - C TCA ATG - 3’

The results demonstrate that two cyclidene complexes can be incorporated consecutively into the phosphate backbone. Interestingly, thermal melting studies indicated that this arrangement gave the duplex formed with a complementary target strand a greater stability than the single cyclidene link modifications, perhaps through increased π-interactions. It is an important demonstration of macrocycles being used to selectively append multiple metal cations to DNA, not dissimilar to some of the metal base pairs previously discussed.[64] The

ability to do this with such robust macrocycle systems has tremendous potential for the fabrication of DNA assemblies with multiple and different metal units.

3.6.2. Synthesis of Triple Cyclidene DNA

After the initial studies, questions remained about the development of such systems. The initial work used copper complexes and it remained to be seen whether the nickel complexes could also be used for multiple incorporations, which would open the door towards hetero-metallic DNA assemblies. As the initial design had the two complexes neighbouring one another, it was decided to design a system in which the metal centres were separated from one another. Therefore, the 30mer sequence in Table 3.5 was synthesised containing three nickel cyclidene link complexes along the phosphate backbone, separated by ten nucleobases. The characterisation data is presented in *Appendix section 6.2.1.*

Table 3.5: The triple-modified DNA strand. X represents the nickel cyclidene link system.

Name	*Sequence*
3NiLink30mer	5’ - TTG TG - **X** - TT ATT GGT CA - **X** - TT AGG TTG AA - **X** - CC GAT - 3’

Despite the advanced design of the **3NiLink30mer**, the strand yields were not dissimilar to those of the mono-modified **NiLink40mer**, indicating again that automated solid-phase synthesis was compatible with the fabrication of longer strands containing several complexes.

3.6.3. UV-vis Characterisation

The bright colours of the cyclidene-metal complexes arise from Soret-like bands.[79] A full account of the UV-vis properties of the various cyclidene systems has been given previously.[92] The complexes are so intense that the cyclidene-modified strands appear coloured by eye at micromolar concentrations. This is neatly demonstrated by comparing solutions of **NiLink40mer** and **3NiLink30mer**; the mono-cyclidene strand at 1 µM has a weak orange colour, whilst the sequence containing three nickel cyclidene complexes at the same concentration is a stronger, deeper orange. These observations were supported by the UV-vis absorption spectra of the strands in Figure 3.30.

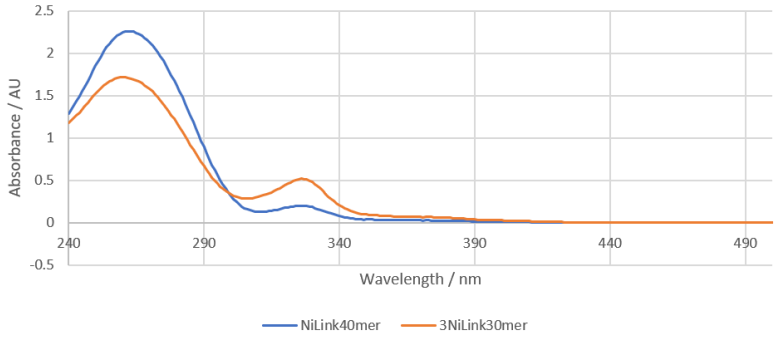

Figure 3.30: Baseline-corrected UV-vis spectrum displaying the absorbances for NiLink40mer and 3NiLink30mer (1 µM) in 10 mM sodium phosphate buffer (pH 7.0) 100 mM NaCl, 20 °C.

The spectrum possesses an intense peak at 260 nm that corresponds to nucleobase absorption. The strong band from 300-350 nm arises from a π-π* transition, whilst the weak shoulder from 340-390 nm is attributed to a Q band.[79, 92] Both these absorbances originate from the nickel cyclidene complex. The two spectra are in keeping with the structural features of each strand; the longer **NiLink40mer** has a more intense peak at 260 nm by virtue of its longer DNA sequence, whilst **3NiLink30mer** displays stronger absorbances between 300 and 390 nm due to it having three times the number of nickel cyclidene units.

3.6.4. Electrochemical Analysis

Following the success of the BDD electrode with the nickel cyclidene-DNA conjugates detailed previously, the **3NiLink30mer** was subjected to electrochemical analysis *via* cyclic voltammetry. The strand was visualised using the same buffer conditions and low scan rates employed for **NiLink40mer**.

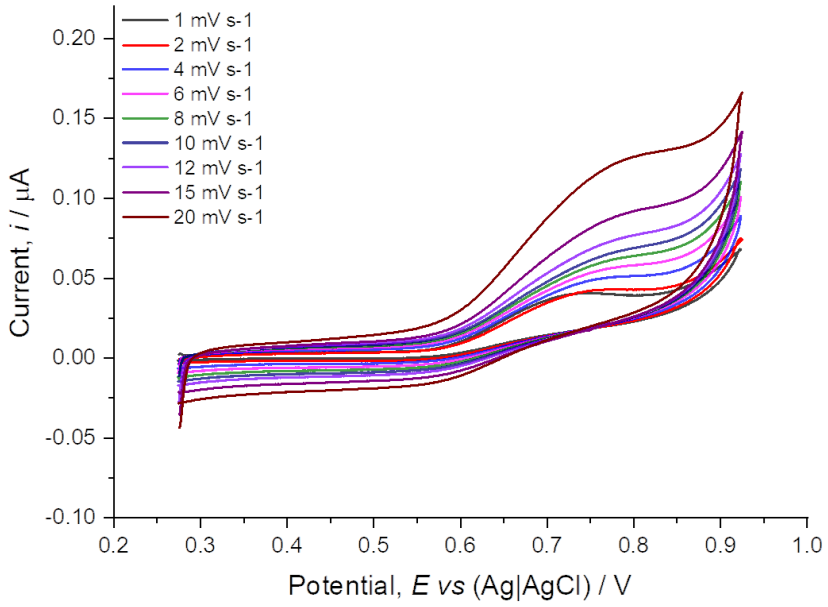

Figure 3.31: CVs of 50 µM 3NiLink30mer oligonucleotide in a 10 mM tris HCl buffer (pH 7.0), 1 M NaCl solution recorded using the boron-doped diamond working electrode. Potential window: 275 mV to 925 mV.

From the cyclic voltammogram presented above in Figure 3.31 there are two main observations. The oxidation peak, in comparison to CVs run on the nickel cyclidene oligos previously, occurs at a more positive potential, at 739 mV. This indicates that oxidising three nickel centres is more unfavourable than oxidising one, possibly due to the fact that three positively charged complexes are being formed. The second observation is that there is no return (reduction) peak. This indicates that following the electrochemical oxidation, some sort of physicochemical process occurs more quickly than the time taken to sweep back at the fastest scan rate. A simple explanation for this is that the oxidation event has caused the

strand to degrade, whilst it is also possible that a chemical reaction or electrode adsorption has occurred. Whilst the exact reason for this lack of reversibility is unclear, an interesting test would be to make the equivalent copper cyclidene strand and probe its electrochemistry.

3.6.5. Conclusion

An oligonucleotide has been synthesised containing three separate nickel cyclidene link moieties. Initial investigations into the properties of this sequence have begun, with the absorbance and electrochemical characteristics reported. Future investigations should investigate duplex formation of the strand, and circular dichroism and thermal melt studies would further inform its structural properties. For such systems to be of use in the construction of multi-component redox-active assemblies, its electrochemical properties would have to be improved. The substitution of nickel with a copper redox centre could be a solution in this regard or surface immobilisation (as discussed in the next chapter).

The successful development of **3NiLink30mer** also raises the intriguing possibility of a linear, or even circular,[95, 96] DNA strand containing multiple cyclidene complexes possessing a combination of copper and nickel cations. A precedent of combining the two metals has been set by Korybut-Daszkiewicz *et al.* with the creation of a dual-link system. The electrochemical properties of the molecule have also been reported, which would provide a useful reference to any studies on a hetero-metallic system.[97]

3.7. Conclusions and Future Work

Robust methodologies for the synthesis of the cyclidene macrocycle, its copper and nickel complexes, and subsequent construction of the tag and link systems have been established within the group for the first time. The complexes were incorporated into a range of oligonucleotides. The work reported in this thesis, alongside the previously published work, has led to the development of a family of metal-functionalised oligonucleotides, Figure 3.32. The most promising of these systems, that utilises the copper tag for DNA sensing applications, will be discussed in *Chapter 4.*

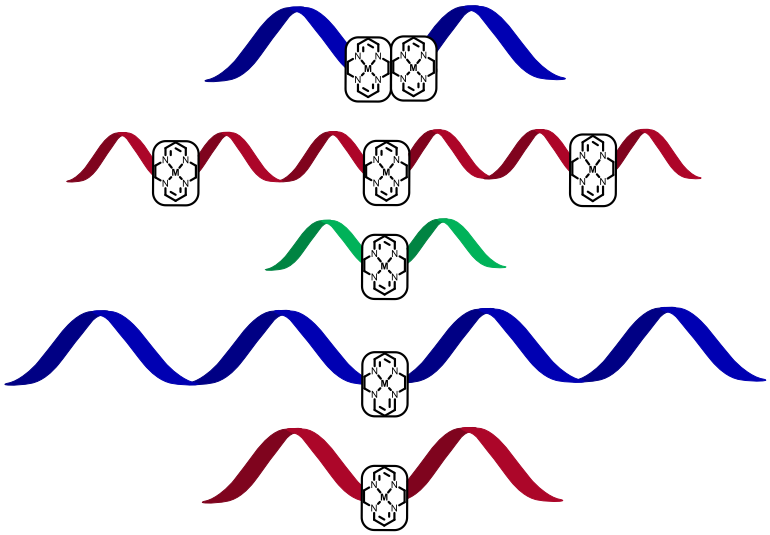

Figure 3.32: A variety of cyclidene-modified oligonucleotides have been synthesised. The family contains DNA of a range of lengths, with a varying number of modification sites.

This work has overcome previously reported issues with the electrochemistry of the nickel complex,[92] allowing future studies to examine the electrochemical sensing ability of the nickel tag for a comparison with the analogous copper system. The ability to incorporate metal complexes at multiple sites along the DNA backbone is an exciting development that could lead to the fabrication of more advanced metal assemblies such as DNA-nanowires. Initial investigations towards utilising such cyclidene systems in self-assembling nanostructures have already been conducted.[98] Of great interest is the prospect of incorporating both the

copper and nickel complexes at multiple sites along the oligonucleotide. This allows a range of metal-modified strands to be created, ranging from robust alternatives to metal-based pairs to an entire metal-containing backbone as in the case of FcNA.[64, 76]

One synthetic challenge that remains to be addressed is pre-programming the chirality of the tag system. The current route creates a stereogenic centre which leads to the production of diastereomers upon incorporation into DNA. At this time, the *R*-isomer is of value in sensing applications, whilst the *S*-isomer, half the material produced, goes to waste. Coupling the macrocycle to an enantiopure linker unit such as a threoninol linker would allow for the sole manufacture of the desired isomer. Investigations into employing the trimethyl aluminium coupling conditions discussed in *Chapter 2* were unsuccessful, due to solubility issues and the low reactivity of the cyclidene methyl ester. Likewise, initial attempts to hydrolyse the ester to a carboxylic acid, a functional group with a greater tendency to couple with the amine unit of the threoninol, were also unsuccessful but are likely to provide a suitable path forward.

3.8. References

1. E. S. Lander, *Nature*, 2011, **470**, 187.
2. F. H. C. Crick, *Nature*, 1970, **227**, 561.
3. J. D. Watson and F. H. C. Crick, *Nature*, 1953, **171**, 737.
4. G. M. Blackburn and M. J. Gait, *Nucleic Acids in Chemistry and Biology*, Royal Society of Chemistry, Cambridge, 1990.
5. L. A. Pray, *Nature Education*, 2008, **100**, 1.
6. A. L. Price, C. C. A. Spencer and P. Donnelly, *Proc. R. Soc. B*, 2015, **282**, 1.
7. D. G. Wang, J.-B. Fan, C.-J. Siao, A. Berno, P. Young, R. Sapolsky, G. Ghandour, N. Perkins, E. Winchester, J. Spencer, L. Kruglyak, L. Stein, L. Hsie, T. Topaloglou, E. Hubbell, E. Robinson, M. Mittmann, M. S. Morris, N. Shen, D. Kilburn, J. Rioux, C. Nusbaum, S. Rozen, T. J. Hudson, R. Lipshutz, M. Chee and E. S. Lander, *Science*, 1998, **280**, 1077.
8. A. J. Brookes, *Gene*, 1999, **234**, 177.
9. R. Karki, D. Pandya, R. C. Elston and C. Ferlini, *BMC Med. Genomics*, 2015, **8**, 37.
10. J. H. A. Duprey, D. M. Bassani, E. I. Hyde, G. Jonusauskas, C. Ludwig, A. Rodger, N. Spencer, J. S. Vyle, J. Wilkie, Z. Zhao and J. H. R. Tucker, *Org. Biomol. Chem.*, 2018, **16**, 6576.
11. K. Nakatani, *ChemBioChem*, 2004, **5**, 1623.
12. J. R. Hart, Y. Zhang, L. Liao, L. Ueno, L. Du, M. Jonkers, J. R. Yates and P. K. Vogt, *PNAS*, 2015, **112**, 1131.
13. I. Ewing, J. J. Hurley, E. Josephides and A. Millar, *Frontline Gastroenterology*, 2014, **5**, 26.
14. E. R. Cantwell-Dorris, J. J. O'Leary and O. M. Sheils, *Mol. Cancer Ther.*, 2011, **10**, 385.
15. Z. Hélias-Rodzewicz, E. Funck-Brentano, L. Baudoux, C. K. Jung, U. Zimmermann, C. Marin, T. Clerici, C. L. Gall, F. Peschaud, V. Taly, P. Saiag and J.-F. Emile, *BMC Cancer* 2015, **15**, 1.
16. H. Davies, G. R. Bignell, C. Cox, P. Stephens, S. Edkins, S. Clegg, J. Teague, H. Woffendin, M. J. Garnett, W. Bottomley, N. Davis, E. Dicks, R. Ewing, Y. Floyd, K. Gray, S. Hall, R. Hawes, J. Hughes, V. Kosmidou, A. Menzies, C. Mould, A. Parker, C. Stevens, S. Watt, S. Hooper, R. Wilson, H. Jayatilake, B. A. Gusterson, C. Cooper, J. Shipley, D. Hargrave, K. Pritchard-Jones, N. Maitland, G. Chenevix-Trench, G. J. Riggins, D. D. Bigner, G. Palmieri, A. Cossu, A. Flanagan, A. Nicholson, J. W. C. Ho, S. Y. Leung, S. T. Yuen, B. L. Weber, H. F. Seigler, T. L. Darrow, H. Paterson, R. Marais, C. J. Marshall, R. Wooster, M. R. Stratton and P. A. Futreal, *Nature*, 2002, **417**, 949.
17. H. Yang, B. Higgins, K. Kolinsky, K. Packman, Z. Go, R. Iyer, S. Kolis, S. Zhao, R. Lee, J. F. Grippo, K. Schostack, M. E. Simcox, D. Heimbrook, G. Bollag and F. Su, *Cancer Res*, 2010, **70**, 5513.
18. W. Kim, S. Lee, H. S. Kim, M. Song, Y. H. Cha, Y.-H. Kim, J. Shin, E.-S. Lee, Y. Joo, J. J. Song, E. J. Choi, J. W. Choi, J. Lee, M. Kang, J. I. Yook, M. G. Lee, Y.-S. Kim, S. Paik and H. Kim, *Genome Res.*, 2018, **28**, 1.
19. A. D. Cox, S. W. Fesik, A. C. Kimmelman, J. Luo and C. J. Der, *Nat. Rev. Drug. Discov.*, 2014, **13**, 828.
20. Y. Imamura, T. Morikawa, X. Liao, P. Lochhead, A. Kuchiba, M. Yamauchi, Z. R. Qian, R. Nishihara, J. A. Meyerhardt, K. M. Haigis, C. S. Fuchs and S. Ogino, *Clin. Cancer Res.*, 2012, **18**, 4753.
21. Y. Samuels and T. Waldman, *Curr. Top. Microbiol. Immunol.*, 2010, **347**, 21.
22. E. Li and Y. Zhang, *Cold Spring Harb. Perspect. Biol.*, 2014, **6**, 1.
23. G. Egger, G. Liang, A. Aparicio and P. A. Jones, *Nature*, 2004, **429**, 457.
24. P. A. Jones and S. B. Baylin, *Nat. Rev. Genet.*, 2002, **3**, 415.
25. S. L. Beaucage and M. H. Caruthers, *Tetrahedron Lett.*, 1981, **22**, 1859.
26. M. H. Caruthers, S. L. Beaucage, C. Becker, J. W. Efcavitch, E. F. Fisher, G. Galluppi, R. Goldman, P. deHaseth, M. Matteucci and L. McBride, *Gene Amplif. Anal.*, 1983, **3**, 1.

27. T. Brown, Solid-Phase Oligonucleotide Synthesis, https://www.atdbio.com/content/17/Solid-phase-oligonucleotide-synthesis, (accessed 22/07/2020).
28. T. Brown, Purification of Oligonucleotides, https://www.atdbio.com/content/7/Purification-of-oligonucleotides, (accessed 22/07/2020).
29. B. Y. Michel, D. Dziuba, R. Benhida, A. P. Demchenko and A. Burger, *Front. Chem.*, 2020, **8**, 112.
30. D. C. Ward and E. Reich, *J. Biol. Chem.*, 1969, **244**, 1228.
31. H. C. Kolb, M. G. Finn and K. B. Sharpless, *Angew. Chem. Int. Ed.*, 2001, **40**, 2004.
32. A. H. El-Sagheer and T. Brown, *Chem. Soc. Rev.*, 2010, **39**, 1388.
33. T. J. Matray and E. T. Kool, *J. Am. Chem. Soc*, 1998, **120**, 6191.
34. T. J. Matray and E. T. Kool, *Nature*, 1999, **399**, 704.
35. E. T. Kool, *Acc. Chem. Res.*, 2002, **35**, 936.
36. T. J. Bandy, A. Brewer, J. R. Burns, G. Marth, T. Nguyen and E. Stulz, *Chem. Soc. Rev.*, 2011, **40**, 138.
37. J.-L. H. A. Duprey, D. M. Bassani, E. I. Hyde, C. Ludwig, A. Rodger, J. S. Vyle, J. Wilkie, Z. Zhao and J. H. R. Tucker, *Supramol. Chem.*, 2011, **23**, 273.
38. J.-L. H. A. Duprey, Z. Zhao, D. M. Bassani, J. Manchester, J. S. Vylec and J. H. R. Tucker, *Chem. Commun.*, 2011, **47**, 6629.
39. F. Eckstein, *J. Am. Chem. Soc*, 1966, **88**, 4292.
40. R. Gan, X. Wu, W. He, Z. Liu, S. Wu, C. Chen, S. Chen, Q. Xiang, Z. Deng, D. Liang, S. Chen and L. Wang, *Sci. Rep.*, 2014, **4**, 1.
41. P. E. Nielsen, M. Egholm, R. H. Berg and O. Buchardt, *Science*, 1991, **254**, 1497.
42. F. Pellestor and P. Paulasova, *Eur. J. Hum. Genet.*, 2002, **12**, 694.
43. K. K. Jensen, H. Orum, P. E. Nielsen and B. Norden, *Biochemistry*, 1997, **36**, 5072.
44. J. Saarbach, P. M. Sabale and N. Winssinge, *Curr. Opin. Chem. Biol.*, 2019, **52**, 112.
45. H. Häkkinen, *Nat. Chem.*, 2012, **4**, 443.
46. M. Hegner, P. Wagner and G. Semenza, *FEBS Lett.*, 1993, **336**, 452.
47. M.-C. Bourg, A. Badia and R. B. Lennox, *J. Phys. Chem. B*, 2000, **104**, 6562.
48. J. L. Zimmermann, T. Nicolaus, G. Neuert and K. Blank, *Nat. Protoc.*, 2010, **5**, 975.
49. B. Kaur, K. Malecka, D. A. Cristaldi, C. S. Chay, I. Mames, H. Radecki and E. Stulz, *Chem. Commun.*, 2018, **54**, 11108.
50. S. Liu, G. H. Clever, Y. Takezawa, M. Kaneko, K. Tanaka, X. Guo and M. Shionoya, *Angew. Chem. Int. Ed.*, 2011, **50**, 8886.
51. J. Richter, *Physica E*, 2003, **16**, 157.
52. J. C. Genereux and J. K. Barton, *Chem. Rev.*, 2010, **110**, 1642.
53. A. Aggarwal, S. Bag, R. Venkatramani, M. Jain and P. K. Mait, *Nanoscale*, 2020, Advance Article.
54. H. Yang, F. Altvater, A. D. d. Bruijn, C. K. McLaughlin, P. K. Lo and H. F. Sleiman, *Angew. Chem. Int. Ed.*, 2011, **50**, 4620.
55. M. E. Morales, R. S. Derbes, C. M. Ade, J. C. Ortego, J. Stark, P. L. Deininger and A. M. Roy-Engel, *PLoS ONE*, 2016, **11**, 1.
56. J. G. Hengstler, U. Bolm-Audorff, A. Faldum, K. Janssen, M. Reifenrath, W. Gotte, D. Jung, O. Mayer-Popken, J. Fuchs, S. Gebhard, H. G. Bienfait, K. Schlink, C. Dietrich, D. Faust, B. Epe and F. Oesch, *Carcinogenesis*, 2003, **24**, 63.
57. S. Katz, *Biochim. Biophys. Acta.*, 1962, **68**, 240.
58. A. Ono, S. Cao, H. Togashi, M. Tashiro, T. Fujimoto, T. Machinami, S. Oda, Y. Miyake, I. Okamoto and Y. Tanaka, *Chem. Commun.*, 2008, 4825.
59. K. Tanaka and M. Shionoya, *J. Org. Chem.*, 1999, **64**, 5002.
60. K. Tanaka, Y. Yamada and M. Shionoya, *J. Am. Chem. Soc*, 2002, **124**, 8802.

61. S. Vecchioni, M. C. Capece, E. Toomey, L. Nguyen, A. Ray, A. Greenberg, K. Fujishima, J. Urbina, I. G. Paulino-Lima, V. Pinheiro, J. Shih, G. Wessel, S. J. Wind and L. Rothschild, *Sci. Rep.*, 2019, **9**, 6942.
62. K. Tanaka, A. Tengeiji, T. Kato, N. Toyama, M. Shiro and M. Shionoya, *J. Am. Chem. Soc*, 2002, **124**, 12494.
63. K. Tanaka, A. Tengeiji, T. Kato, N. Toyama and M. Shionoya, *Science*, 2003, **299**, 1212.
64. K. Tanaka, G. H. Clever, Y. Takezawa, Y. Yamada, C. Kaul, M. Shionoya and T. Carell, *Nat. Nanotechnol.*, 2006, **1**, 190.
65. H. Yang and H. F. Sleiman, *Angew. Chem. Int. Ed.*, 2008, **47**, 2443.
66. H. Yang, A. Z. Rys, C. K. McLaughlin and H. F. Sleiman, *Angew. Chem. Int. Ed.*, 2009, **48**, 9919.
67. M. Balaz, B. C. Li, J. D. Steinkruger, G. A. Ellestad, K. Nakanishi and N. Berova, *Org. Biomol. Chem.*, 2006, **4**, 1865.
68. A. Brewer, G. Siligardi, C. Neylond and E. Stulz, *Org. Biomol. Chem.*, 2011, **9**, 777.
69. I. Grabowska, D. G. Singleton, A. Stachyra, A. Gora-Sochacka, A. Sirko, W. Zagorski-Ostoja, H. Radecka, E. Stulz and J. Radecki, *Chem. Commun.*, 2014, **50**, 4916.
70. P. Bigey, S. H. Sonnichsen, B. Meunier and P. E. Nielsen, *Bioconjugate Chem.*, 1997, **8**, 267.
71. R. C. Mucic, M. K. Herrlein, C. A. Mirkin and R. L. Letsinger, *Chem. Commun.*, 1996, 555.
72. A.-E. Navarro, N. Spinelli, C. Moustrou, C. Chaix, B. Mandrand and H. Brisset, *Nucleic Acids Res.*, 2004, **32**, 5310.
73. M. Nakayama, T. Ihara, K. Nakano and M. Maeda, *Talanta*, 2002, **56**, 857.
74. C. Fan, K. W. Plaxco and A. J. Heeger, *PNAS*, 2003, **100**, 9134.
75. H. V. Nguyen, A. Sallustrau, L. Male, P. J. Thornton and J. H. R. Tucker, *Organometallics*, 2011, **30**, 5284.
76. H. V. Nguyen, Z. Zhao, A. Sallustrau, S. L. Horswell, L. Male, A. Mulas and J. H. R. Tucker, *Chem. Commun.*, 2012, **48**, 12165.
77. E. Leary, B. Limburg, A. Alanazy, S. Sangtarash, I. Grace, K. Swada, L. J. Esdaile, M. Noori, M. T. González, G. Rubio-Bollinger, H. Sadeghi, A. Hodgson, N. Agraıt, S. J. Higgins, C. J. Lambert, H. L. Anderson and R. J. Nichols, *J. Am. Chem. Soc*, 2018, **140**, 12877.
78. W. Xu, E. Leary, S. Hou, S. Sangtarash, M. T. Gonzµlez, G. Rubio-Bollinger, Q. Wu, H. Sadeghi, L. Tejerina, K. E. Christensen, N. Agraït, S. J. Higgins, C. J. Lambert, R. J. Nichols and H. L. Anderson, *Angew. Chem. Int. Ed.*, 2019, **58**, 8378.
79. J.-L. H. A. Duprey, J. Carr-Smith, S. L. Horswell, J. Kowalski and J. H. R. Tucker, *J. Am. Chem. Soc*, 2016, **138**, 746.
80. I. Mames, A. Rodger and J. Kowalski, *Eur. J. Inorg. Chem.*, 2015, 630.
81. R. Haner, F. Garo, D. Wenger and V. L. Malinovskii, *J. Am. Chem. Soc*, 2010, **132**, 7466.
82. N. Elgrishi, K. J. Rountree, B. D. McCarthy, E. S. Rountree, T. T. Eisenhart and J. L. Dempsey, *J. Chem. Educ.*, 2018, **95**, 197.
83. P. T. Kissinger and W. R. Heineman, *J. Chem. Educ.*, 1983, 702.
84. A. J. Bard and L. R. Faulkner, *Electrochemical Methods: Fundamentals and Applications*, Wiley and Sons, 2 edn., 2001.
85. B. Korybut-Daszkiewicz, A. Wieckowska, R. Bilewicz, S. Domagała and K. Wozniak, *J. Am. Chem. Soc*, 2001, **123**, 9356.
86. U. E. Wawrzyniak, M. Wozny, J. Kowalski, S. Domagała, E. Maicka, R. Bilewicz, K. Wozniak and B. Korybut-Daszkiewicz, *Chem. Eur. J.*, 2009, **15**, 149.
87. M. Nakane, H. Gollman, C. R. Hutchinson and P. L. Knutson, *J. Org. Chem.*, 1980, **45**, 2536.
88. S. Takamura, T. Yoshimiya, S. Kameyama, A. Nishida, H. Yamamoto and M. Noguchi, *Synthesis*, 2000, **5**, 637.
89. A. Rybka, R. Kolinski, J. Kowalski, R. Szmigielski, S. Domagała, K. Wozniak, A. Wieckowska, R. Bilewicz and B. Korybut-Daszkiewicz, *Euro. J. Inorg. Chem.*, 2007, 172.
90. C. R. Hutchinson, M. Nakane, H. Gollman and P. L. Knutson, *Org. Synth.*, 1986, **64**, 144.

91. A. Wieckowska, M. Wisniewska, M. Chrzanowski, J. Kowalski, B. Korybut-Daszkiewicz and R. Bilewicz, *Pure. Appl. Chem.*, 2007, **79**, 1077.
92. J. Carr-Smith, PhD Thesis, University of Birmingham, 2015.
93. J. V. Macpherson, *Phys. Chem. Chem. Phys.*, 2015, **17**, 2935.
94. S. J. Cobb, Z. J. Ayres and J. V. Macpherson, *Ann. Rev. Anal. Chem.*, 2018, **11**, 463.
95. P. Liu, P. Neuhaus, D. V. Kondratuk, T. S. Balaban and H. L. Anderson, *Angew. Chem. Int. Ed.*, 2014, **53**, 7770.
96. P. S. Bols and H. L. Anderson, *Acc. Chem. Res.*, 2018, **51**, 2083.
97. I. Mames, U. E. Wawrzyniak, M. Woźny, R. Bilewicz and B. Korybut-Daszkiewicz, *Dalton Trans.*, 2013, **42**, 2382.
98. S. Todd, MSci Dissertation, University of Birmingham, 2019.

4. Electrochemical Sensing with Metal-Modified Nucleic Acid Probes

4.1. Introduction to DNA Sensing

4.1.1. Overview of Nucleic Acid Probes

Modified oligonucleotides are useful tools for biological sensing, from identifying the presence of a specific biomarker released by the body in response to trauma, to the detection of more subtle targets such as a single point variant (SPV). The basic premise involves attaching a reporter group, for example a fluorescent or redox-active molecule, to the DNA strand and monitoring its output signal. The recognition capabilities of the nucleobases allow the composition of the strand to be tailored to the desired target, making nucleic acid probes highly selective towards it in a multicomponent sample. In the example outlined in Figure 4.1, the DNA probe is modified with a redox-active group and an electrochemical current signal is observed. Upon addition of the target nucleic acid, which has the complementary nucleobase sequence to the probe, a duplex is formed as the probe binds the target. This DNA hybridisation process results in a decrease in the current signal as the immediate environment of the reporter group has changed, revealing the presence of the analyte.

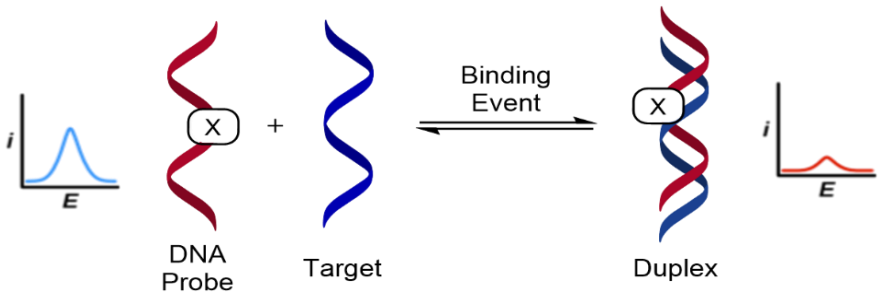

Figure 4.1: A basic schematic of sensing using modified nucleic acid probes. X = reporter group modification.

4.1.2. DNA Sequencing

One competing technology to hybridisation sensing using nucleic acid probes is DNA sequencing. This approach, which determines the specific order of nucleotides that make up nucleic acid sequence, has been crucial in determining the composition of the human genome and has been invaluable for both medical and biological research.[1-5] The ability to identify each individual nucleobase makes sequencing ideally suited to the detection of disease biomarkers including SPVs. However, the methods employed are currently expensive (*e.g.* in next-generation sequencing, NGS) and often time-consuming, requiring specialist training and equipment. This makes the use of NGS in certain situations less useful, for example where instant results are desired, such as in a laboratory linked to a patient clinic that screens patient blood or saliva samples. As the COVID-19 pandemic has shown, the challenge for many tests is to provide a reliable result well within one hour. This is where modified nucleic acid probes still have value, with the potential to provide a cheap, rapid and simple (*i.e.* yes/no) diagnosis by targeting a specific sequence.

4.1.3. Commercial Sensing Probes

4.1.3.1. Overview

Many of the nucleic acid probes employed for biosensing are modified with a fluorescent reporter group.[6, 7] Fluorescence is a popular readout method because of the relative simplicity of the equipment, its high sensitivity and its effectiveness at low concentrations, often sub micromolar. When compared to sequencing, the technique can generate a result for a doctor or patient in a fraction of the time at a reduced cost.

The disadvantage of many of these fluorescence-based probes is that a detection limit in the low micromolar or high nanomolar range is often insufficient to identify the trace amounts of nucleic acid biomarkers in a patient sample. To combat this, they are often used in tandem with DNA amplification methods such as the polymerase chain reaction, PCR. Once the patient sample has been received for analysis, it is first subjected to amplification to increase the amount of DNA so that it can be detected with the fluorescence technique. The amplification process routinely increases the concentration of patient DNA from femtomolar levels to nanomolar, a several orders of magnitude increase. PCR is beneficial as it is capable of amplifying only the DNA sequence of interest at the expense of other species present in the patient sample which may interfere with the subsequent sensing. Whilst offering a solution to one problem, the amplification process itself is time-consuming, which delays the time to make a diagnosis.

4.1.3.2. Molecular Beacons

Molecular beacons employ hairpin DNA probes that have a fluorophore attached at one end and a quencher at the other. When unbound, the probe adopts a folded structure due to self-complementary regions in its nucleobase make up. This conformation positions the fluorophore and quencher in close proximity, keeping the fluorescent output signal at a minimum. Binding the target causes the probe to become linear and position the fluorophore away from the quencher, resulting in an increase in fluorescence, Figure 4.2.[8]

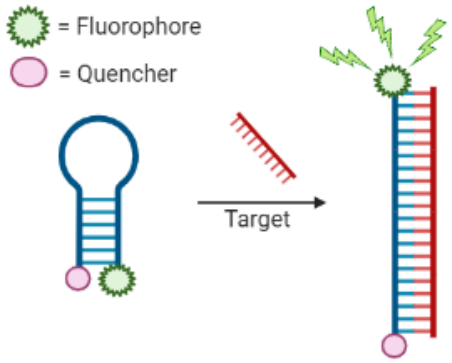

Figure 4.2: Schematic showing a molecular beacon in action. Fluorescence signal increases upon target binding.

As well as identifying the presence of a specific species, molecular beacons can be used for single nucleotide polymorphism (SNP) detection.[9] The method is dependent on differences in binding strength of the probe and two different targets. The DNA sequence of the healthy wild-type DNA differs from the mutant DNA by just one nucleobase. This is enough, however, to weaken the binding affinity for the mismatched sequence, resulting in a greater amount of the probe remaining in the hairpin structure and a weaker fluorescence signal being observed. Whilst this enables the technique to be used to distinguish between the presence of wild type and mutant target, the dependence on binding strength does lead to some false-positive results.[10]

4.1.3.3. TaqMan Assay

A commercial fluorescence-based technique for SPV detection is the TaqMan™ assay which combines the sensing step with the PCR amplification process to reduce readout times. It employs a molecular beacon-type probe, with a fluorophore at one end of the strand and a quencher at the other. However, these probes are linear and shorter in length, allowing the quencher to reduce greatly the output signal of the fluorophore without forming a hairpin. The nucleobase sequence of the probe is complementary to the specific point variant. During amplification, the probe binds the target and is degraded by the DNA Thermus aquaticus

polymerase (Taq), separating the fluorophore from the quencher, subsequently increasing the fluorescence signal. The intensity of the signal increases with each round of amplification as increasing amounts of the target, now binding the TaqMan probe, are generated. Following PCR, the presence of the SPV is determined by comparing the fluorescence signal from the probe to that of control sequences that are also included in the amplification process.[11, 12]

The control strands increase the reliability of the assay compared to molecular beacons, but the method still has drawbacks. The short probes used require a strict, elevated temperature window to efficiently bind their targets, meaning the method cannot be conducted at room temperature. A significant benefit to a clinic-based sensor would be the ability to screen a patient sample for a variety of SPVs in one test, like the sensors developed for cations by de Silva that were mentioned in *Chapter 1*. Unfortunately, the design of the TaqMan assay does not allow multiplexed sensing of this nature to occur.

Other techniques have followed suit and harnessed PCR. Scorpion primers combine PCR with the hairpin loops familiar in molecular beacons and do not require the control strands employed by TaqMan. Scorpions boast a reduced sensing time and the potential to be utilised in high throughput systems for SPV detection.[13] Roche Diagnostics have produced the Cobas® system that, although little in the public domain is known about its operation, is driven by fluorescence and can rapidly screen samples. The Cobas technology is largely automated and needs minimal operating, which is beneficial for clinicians but its high cost prices out many suitors.

4.1.4. Electrochemical Methods

Compared to the wealth of fluorescent probes for DNA available, there are a smaller number of electrochemical nucleic acid probes known. However, with many designs offering advantages over the routine fluorescence-based systems, it is an active and growing area of research.

One of the advantages electrochemical DNA sensors hold over their fluorescence counterparts is a lower limit of detection. Whilst electrochemical probes enjoy a low background signal, fluorescence-based approaches compete against autofluorescence from biological media including the DNA itself,[14] limiting sensitivity. Electrochemical DNA probes can also be routinely attached to the surface of the working electrode (*e.g.* as self-assembled monolayers or SAMs) to increase the quality and intensity of the readout signal. Surface-immobilisation requires a fraction of the material needed for solution-based sensing and the increased sensitivity reduces the limits of detection of the system by several orders of magnitude.

As mentioned in *Chapter* 3, Plaxco adapted the molecular beacon design for electrochemical sensing by attaching a ferrocene unit to the end of a surface-bound hairpin probe, Figure 4.3a.

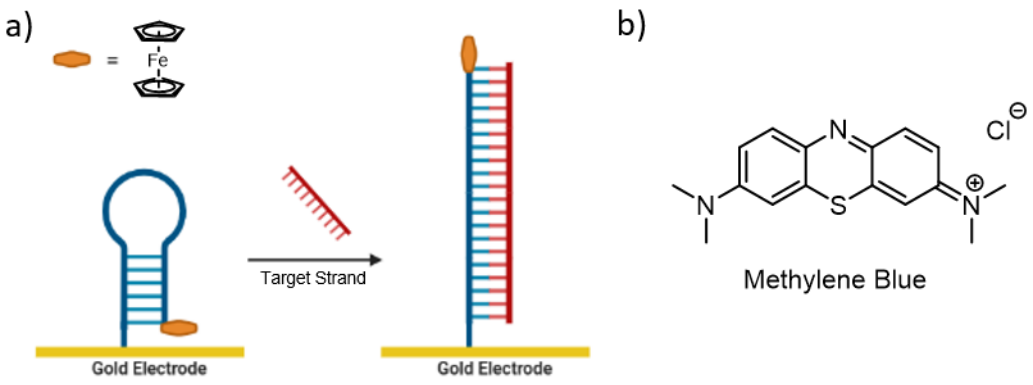

Figure 4.3: a) An electrochemical adaption of a molecular beacon utilizing the redox properties of ferrocene. b) The redox active molecule methylene blue.

In this instance, the change to a linear conformation upon binding the target moves the electrochemical reporter group away from the electrode surface, reducing the rate of electron transfer and subsequently the intensity of the signal.[15] Other redox active groups including methylene blue, Figure 4.3b, have been employed as the reporter group.[16]

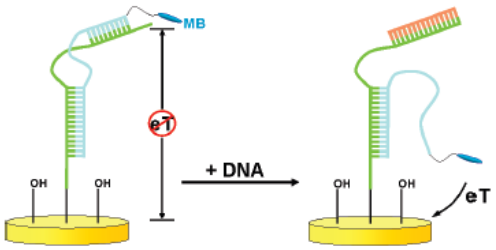

Figure 4.4: Plaxco et al. electrochemical probe based off the displacement of the methylene blue reporter group. Figure adapted from reference 16.

Subsequent studies have explored more creative probe designs for inducing a change in signal through conformational changes. Plaxco's system in Figure 4.4 comprises two strands, a surface bound capture probe (green) and a methylene blue-labelled signalling probe (blue), with complementary regions that allow partial binding. When bound to each other the reporter group is positioned far away from the electrode, limiting electron transfer. Addition of the target DNA leads to the displacement of the upper section of the signalling probe, moving the methylene blue unit closer to the surface to transfer electrons more efficiently, increasing the electrochemical signal. Impressively, the probe boasts a 400 fM detection limit, far superior to any fluorescent alternatives.[17]

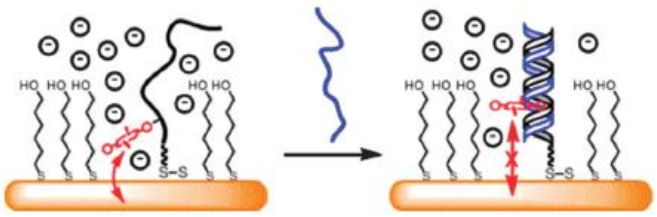

Figure 4.5: Stulz et al. designed a porphyrin-cobalt complex electrochemical sensor. Adapted from reference 18.

Stulz and co-workers moved away from distance-driven sensing mechanisms with their design which attached a porphyrin-cobalt complex to a nucleobase in the centre of a surface-bound

strand. Unlike the systems described above, hybridisation of this probe with its target does not lead to a significant change in the position of the porphyrin complex and so the change in redox signal occurs for different reasons. The observed changes are likely to be due to the change in the immediate environment of the porphyrin complex as the probe binds its target. The macrocycle will be at least partially embedded into the duplex formed with the target strand and this, alongside the increased negative charge introduced by the duplex, will lead to the redox centres being shielded from anionic counterions in the buffer solution. Such changes to the hydrophobic environment of a redox centre have been shown to lead to decreases in current signal, and this probe successfully harnessed this for a sensing output.[18]

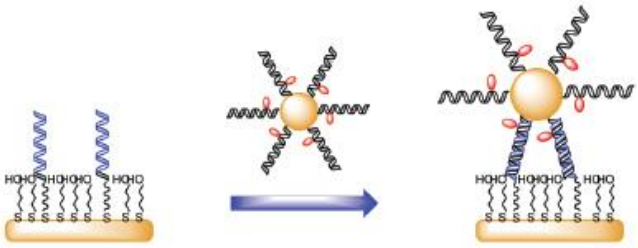

Figure 4.6: The porphyrin complex probe was attached to a gold nanoparticle to achieve greater limits of detection. Adapted from reference 19.

Although the probe was able to detect a virus biomarker at femtomolar concentrations, the system was combined with gold nanoparticles to further improve sensitivity, Figure 4.6. A self-assembled monolayer (SAM) was formed on the electrode surface containing a capture strand. This was used to anchor the nanoparticles which themselves were coated with the redox-active probe strand. The target was added and, following a two-hour hybridisation time, a decrease in the current signal indicated successful binding. Studies found that the use of nanoparticles decreased the limit of detection, with calculations suggesting the system may be able to detect attomolar target concentrations. This improvement is thought to be due to the nanoparticles allowing an increased number of redox centres to be positioned close to the electrode surface. An exciting idea is if different probes could be attached to the

same nanoparticle, this sensing arrangement could be utilised in multiplexing devices to detect a variety of targets in the same sample.[19]

As discussed in *Chapter 3*, Tucker and co-workers reported a metal-modified DNA strand that could discriminate between all four nucleobases using electrochemistry, Figure 4.7a. A copper-cyclidene complex was incorporated into the phosphate backbone of the 15-mer in a tag configuration. It was thought that the structural positioning of the macrocycle was crucial for nucleobase identification; one possibility, pictured in Figure 4.7b, is that the cyclidene unit intercalates into the duplex and adopts a different position depending on the nucleobase situated opposite it. A second possibility is that the cyclidene itself is partially displaced from the duplex, with the extent of the distortion related to the identity of the neighbouring nucleobase. Although the variation in the macrocycle's position is likely to be minor, it is clearly sufficient to induce a change in the electron transfer rate and subsequently the electrochemical readout signal. The probe has the potential to be the foundations of a sensing system capable of detecting SPVs.[20]

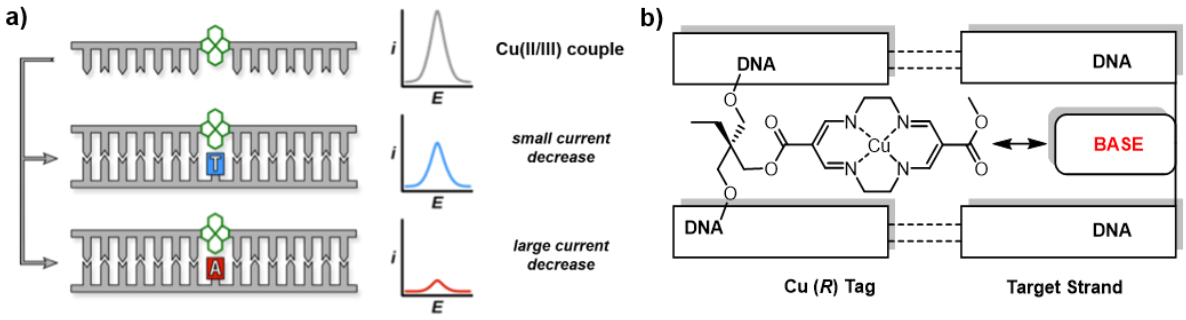

Figure 4.7: a) Copper-cyclidene (R) tag system was capable of electrochemically discriminating between all four nucleobases when incorporated into DNA. b) The key to this base discrimination is thought to be the intercalating ability of the cyclidene macrocycle. Figure adapted from reference 20.

The initial sensing studies were carried out in solution as opposed to anchoring the probe on the surface. Consequently, the sensing mechanism does not involve altering the distance of the redox centre from the electrode surface as seen previously but, like the system developed

by Stulz and colleagues, responds instead to a change in environment experienced by the redox centre as the target is bound. However, in addition to the cyclidene complex being stable to demetallation under automated synthesis conditions, its smaller size means that it can intercalate further into the duplex and interact with the bases stationed opposite it. In particular the bigger purine bases, adenine and guanine, are thought to subtly alter the position of the macrocycle in the duplex; this leads to differences in the electrochemical readout signal, allowing each base to be identified.[20]

4.2. Aims and Objectives

Following the synthesis of the monomers in *Chapter 3*, it was decided to synthesise more copper cyclidene tag-modified oligonucleotide probes in order to build on the sensing results previously reported and develop a sensing system capable of accurate, reliable SPV detection. The first objective was to immobilise the cyclidene probe onto the electrode surface as a self-assembled monolayer (SAM) and explore the electrochemical sensing ability using target-DNA strands, Figure 4.8.

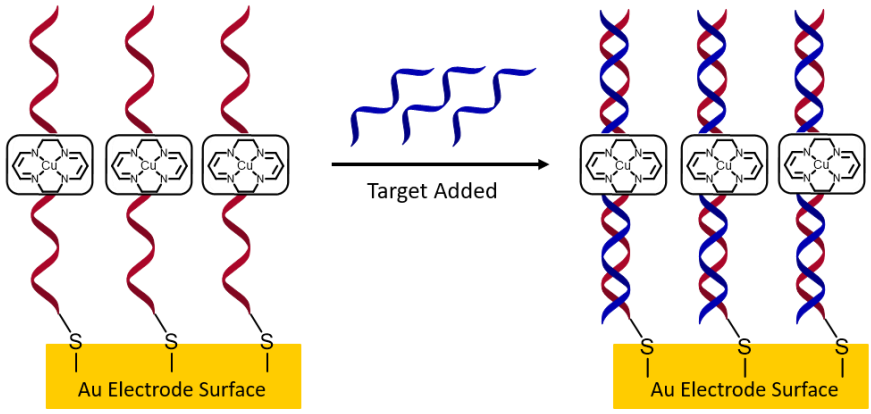

Figure 4.8: A schematic representation of the cyclidene-modified probe attached to a gold electrode surface as a self-assembled monolayer.

If the surface-bound probe exhibited the previously observed nucleobase discrimination found in solution, studies could progress further towards developing a functional sensing system. Key challenges would include determining the limit of detection and the minimal time required to generate a reliable sensing readout, as well as the feasibility of a reusable probe.

Whilst initial studies would take place on a previously developed in-house test sequence, the final objective would be to test the sensing system on real SPVs, such as the cancer biomarkers BRAF V600E and KRAS G12V.

4.3. First Generation Probe

4.3.1. Probe Design and Synthesis

With it well documented that thiols can be used to anchor DNA to a gold surface, including in the redox-active systems described above, it was envisaged that a polycrystalline gold electrode would be the ideal surface upon which to form a SAM.[21]

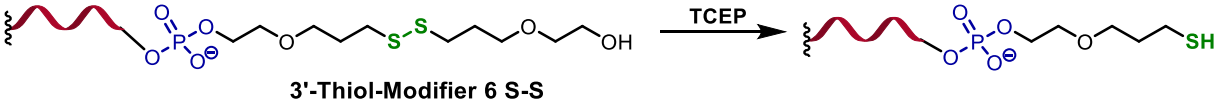

Scheme 4.1: The nucleic acid probes were modified at the 3'-terminal with a 3'-thiol-modifier 6 SS. This appends a disulfide unit to the DNA strand which can be reduced to afford a thiol.

The DNA probes in this work were functionalised with a 3'-thiol-modifier 6 SS unit during solid-phase DNA synthesis, pictured in Scheme 4.1 above. The disulfide bond can be reduced using tris(2-carboxyethyl) phosphine (TCEP) to reveal a thiol moiety which can subsequently be used to attach the DNA to the gold electrode.

Table 4.1: The oligonucleotides synthesised for initial surface-based electrochemical sensing studies. X = copper cyclidene tag system. SS = 6 SS 3' disulphide modification.

Name	*Sequence*
CycNINA	5'– TGG ACT C **X** C TCA ATG **SS** - 3'
Target-A	5' – CAT TGA G**A**G AGT CCA – 3'
Target-C	5' – CAT TGA G**C**G AGT CCA – 3'
Target-G	5' – CAT TGA G**G**G AGT CCA – 3'
Target-T	5' – CAT TGA G**T**G AGT CCA – 3'

The sequences of the nucleic acid probe and nucleic acid target strands synthesised are presented in Table 4.1. The sensing probe, CycNINA, is 15 nucleobases long with the copper

cyclidene tag incorporated into the backbone in place of the central nucleotide and a 3'-disulfide-modifier unit. The probe is programmed with an in-house nucleobase test sequence, known as the NINA sequence, that has been fully characterised, allowing any deviations in behaviour to be attributed to the cyclidene modification. This is the same sequence employed in the initial studies.[20]

The target strands consist of the complementary nucleobase sequence to the probe, with each target possessing a different nucleobase at its centre, allowing the nucleobase situated opposite the cyclidene modification in the probe-target duplex to be varied. This single nucleobase variation in the sequence acts as a test single point-variant site. If the probe proves capable of identifying nucleobase variations in the NINA sequence, the sequence of real SPV sites that are cancer biomarkers can be programmed into future probes.

4.3.2. Purification and Characterisation

Following automated solid-phase DNA synthesis, the crude DNA mixtures were purified by reverse-phase HPLC. The full conditions used are detailed in *Chapter 5: Experimental section 5.5.2.2*, with the subsequent characterisation by mass spectrometry and analytical HPLC listed in *Appendix section 6.3.1*.

Whilst the crude mixtures of the unmodified sequences and the previously described cyclidene link systems possessed one major product peak in the analytical HPLC trace, the mixture containing the cyclidene tag sequence gave two major peaks, as shown below in Figure 4.9. This was also observed in the previously reported work and is due to the chirality of the tag system.[20] The two diastereomers adopt different positions in the DNA strand due to their respective stereochemical conformations. The greater retention time of the (*R*)

diastereomer suggests it adopts a conformation where it protrudes from the oligonucleotide more so than its (*S*) counterpart. Similar trends are observed in previously synthesised intercalators with threoninol and serinol linkers.[22, 23] Inspection of the HPLC traces identified that the addition of the 3'-disulfide moiety to the strand had little effect on its retention time through the HPLC column compared to the previously reported probes in the same eluent conditions.[24]

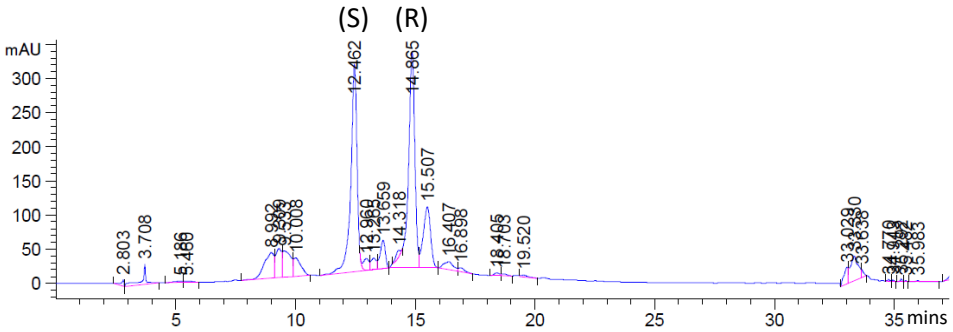

Figure 4.9: Analytical HPLC trace of CycNINA crude mixture. Phenomenex Clarity 5 µM Oligo-RP LC 250x10 mm column. 0.1M TEAA in HPLC water:MeCN gradient (15 to 25% MeCN) for 30 mins followed by 100% MeCN for 10 mins. Absorbance at 260 nm shown.

The ability to separate the diastereomers was crucial to the initial success of the sensing system as the (*R*) isomer was found to be far superior at electrochemical sensing than the (*S*). Guided by the initial results, whilst both isomers were isolated pure from the crude mixture, the (*R*) isomer strands were predominantly used for the sensing experiments that are reported herein.

4.3.3. Thermal Melting Studies

Thermal melting (T_m) is used to probe the stability of a DNA duplex and proves a useful characterisation technique for examining the impact of a modification on the oligonucleotide. The experiment raises the DNA sample to elevated temperatures, resulting in the duplex denaturing and splitting into two single strands. The temperature at which 50% of the duplexes in the sample have denatured is the T_m value, with a higher melting temperature indicating a more stable duplex. Generally, sequences with a greater guanine-cytosine population possess a higher T_m value as a result of the additional stability afforded from the three hydrogen bonds between the two bases. Likewise, a longer strand will have a higher T_m value than a shorter strand because of the increased number of hydrogen bonds.[25]

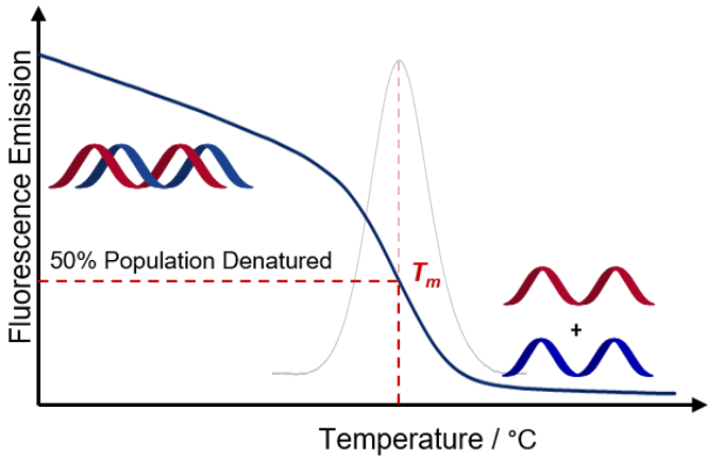

Figure 4.10: A thermal melting curve following the emission profile of SYBR Green.

The technique traditionally follows the absorption profile of DNA at 260 nm, with large increases in absorption observed upon denaturing of the duplex.[26-28] More recently, fluorescence has been employed by the Tucker group to monitor DNA denaturation, monitoring the emission profile of the DNA intercalating dye, SYBR Green. The dye is highly fluorescent when intercalating into the DNA duplex but once the duplex is denatured intercalation is no longer possible and a significant decrease in the fluorescent signal is

observed.[29] As in Figure 4.10, the fluorescence emission is plotted against temperature. The T_m value is subsequently determined from the first derivative of the data, with the mid-point of the curve highlighting the point at which 50% of the population is denatured and subsequently the T_m value.[25] The values reported in this work are the average of at least three measurements.

In the initial studies of cyclidene-modified oligos, trends in the T_m values helped explain the differences in sensing ability between the (*R*) and (*S*) copper cyclidene tag units. The melting temperatures of the (*R*) isomer were lower than those of the (*S*) isomer by a couple of degrees, suggesting the (*R*) tag was capable of intercalating further into the duplex and causing greater destabilisation to the structure. The values also varied depending on the identity of the target nucleobase, with lower T_m values recorded when the larger purine bases were stationed opposite the modification site in the duplex. This suggested that the cyclidene moiety could interact with the base opposite and partially displace it, distorting the duplex structure. The larger the nucleobase, the greater the distortion. As the (*R*) isomer appeared capable of greater intercalation, it is likely that this quality relates to its superior electrochemical sensing ability.[20, 24]

The same trends were observed in the T_m values of the thiolated CycNINA probe, presented in Table 4.2. This was expected as the same sequences were assessed as before and the presence of the disulfide unit at the 3' terminal was highly unlikely to affect the binding ability of the probe. The result was promising and suggested that the probes would be capable of replicating the previously observed nucleobase discrimination during surface-based electrochemical experiments. Higher T_m values were obtained than previously reported as a

result of the change from an absorbance-based melting temperature experiment to a fluorescence-based set-up, with the use of SYBR Green as an intercalating dye known to increase the melting temperature by several degrees.[30]

Table 4.2: Thermal melt values of the CycNINA nucleic acid probes binding the target strands. The T_m value of the unmodified sequence was 64.0 °C. [DNA] = 10 μM in 10 mM sodium phosphate buffer (pH 7.0), 100 mM NaCl.

Base Opposite Cyclidene	*CycNINA / °C*	
	(*S*)	(*R*)
A	63.0	59.1
C	64.8	60.9
G	61.5	59.3
T	64.0	61.3

4.3.4. Electrochemical Sensing

4.3.4.1. An Introduction to Surface-Based Electrochemistry

Whereas the electrochemistry described in *Chapter 3* concerned solution-based species and measurements, this Chapter describes electrochemical measurements of redox-active species that are bound to the surface of the electrode. The experimental set up is as previously described with the DNA-coated electrode suspended in a buffer solution but, whilst the target species are present in the solution, all activity occurs at the electrode surface. Consequently, electron transfer is no longer reliant on diffusion, which changes the appearance of the cyclic voltammogram (CV) and subsequent analysis.

For electrochemical sensing, using a surface allows a significantly smaller amount of redox-active probe to be used relative to solution-based sensing systems, which must operate at high concentrations to compete with a higher background signal that often consumes the redox peak of interest. Secondly, the peak separation, ΔE_p, of the anodic and cathodic peaks in the CV is very close to 0 mV, with the peaks sitting almost directly on top of one another.

A further difference from a solution-based CV is that the current should increase proportionally with the scan rate, rather than the square root of the scan rate, according to Equation 4.1.[31]

Equation 4.1 $$i_p = \frac{n^2F^2}{4RT} v A_{sur} \Gamma$$

Where:

i_p = peak current (A)

n = no. of electrons transferred per molecule

F = Faraday's constant (C mol^{-1})

A_{sur} = microscopic working electrode surface area (cm^2)

T = temperature (K)

Γ = surface coverage (mol cm^{-2})

v = scan rate (V s^{-1})

R = Molar Gas constant (V C K^{-1} mol^{-1})

The information obtained from recording a CV can be used with Equation 4.1 to determine the number of redox-active species on the working electrode surface. For this to be possible, the microscopic area of the working electrode, A_{sur}, must be determined after the polishing and cleaning steps in each experiment. Characterising the electrode surface is particularly important with polycrystalline gold electrodes as the surfaces naturally vary and are affected by each act of polishing, resulting in each electrode having a unique structure and roughness. A high microscopic surface area suggests a rough electrode surface, with more sites available

for redox chemistry. Meanwhile, a low surface area betrays the presence of contaminants absorbed on the surface, for example those that have survived the cleaning process between experiments.

The microscopic surface area, A_{sur}, is calculated by multiplying the geometric surface area of the working electrode by a roughness factor, *r*, which gives an indication of surface roughness. The roughness factor can be calculated with Equation 4.2.

Equation 4.2

$$r = \frac{Q/A}{482\ \mu C\ cm^{-2}}$$

Where:

r = surface roughness

Q = Charge (μC)

A = geometric working electrode surface area (cm^2)

When a gold electrode is placed in acidic solution, the surface is covered by a layer of gold oxide. The charge required to remove the layer is obtained by integrating the cathodic peak relating to the reduction of the gold oxide, observed around 900 mV in a CV recorded in 0.5 M sulfuric acid. Equation 4.2 compares this charge with the literature value for the removal of an oxygen monolayer from gold, 482 μC cm^{-2}, to calculate the roughness factor.[32, 33]

4.3.4.2. Self-Assembled Monolayer Formation

Self-assembled monolayers (SAMs) of CycNINA were formed on polycrystalline gold electrodes as detailed in *Chapter 5: Experimental section 5.6.3.1*. The gaps between the anchored nucleic acid probes were filled with 6-mercapto-1-hexanol, which prevents non-specific contacts between the probes and the electrode surface.[34] Four electrodes were chosen for the sensing studies, two of which were older with a higher roughness and surface areas between 0.030 – 0.040 cm^2 for each experiment, and two brand new electrodes with lower surface areas routinely between 0.018 – 0.029 cm^2. The electrodes chosen would test the performance of probes on a variety of gold surfaces and allow the development of a sensing system that is reliable across a range of polycrystalline gold electrodes, not just one specific electrode in a single lab.

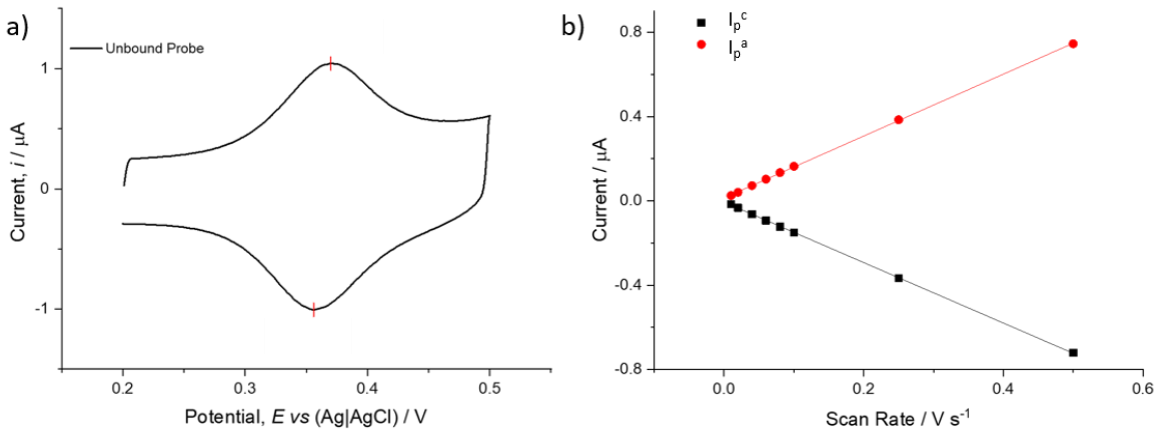

Figure 4.11: a) Cyclic voltammogram of CycNINA probe in 10 mM tris HCl buffer pH 7.0, 100 mM NaCl at 1000 mV s^{-1}. b) Scan rate dependence of the current for the surface-bound system.

Cyclic voltammetry confirmed the probes were attached to the electrode surface. The ΔE_p of the cyclidene redox peak was 6 mV, Figure 4.11a, a significant decrease from the previously reported 64 mV for the solution-based electrochemical studies.[20] Figure 4.11b compares the current against the scan rate. The linear relationship between the two is characteristic of a surface bound system and confirms the successful formation of the CycNINA SAM.[31]

4.3.4.3. Detecting Binding Events

Attention turned to the electrochemical sensing ability of the surface-bound cyclidene probes and the first challenge was to exhibit changes in current upon binding the complementary target-DNA sequence. Alongside cyclic voltammetry, square wave voltammetry (SWV) was used for the sensing experiments. SWV is a pulse voltammetry technique which combines staircase and square wave forms to remove the large background currents observed in CV resulting from capacitive charging.[35] Consequently, the technique possesses a sensitivity several orders of magnitude greater the CV which, alongside its rapid data acquisition, makes it ideally suited for sensing experiments.[36] SWV was employed in the initial solution investigations with cyclidene probes.[20]

After addition of the complementary target sequence (at 1 µM), a 20-minute hybridisation time followed to ensure binding with CycNINA before the electrochemical measurements were repeated, with the results presented in Figure 4.12 below.

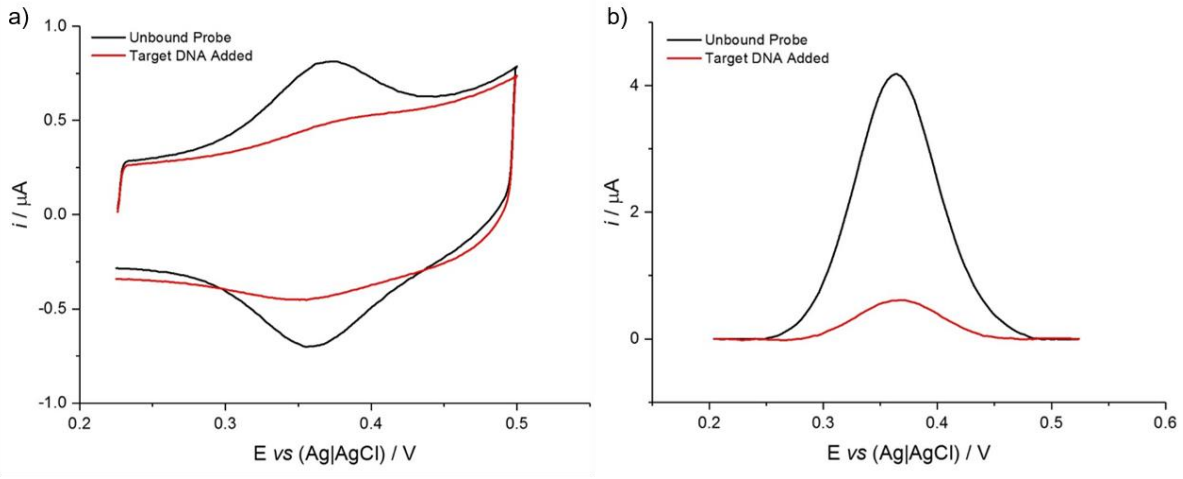

Figure 4.12: Electrochemical sensing with CycNINA. A change in current signal is observed when CycNINA binds its complementary target in both a) cyclic voltammetry and b) square wave voltammetry. [Target DNA] = 1 µM in 10 mM tris-HCl Buffer (pH 7.0), 100 mM NaCl.

A significant decrease in the copper redox signal was observed in both the CVs and SWVs, indicating a significant change to the environment of the cyclidene complex on the formation of the probe-target duplex. Very minor shifts in peak position (*ca.* 2 mV) were also observed upon target binding. The change in signal observed in Figure 4.12a was a promising development as sensing *via* CV had not been previously investigated with cyclidene-modified DNA, raising the possibility of using both electrochemical techniques for electrochemically sensing biomarkers.

4.3.4.4. Nucleobase Discrimination

The nucleobase situated directly opposite the cyclidene unit in the duplex was varied to assess the ability of the probe to distinguish between individual bases, Figure 4.13. The ability to distinguish between individual nucleobases is essential for the system to successfully identify single point variants (SPVs). The initial studies formed SAMs of CycNINA on three gold electrodes and recorded CVs and SWVs of the unbound probe before adding the target-DNA.

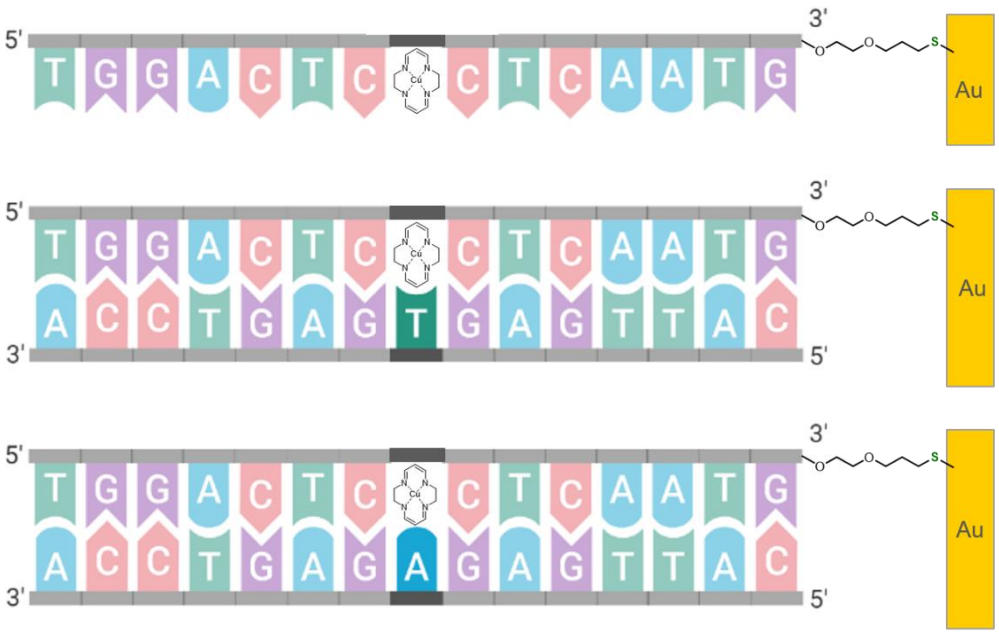

Figure 4.13: Schematic representation of the surface bound CycNINA probe binding the thymine and adenine nucleobase target strands, Target-T and Target-A, respectively.

The first study stationed thymine opposite the cyclidene unit, the second study investigated adenine opposite. The square wave voltammograms were compared and the sensing output assessed for the three different electrodes, with the changes in the current signal detailed in Figure 4.14.

a)

Electrode	*% Decrease in Current Upon Target Addition*	
	A	T
1	21.4	80.9
2	62.0	90.3
3	72.6	87.2

b)

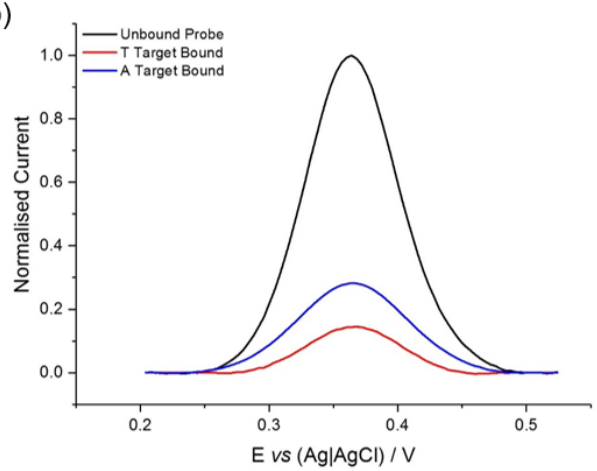

Figure 4.14: a) Table depicting the % change in current of the copper cyclidene redox signal of in SWV upon addition of each target. b) Square wave voltammogram of electrode 3 showing the change in current signal between the unbound probe and when thymine and adenine targets are added. [Target-DNA] = 1 µM in 10 mM tris-HCl Buffer (pH 7.0), 100 mM NaCl.

The results clearly show that the probe is capable of nucleobase discrimination through differences in the change in current upon target addition, in this instance a thymine-adenine variation which is the nucleobase change observed in the BRAF V600E mutation. Interestingly, although these results support the solution-based studies in detecting a thymine-adenine change, with the probe immobilised on a surface, the inverse to what was observed for the freely diffusing system was observed in regards to the change in current; for the SAM, the larger decrease occurs when thymine is opposite the cyclidene tag, rather than adenine. Whilst this effect is difficult to explain, it is likely that removal of the influence of diffusion on the electron transfer process must play a role.[20]

Despite the success of the system at nucleobase discrimination, when comparing the results across the three electrodes it is evident that the system is not consistent; the same trends are

observed regarding which nucleobase gives a greater decrease in current signal but different percentage decreases are observed for each electrode. This unreliability is further highlighted when different measurements of the measurements on freshly formed SAMs gave differing results. On electrode 1, for example, the percentage decrease on addition of the adenine target was initially 21.4% but increased to 77.5% when repeated. Whilst these were only initial studies on the system, such variation in measurements of the same target is a major issue. For a sensing system to be applied to patient samples and be of use in a medical environment, far greater levels of consistency and reliability are required.

4.3.4.5. Reusability Studies

It is highly desirable for the sensing system to be able to be used multiple times, reducing expenditure and waste generated by the end user. An advantage of using a surface-bound sensing system is that the electrode coated with the probe can be transferred between solutions with washing steps in between. The strength of the gold-sulfur bond ensures the SAM is not damaged and completely lost during the washing steps and enables the probes to be moved from a solution of target to a urea solution, which is known to denature the duplex and regenerate the unbound probe.[37] Following a period of time soaking, the electrode can be washed and then transferred into a solution of buffer before the electrochemical sensing process is repeated.

The SWV results for repeat experiments on the same electrode are detailed in Figure 4.15 below. Following the expected decrease in current upon addition of the Target-T strand, a soak in a 10 µM urea solution for one hour resulted in partial regeneration of the signal. Immersing the electrode in a fresh solution of Target-T resulted in a second decrease in current, signifying the binding event.

a)

Probe Status	*Current / µA*	*% Change*
Unbound Probe	12.54	-
Target T Added	3.55	- 71.7
Regenerated Probe	7.52	+ 44.1
Second Target T Addition	1.08	- 85.6

b)

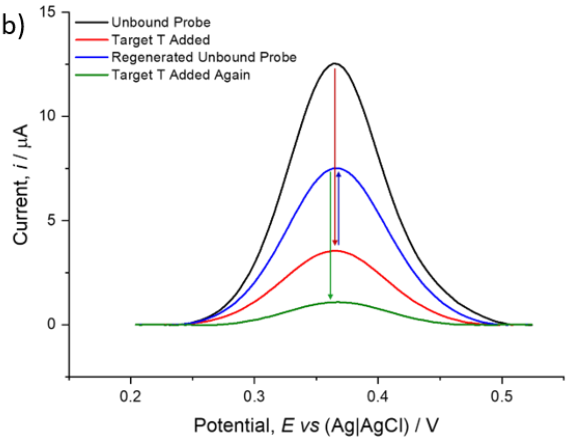

Figure 4.15: a) Table depicting the % change in current of the copper cyclidene redox signal in SWV upon addition of Target-T, regeneration of the unbound probe by soaking in 10 µM urea solution and subsequent target re-addition. b) Corresponding SWV showing the change in current signal. [Target DNA] = 1 µM in 10 mM tris-HCl Buffer (pH 7.0), 100 mM NaCl.

Whilst the significant decrease seen upon addition of target-DNA to the regenerated probe suggests a significant proportion of unbound probes were regenerated by the urea soak, the signal regeneration was quite poor at only 44%, which may be because only some of the target strands are displaced by the addition of urea. However a second reason is that some of the probes could have become detached from the surface of the electrode during the washing steps, resulting in the weaker redox signal.

The evidence of at least partial regeneration of the unbound probe and ability to sense a second binding event is promising but the studies again highlight flaws in this sensing system. It is not possible to accurately gauge the extent of regeneration from one redox signal without the presence of a reference, whilst the probe again shows a limited reliability in terms of its

signal readout. For it to be successful in its application, the readout must be consistent for each target sequence. It became apparent that whilst the foundations of a promising sensing system were present, further development of the nucleic acid probe was required to make it a viable sensing system.

4.4. Ratiometric Sensing

In an attempt to increase the reproducibility, consistency and reusability of the sensing system, a ferrocene unit was installed at the 5' terminus of the probe, thus creating a novel heterometallic nucleic acid sensing system. It was considered that the structure and position of this second redox centre should result in its being unaffected by a binding event, unlike the cyclidene complex, allowing it to act as an internal reference signal. This in turn would allow for a ratiometric approach to electrochemical sensing; measuring the decrease in current observed in the copper redox signal against the unchanged iron redox signal of ferrocene.

There is some precedent in the literature of ratiometric electrochemical sensing. Ellington and co-workers adapted Plaxco's molecular beacon design by attaching methylene blue to the 5' terminal of a hairpin loop, whilst the 3' end possessed a ferrocene unit and was anchored to the surface. Hybridisation of the probe with its target induced a conformational rearrangement, moving the methylene blue unit away from the surface. This resulted in a decrease of the methylene blue redox signal whilst the ferrocene unit, whose proximity to the surface was unchanged, saw its current signal stay constant.[38] Chen and co-workers similarly combined ferrocene, methylene blue and a hairpin structure in their design, but also employed Exonuclease III as target recycling amplification strategy. Target binding saw changes to both the redox signals. The sensing system boasts an impressive detection limit of

4.16 fM.[39] Both designs rely on conformational rearrangements upon target binding to induce a change in redox signal, a significantly different strategy to the one presented here with the cyclidene-ferrocene probe.

4.4.1. Probe Design and Synthesis

The composition of the ratiometric sensing probe, FcCycNINA, is shown in Table 4.3. The probe is a simple variation on the original CycNINA strand: a 15-base long sequence with a copper cyclidene tag unit replacing the middle nucleotide unit, a 3' disulfide modification and a ferrocene unit tagged to the 5' terminal. As the strand was programmed with the NINA nucleobase sequence, it was compatible with the previously synthesised target-DNA. Due to the susceptibility of the cyclidene unit and disulfide modification to oxidation, ultra-mild synthesis conditions were employed.

Table 4.3: The ratiometric sensing probe synthesised was programmed with the NINA test sequence. X = copper cyclidene tag system. Fc = ferrocene modification. SS = 6 SS 3' disulphide modification.

Name	*Sequence*
FcCycNINA	5'– **Fc** TGG ACT C **X** C TCA ATG **SS** - 3'

4.4.2. Characterisation and Purification

As the analytical HPLC trace in Figure 4.16 shows, the previous eluent system was capable of sufficiently separating the (*R*) and (*S*) diastereomers and was therefore employed to purify FcCycNINA. The addition of the ferrocene moiety to the 5' terminal increased the retention time on the HPLC column by 10 minutes due to an increased hydrophobicity of the strand. An interesting feature in the analytical HPLC trace of the crude mixture is the two peaks at 15.0 and 17.4 minutes. They represent the truncated sequences where the final coupling step to attach the ferrocene unit failed, essentially producing CycNINA.

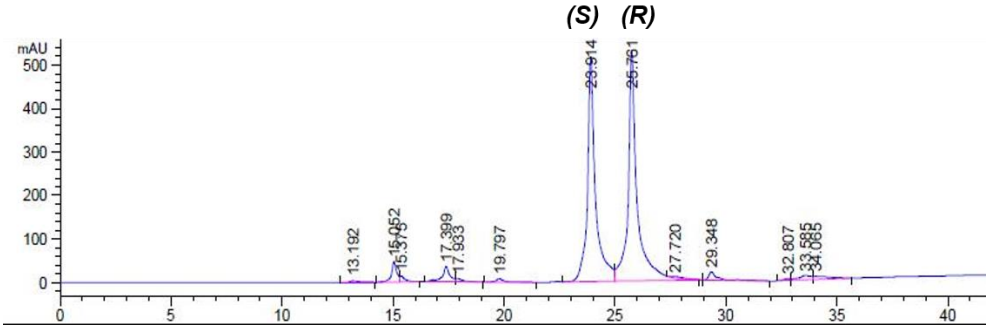

Figure 4.16: Analytical HPLC trace of FcCycNINA crude mixture. Phenomenex Clarity 5 µM Oligo-RP LC 250x10 mm column. 0.1 M TEAA in HPLC water:MeCN gradient (15 to 25% MeCN) for 30 min followed by 100% MeCN for 10 min. Absorbance at 260 nm shown.

Following purification by semi-preparative HPLC using the conditions outlined in *Chapter 5: Experimental section 5.5.2.2*, the purity of the probes was confirmed with analytical HPLC and the probes were then characterised with mass spectrometry, *Appendix section 6.3.1.2.*

4.4.3. Thermal Melting Studies

The impact of the 5' ferrocene modification on the structure of the DNA probe was assessed using thermal melting studies. The results are displayed in Table 4.4 and compare the values for ratiometric FcCycNINA with the initial CycNINA probe.

Table 4.4: Thermal melt values of the CycNINA and FcCycNINA nucleic acid probes binding the target strands. The T_m value of the unmodified sequence was 64.0 °C. [DNA] = 10 µM in 10 mM sodium phosphate buffer (pH 7.0), 100 mM NaCl.

Base Opposite Cyclidene	*CycNINA / °C*		*FcCycNINA / °C*	
	(*S*)	(*R*)	(*S*)	(*R*)
A	63.0	59.1	62.0	55.7
C	64.8	60.9	64.5	61.0
G	61.5	59.3	61.5	59.5
T	64.0	61.3	63.7	59.5

Overall, the similar T_m values suggest the addition of the ferrocene moiety has little impact on the stability of the probe-target duplexes. This was expected as the position of the ferrocene at the 5' terminal largely prevents it from disrupting hybridisation. This suggests the ferrocene will be ideally suited to its role as an internal electrochemical reference. It is interesting to note however that the values for the (*R*) isomer binding Target-T and Target-A were slightly lower than expected. Nevertheless, the same trends were observed as before; the (*R*) isomer afforded lower melting temperatures than the (*S*) isomer and the larger purine nucleobases destabilised the duplex more when stationed opposite the cyclidene complex than the smaller pyrimidines. Together these observations indicated that the cyclidene macrocycle was behaving as expected.

4.4.4. Electrochemical Sensing

4.4.4.1. Initial Studies: Cyclic Voltammetry

For the two independent redox centres in the probe to work together and be an effective sensing readout, it was important that the two signals would not overlap with one another in the CV or SWV. The cyclic voltammogram in Figure 4.17 shows that the iron and the copper redox signals are sufficiently separated, possessing a difference in $E_{1/2}$ values of over 250 mV, which ensures neither signal distorts the shape of the other. An interesting observation was that the ratio in current signals of the two redox peaks was approximately 1.3:1, with the cyclidene peak possessing a greater current magnitude because of its closer proximity to the surface of the electrode relative to the ferrocene. This was consistent across all four polycrystalline gold electrodes used.

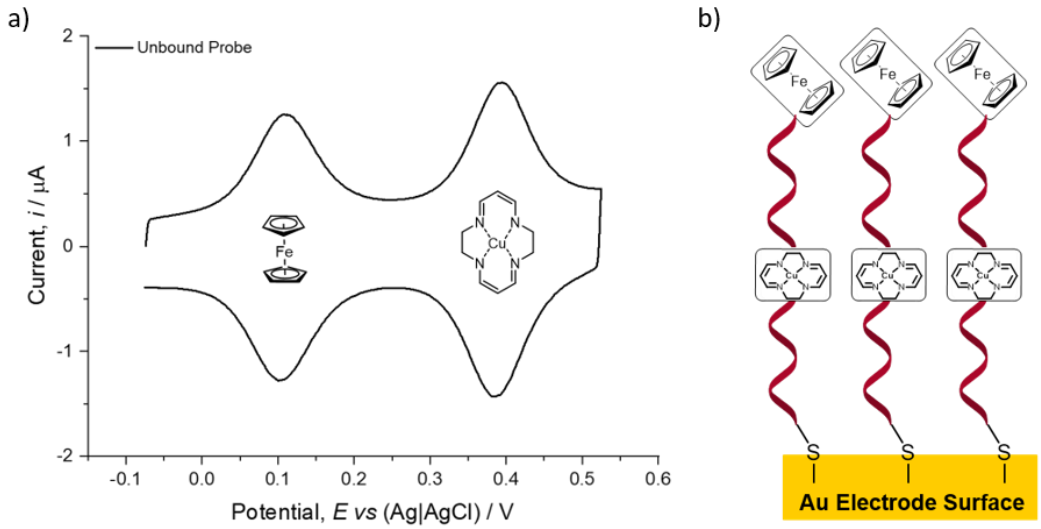

Figure 4.17: a) Cyclic voltammogram of the unbound ratiometric FcCycNINA probe. Recorded in 10 mM sodium phosphate buffer (pH 7.0), 1 M $NaClO_4$ at 1000 mV s^{-1}. b) A schematic representation of the unbound probe on the electrode surface.

Addition of target-DNA resulted in a significant decrease of the cyclidene current, whereas the ferrocene signal was relatively unchanged, Figure 4.18. These results were seen not only in the 10 mM tris-HCl buffer (pH 7.0), 100 mM NaCl conditions previously examined, but also in 10 mM sodium phosphate buffer (pH 7.0), 1 M $NaClO_4$, pictured in Figure 4.18a.

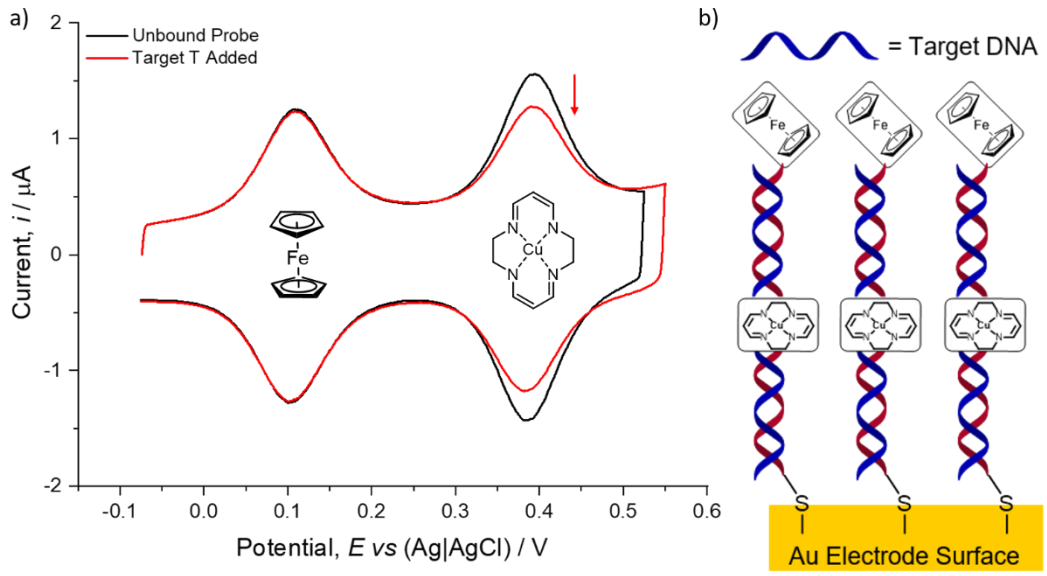

Figure 4.18: a) Cyclic voltammogram of the ratiometric FcCycNINA probe binding Target-T. Recorded in 10 mM sodium phosphate buffer (pH 7.0), 1 M $NaClO_4$ at 1000 mV s^{-1}. [Target-T] = 1 µM. b) A schematic representation of the probe binding target DNA on the electrode surface.

This behaviour was exactly as expected; as the probe strand does not experience a conformational change like previously reported systems, changes in signal were only expected to be induced by interactions with the target strand. Upon hybridisation with the target-DNA, the cyclidene unit at the centre of the strand experiences a significant change in its surrounding environment as it is now embedded in a duplex. As it intercalates into the duplex, the rate of electron transfer decreases relative to the unbound probe, resulting in the decrease in current signal. Meanwhile, the immediate environment of the terminal ferrocene unit is relatively unchanged as it is situated away from the duplex, Figure 4.18b. Therefore, only a minimal change to its current signal is experienced, allowing it to behave as an internal reference signal which the copper cyclidene current can be monitored against.

The presence of the stable redox signal originating from the ferrocene allowed for the quantification of FcCycNINA on the working electrode surface. In comparison, the cyclidene signal is unsuitable for such an approximation as it varies depending on the probe's binding state. Following the determination of a roughness factor after polishing for each electrode according to Equation 4.2, the current of the iron redox signal was used with Equation 4.1 to determine the surface coverage, *Γ*, Table 4.5.

Table 4.5: The surface coverage of FcCycNINA in single stranded (unbound probe) and double stranded form (target bound). Current taken from CV recorded at 1000 mV s^{-1} in 10 mM tris HCl (pH 7.0) 100 mM NaCl.

	Surface Coverage / mol cm^{-2}	
Electrode	**Unbound Probe**	**Target Bound**
1	1.65×10^{-11}	1.48×10^{-11}
2	1.41×10^{-11}	1.46×10^{-11}
3	1.11×10^{-11}	1.04×10^{-11}
4	1.02×10^{-11}	9.92×10^{-12}

The values obtained were in agreement with literature values for similar ferrocene-labelled DNA[40, 41] and indicate that there are approximately 10^{13} molecules of DNA per cm^2, with a distance of approximately 30 Å between each surface-bound DNA strand. This inter-strand separation raises the possibility of the DNA being able to lean and interact with each other. This is more likely to occur with the more flexible single strands, which are thought to adopt a more uniform and rigid arrangement upon duplex formation. Ellipsometry studies would provide further insight into the behaviour and arrangement of the surface-bound strands, allowing changes in the thickness of the SAM to be monitored upon hybridisation.

The observed trends were as expected; the electrodes with the larger surface area, 1 and 2, possessed a higher coverage whilst the formation of a duplex resulted in a minor decrease in coverage. The surface coverage offers an insight into the consistency in CV appearance across multiple electrodes. Whilst the surface areas and conditions differ, in some cases significantly so, the coverage is only marginally different, with each SAM containing similar amounts of FcCycNINA. Hence a similar electrochemical readout is observed in the CV.

4.4.4.2. Initial Studies: Square Wave Voltammetry

Whilst the CVs were consistent across all electrodes and from one SAM to another, the SWVs were found to vary significantly. The condition of the electrode had a drastic effect on the appearance of the SWV. The SWV of a FcCycNINA SAM on the older, rougher gold electrodes with a higher surface area had a copper cyclidene current signal which was approximately 1.3 times the ferrocene current signal, similar to that observed in the CV, Figure 4.19a. On the other hand, the cyclidene signal was over 3 times stronger than the ferrocene signal in the SWV of a FcCycNINA SAM on the newer, smoother electrodes with a lower surface area, Figure 4.19b. The differences between SWVs recorded using different electrodes are thought to be due to the increased sensitivity of SWV relative to CV, with SWV seemingly capable of detecting subtle differences in the structure of the SAM, such as individual orientations, that are not detectable with CV.[42]

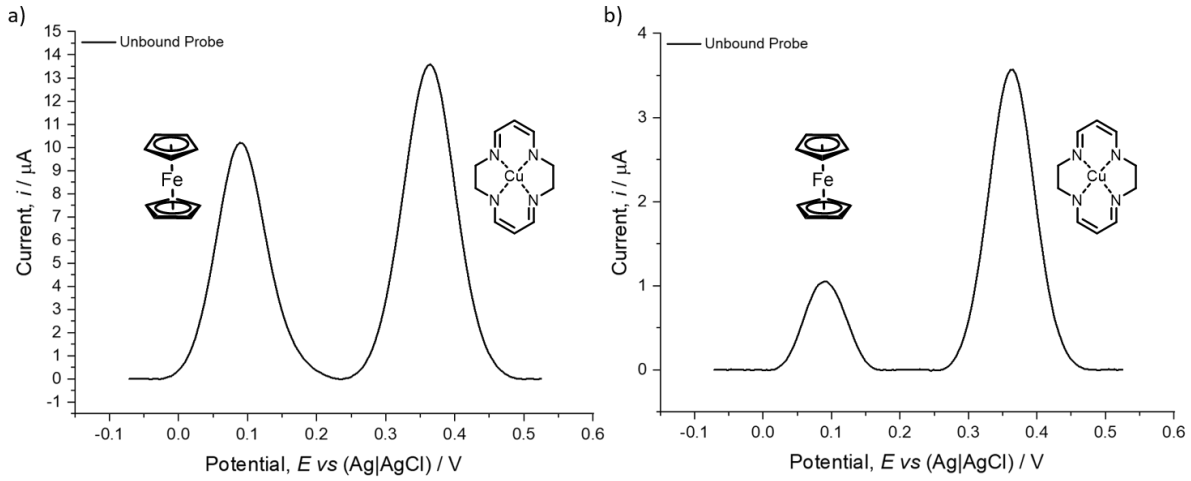

Figure 4.19: Square wave voltammograms of the unbound FcCycNINA probe in 10 mM tris HCl buffer (pH 7.0), 100 mM NaCl on a) electrode 1 (high surface area) and b) electrode 3 (low surface area).

The choice of buffer conditions also affected the SWV appearance. As shown in Figure 4.20, switching from a tris HCl buffer to a sodium phosphate buffer system results in a significant decrease in the ferrocene current relative to the copper cyclidene signal. Again, the highly sensitive technique appears to be able to detect any subtle interactions with the surface bound probe by the species present in the buffer. The change in buffer conditions also caused a shift in peak position which was also observed in CV, with more positive potentials recorded in the phosphate buffer.

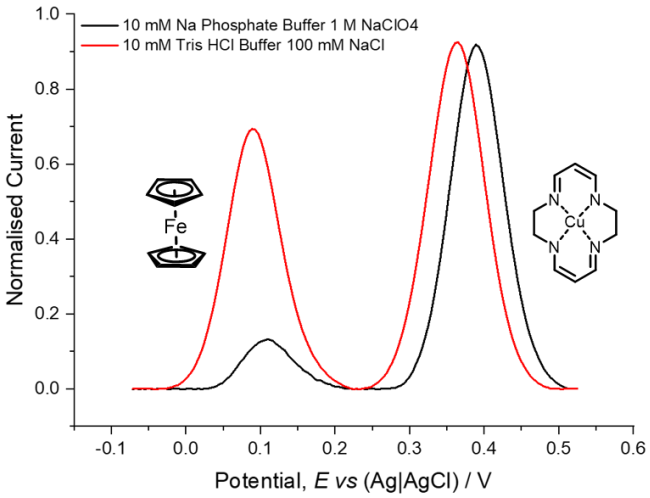

Figure 4.20: Square wave voltammograms of FcCycNINA comparing the effect of different buffer conditions on the current ratio of the ferrocene and cyclidene redox signals.

Addition of the target species resulted in a decrease in the cyclidene current signal, but varied changes were also observed in the ferrocene signal, Figure 4.21. The high surface area electrodes, Figure 4.21a, saw a decrease in cyclidene signal alongside a minor decrease in the ferrocene current, similar to that observed in the CV. The low surface area electrodes however saw a significant decrease in cyclidene signal upon target binding as expected, but also experienced a significant increase in the ferrocene signal, Figure 4.21b. An increase in current signal suggests the ferrocene tag has been moved closer to the electrode surface during the binding event to better facilitate electron transfer. However, this is not reflected

in the SWV of other electrodes and even in a CV recorded of the same electrode and SAM immediately after the SWV. Further sensing studies revealed similar discrepancies between current signals in SWV compared to CV.

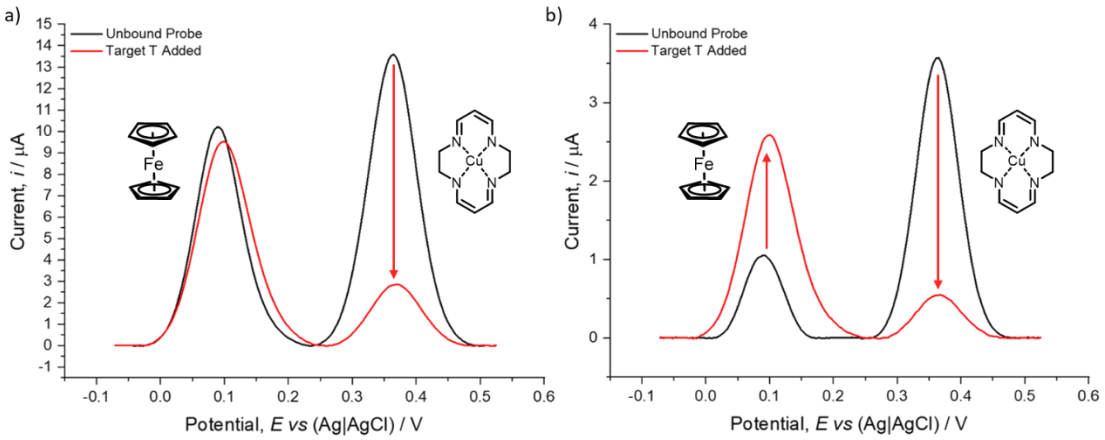

Figure 4.21: Square wave voltammogram of FcCycNINA probe unbound and following addition of Target-T strand. a) electrode 1 (high surface area). b) electrode 3 (low surface area). [Target-T] = 1 µM. Recorded in 10 mM tris HCl buffer (pH 7.0), 100 mM NaCl.

Cyclic voltammetry was found to be a much more consistent electrochemical sensing technique, with the changes observed being consistent and repeatable across different electrodes and SAMS, whereas square wave voltammetry produced a variety of results that were dependent on not only the electrode used, but also the quality of the SAM, with limited reproducibility. This was far from ideal for a sensing readout and so the subsequent analysis focuses on cyclic voltammetry.

However, the high sensitivity of SWV proved to be a valuable characterisation technique for the newly formed SAM. The technique could identify traces of mercaptohexanol that remained trapped between the DNA strands of the SAM following the backfilling step during SAM fabrication. These traces could distort the electrochemical signal through hydrogen bonding with the DNA, shifting the signal to a more positive potential. The rapid scan time and high sensitivity of SWV made it ideal to characterise the SAM before sensing and identify if further washing steps were required.

4.4.4.3. Determining the Cyclidene:Ferrocene Current Ratio

The ratiometric sensing approach resulted in changes to the electrochemical current signal induced by target binding being described in terms of the change experienced by the cyclidene sensing signal relative to the ferrocene reference signal. This was expressed in terms of the change in the cyclidene:ferrocene current ratio (Cyc:Fc ratio), Equation 4.3.

Equation 4.3 Cyclidene:Ferrocene Current Ratio = *Cyc i* / *Fc i*

Figure 4.22 outlines how the information required to calculate the Cyc:Fc ratio from the cyclic voltammogram was obtained. The red dotted line underneath each redox peak is the baseline and each peak current is determined from the baseline to the highest point of the peak, as is common practice.[43] Following determination of both the oxidation and the reduction peak currents, i_{ox} and i_{red}, respectively, the cyclidene current is divided by the ferrocene current to give the Cyc:Fc ratio. The ratio of the unbound probe and the hybridised probe following

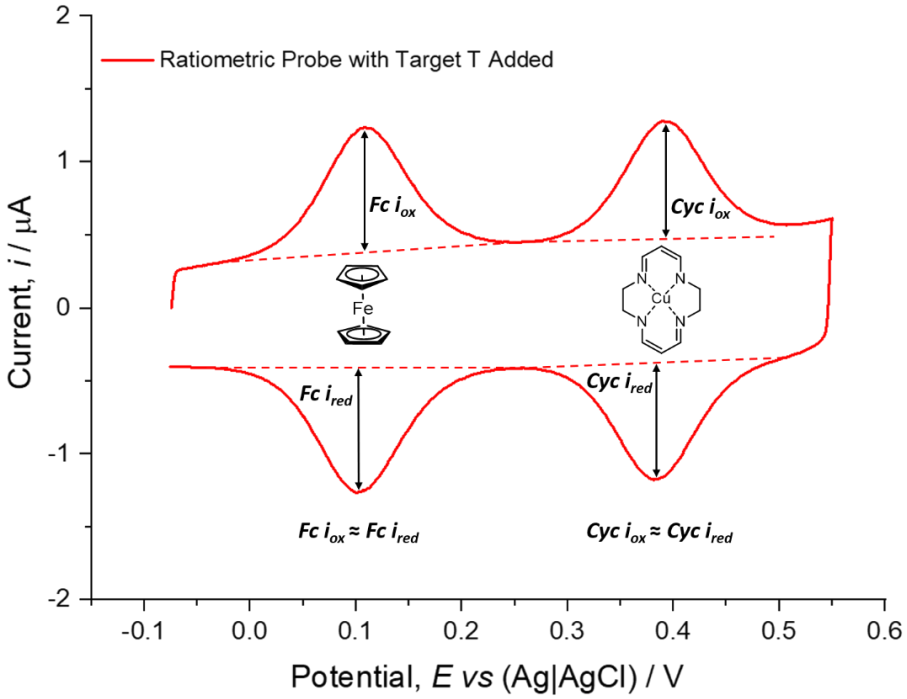

Figure 4.22: Cyclic voltammogram depicting the components that are considered in calculating the Cyc:Fc current ratio for electrochemical sensing. CV recorded at 1000 mV s^{-1} in 10 mM sodium phosphate buffer (pH 7.0), 1 M $NaClO_4$. [Target-T] = 1 µM Fc = Ferrocene. Cyc = Copper Cyclidene Tag. i = Current. Ox = Oxidation. Red = Reduction.

target addition can be compared and a percentage change in ratio can subsequently be calculated.

As the electrochemistry of both the ferrocene and the copper cyclidene units are near-reversible, the magnitudes of i_{ox} and i_{red} are expected to be the same, enabling the ratio to be calculated from either of the oxidation or reduction peaks. As the shape of the cyclidene oxidation signal in particular is susceptible to distortion from background signals from the buffer, such as the chloride adsorption described in *Chapter 3*, the reduction peaks are sometimes a more reliable source of information. If there is a significant difference in the magnitudes of the currents, this may indicate damage to the SAM or the presence of an interfering species, for example mercaptohexanol.

4.4.4.4. Varying the Nucleobase Target

The sensing ability of the probe was assessed by varying the nucleobase situated directly opposite the cyclidene complex in the probe-target duplex, as shown in Figure 4.23. Using cyclic voltammetry as the electrochemical readout method, the FcCycNINA probe was capable of distinguishing between all four canonical DNA nucleobases. Significantly, the

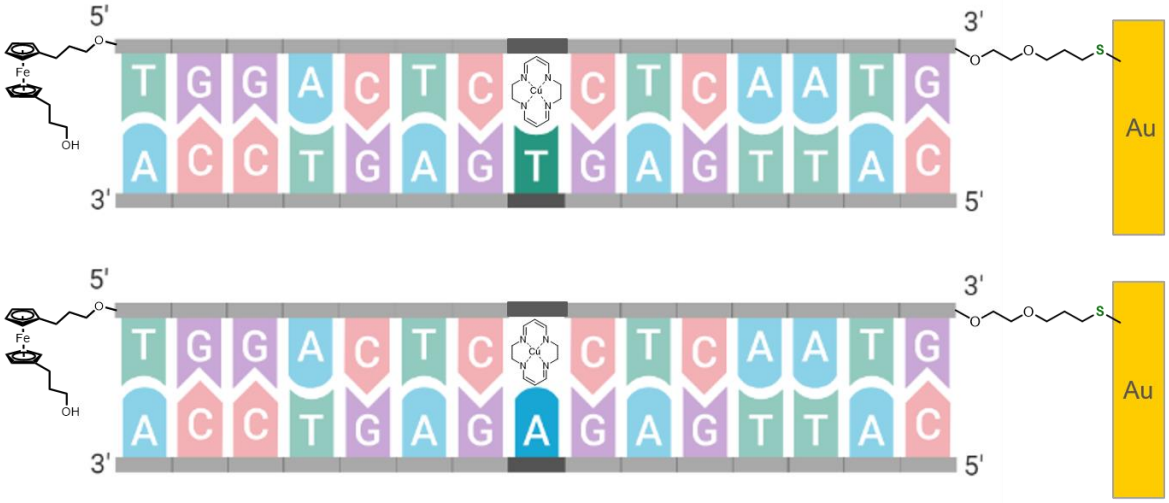

Figure 4.23: Schematic representation of the FcCycNINA probe sensing the single nucleobase change at the test single point-variant site in the NINA sequence.

changes in current observed were consistent across all four working electrodes and were reproducible using fresh SAMs. It was interesting to note that the sensing output of the probe was affected by the buffer conditions employed. As the results in Figs 4.24 and 4.25 show, the choice of buffer could be tailored to adapt the sensing output to the single point variation to be detected.

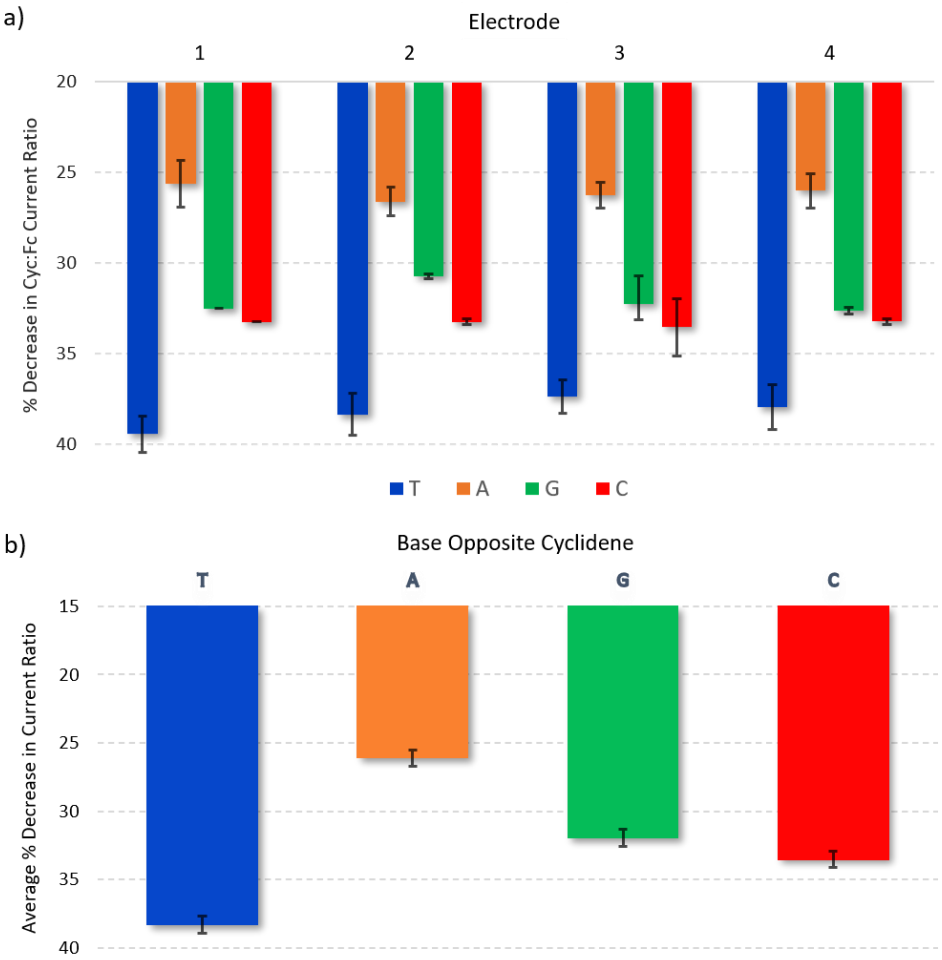

*Figure 4.24: The percentage decreases observed in the Cyc:Fc ratio upon varying the nucleobase opposite the cyclidene unit in the FcCycNINA Probe-Target duplex in **10 mM tris HCl buffer (pH 7.0), 100 mM NaCl.** a) Sensing results across each gold working electrode. b) Average sensing results. [Target DNA] between 1 μM to 10 fM. Error values are reported at a 95% confidence level of the standard error of the mean.*

In 10 mM tris HCl buffer (pH 7.0), 100 mM NaCl, FcCycNINA was able to distinguish between all four canonical nucleobases and proved particularly capable of discriminating between a thymine-adenine variation, Figure 4.24. The 12% difference between the two signal readouts was comfortably outside the margin of error, allowing it to identify the nucleobase with a

high degree of confidence. This is the nucleobase change observed in the BRAF V600E biomarker and appears to be an ideal candidate sequence with which to assess the ratiometric sensing system.

Although the difference between cytosine and guanine was minimal at only 2%, the consistency of the probe ensures that even this small difference in signal readout falls outside of the margins of error for each reading. Whilst the system could identify a guanine-cytosine variation using pure target samples, ideally the difference in readout would be larger to allow more leeway when analysing more complicated mixtures, such as patient samples, where other species may interfere with the electrochemical readout.

Sensing in 10 mM sodium phosphate buffer (pH 7.0), 1 M sodium perchlorate conditions altered the signal readout for the nucleobases and resulted in a better differentiation

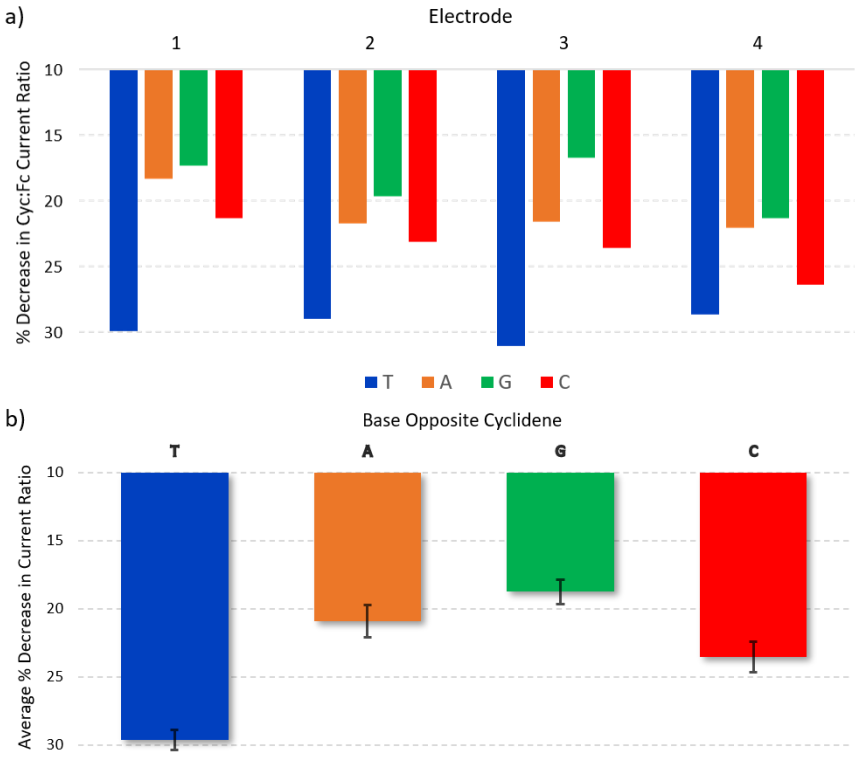

*Figure 4.25: The percentage decreases observed in the Cyc:Fc ratio upon varying the nucleobase opposite the cyclidene unit in the FcCycNINA Probe-Target duplex in **10 mM Sodium Phosphate buffer (pH 7.0), 1 M $NaClO_4$.** a) Sensing results across each gold working electrode. b) Average sensing results. [Target DNA] between 1 µM to 10 fM. Error values are reported at a 95% confidence level of the standard error of the mean.*

between certain variations, Figure 4.25. Overall, smaller decreases in the Cyc:Fc current ratio were observed for each nucleobase, with thymine seeing the biggest decrease at 30%. The readout for guanine was particularly affected, seeing a significant decrease relative to the other nucleobases. This was beneficial for identifying a guanine-cytosine variant, with the difference in percentage decrease in Cyc:Fc ratio increasing to 5%. The conditions were also well suited to detect a thymine-guanine variation, with a difference in 11% between the signal readouts of the two bases. These conditions appear favourable for a mutation such as the KRAS G12V, where the healthy wild-type guanine at position 35 is replaced with thymine in the mutant strain.

The buffer conditions were further varied by altering the accompanying salts, with a full summary included in the *Appendix section 6.3.5*. These included 10 mM sodium phosphate buffer (pH 7.0), 100 mM NaCl, which are comparable conditions to phosphate-buffered saline solutions used for biological research. Whilst the sensing results were promising, the readouts for adenine and cytosine were just within error of one another and so the conditions were not as suitable as the buffers detailed above. Sensing with FcCycNINA in 10 mM tris HCl buffer (pH 7.0), 1 M $NaClO_4$ gave the poorest SPV sensing readout, with Cyc:Fc ratios for adenine, cytosine and guanine similar and within error. However, the cyclidene signal saw a significantly larger decrease in these conditions than any other assessed and some peak shifts were observed. Use of FcCycNINA in this buffer may be suitable for the detection of other, less subtle biomarkers, including circulating free DNA, which can indicate a trauma injury or a stroke among other afflictions.[44]

The success with 10 mM tris HCl buffer, 100 mM NaCl and 10 mM sodium phosphate buffer, 1 M $NaClO_4$ led us to select these two conditions for the subsequent ratiometric sensing experiments.

4.4.4.5. Selectivity Studies

The complementary nature of DNA, arising from the hydrogen bonding of the nucleobases, ensures that the probe has an affinity for its preprogramed target over other nucleic acid sequences. Such selectivity is vital for the success of the probe when analysing more complex mixtures such as a blood or saliva sample, which contain a variety of DNA species. To assess the selectivity of the FcCycNINA probe, a target strand consisting of an uncomplementary nucleobase sequence was synthesised, Table 4.6.

Table 4.6: The uncomplementary target strand. Scrambled Target possesses the same nucleobase composition as Target-T but the order of the bases has been scrambled to prevent duplex formation.

Name	*Sequence*
Scrambled Target	5’ - ACA GCT TCA TGG AAG - 3’

Addition of the Scrambled Target strand to the FcCycNINA probe resulted in a minor decrease in the Cyc:Fc current ratio, often less than 5%, Figure 4.26. This is considerably lower than the smallest decrease observed when sensing the target-DNA strands. The small decrease in the cyclidene redox signal is thought to be due to non-specific hydrogen bonding interactions between the nucleobases of the probe and those of the Scrambled Target. The terminally bound ferrocene unit experiences little change to its redox signal due to its distance from any

nucleobase interactions. Thermal melting studies confirmed that FcCycNINA did not form a duplex with Scrambled Target, with no melting temperature obtained.

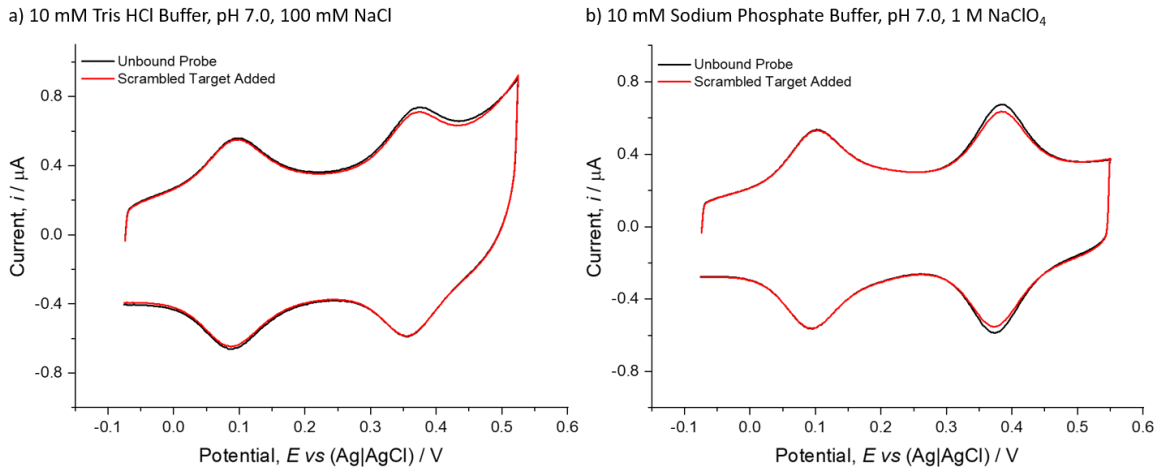

Figure 4.26: Cyclic voltammograms showing the FcCycNINA probe with the Scrambled Target in a) 10 mM tris HCl buffer (pH 7.0), 100 mM NaCl, [Scramblted Target] = 100 pM and b) 10 mM sodium phosphate buffer (pH 7.0), 1 M NaClO4, [Scrambled Target] = 10 fM. Scan rate = 1000 mV s^{-1}

The FcCycNINA probe was then subjected to a competitive selectivity test; it was immersed in a 1:1 solution of Target-T and Scrambled Target and the sensing output from the CV was analysed, Figure 4.27. The probe demonstrated its selectivity, forming a duplex with its complementary sequence Target-T, as evidenced by the substantial decrease in the cyclidene current signal. In 10 mM tris HCl buffer (pH 7.0), 100 mM NaCl conditions, a decrease of 36.3%

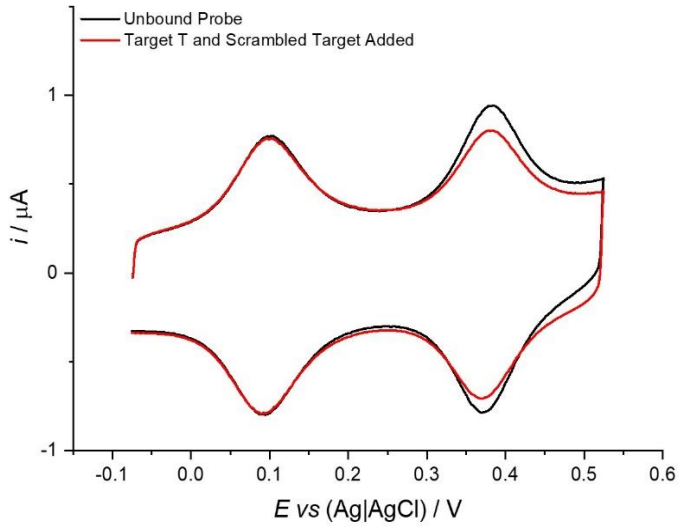

Figure 4.27: Cyclic Voltammogram depicting the FcCycNINA sensing in a mixture of Target-T and Scrambled Target in 10 mM sodium phosphate buffer (pH 7.0), 1 M $NaClO_4$ [Target DNA] = 10 fM.

was observed, compared to the 38.3% ± 0.6 expected for Target-T. Whilst the readout was outside the margin of error expected, the error was calculated for pure samples of target and so it is promising that the introduction of a competing species has led to a only a very minor variation in the sensing output. That the readout signal did not fall within the error window of any of the other nucleobase targets was also very positive and highlighted the necessity to have as large signal difference between targets as possible.

4.4.4.6. Limit of Detection

To determine the lowest target concentration that FcCycNINA could reliably distinguish each nucleobase, the sensing experiments were repeated with a reduced quantity of target-DNA. The concentration of Target-T was decreased by an order of magnitude in each experiment and the Cyc:Fc current ratio was monitored across multiple electrodes, Figure 4.28.

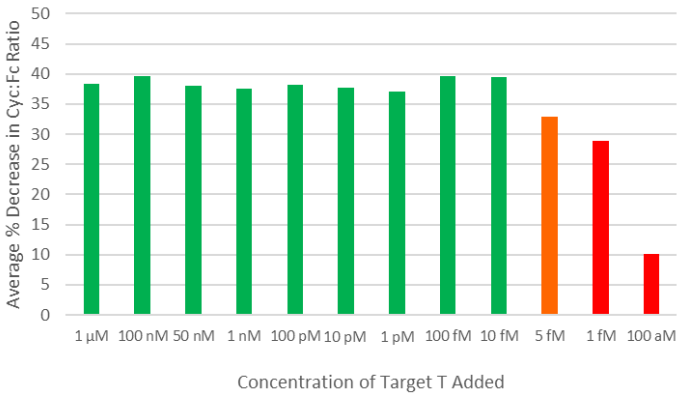

Figure 4.28: Average percentage decrease in Cyc:Fc ratio upon target binding at a variety of target concentrations. [Target-T] = 1 µM to 100 aM. CVs performed in 10 mM tris HCl buffer (pH 7.0), 100 mM NaCl.

From target concentrations of 1 µM to 10 fM the decreases in Cyc:Fc current ratio were as expected and within error of the average value. Lowering the concentration further to 5 and 1 fM also induced significant decreases in current ratio but they were outside the margin of error expected for Target-T and could falsely suggest another nucleobase target was present. Decreasing the target concentration by a further order of magnitude to 100 aM induced a

decrease of only 10%, far lower than the expected value for any nucleobase. Following the initial study with Target-T, sensing with the other nucleobase targets was performed at picomolar and femtomolar concentrations, and the sensing readouts obtained matched the results from the earlier experiments at higher target concentrations.

The results demonstrated that nucleobase discrimination can be performed with confidence at a 10 fM target concentration. The small deviations from the expected value at lower femtomolar concentrations may suggest that not all FcCycNINA probes of the SAM are bound to the target, as shown in Figure 4.29a, hence smaller changes in cyclidene current were observed. Decreasing the concentration to 100 aM would further increase the number of unbound probes, hence the smaller current decrease, Figure 4.29b. Whilst unable to discriminate subtle genetic variations at these lower concentrations, FcCycNINA appears capable of monitoring the binding of biomarkers down to low femtomolar levels.

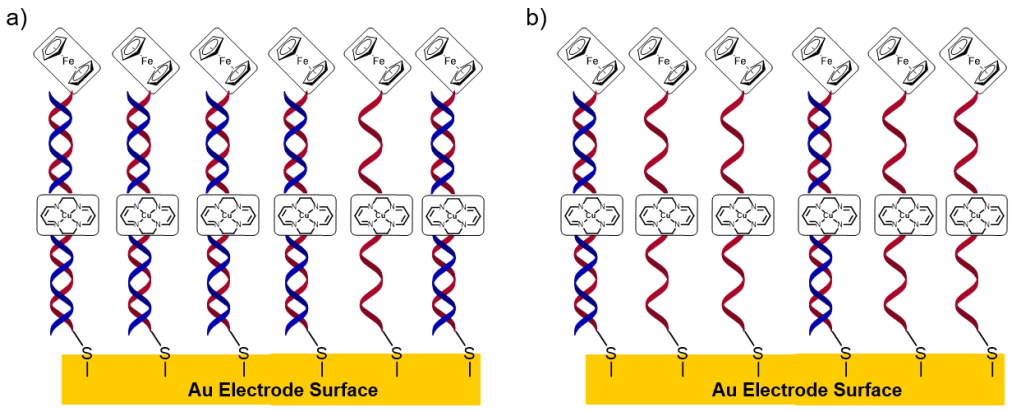

Figure 4.29: Schematic representation of the FcCycNINA SAM. a) Majority of sensing probes are binding target DNA. b) Minority of probes binding target DNA.

The ability of the ratiometric probe to discriminate between nucleobases and allow SPV detection in the femtomolar range is unprecedented and crucially would allow for the detection of such biomarkers without the need for much, or perhaps any, PCR amplification. If this could be replicated on patient samples, it would save valuable time and reduce the cost

of the sensing assay, making such a system highly beneficial for an end user such as an NHS medical practice or hospital. The ability to monitor binding events at low-femtomolar concentrations is in keeping with other reported surface-bound nucleic acid probes.[18, 19, 39] However, it appears that this is the first nucleic acid probe that is capable of distinguishing between nucleobases (i.e. discern SPVs) at such low concentrations.

4.4.4.7. Reusability and Unbound Probe Regeneration

Alongside a rapid, accurate sensing readout at low cost, a reusable sensing probe would be highly desirable for an end user in medical screening. The initial studies with the CycNINA probe investigated the use of urea as a means of denaturation, section 4.3.4.5. Although it proved capable of regenerating some of the unbound probes, the results were varied and at best, only partial regeneration occurred. The new heterometallic probe FcCycNINA was also soaked in a urea solution but again, the results were inconsistent.

Sonication of the SAM-coated electrode has been previously explored as an alternative means of denaturation, with evidence of denaturation in a matter of minutes reported.[45] Following sensing of Target-A, the FcCycNINA-coated electrode was sonicated in ultrapure water for 90

a)

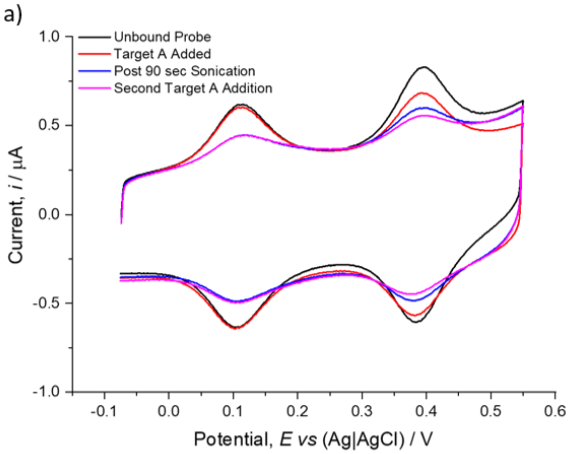

b)

	Cyc:Fc	*% Decrease*
Unbound Probe	1.266	-
Target-A Added (10 fM)	0.987	22.04
Post Sonication	1.280	-
Second Target-A Addition	0.999	22.01

Figure 4.30: a) CV showing the reusability of the FcCycNINA probe. Scan rate = 1000 mV s^{-1}. b) Table outlining the sensing results from the CV in a). CV recorded in 10 mM sodium phosphate buffer (pH 7.0), 1 M $NaClO_4$. [Target-A] = 10 fM.

seconds. The electrode was returned to a solution of buffer and the sensing process repeated, with the results shown in Figure 4.30. The sonication denatured the probe-target duplex and regenerated the unbound probe, as evidenced by the recovery of the Cyc:Fc ratio to the initial value. Upon addition of Target-A, the cyclidene current decreased again by a consistent amount.

Whilst the result was encouraging, it is important to note that this method does not result in a sensing system that could be used an infinite number of times. As evidenced by Figure 4.30a, sonication led to a decreased current signal for both the cyclidene and the ferrocene redox peaks. Therefore, sonication of the electrode causes some of the gold-sulfur bonds of the SAM to be broken, causing some of the FcCycNINA probe to be lost from the surface. Washing steps following sonication ensured the detached probes did not contaminate the buffer solution and contribute to the sensing signal. It is also important not to sonicate the working electrode excessively, as extended sonication is known to damage the polycrystalline gold surface.

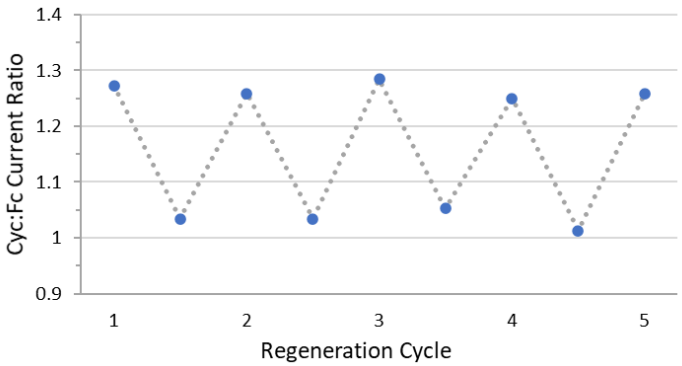

Figure 4.31: The change in the Cyc:Fc current ratio over multiple regeneration cycles. Sensing performed in 10 mM sodium phosphate buffer (pH 7.0), 1 M $NaClO_4$. [Target-G] = 10 fM. 1 min sonication in ultrapure water per cycle.

Nevertheless, the method could reliably denature the probe-target duplex, with the freshly regenerated probe providing a consistent and accurate sensing output multiple times, Figure 4.31. Incorporating the ferrocene reference molecule into the same probe as the cyclidene

complex was vital for this success, as the loss of probe from the electrode surface does not result in an imbalance in the ratio of the two redox centres, thus proving that the unbound probe has been regenerated completely.

4.4.4.8. Epigenetic Sensing

After the success of identifying the four canonical DNA nucleobases with FcCycNINA, Target-5mC was synthesised, Table 4.7, presenting the challenge of sensing the epigenetic biomarker, 5-methylcytosine.

Table 4.7: The epigenetic target strand consists of the NINA nucleobase sequence with 5-methylcytosine at its centre.

Name	*Sequence*
Target-5mC	5’ - CAT TGA G **5mC** G AGT CCA - 3’

The FcCycNINA probe was able to discriminate between the healthy nucleobase and the epigenetic biomarker, Figure 4.32. The smaller decrease in signal for 5-methylcytosine relative to cytosine was in keeping with the observations between the canonical nucleobases, where smaller decreases in Cyc:Fc ratio were observed for the physically larger purines, adenine and guanine, compared to the pyrimidines. The result demonstrated the remarkable sensitivity of the copper cyclidene complex and its ability to detect even subtle variations in

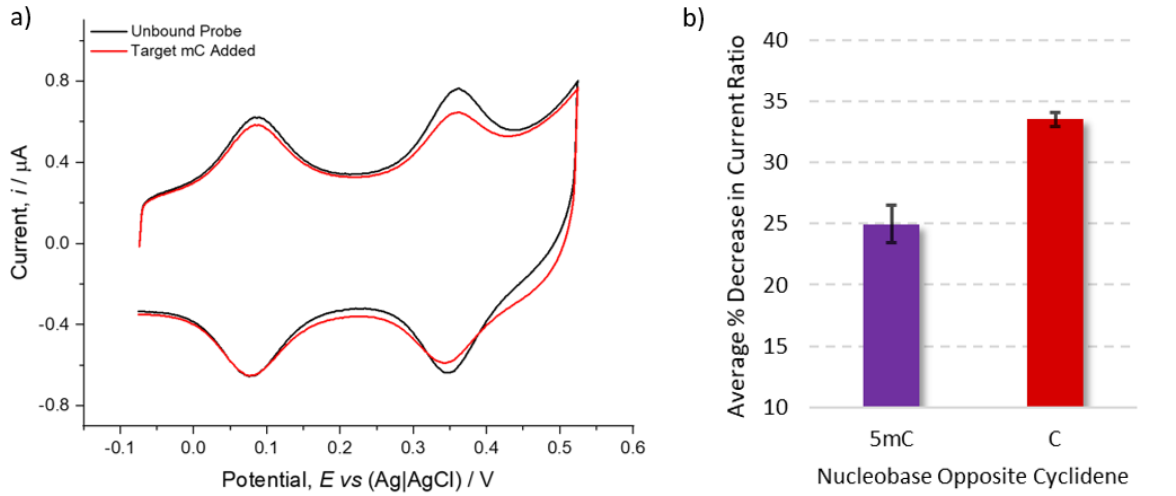

Figure 4.32: Sensing Target-5mC. a) Cyclic voltammogram, scan rate = 1000 mV s-1. 10 mM tris HCl buffer (pH 7.0), 100 mM NaCl. [Target-5mC] = 100 pM. b) Comparing 5mC and C sensing. [Target DNA] = 100 pM to 10 fM. Error values are reported at a 95% confidence level of the standard error of the mean.

its immediate environment, presumably through intercalation. In this instance, the addition of a methyl group is sufficient to adjust the position of the tag in the duplex, subsequently altering the electron transfer rate and allowing the identification of the mutation. This quality appears unique to the cyclidene complex in the (*R*) tag conformation, as outlined below.

4.4.4.9. Sensing with (*S*)-FcCycNINA

The experiments detailed above have used the (*R*) diastereomer of the FcCycNINA probe because of its performance during the initial solution studies.[20] This superior sensing ability was confirmed when sensing with the (*S*) diastereomer of FcCycNINA was conducted, Table 4.8.

Table 4.8: The percentage decrease in the Cyc:Fc current ratio of (S) FcCycNINA probe in 10 mM tris HCl buffer (pH 7.0), 100 mM NaCl.

	Base Opposite Cyclidene			
Electrode	T / %	A / %	G / %	C / %
1	25.06	24.68	n.d.	26.86
2	25.54	25.29	23.52	26.12
3	29.35	23.82	24.21	22.37
4	28.11	25.84	25.90	23.11

As expected, the (*S*) probe was capable of sensing target binding, as evidenced by the drop in Cyc:Fc ratio, however the percentage decreases for each target-DNA species were very similar and nucleobase identification was not possible. The is what was found in the solution work[24] and must somehow be associated with the conformation adopted by the (*S*) cyclidene tag, which prevents it from intercalating as far into the duplex as the (*R*) tag and interacting with its opposite nucleobase in the probe-target duplex to the same extent. This theory is

supported by the T_m data in Table 4.4 and previously reported computational models for the solution-based probes.[20]

4.4.4.10. Summary

The FcCycNINA probe has been proven capable of discriminating between all four canonical nucleobases and the epigenetic biomarker 5-methylcytosine at low femtomolar concentrations using a ratiometric electrochemical sensing approach. The key to the nucleobase detection is the copper cyclidene complex situated at the centre of the DNA strand, whose intercalating ability allows it to respond to the subtle changes in environment that accompany a nucleobase variation. The use of an internal reference molecule, ferrocene, allows for a more accurate, reproducible and consistent sensing readout, whilst also enabling the probe to be reliably reused. The sensing readout can be obtained in under half an hour, with a 20-minute hybridisation proving more than sufficient to bind the target-DNA. The probe's development appears a promising step to detecting important biomarkers such as SPVs without the need for target amplification steps such as PCR, which take time and are costly.

Whilst these studies with the ratiometric sensing system are promising, they have so far been carried out using an in-house test DNA sequence. The next stage of the technology's development examines the use of DNA sequences taken from genes that contain a known cancer mutation site. If successful, such probes could then be applied to patient samples to assess their suitability as a clinical diagnostic device.

4.5. Ratiometric Electrochemical Sensing of Natural SPVs

4.5.1. Sequence Selection

Two single point variant sites were selected as suitable targets and the appropriate sequences were programmed into the ratiometric sensing probe, Table 4.9.

Table 4.9: The BRAF and KRAS ratiometric probes synthesised alongside their complementary wild type and mutant DNA targets. X = Copper cyclidene tag. Fc = Ferrocene. SS = 6 SS 3' disulphide modification.

Name	*Sequence*
FcCycBRAF	5' – Fc AGA TTT C X C TGT AGC SS – 3'
BRAF Target-T	5' – GCT ACA GTG AAA TCT – 3'
BRAF Target-A	5' – GCT ACA GAG AAA TCT – 3'
FcCycKRAS	5' – Fc TAC GCC A X A AGC TCC SS – 3'
KRAS Target-G	5' – GGA GCT GGT GGC GTA – 3'
KRAS Target-T	5' – GGA GCT GTT GGC GTA – 3'
KRAS Target-A	5' – GGA GCT GAT GGC GTA – 3'

The BRAF V600E mutation is prevalent in several cancers, including bowel cancer and melanoma, and sees a thymine to adenine variation at position 1799 of the BRAF gene. The FcCycBRAF probe was accordingly programmed with the complementary sequence to a 15-base-long section centred about the mutation site.[46] The FcCycKRAS probe targets an SPV site at position 35 of the KRAS gene, codon 12, where the healthy wild type guanine is known to mutate to both thymine and adenine, termed the KRAS G12V and G12D mutations, respectively. The mutant species are important biomarkers for bowel cancer, with the

guanine-thymine variation the more common of the two.[47] This particular KRAS target is an attractive challenge for the ratiometric system not only because of its medical significance, but that the ratiometric probe must be able to distinguish between three nucleobase targets.

As the only change to the composition of the new ratiometric probes is the nucleobase sequence, they were synthesised, purified and characterised as detailed for the FcCycNINA system. Specific information including characterisation by mass spectrometry and HPLC can be found in *Appendix section 6.3.1.2.*

4.5.2. Thermal Melting Studies

Thermal melting studies confirmed that the change in the nucleobase coding of the ratiometric probe did not alter the behaviour of the copper cyclidene complex, with similar trends observed compared to FcCycNINA. The results displayed in Table 4.10 outline that the (*S*) isomer forms more stable duplexes than the (*R*) isomer, whilst stationing a larger purine nucleobase opposite the cyclidene modification site destabilises the duplex relative to a pyrimidine. The one exception to this was the high value of the FcCycKRAS (*R*) isomer when binding KRAS Target-G. The KRAS probes possessed a far higher melting value than their NINA and BRAF counterparts, with the additional stability resulting from the high guanine and cytosine content in the nucleobase sequence. It is possible that the presence of the guanine nucleobase in the target position contributes to that stability through hydrogen bonding.

Table 4.10: Thermal melt values of the FcCycNINA, FcCycBRAF and FcCycKRAS probes binding the target strands. The T_m value of the unmodified NINA sequence was 64.0 °C, unmodified BRAF was 63.0 °C and the unmodified KRAS was 73.8 °C. [DNA] = 10 µM in 10 mM sodium phosphate buffer (pH 7.0), 100 mM NaCl.

Base Opposite Cyclidene	*FcCycNINA / °C*		*FcCycBRAF / °C*		*FcCycKRAS / °C*	
	(*S*)	(*R*)	(*S*)	(*R*)	(*S*)	(*R*)
A	62.0	55.7	61.0	55.3	72.4	69.0
C	64.5	61.0	n.d.	n.d.	n.d.	n.d.
G	61.5	59.5	n.d.	n.d.	72.7	71.0
T	63.7	59.5	62.2	60.8	73.3	69.9

That the same trends are observed, compared to the FcCycNINA probe, suggests that the cyclidene complex is behaving and interacting with the surrounding environment in the

probe-target duplex as expected, which is encouraging for the prospect of electrochemically differentiating between the nucleobases.

4.5.3. Electrochemical Sensing

4.5.3.1. BRAF V600E

The FcCycBRAF probe was capable of electrochemically identifying the BRAF V600E mutation at concentrations as low as 10 fM. As expected, the 10 mM tris HCl buffer (pH 7.0), 100 mM NaCl buffer conditions were best suited to sensing the SPV, with the results shown in Figure 4.33.

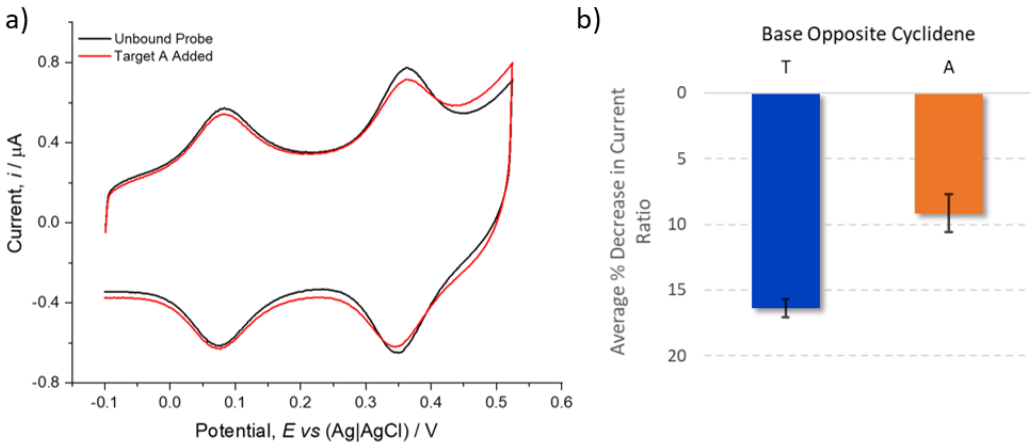

Figure 4.33: a) Cyclic voltammogram showing FcCycBRAF probe sensing Target-A in 10 mM tris HCl buffer (pH 7.0), 100 mM NaCl. [Target-A] = 10 fM. b) The average percentage decrease in Cyc:Fc current ratio upon target binding of FcCycBRAF probe in 10 mM tris HCl buffer (pH 7.0), 100 mM NaCl. [Target DNA] = 100 pM to 10 fM. Error values are reported at a 95% confidence level of the standard error of the mean.

The percentage decrease in the Cyc:Fc current ratio was considerably smaller for both targets compared to the equivalent results with the FcCycNINA test probe, with a decrease of 16.4 ± 0.7 observed upon binding the wild type thymine target and just 9.2% ± 1.4 for the mutant adenine target. Despite the smaller decreases in the readout signal, the FcCycBRAF probe was comfortably capable of consistently and accurately detecting the specific nucleobase target. The 7% difference in the readout signals was not as large as the thymine-adenine difference

observed in the same buffer conditions with the FcCycNINA probe, but the low error in the values mean it is a more than acceptable gap.

One concern around the lower readout signal changes, especially the mere 9% decrease for adenine, was whether the FcCycBRAF probe would be able to distinguish between a binding event and minor interactions with other DNA species in a complex solution. It was interesting to note then that addition of the uncomplementary Scrambled Target strand followed the same trend, with a far smaller decrease in Cyc:Fc ratio of less than 2% observed, Figure 4.34. Due to the consistency of the signal readout, such a small decrease is unlikely to interfere with the sensing of a binding event.

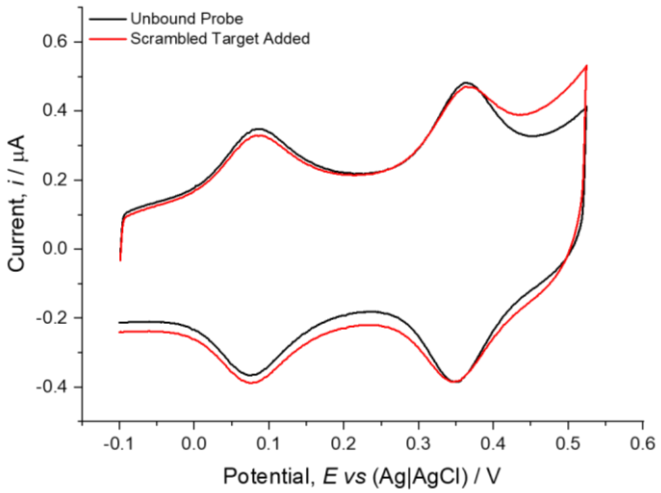

Figure 4.34: Cyclic voltammogram outlining the selectivity of the FcCycBRAF probe. A decrease of only 1.66% is observed upon binding Scrambled Target. Scan rate = 1000 mV s^{-1}. 10 mM tris HCl buffer (pH 7.0), 100 mM NaCl. [Scrambled Target] = 10 fM.

Performing the electrochemical sensing in the sodium phosphate buffer system led to very poor nucleobase discrimination, as expected from the earlier studies with FcCycNINA. These results in included in the *Appendix section 6.3.3*.

4.5.3.2. KRAS G12V and G12D

The detection of the KRAS gene variation presented a greater challenge for the ratiometric sensing system due to the need to discriminate between three nucleobases: the healthy wild type guanine and the mutants adenine and thymine. Whereas the sensing readout for the BRAF biomarker simply needed to identify whether the wildtype had mutated into its single alternative nucleobase, requiring buffer conditions which gave the clearest separation between the thymine and adenine readouts, the FcCycKRAS probe had to deliver an accurate and consistent sensing readout that could unequivocally identify one of two possible mutations present at the SPV site.

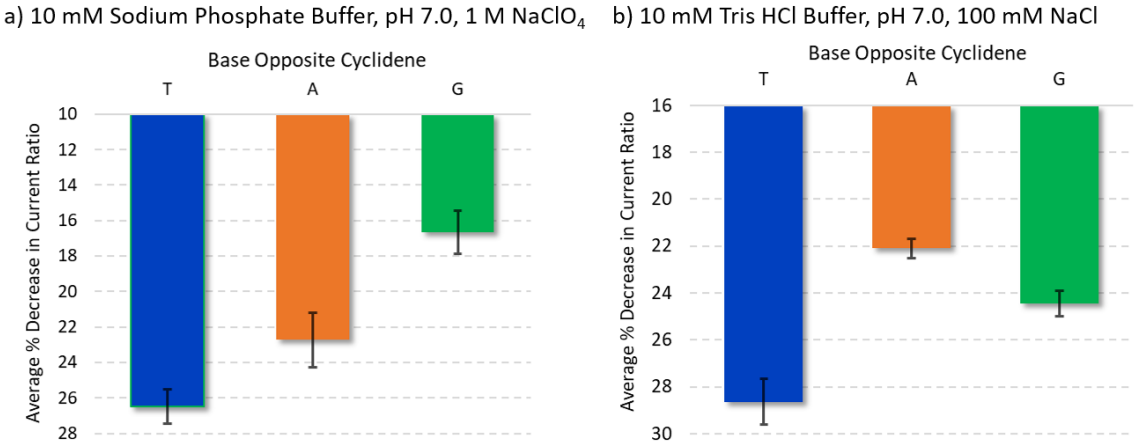

Figure 4.35: The average percentage decrease in the Cyc:Fc current ratio upon target binding of the FcCycKRAS probe in a) 10 mM Na phosphate buffer (pH 7.0), 1 M $NaClO_4$ and b) 10 mM tris HCl buffer (pH 7.0), 100 mM NaCl. [Target DNA] = 10 fM. Error values are reported at a 95% confidence level of the standard error of the mean.

Both sets of buffer conditions were explored to determine the best sensing set up. The studies indicated that each buffer was capable of distinguishing between the three nucleobases, Figure 4.35. As seen previously with the FcCycNINA probe, the sodium phosphate buffer conditions excelled at discriminating between the guanine-thymine variant of KRAS G12V, Figure 4.36, alongside the KRAS G12D guanine-adenine variant. That the signal readouts for thymine and adenine were sufficiently separated and out of error was equally important, allowing the FcCycKRAS probe to not only identify a wild-type to mutant change, but to

specify which mutant nucleobase. Whilst the tris HCl buffer conditions could also detect the nucleobase variations, the difference in the signal readout between the nucleobases was not as substantial as that offered by the phosphate buffer. However, despite the smaller separation, the margin of error in the readings are very small due to the excellent consistency of the probe.

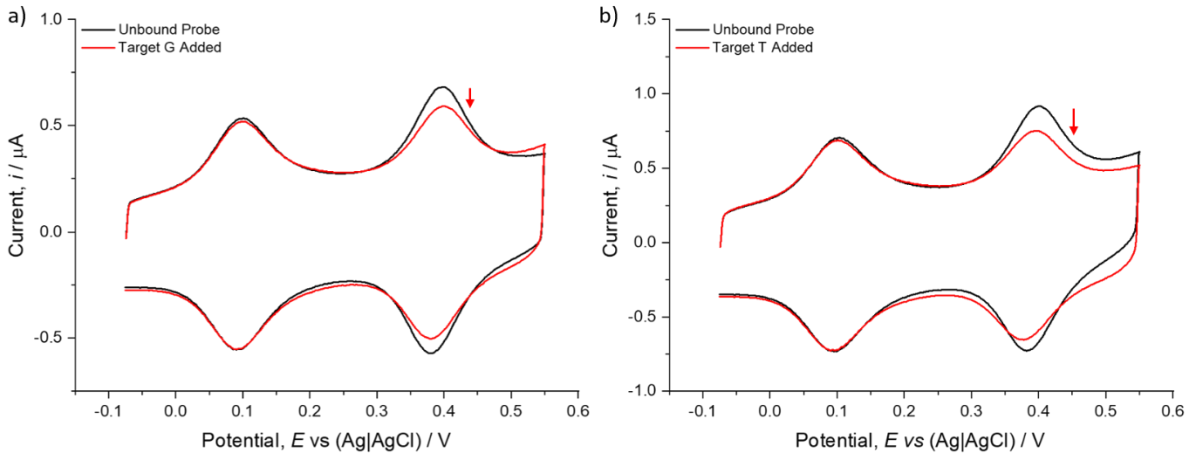

Figure 4.36: CVs of FcCycKRAS showing the smaller decrease in cyclidene current for Target-G (a) compared to the larger decrease for Target-T (b). 10 mM Na Phosphate buffer (pH 7.0), 1 M $NaClO_4$. Scan rate = 1000 mV s^{-1}. [Target DNA] = 10 fM.

The FcCycKRAS probe offered the same selectivity as its counterparts, with a minor decrease in the Cyc:Fc ratio of 5-8% observed with the scrambled target strand, Figure 4.37. The change in ratio for the noncomplementary sequence is significantly lower than the smallest decrease observed for a complementary target-DNA strand.

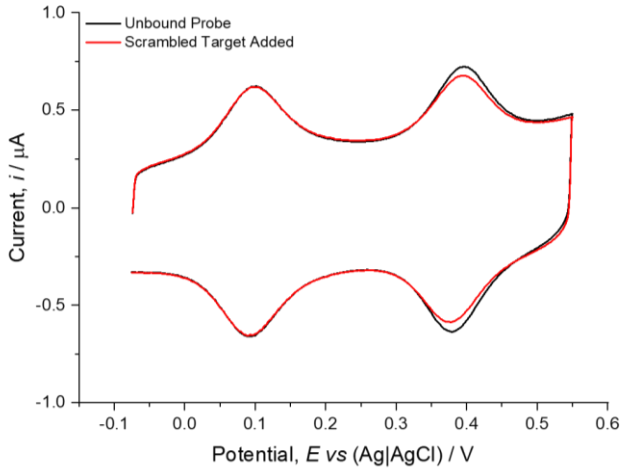

Figure 4.37: Cyclic voltammogram showing the FcCycKRAS probe with the Scrambled Target strand. 10 mM sodium phosphate buffer (pH 7.0), 1 M $NaClO_4$. Scan rate = 1000 mV s^{-1}. [Scrambled Target] = 10 fM.

The magnitude of the FcCycKRAS signal decreases induced by target binding were comparable to the values observed with FcCycNINA, as were the changes observed upon addition of the uncomplementary Scrambled Target. All the changes in readout signal were far larger than those observed for the BRAF sensing system. This unusual trend implies the nucleobase sequence of the DNA strand has an impact on the signal decreases. The BRAF sequence is thymine-rich, including a stretch of three consecutive thymine units. It is possible that the flexibility of FcCycBRAF is subsequently greater and the conformation adopted in the probe-target duplex better facilitates the electron transfer from the copper cyclidene complex to the electrode surface relative to the other two probes, hence the reduced signal decrease upon target binding.

a)

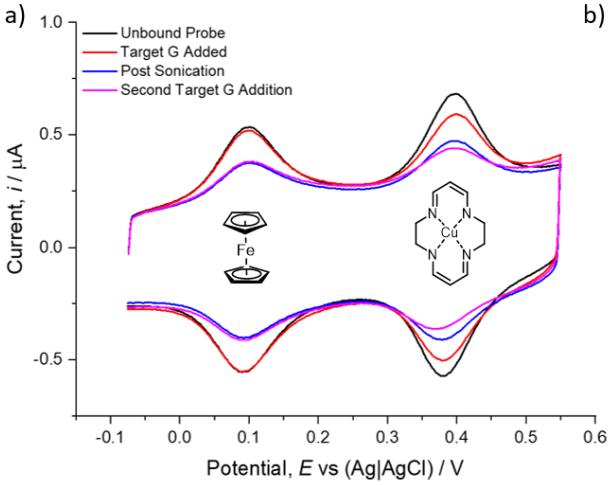

b)

	Cyc:Fc	*% Decrease*
Unbound Probe	1.246	-
Target-G Added (10 fM)	1.029	17.42
Post 60 sec Sonication	1.227	-
Second Target-G Addition	1.017	17.11

Figure 4.38: a) Cyclic voltammograms displaying the reusability of the FcCycKRAS probe. 10 mM sodium phosphate buffer (pH 7.0), 1 M $NaClO_4$. [Target G] = 10 fM. Sonication time = 1 min. Scan rate = 1000 mV s^{-1}. b) Cyc:Fc Current ratio analysis of CV.

In Figure 4.38, FcCycKRAS showcases the reusability of the ratiometric probes, achieving full signal recovery from a 60 second sonication in ultra-pure water before sensing Target-G for a second time with a consistent drop in the Cyc:Fc ratio. An interesting future experiment would be to add a different target strand after denaturation and see if the expected signal decrease is observed.

4.5.4. Summary

The ratiometric sensing system has adapted to two SPV sites in the BRAF and KRAS genes and is successfully able to distinguish between the healthy wild type and the mutant nucleobases. The FcCycBRAF and FcCycKRAS probes performed the electrochemical sensing with the same precision, consistency and reproducibility as exhibited in the FcCycNINA test probe, producing a reliable sensing readout. They demonstrated that the nucleobase composition of the probe may be tailored to any specific target species without affecting the behaviour of the two metal redox centres and the sensing ability of the ratiometric system. Most importantly, the probes could be used to detect the target species at a concentration of 10 fM, raising the possibility of detecting these medically important biomarkers without the need for target amplification.

4.6. Conclusions and Future Work

A novel hetero-bimetallic nucleic acid strand which is capable of electrochemically detecting single point variants at a concentration of 10 fM *via* a ratiometric approach has been developed. The surface-based sensing system was built on the previously published work which discovered the nucleobase-discriminating ability of an intercalating copper cyclidene complex tagged into the backbone of a DNA strand. This new design attaches an additional redox-active metal to the 5'-terminal of the strand in the form of a ferrocene molecule, which acts as an internal electrochemical reference with which the signal changes in the copper cyclidene signal can be compared upon target binding, allowing a more consistent sensing readout. The ratiometric approach, which also enables the probe to be reused, has been employed to detect disease biomarkers including bowel cancer.

The low limit of detection offered by the ratiometric system is an exciting development which raises the possibility of detecting nucleic acid biomarkers without the need for amplification, an expensive and time-consuming process which sees patients wait days to receive a prognosis. The potential to provide a medical professional with vital information, ranging from an initial diagnosis to how a patient is responding to treatments, in under 30 minutes without the need for expensive, specialist equipment would be of huge value to health services such as the NHS. In light of this, and owing to the novel probe design, a patent application has been filed for the heterometallic ratiometric sensing system.[48]

The future development of the sensing system will explore two areas. Studies to improve the design of the probe will aim to maximise the strength of the electrochemical signal and explore increasing the binding-induced decrease of the cyclidene redox signal. Initial experiments will focus on shifting the position of the cyclidene and ferrocene tags along the DNA strand and finding the optimum arrangement for the clearest sensing readout. This includes maximising the difference in sensing readout for each target nucleobase. The second area of development will look to test the BRAF and KRAS-specific probes on patient samples after the initial success with synthetic targets. The performances of the probes with such complex mixtures will inform the development of the probe design as well as indicating whether the detection limits of the probe are low enough to sense biomarkers without the need for target amplification. It will be an excellent test of the sensing capability and whether the detection of subtle genetic differences are possible in patient samples, or if the system will be better suited to the rapid detection of biomarkers such as circulating free DNA, which may simply require registering the binding event.

4.7. References

1. R. Wu, *Nature New Biol.*, 1972, **236**, 198.
2. International_Human_Genome_Sequencing_Consortium, *Nature*, 2001, **409**, 860.
3. International_Human_Genome_Sequencing_Consortium, *Science*, 2001, **291**, 1304.
4. International_Human_Genome_Sequencing_Consortium, *Nature*, 2004, **431**, 931.
5. C. S. Pareek, R. Smoczynski and A. Tretyn, *J. Appl. Genetics*, 2011, **52**, 413.
6. R. T. Ranasinghe and T. Brown, *Chem. Commun.*, 2005, 5487.
7. S. Banerjee, E. B. Veale, C. M. Phelan, S. A. Murphy, G. M. Tocci, L. J. Gillespie, D. O. Frimannsson, J. M. Kelly and T. Gunnlaugsson, *Chem. Soc. Rev.*, 2013, **42**, 1601.
8. P. Zhang, T. Beck and W. Tan, *Angew. Chem. Int. Ed.*, 2001, **40**, 402.
9. J. Guo, J. Ju and N. J. Turro, *Anal. Bioanal. Chem.*, 2012, **402**, 3115.
10. P. J. Santangelo, B. Nix, A. Tsourkas and G. Bao, *Nucleic Acids Res.*, 2004, **32**, 57.
11. K. J. Livak, S. J. A. Flood, J. Marmaro, W. Giusti and K. Deetz, *Genome Res.*, 1995, **4**, 357.
12. F. E. A. McGuigan and S. H. Ralston, *Psychiat. Genet.*, 2002, **12**, 133.
13. N. Thelwell, S. Millington, A. Solinas, J. Booth and T. Brown, *Nucleic Acids Res.*, 2000, **28**, 3752.
14. M. Monici, *Biotechnol. Annu. Rev.*, 2005, **11**, 227.
15. C. Fan, K. W. Plaxco and A. J. Heeger, *PNAS*, 2003, **100**, 9134.
16. A. A. Lubin and K. W. Plaxco, *Acc. Chem. Res.*, 2010, **43**, 496.
17. Y. Xiao, A. A. Lubin, B. R. Baker, K. W. Plaxco and A. J. Heeger, *PNAS*, 2006, 16677.
18. I. Grabowska, D. G. Singleton, A. Stachyra, A. Gora-Sochacka, A. Sirko, W. Zagorski-Ostoja, H. Radecka, E. Stulz and J. Radecki, *Chem. Commun.*, 2014, **50**, 4916.
19. B. Kaur, K. Malecka, D. A. Cristaldi, C. S. Chay, I. Mames, H. Radecki and E. Stulz, *Chem. Commun.*, 2018, **54**, 11108.
20. J.-L. H. A. Duprey, J. Carr-Smith, S. L. Horswell, J. Kowalski and J. H. R. Tucker, *J. Am. Chem. Soc*, 2016, **138**, 746.
21. M. Hegner, P. Wagner and G. Semenza, *FEBS Lett.*, 1993, **336**, 452.
22. J.-L. H. A. Duprey, D. M. Bassani, E. I. Hyde, C. Ludwig, A. Rodger, J. S. Vyle, J. Wilkie, Z. Zhao and J. H. R. Tucker, *Supramol. Chem.*, 2011, **23**, 273.
23. Z. Zhao, M. San, J.-L. H. A. Duprey, J. R. Arrand, J. S. Vyle and J. H. R. Tucker, *Bioorg. Med. Chem. Lett.*, 2012, **22**, 129.
24. J. Carr-Smith, PhD Thesis, University of Birmingham, 2015.
25. J.-L. Mergny and L. Lacroix, *Oligonucleotides*, 2003, **13**, 515.
26. R. Thomas, *Biochim. Biophys. Acta.*, 1954, **14**, 231.
27. R. Thomas, *Gene*, 1993, **135**, 77.
28. S. A. Rice and P. Doty, *J. Am. Chem. Soc*, 1957, **79**, 3937.
29. C. T. Wittwer, M. G. Herrmann, A. A. Moss and R. P. Rasmussen, *Biotechniques*, 1997, **22**, 130.
30. H. Gudnason, M. Dufva, D. D. Bang and A. Wolff, *Nucleic Acids Res.*, 2007, **35**, 127.
31. A. J. Bard and L. R. Faulkner, *Electrochemical Methods: Fundamentals and Applications*, Wiley and Sons, 2 edn., 2001.
32. J. C. Hoogvliet, M. Dijksma, B. Kamp and W. P. v. Bennekom, *Anal. Chem.*, 2000, **72**, 2016.
33. E. F. D. Jr., P. F. Driscoll, D. Liu, N. A. Burnham, C. R. Lambert and W. G. McGimpsey, *Anal. Chem.*, 2008, **80**, 7670.
34. R. Levicky, T. M. Herne, M. J. Tarlov and S. K. Satija, *J. Am. Chem. Soc*, 1998, **120**, 9787.
35. M. S. Krause and L. Ramaley, *Anal. Chem.*, 1969, **41**, 1362.
36. J. G. Osteryoung and R. A. Osteryoung, *Anal. Chem.*, 1985, **57**, 101.
37. T. T. Herskovits, *Biochemistry*, 1963, **2**, 335.
38. Y. Du, B. J. Lim, B. Li, Y. S. Jiang, J. L. Sessler and A. D. Ellington, *Anal. Chem.*, 2014, **86**, 8010.
39. E. Xiong, X. Zhang, Y. Liu, J. Zhou, P. Yu, X. Li and J. Chen, *Anal. Chem.*, 2015, **87**, 7291.

40. A. Anne, A. Bouchardon and J. Moiroux, *J. Am. Chem. Soc*, 2003, **125**, 1112.
41. M. Chahma, J. S. Lee and H.-B. Kraatz, *J. Electroanal. Chem.*, 2004, **567**, 283.
42. H. Roberts, PhD, University of Birmingham, 2018.
43. N. Elgrishi, K. J. Rountree, B. D. McCarthy, E. S. Rountree, T. T. Eisenhart and J. L. Dempsey, *J. Chem. Educ.*, 2018, **95**, 197.
44. A. N. Butt and R. Swaminathan, *Ann. N. Y. Acad. Sci.*, 2008, **1137**, 236.
45. X. Wang, H. J. Lim and A. Son, *Environ. Anal. Health Toxicol.*, 2014, **29**, 1.
46. G. R. B. H. Davies, C. Cox, P. Stephens, S. Edkins, S. Clegg, J. Teague, H. Woffendin, M. J. Garnett, W. Bottomley, N. Davis, E. Dicks, R. Ewing, Y. Floyd, K. Gray, S. Hall, R. Hawes, J. Hughes, V. Kosmidou, A. Menzies, C. Mould, A. Parker, C. Stevens, S. Watt, S. Hooper, R. Wilson, H. Jayatilake, B. A. Gusterson, C. Cooper, J. Shipley, D. Hargrave, K. Pritchard-Jones, N. Maitland, G. Chenevix-Trench, G. J. Riggins, D. D. Bigner, G. Palmieri, A. Cossu, A. Flanagan, A. Nicholson, J. W. C. Ho, S. Y. Leung, S. T. Yuen, B. L. Weber, H. F. Seigler, T. L. Darrow, H. Paterson, R. Marais, C. J. Marshall, R. Wooster, M. R. Stratton and P. A. Futreal, *Nature*, 2002, **417**, 949.
47. W. Kim, S. Lee, H. S. Kim, M. Song, Y. H. Cha, Y.-H. Kim, J. Shin, E.-S. Lee, Y. Joo, J. J. Song, E. J. Choi, J. W. Choi, J. Lee, M. Kang, J. I. Yook, M. G. Lee, Y.-S. Kim, S. Paik and H. Kim, *Genome Res.*, 2018, **28**, 1.
48. J. H. R. Tucker and Co-workers, UK Patent Application No. 2008017.2, 2020.

5. Experimental

All reagents and solvents were purchased from Sigma-Aldrich, Acros Organics, Alfa Aesar, Fisher Scientific, VWR and LGC Genomics and used as received. Dry solvents were either purchased as such or obtained from a Pure Solv-MD solvent purification system and transported under an atmosphere of argon. Reactions using anhydrous solvents were performed in oven-dried glassware under an atmosphere of argon. Thin-layer chromatography (TLC) was performed on Merck silica gel 60 plates and visualised using short-wave UV light (254 nm). Flash column chromatography was performed using Merck silica 60. ^{1}H NMR and ^{31}P NMR spectra were recorded on a Bruker AVIII 300 NMR spectrometer, recorded at 300 MHz. ^{13}C NMR spectra were recorded on a Bruker AVIII 400 spectrometer, recorded at 101 MHz. Chemical shifts (δ) are reported in ppm and are relative to the residual solvent peak. Data were acquired using Bruker Topspin v3.2 and analysed with MestReNova v12.0.3-21384. Electrospray mass (ESI-MS) spectra were acquired by either Waters Micromass LCT Electrospray Time-of-Flight (ES-TOF), Waters Xevo G2-XS, or Synapt G2S mass spectrometers. FT–IR spectra were recorded using a PerkinElmer 100FT–IR spectrometer with ATR attachment. Only diagnostic and/or intense peaks are reported. Melting points were carried out in triplicate and an average of the values recorded and reported as a range using Stuart SMP10 melting point apparatus with open glass capillary tubes.

5.1. Synthesis of Cobalt Sandwich Complexes

5.1.1. Synthesis of Alkyne Precursors:

5.1.1.1. Trimethyl(*o*-tolylethynyl)silane:

Known Compound. Characterisation matches the literature data.[1]

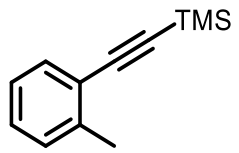

2.1

Bis(triphenylphosphine)palladium(II) dichloride (0.730 g, 5 mol %) and copper iodide (0.438 g, 10 mol %) were added to a stirred solution of 2-iodotoluene (2.92 ml, 22.93 mmol, 1 equiv.) and dry trimethylamine (37.5 ml). Ethynyl trimethylsilane (3.85 ml, 27.05 mmol, 1.2 equiv.) was added dropwise at 0 ˚C and the resulting mixture was stirred for 24 h at rt. The solvent was removed under vacuum, the residue was filtered through celite and the celite pad was washed with hexane (30 ml) and ethyl acetate (30 ml). The filtrate was concentrated under reduced pressure and the crude residue purified by column chromatography (silica gel; eluent system of 95:5 hexane:ethyl acetate). The appropriate fractions were combined and the solvent removed to yield a yellow oil (4.284 g, 22.78 mmol, 99%). ^{1}H NMR (300 MHz, $CDCl_3$) δ 7.32 (d, J = 7.4 Hz, 1H, *PhCH₃ C**H***), 7.12 – 7.03 (m, 2H, *PhCH₃ C**H***), 7.03 – 6.96 (m, 1H, *PhCH₃ C**H***), 2.33 (s, 3H, *PhC**H₃***), 0.17 (s, 9H, *(C**H₃**)₃Si*). ^{13}C NMR (101 MHz, $CDCl_3$) δ 140.48 (*PhCH₃ **C**CH₃*), 132.02 (*PhCH₃ **C**H*), 129.26 (*PhCH₃ **C**H*), 128.38 (*PhCH₃ **C**H*), 125.35 (*PhCH₃ **C**H*), 122.85 (*PhCH₃ **C***), 104.01 (***C***≡*C-TMS*), 98.06 (*C≡**C**-TMS*), 20.54 (*Ph**C**H₃*), 0.00 (*Si**C**H₃*).

5.1.1.2. 1-Ethynyl-2-methylbenzene:

Known Compound. Characterisation matches the literature data.[2]

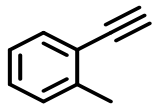

2.2

Trimethyl(*o*-tolylethynyl)silane (1.720 g, 9.145 mmol, 1 equiv.) was dissolved in dry methanol (15 ml) before potassium carbonate (2.528 g, 18.29 mmol, 2 equiv.) was added and the resulting mixture was stirred at rt for 16 h. The resulting mixture was quenched with water (50 ml), before being washed with diethyl ether (3 x 50 ml). The organic washings were combined and washed with brine (30 ml) before the solvent was removed under reduced pressure to afford a pale-yellow oil (0.849 g, 7.319 mmol, 80 %). ^{1}H NMR (300 MHz, $CDCl_3$) δ 7.46 (d, J = 8.3 Hz, 1H, *PhCH₃ C**H***), 7.27 – 7.17 (m, 2H, *PhCH₃ C**H***), 7.16 – 7.09 (m, 1H, *PhCH₃ C**H***), 3.27 (s, 1H, *C≡C-**H***), 2.45 (s, 3H, *PhC**H₃***). ^{13}C NMR (101 MHz, $CDCl_3$) δ 140.78 (*PhCH₃ **C**CH₃*), 132.53 (*PhCH₃ **C**H*), 129.46 (*PhCH₃ **C**H*), 128.75 (*PhCH₃ **C**H*), 125.53 (*PhCH₃ **C**H*), 121.94 (*PhCH₃ **C***), 82.54 (***C***≡*C-H*), 80.95 (*C≡**C**-H*), 20.60 (*Ph**C**H₃*). LRMS (TOF MS EI$^+$) (m/z) calculated for C_9H_8: 116.06 found: 116.1 $[M]^+$

5.1.2. Alkyne Functionalisation:

5.1.2.1. 4'-(*o*-tolylethynyl)benzo-18-crown-6 ether:

Novel compound.

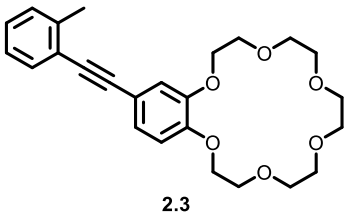

2.3

4-bromo-benzo-18-crown-6 ether (4.998 g, 12.81 mmol, 1 equiv.) was dissolved in dry diisopropylamine (50 ml) before $PdCl_2(PPh_3)_2$ (0.449 g, 5 mol %) and copper iodide (0.122 g, 5 mol %) were added. The resulting mixture was deoxygenated with argon for 45 min before 2-ethynyl toluene (2.08 g, 17.93 mmol, 1.4 equiv.) was added dropwise over 30 min at 0 °C. The resulting mixture was then heated at 90 ˚C for 3 nights. The reaction mixture was cooled to rt before the solvent was removed under reduced pressure. The residue was redissolved in ethyl acetate and passed through a pad of celite. The celite pad was washed with ethyl acetate and then hexane until the washings were clear. The filtrate was collected and the solvent removed under reduced pressure before the crude residue was purified by column chromatography (silica gel, eluent system of 96:4 dichloromethane:methanol). The appropriate fractions were combined and the solvent removed to yield a thick, light brown oil (5.136 g, 12.05 mmol, 94%). ^{1}H NMR (400 MHz, $CDCl_3$) δ 7.47 (d, J = 7.3 Hz, 1H, *PhCH₃ C**H***), 7.22 (d, J = 1.0 Hz, 1H, *PhCH₃ C**H***), 7.21 (m, 1H, *PhCH₃ C**H***), 7.19 – 7.14 (m, 1H, *PhCH₃ C**H***), 7.11 (dd, J = 8.3, 1.9 Hz, 1H, *Ph-crown C**H***), 7.04 (d, J = 1.9 Hz, 1H, *Ph-crown C**H***), 6.83 (d, J = 8.3 Hz, 1H, *Ph-crown C**H***), 4.20 – 4.15 (m, 4H, *crown-OC**H₂***), 3.95 – 3.91 (m, 4H, *crown-OC**H₂***), 3.78 (dd, J = 6.0, 2.9 Hz, 4H, *crown-OC**H₂***), 3.72 (dd, J = 6.1, 3.1 Hz, 4H, *crown-OC**H₂***), 3.69 (s, 4H, *crown-OC**H₂***), 2.50 (s, 3H, *PhC**H₃***). ^{13}C NMR (101 MHz, $CDCl_3$) δ 149.37 (*Ph-crown **C**OCH₂*), 148.49 (*Ph-crown **C**OCH₂*), 139.98 (*PhCH₃ **C**CH₃*), 131.69 (*PhCH₃ **C**H*), 129.44 (*PhCH₃ **C**H*), 128.07 (*PhCH₃ **C**H*), 125.57 (*PhCH₃ **C**H*), 125.28 (*Ph-crown **C**H*), 123.19 (*PhCH₃ **C***), 116.77 (*Ph-crown **C**H*), 116.15 (*Ph-crown **C***), 113.48 (*Ph-crown **C**H*), 93.38 (***C***≡*C-PhCH₃*), 86.97 (*C≡**C**-PhCH₃*), 70.79 (*crown O**C**H₂*), 70.67 (*crown O**C**H₂*), 69.47 (*crown O**C**H₂*), 69.01 (*crown O**C**H₂*), 68.89 (*crown O**C**H₂*), 20.79 (*Ph**C**H₃*). HRMS (TOF MS EI$^+$) (m/z) calculated for $C_{25}H_{30}O_6$: 426.2042, $C_{25}H_{30}O_6Na$: 449.1940 found: 449.1944 $[M+Na]^+$

5.1.2.2. 4'-(*o*-tolylethynyl)veratrole:

Novel compound.

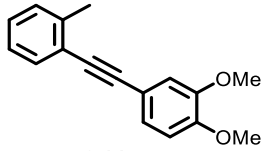

2.14

4-bromoveratrole (0.66 ml, 4.607 mmol, 1 equiv.) was dissolved in dry diisopropylamine (10 ml) before $PdCl_2(PPh_3)_2$ (0.162 g, 5 mol %) and copper iodide (0.044 g, 5 mol %) were added. The resulting mixture was deoxygenated for 45 min before 2-ethynyl toluene (0.70 ml, 6.450 mmol, 1.4 equiv.) was added dropwise over 30 min at 0 °C. The resulting mixture was then heated at 90 ˚C for 3 nights. The reaction was cooled to rt and passed through celite. The celite pad was washed with ethyl acetate until the washings were colourless and then washed with hexane (10 ml). The filtrate was collected and the solvent removed under reduced pressure before the crude residue was purified by column chromatography (silica gel; eluent system of 9:1 hexane:ethyl acetate) which yielded a light brown oil (1.033 g, 4.097 mmol, 89%). ^{1}H NMR (300 MHz, $CDCl_3$) δ 7.49 (d, *J* = 7.1 Hz, 1H, *PhCH₃ C**H***), 7.25 – 7.12 (m, 4H, *PhCH₃ C**H**, Ph(OCH₃)₂ C**H***), 7.04 (t, *J* = 2.0 Hz, 1H, *Ph(OCH₃)₂ C**H***), 6.84 (d, *J* = 8.3 Hz, 1H, *Ph(OCH₃)₂ C**H***), 3.91 (d, *J* = 2.8 Hz, 6H, *Ph(OC**H₃**)₂*), 2.52 (s, 3H, *PhC**H₃***). ^{13}C NMR (101 MHz, $CDCl_3$) δ 149.46 (*Ph(OCH₃)₂ **C**OCH₃*), 148.68 (*Ph(OCH₃)₂ **C**OCH₃*), 139.98 (*PhCH₃ **C**CH₃*), 131.71 (*PhCH₃ **C**H*), 129.44 (*PhCH₃ **C**H*), 128.07 (*PhCH₃ **C**H*), 125.57 (*PhCH₃ **C**H*), 124.83 (*Ph(OCH₃)₂ **C**H*), 123.38 (*PhCH₃ **C***), 114.17 (*Ph(OCH₃)₂ **C***), 112.48 (*Ph(OCH₃)₂ **C**H*), 111.07 (*Ph(OCH₃)₂ **C**H*), 93.42 (***C**≡C-PhCH₃*), 86.91 (*C≡**C**-PhCH₃*), 55.93 (*Ph(O**C**H₃)₂*), 20.81 (*Ph**C**H₃*). LRMS (TOF MS EI$^+$) (m/z) calculated for $C_{17}H_{16}O_2$: 252.12 found: 252.2 M^+

5.1.3. Sandwich Complex Formation:

5.1.3.1. Chlorotris(triphenylphosphine) Cobalt

Known compound.[3]

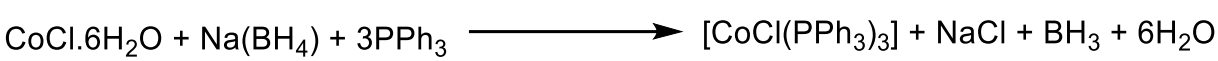

Cobalt (II) chloride hexahydrate (4.80 g, 20.20 mmol, 1 equiv.) and triphenyl phosphine (16.00 g, 61.00 mmol, 3 equiv.) were stirred in deoxygenated ethanol (300 ml) and the resulting mixture was heated at 70 ˚C for 30 min. The reaction mixture was cooled to rt before sodium borohydride (0.80 g, 20.20 mmol, 1 equiv.) was added in several small portions over 10 min. The brown precipitate was collected *via* filtration and washed sequentially with ethanol (10 ml), water (10 ml), ethanol (10 ml) and hexane (10 ml). The precipitate was collected and dried under high vacuum to yield the desired product as a chocolate brown powder (15.45 g, 17.50 mmol, 87%).

5.1.3.2. (η^4-1,3-*o*-Tolyl-2,4-benzo-18-crown-6-ether-cyclobutadiene)(η^5-carbomethoxycyclopentadienyl) Cobalt:

Novel Compound. Adapted from Richards *et al.*[4, 5]

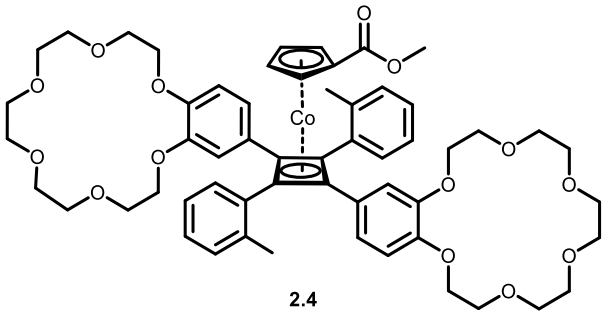

2.4

Dimethyl carbonate (0.87 ml, 10.26 mmol, 3.4 equiv.) was added to a solution of sodium cyclopentadienylide (2 M in THF) (1.51 ml, 3.318 mmol, 1.1 equiv.) in dry THF (4 ml) and the solution was heated at 75 ˚C for 4 h. The solution was cooled to rt before dry toluene (32 ml), $CoCl(PPh_3)_3$ (2.66 g, 3.017 mmol, 1 equiv.) and 4'-(*o*-tolylethynyl)benzo-18-crown-6 ether (2.70 g, 6.335 mmol, 2.1 equiv.) were added sequentially. The resulting mixture was heated at 120 ˚C for 16 h. The reaction mixture was cooled and the solvent removed under reduced pressure before the crude residue was redissolved in dichloromethane and passed through celite. The celite pad was washed with dichloromethane (60 ml) until the washings were colourless. The filtrate was collected and the solvent removed under vacuum, before the crude residue was purified by column chromatography (silica gel; gradient eluent system 100 % dichloromethane to 9:1 dichloromethane:methanol). The final yellow band was collected and the solvent removed to yield a yellow oil. This mixture of metallocene isomers was further purified by preparative HPLC (C18 column; gradient eluent system of 1:1 acetonitrile:water to 100 % acetonitrile over 30 min, monitored by 375 nm). The appropriate fractions were combined and the solvent removed to afford the desired *trans* isomer as a yellow solid (0.892 g, 0.862 mmol, 29%). Ratio of crude yield: *cis*:*trans*: 1:2.5 (determined by ^{1}H NMR). ^{1}H NMR (400 MHz, $CDCl_3$) δ 8.30 (d, J = 6.6 Hz, 2H, *PhCH₃ C**H***), 7.38 (t, J = 7.1 Hz, 2H, *PhCH₃ C**H***), 7.32 (t, J = 6.8 Hz, 2H, *PhCH₃ C**H***), 7.20 (d, J = 7.3 Hz, 2H, *PhCH₃ C**H***), 6.46 (t, J = 7.5 Hz, 2H, *Ph-crown C**H***), 6.36 (dd, J = 8.4, 1.7 Hz, 2H, *Ph-crown C**H***), 6.29 (d, J = 1.7 Hz, 2H, *Ph-crown C**H***), 5.69 (t, J = 2.0 Hz, 2H, *Cp C**H***), 4.81 (t, J = 2.0 Hz, 2H, *Cp C**H***), 4.03 – 3.97 (m, 4H, *crown OC**H₂***), 3.87 – 3.81 (m, 4H, *crown OC**H₂***), 3.73 – 3.62 (m, 28H, *crown OC**H₂***), 3.60 (d, J = 4.6 Hz, 4H, *crown OC**H₂***), 3.18 (s, 3H, *COOC**H₃***), 2.19 (s, 6H, *PhC**H₃***). ^{13}C NMR (101 MHz, $CDCl_3$) δ 166.45 (***C***=*O*), 148.20 (*Ph-crown **C**OCH₂*), 147.12 (*Ph-crown **C**OCH₂*), 138.31 (*PhCH₃ **C**Cb*), 133.48 (*PhCH₃*

C**CH₃*), 133.43 (*PhCH₃ **C**H*), 130.42 (*Ph-crown **C**Cb*), 129.69 (*PhCH₃ **C**H*), 128.00 (*PhCH₃ **C**H*), 126.01 (*PhCH₃ **C**H*), 117.74 (*Ph-crown **C**H*), 113.70 (*Ph-crown **C**H*), 109.64 (*Ph-crown **C**H*), 85.80 (*Cp **C), 85.47 (*Cp **C**H*), 83.87 (*Cp **C**H*), 78.59 (*Cb **C***), 77.22 (*Cb **C***), 70.49 (*crown O**C**H₂*), 69.27(*crown O**C**H₂*), 69.05 (*crown O**C**H₂*), 67.64 (*crown O**C**H₂*), 67.47 (*crown O**C**H₂*), 51.17 (*COO**C**H₃*), 21.09 (*Ph**C**H₃*) LRMS (TOF MS EI$^+$) (m/z) calculated for $C_{57}H_{67}O_{14}CoNa$: 1057.37 found: 1057.39 $[M+Na]^+$.

5.1.3.3. (η^4-1,3-*o*-Tolyl-2,4-veratrole-cyclobutadiene)(η^5-carbomethoxy-cyclopentadienyl) Cobalt:

Novel Compound. Adapted from Richards *et al.*[4, 5]

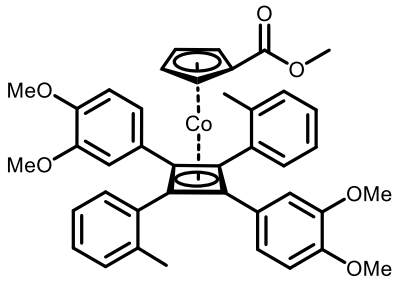

2.15

Dimethyl carbonate (0.47 ml, 5.556 mmol, 3.5 equiv.) was added to a solution of sodium cyclopentadienylide (2 M in THF) (0.90 ml, 1.797 mmol, 1.1 equiv.) in dry THF (4 ml), before the resulting solution was heated at 75 ˚C for 4 h. The reaction mixture was cooled to rt before dry toluene (32 ml), $CoCl(PPh_3)_3$ (1.44 g, 1.634 mmol, 1 equiv.) and 4'-(*o*-tolylethynyl)veratrole (0.865 g, 3.432 mmol, 2.1 equiv.) were added sequentially. The resulting mixture was heated at 120 ˚C for 16 h. The reaction mixture was cooled to rt and the solvent was removed under reduced pressure before the crude residue was redissolved in dichloromethane and passed through celite. The celite pad was washed with dichloromethane until the washings were

colourless. The filtrate was collected and the solvent removed under vacuum, before the crude residue was purified by column chromatography (silica gel; 7:3 hexane:ethyl acetate). The first yellow band was collected and the solvent removed to yield the desired *trans* isomer as a yellow oil (0.314 g, 0.457 mmol, 28%). Ratio of crude yield: *cis*:*trans*: 1:2.5 (determined by ^{1}H NMR). ^{1}H NMR (300 MHz, $CDCl_3$) δ 8.35 (dd, *J* = 7.4, 1.4 Hz, 2H, *PhCH₃ C**H***), 7.44 – 7.29 (m, 4H, *PhCH₃ C**H***), 7.22 (d, *J* = 7.1 Hz, 2H, *PhCH₃ C**H***), 6.50 (d, *J* = 8.4 Hz, 2H, *Ph(OCH₃)₂ C**H***), 6.41 (dd, *J* = 8.3, 1.9 Hz, 2H, *Ph(OCH₃)₂ C**H***), 6.36 (d, *J* = 1.9 Hz, 2H, *Ph(OCH₃)₂ C**H***), 5.72 (t, *J* = 2.1 Hz, 2H, *Cp C**H***), 4.83 (t, *J* = 2.1 Hz, 2H, *Cp C**H***), 3.75 (s, 6H, *PhOC**H₃***), 3.37 (s, 6H, *PhOC**H₃***), 3.17 (s, 3H, *COOC**H₃***), 2.23 (s, 6H, *PhC**H₃***) ^{13}C NMR (101 MHz, $CDCl_3$) δ 166.41 (***C***=*O*), 148.71 (*Ph(OCH₃)₂ **C**OCH₃*), 147.62 (*Ph(OCH₃)₂ **C**OCH₃*), 138.31 (*PhCH₃ **C**Cb*), 133.55 (*PhCH₃ **C**CH₃*), 133.48 (*PhCH₃ **C**H*), 129.98 (*Ph(OCH₃)₂ **C**Cb*), 129.62 (*PhCH₃ **C**H*), 128.02 (*PhCH₃ **C**H*), 126.00 (*PhCH₃ **C**H*), 117.40 (*Ph(OCH₃)₂ **C**H*), 111.36 (*Ph(OCH₃)₂ **C**H*), 107.98 (*Ph(OCH₃)₂ **C**H*), 85.85 (*Cp **C***), 85.39 (*Cp **C**H*), 83.89 (*Cp **C**H*), 78.57 (*Cb **C***), 55.70 (*PhO**C**H₃*), 55.11 (*PhO**C**H₃*), 51.02 (*COO**C**H₃*), 21.10 (*Ph**C**H₃*) LRMS (TOF MS EI^{+}) (m/z) calculated for $C_{41}H_{39}O_6CoNa$: 709.20 found: 709.20 $[M+Na]^{+}$

5.1.3.4. (η^5-Carbomethoxycyclopentadienyl)(η^4-tetraphenylcyclobutadiene) Cobalt:

Known compound. Characterisation matches the literature data.[4]

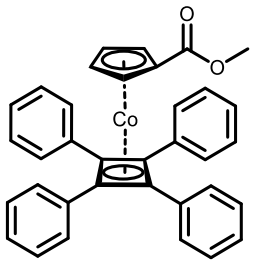

2.6

Dimethyl carbonate (0.38 ml, 4.542 mmol, 3.4 equiv.) was added to a solution of sodium cyclopentadienylide (2 M in THF) (0.74 ml, 1.469 mmol, 1.1 equiv.) in dry THF (4 ml) and the solution was heated at 70 ˚C for 4 h. The solution was cooled to rt before dry toluene (32 ml), $CoCl(PPh_3)_3$ (1.17 g, 1.336 mmol, 1 equiv.) and diphenyl acetylene (0.500 g, 2.805 mmol, 2.1 equiv.) were added sequentially. The resulting mixture was heated at 120 ˚C for 16 h. The reaction was cooled to rt and the solvent was removed under vacuum before the crude residue was redissolved in dichloromethane and passed through celite. The celite pad was washed with dichloromethane until the washings were colourless. The filtrate was collected and the solvent removed under vacuum, before the crude residue was purified by column chromatography (silica gel; gradient eluent system of 3:7 dichloromethane:hexane increasing to 7:3 dichloromethane:hexane). The yellow band was collected and the solvent removed to yield a dark yellow solid (0.460 g, 0.854 mmol, 64%). ^{1}H NMR (300 MHz, $CDCl_3$) δ 7.43 (dd, *J* = 7.9, 1.5 Hz, 8H, *Ph C**H***), 7.30 – 7.15 (m, 12H, *Ph C**H***), 5.19 (t, *J* = 2.1 Hz, 2H, *Cp C**H***), 4.76 (t, *J* = 2.1 Hz, 2H, *Cp C**H***), 3.21 (s, 3H, *COOC**H₃***). ^{13}C NMR (101 MHz, $CDCl_3$) δ 166.38 (***C***=*O*), 135.11 (*Ph **C***), 128.87 (*Ph **C**H*), 128.08 (*Ph **C**H*), 126.72 (*Ph **C**H*), 86.69 (*Cp **C***), 86.39 (*Cp **C**H*), 84.55 (*Cp **C**H*), 76.40 (*Cb **C***), 51.21 (*COO**C**H₃*). LRMS (TOF MS EI$^+$) (m/z) calculated for $C_{35}H_{27}O_2Co$: 538.12 found: 538.1 M^+

5.1.4. Synthesis of Cobalt Sandwich Complex Rotary System:

5.1.4.1. (η^4-1,3-*o*-Tolyl-2,4-benzo-18-crown-6-ether-cyclobutadiene)(η^5-*N*-3-(aminomethyl)benzylaminecyclopentadienyl) Cobalt:

Novel compound. Adapted from literature.[6, 7]

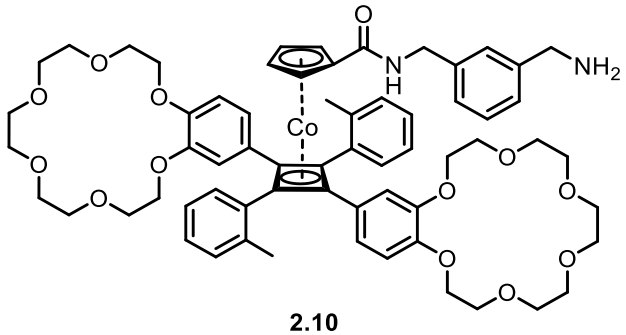

2.10

Trimethyl aluminium (2 M in toluene) (0.06 ml, 0.116 mmol, 3 equiv.) was added dropwise at 0 ˚C to a solution of *m*-xylylene diamine (0.015 ml, 0.116 mmol, 3 equiv.) in dry toluene (2 ml). The resultant solution was allowed to warm to rt and stirred for 1 h. A solution of (η^4-1,3-*o*-tolyl-2,4-benzo-18-crown-6-ether-cyclobutadiene) (η^5-carbomethoxycyclopentadienyl) cobalt (0.040 g, 0.0387 mmols, 1 equiv.) in dry toluene (2 ml) was added dropwise at rt before the resulting mixture was heated at 120 ˚C overnight. The reaction mixture was cooled to rt before dichloromethane (10 ml) and aq. potassium sodium tartrate solution (1.3 M, 10 ml) were added, and the aqueous phase was washed with dichloromethane (3 x 10 ml). The organic phases were combined, washed with brine (10 ml) and dried over anhydrous magnesium sulphate. The solvent was removed under reduced pressure and the crude residue purified by column chromatography (neutral alumina; 97:3 dichloromethane:methanol). The yellow band was collected and solvent removed to yield a yellow oil (0.030 g, 0.0263 mmol, 68%). ^{1}H NMR (400 MHz, CD_3OD) δ 8.45 (d, *J* = 7.5 Hz, 2H, *PhCH₃ C**H***), 7.46 (t, *J* = 7.4 Hz, 2H, *PhCH₃ C**H***), 7.38 (t, *J* = 7.3 Hz, 2H, *PhCH₃ C**H***), 7.29 – 7.19 (m,

5H, *PhCH₃* ***CH****, PhCH₂NH₂* ***CH***), 6.66 (s, 1H, *PhCH₂NH₂* ***CH***), 6.56 (d, *J* = 8.5 Hz, 2H, *Ph-crown* ***CH***), 6.45 (dd, *J* = 8.4, 1.3 Hz, 2H, *Ph-crown* ***CH***), 6.33 (s, 2H, *Ph-crown* ***CH***), 5.84 (t, J = 2.0 Hz, 2H, *Cp* ***CH***), 4.77 (t, J = 2.0 Hz, 2H, *Cp* ***CH***), 4.14 (s, 2H, *PhC****H₂****CO*), 3.94 (s, 6H, *PhC****H₂****NH₂, crown OC****H₂***), 3.80 – 3.57 (m, 32H, *crown OC****H₂***), 3.51 (m, 4H, *crown OC****H₂***), 2.18 (s, 6H, *PhC****H₃***). ^{13}C NMR (101 MHz, CD_3OD) δ 168.72 (***C****=O*), 148.78 (*Ph-crown* ***C****OCH₂*), 147.64 (*Ph-crown* ***C****OCH₂*), 140.27 (*PhCH₂NHCO* ***C***), 139.36 (*PhCH₃* ***C****Cb*), 135.08 (*PhCH₃* ***C****H*), 134.65 (*PhCH₃* ***C****CH₃*), 133.92 (*PhCH₂NH₂* ***C***), 131.96 (*Ph-crown* ***C****Cb*), 130.75 (*PhCH₃* ***C****H*), 130.18 (*PhCH₃* ***C****H*), 129.89 (*PhCH₂NH₂* ***C****H*), 129.59 (*PhCH₂NH₂* ***C****H*), 129.36 (*PhCH₂NH₂* ***C****H*), 128.83 (*PhCH₂NH₂* ***C****H*), 127.33 (*PhCH₃* ***C****H*), 119.35 (*Ph-crown* ***C****H*), 114.14 (*Ph-crown* ***C****H*), 110.08 (*Ph-crown* ***C****H*), 90.67 (*Cp* ***C***), 86.72 (*Cp* ***C****H*), 83.12 (*Cp* ***C****H*), 79.90 (*Cb* ***C***), 78.37(*Cb* ***C***), 71.73 (*crown O****C****H₂*), 71.55 (*crown O****C****H₂*), 71.41 (*crown O****C****H₂*), 71.32 (*crown O****C****H₂*), 71.16 (*crown O****C****H₂*), 71.02 (*crown O****C****H₂*), 70.38 (*crown O****C****H₂*), 70.17 (*crown O****C****H₂*), 69.16 (*crown O****C****H₂*), 68.43 (*crown O****C****H₂*), 44.60 (*Ph****C****H₂CO*), 44.26 (*Ph****C****H₂NH₂*), 21.41 (*Ph****C****H₃*). HRMS: (TOF MS ES$^+$) (m/z) calculated for $C_{62}H_{75}N_2O_{13}Co$:1138.4601, $C_{62}H_{76}N_2O_{13}Co$: 1139.4679 found: 1139.4674 $[M+H]^+$

5.1.5. Synthesis of Cobalt Sandwich Complex Control Compounds:

5.1.5.1. (η^4-1,3-o-Tolyl-2,4-veratrole-cyclobutadiene) (η^5-*N*-3-(amino-methyl)benzylaminecyclopentadienyl) Cobalt:

Novel compound. Adapted from literature.[6, 7]

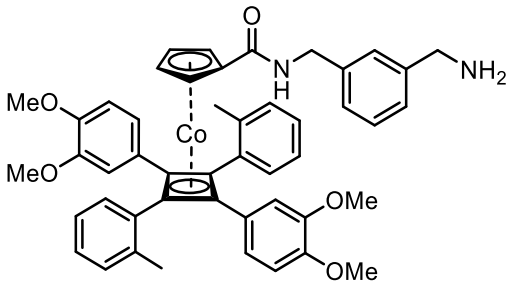

2.13

Trimethyl aluminium (2 M in toluene) (0.42 ml, 0.825 mmol, 3 equiv.) was added dropwise at 0˚C to a solution of *m*-xylylene diamine (0.11 ml, 0.825 mmol, 3 equiv.) in dry toluene (3 ml). The resulting solution was allowed to warm to rt and stirred for 1 h. A solution of η^4-1,3-o-tolyl-2,4-veratrole-cyclobutadiene)(η^5-carbomethoxy-cyclopentadienyl) cobalt: (0.18 g, 0.275 mmol, 1 equiv.) in dry toluene (8 ml) was added dropwise at rt before the resulting mixture was heated at 120 ˚C overnight. The reaction mixture was cooled to rt before dichloromethane (10 ml) and aq. potassium sodium tartrate solution (1.3 M, 10 ml) were added, and the aqueous phase was washed with dichloromethane (3 x 10 ml). The organic phases were combined, washed with brine (10 ml) and dried over anhydrous magnesium sulphate. The solvent was removed under reduced pressure and the crude residue purified by column chromatography (silica gel; 9:1 dichloromethane:methanol). The yellow band was collected and solvent removed to yield a yellow oil (0.111 g, 0.140 mmol, 51%). ^{1}H NMR (300 MHz, CD_3CN) δ 8.39 (dd, *J* = 7.3, 1.7 Hz, 2H, *PhCH₃ C**H***), 7.45 – 7.16 (m, 9H, *PhCH₃ C**H,** PhCH₂NH₂ C**H***), 7.08 (d, *J* = 7.5 Hz, 1H, *PhCH₂NH₂ C**H***), 6.52 (d, *J* = 8.2 Hz, 2H, *Ph(OCH₃)₂ C**H***), 6.35 (q, *J* = 2.0 Hz, 2H, *Ph(OCH₃)₂ C**H***), 6.32 (d, *J* = 2.0 Hz, 2H, *Ph(OCH₃)₂ C**H***), 6.21 (t, *J* = 5.7 Hz, 1H, *CON**H***), 5.71 (t, *J* = 2.1 Hz, 2H, *Cp C**H***), 4.81 (t, *J* = 2.1 Hz, 2H, *Cp C**H***), 3.95 (s, 2H, *PhC**H₂**NH₂*), 3.75 (d, *J* = 5.7 Hz, 2H, *PhC**H₂**NHCO*), 3.65 (s, 6H, *PhOC**H₃***), 3.28 (s, 6H, *PhOC**H₃***), 2.20 (s, 3H, *PhC**H₃***). ^{13}C NMR (101 MHz, CD_3CN) δ 165.44 (***C***=*O*), 149.41 (*Ph **C**OCH₃*) , 148.35 (*Ph **C**OCH₃*), 140.25 (*PhCH₂NHCO **C***), 138.65 (*PhCH₃ **C**Cb*), 134.49 (*PhCH₃ **C**H*), 134.12 (*PhCH₃ **C**CH₃*), 130.53 (*PhCH₂NH₂ **C***), 130.00 (*Ph **C**Cb*), 129.27 (*PhCH₃ **C**H*), 128.79 (*PhCH₃ **C**H*), 128.64 (*PhCH₂NH₂ **C**H*), 128.33 (*PhCH₂NH₂ **C**H*), 126.68 (*PhCH₂NH₂ **C**H*), 117.90 (*PhCH₂NH **C**H*), 112.33 (*Ph **C**H*), 108.91 (*Ph **C**H*), 90.46 (*Cp **C***), 85.23 (*Cp **C**H*), 82.65 (*Cp **C**H*), 78.77 (*Cb **C***),7.43 (*Cb **C***), 55.82 (*Ph CO**C**H₃*),

55.12 (*Ph CO**C**H₃*), 43.67 (*Ph**C**H₂CO*), 43.21 (*Ph**C**H₂NH₂*), 20.92 (*Ph**C**H₃*). HRMS: (TOF MS ES⁺) (m/z) calculated for $C_{48}H_{48}N_2O_5Co$: 791.2895 found: 791.2895

5.1.5.2. (η^5-*N*-3-(aminomethyl)benzylaminecyclopentadienyl)(η^4-tetraphenylcyclobutadiene) Cobalt:

Novel compound. Adapted from literature.[6, 7]

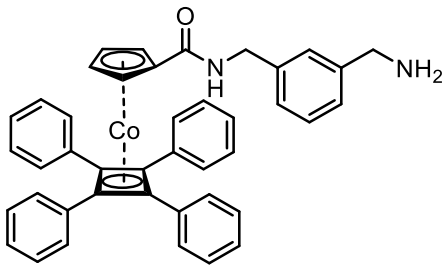

2.9

Trimethyl aluminium (2 M in toluene) (0.04 ml, 0.409 mmol, 2.2 equiv.) was added dropwise at 0˚C to a solution of *m*-xylylene diamine (0.03 ml, 0.223 mmol, 1.2 equiv.) in dry toluene (2 ml). The resulting solution was allowed to warm to rt and stirred for 1 h, before a solution of (η^5-carbomethoxycyclopentadienyl)(η^4-tetraphenylcyclobutadiene) cobalt (0.100 g, 0.186 mmol, 1 equiv.) in dry toluene (3 ml) was added dropwise at rt and the resulting mixture was heated at 120 °C overnight. The reaction mixture was cooled to rt before dichloromethane (10 ml) and aq. potassium sodium tartrate solution (1.3 M, 10 ml) were added, and the aqueous phase was washed with dichloromethane (3 x 10 ml). The organic phases were combined, washed with brine (10 ml) and dried over anhydrous magnesium sulphate. The solvent was removed under reduced pressure and the crude residue purified by column chromatography (silica gel; gradient eluent system starting with 99:1 dichloromethane:triethylamine and ending in 89:10:1 dichloromethane:meth-

anol:triethylamine). The yellow band was collected and solvent removed to yield an orange solid (0.0838 g, 0.130 mmol, 70%). ^{1}H NMR (300 MHz, CD_3CN) δ 7.47 – 7.41 (m, 8H, *Ph C**H***), 7.36 – 7.18 (m, 14H, *Ph C**H**, PhCH₂NH₂ C**H***), 7.13 (s, 1H, *PhCH₂NH₂ C**H***), 6.98 (d, J = 6.9 Hz, 1H, *PhCH₂NH₂ C**H***), 6.45 (t, J = 6.0 Hz, 1H, *CON**H***), 5.18 – 5.16 (m, 2H, *Cp C**H***), 4.79 – 4.76 (m, 2H, *Cp C**H***), 3.93 (d, J = 6.0 Hz, 2H, *PhC**H₂**NHCO*), 3.75 (s, 2H, *PhC**H₂**NH₂*).^{13}C NMR (101 MHz, CD_3CN) δ 165.25 (***C**=O*), 140.43 (*PhCH₂NHCO **C***), 136.16 (*Ph **C***), 129.72 (*PhCH₂NH₂ **C**H*), 129.27 (*PhCH₂NH₂ **C**H*), 129.06 (*PhCH₂NH₂ **C**H*), 127.71 (*PhCH₂NH₂ **C**H*), 127.25 (*Ph **C**H*), 126.59 (*Ph **C**H*), 91.91 (*Cp **C***), 86.52 (*Cp **C**H*), 83.26 (*Cp **C**H*), 77.17 (*Cb **C***), 46.67 (*Ph**C**H₂NH₂*), 43.73 (*Ph**C**H₂NHCO*). HRMS (TOF MS ES$^+$) calculated for $C_{42}H_{35}CoN_2O$: 642.2081, $C_{42}H_{36}CoN_2O$: 643.2160 found: 643.2157 $[M+H]^+$

5.1.5.3. (η^5-*N*-(3-methylbenzylaminecyclopentadienyl)(η^4-tetraphenylcyclobutadiene) Cobalt:

Novel compound. Adapted from literature.[6, 7]

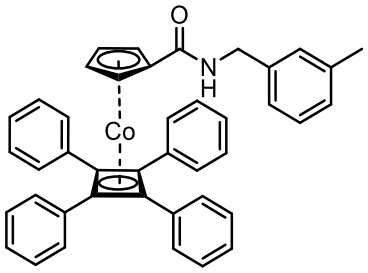

2.12

Trimethyl aluminium (2 M in toluene) (0.78 ml, 1.561 mmol, 3.5 equiv.) was added dropwise at 0˚C to a solution of 3-methyl benzylamine (0.17 ml, 1.338 mmol, 3 equiv.) in dry toluene (3 ml). The resulting solution was allowed to warm to rt and stirred for 1 h, before a solution of

(η^5-carbomethoxycyclopentadienyl)(η^4-tetraphenylcyclobutadiene) cobalt (0.240 g, 0.446 mmol, 1 equiv.) in dry toluene (3 ml) was added dropwise at rt and the resulting mixture was heated at 120 °C overnight. The reaction mixture was cooled to rt before dichloromethane (20 ml) and aq. potassium sodium tartrate solution (1.3 M, 10 ml) were added, and the aqueous phase was washed with dichloromethane (3 x 10 ml). The organic phases were combined, washed with brine (10 ml) and dried over anhydrous magnesium sulphate. The solvent was removed under reduced pressure and the crude residue purified by column chromatography (silica gel; gradient eluent system starting in 7:3 dichloromethane:hexane ending in 100% dichloromethane). The yellow band was collected and solvent removed to yield a yellow oil (0.111 g, 0.177 mmol, 40%). ^{1}H NMR (400 MHz, CD_3CN) δ 7.49 – 7.41 (m, 8H, *Ph C**H***), 7.35 – 7.29 (m, 4H, *Ph C**H***), 7.29 – 7.23 (m, 8H, *Ph C**H***), 7.17 (t, *J* = 7.6 Hz, 1H, *PhCH$_2$NH$_2$ C**H***), 7.06 (d, *J* = 7.6 Hz, 1H, *PhCH$_2$NH$_2$ C**H***), 6.98 (s, 1H, *PhCH$_2$NH$_2$ C**H***), 6.93 (d, *J* = 7.6 Hz, 1H, *PhCH$_2$NH$_2$ C**H***), 6.38 (s, 1H, *CON**H***), 5.17 (t, *J* = 2.2 Hz, 2H, *Cp C**H***), 4.78 (t, *J* = 2.2 Hz, 2H, *Cp C**H***), 3.92 (d, *J* = 5.8 Hz, 2H, *PhC**H$_2$**NHCO*), 2.30 (s, 3H, *PhC**H$_3$***). ^{13}C NMR (101 MHz, CD_3CN) δ 164.78 (***C***=*O*), 139.96 (*PhCH$_2$NHCO **C***), 138.48 (*PhCH$_3$ **C***), 135.76 (*Ph **C***), 129.32 (*PhCH$_3$ **C**H*), 128.81 (*PhCH$_3$ **C**H*), 128.68 (*PhCH$_3$ **C**H*), 128.03 (*PhCH$_3$ **C**H*), 127.32 (*Ph **C**H*), 125.12 (*Ph **C**H*), 91.52 (*Cp **C***), 86.12 (*Cp **C**H*), 82.85 (*Cp **C**H*), 76.74 (*Cb **C***), 43.27 (*Ph**C**H$_2$NHCO*), 20.99 (*Ph**C**H$_3$*). HRMS: (TOF MS ES+) (m/z) calculated for $C_{42}H_{34}NOCo$: 627.1972, $C_{42}H_{34}NOCoNa$: 650.1870 found: 650.1870 $[M+Na]^+$

5.1.5.4. (η^4-1,3-*o*-Tolyl-2,4-benzo-18-crown-6-ether-cyclobutadiene)(η^5-*N*-(3-methylbenzylaminecyclopentadienyl) Cobalt:

Novel compound. Adapted from literature.[6, 7]

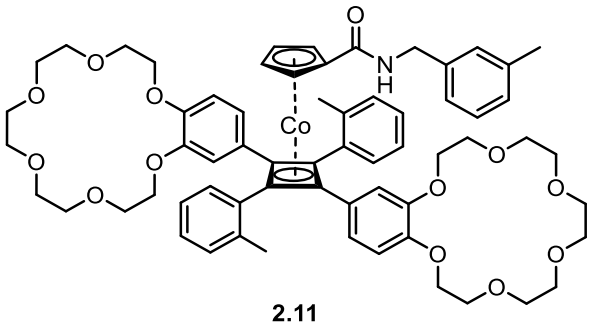

2.11

Trimethyl aluminium (2 M in toluene) (0.20 ml, 0.401 mmol, 3 equiv.) was added dropwise at 0˚C to a solution of 3-methyl benzylamine (0.025 ml, 0.201 mmol, 1.5 equiv.) in dry toluene (3 ml). The resultant solution was allowed to warm to rt and stirred for 1 h, before a solution of (η^4-1,3-o-tolyl-2,4-benzo-18-crown-6-ether-cyclobutadiene) (η^5-carbomethoxy-cyclopentadienyl) cobalt (0.130 g, 0.134 mmol, 1 equiv.) in toluene (3 ml) was added dropwise at rt and the resulting mixture was heated at 120 °C overnight. The reaction mixture was cooled to rt before dichloromethane (10 ml) and aq. potassium sodium tartrate solution (1.3 M, 10 ml) were added, and the aqueous phase was washed with dichloromethane (3 x 10 ml). The organic phases were combined, washed with brine (10 ml) and dried over anhydrous magnesium sulphate. The solvent was removed under reduced pressure and the crude residue purified by column chromatography (alumina; dichloromethane with 2% methanol) The yellow band was collected and solvent removed to afford the product as a yellow oil (0.117 g, 0.104 mmol, 78%). ^{1}H NMR (300 MHz, CD_3CN) δ 8.38 (dd, *J* = 7.1, 2.0 Hz, 2H, *PhCH₃ **CH***), 7.45 – 7.32 (m, 4H, *PhCH₃ **CH***), 7.29 – 7.24 (m, 2H, *PhCH₃ **CH***), 7.11 (t, *J* = 7.5 Hz, 1H, *PhCH₂NH₂ **CH***), 7.01 (d, *J* = 7.6 Hz, 1H, *PhCH₂NH₂ **CH***), 6.95 – 6.86 (m, 2H, *PhCH₂NH₂ **CH***), 6.47

(d, *J* = 8.3 Hz, 2H, *Ph-crown C**H***), 6.33 – 6.26 (m, 4H, *Ph-crown C**H***), 6.14 (t, *J* = 6.0 Hz, 1H, *CON**H***), 5.58 (t, *J* = 2.1 Hz, 2H, *Cp C**H***), 4.84 (t, *J* = 2.1 Hz, 2H, *Cp C**H***), 4.01 – 3.93 (m, 4H, *crown OC**H₂***), 3.83 (d, *J* = 6.0 Hz, 2H, *PhC**H₂**CO*), 3.67 – 3.61 (m, 4H, *crown OC**H₂***), 3.60 – 3.45 (m, 28H, *crown OC**H₂***), 3.43 – 3.37 (m, 4H, *crown OC**H₂***), 2.25 (s, 3H, *NHCH₂PhC**H₃***), 2.21 (s, 6H, *PhC**H₃***). ^{13}C NMR (101 MHz, CD_3CN) δ 165.19 (***C***=*O*), 148.13 (*Ph-crown **C**OCH₂*), 147.37 (*Ph-crown **C**OCH₂*), 140.06 (*PhCH₂NHCO **C***), 138.71 (*PhCH₃ **C**Cb*), 138.40 (*PhCH₃ **C**H)*, 134.41 (*PhCH₃ **C**CH₃)*, 134.22 (*PhCH₂NH₂ **C***), 130.34 (*Ph-crown **C**Cb*), 130.03 (*PhCH₃ **C**H*), 128.75 (*PhCH₃ **C**H*), 128.59 (*PhCH₃ **C**H*), 127.97 (*PhCH₂NH₂ **C**H*), 126.66 (*PhCH₂NH₂ **C**H*), 125.07 (*PhCH₂NH₂ **C**H*), 117.90 (*PhCH₂NH₂ **C**H*), 117.43(*Ph-crown **C**H*), 112.55 (*Ph-crown **C**H*), 109.13 (*Ph-crown **C**H*), 90.78 (*Cp **C***), 85.35 (*Cp **C**H*),, 82.21 (*Cp **C**H*), 78.67 (*Cb **C***), 77.32 (*Cb **C***), 70.64 (*crown O**C**H₂*), 70.53 (*crown O**C**H₂*), 69.25 (*crown O**C**H₂*), 68.87 (*crown O**C**H₂*), 68.09 (*crown O**C**H₂*), 67.28 (*crown O**C**H₂*), 43.16 (*Ph**C**H₂CO*), 21.00 (*Ph**C**H₃*), 20.95 ($NHCOCH_2$ *Ph**C**H₃*). HRMS: (TOF MS ES$^+$) (m/z) calculated for $C_{64}H_{74}NO_{13}Co$: 1123.4492, $C_{64}H_{74}NO_{13}CoNa$: 1146.4390 found: 1146.4391 $[M+Na]^+$

5.1.5.5. (η^5-pentylaminecyclopentadienyl)(η^4-tetraphenylcyclobutadiene) Cobalt:

Novel compound. Adapted from literature.[6, 7]

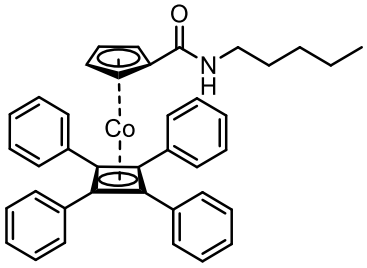

2.7

Trimethyl aluminium (2 M in toluene) (0.03 ml, 0.338 mmol, 2.6 equiv.) was added dropwise at 0˚C to a solution of pentylamine (0.02 ml, 0.172 mmol, 1.3 equiv.) in toluene (1.5 ml). The resultant solution was allowed to warm to rt and stirred for 45 min. A solution of (η^5-carbomethoxycyclopentadienyl) (η^4-tetraphenylcyclobutadiene) cobalt (0.070 g, 0.130 mmol, 1 equiv.) in toluene (3 ml) was added dropwise at rt and the resulting mixture was heated at 112 °C overnight. The reaction mixture was cooled to rt before dichloromethane (10 ml) and aq. potassium sodium tartrate solution (1.3 M, 10 ml) were added, and the aqueous phase was washed with dichloromethane (3 x 10 ml). The organic phases were combined, washed with brine (10 ml) and dried over anhydrous magnesium sulphate. The solvent was removed under reduced pressure and the crude residue purified by column chromatography (silica gel; gradient eluent system starting in dichloromethane ending in 98:2 dichloromethane:methanol) The first yellow band was collected and solvent removed to give the product as an orange oil (0.0529 g, 0.0892 mmol, 69%). ^{1}H NMR (300 MHz, $CDCl_3$) δ 7.51 – 7.40 (m, 8H, *Ph C**H***), 7.31 – 7.19 (m, 12H, *Ph C**H***), 5.01 (t, *J* = 2.1 Hz, 2H, *Cp C**H***), 4.93 (t, *J* = 5.7 Hz, 1H, *CON**H***), 4.68 (t, *J* = 2.1 Hz, 2H, *Cp C**H***), 2.82 (q, *J* = 6.6 Hz, 2H, *NHC**H₂**CH₂*), 1.36 – 1.04 (m, 6H, *C**H₂**C**H₂**C**H₂**CH₃*), 0.87 (t, *J* = 7.1 Hz, 3H, *CH₂C**H₃***). ^{13}C NMR (101 MHz, $CDCl_3$) δ 165.3 (***C***=*O*), 135.4 (*Ph **C***), 128.8 (*Ph **C**H*), 128.1 (*Ph **C**H*), 126.7 (*Ph **C**H*), 90.8 (*Cp **C***), 86.2 (*Cp **C**H*), 82.1 (*Cp **C**H*), 76.1 (*Cb **C***), 39.7 (*NH**C**H₂CH₂*), 29.1 (***C**H₂CH₂CH₂CH₃*), 29.0 (*CH₂**C**H₂CH₂CH₃*), 22.4 (*CH₂CH₂**C**H₂CH₃*), 14.0 (*CH₂**C**H₃*). LRMS: (TOF MS ES$^+$) (m/z) calculated for $C_{39}H_{36}NOCo$: 593.21 found: 594.24

5.1.6. X-Ray Diffraction

An Agilent SuperNova diffractometer equipped with an Atlas detector was used for the measurement of all datasets. The crystal was kept at 100.00 K during data collection. All data collections were driven and processed using CrysAlisPro. ShelXS was used to solve all the structures and refinement using a full matrix least-squares procedure on F2 was performed in ShelXL. OLEX2 was used to generate all reports and figures.

5.2. Variable Temperature NMR Studies:

5.2.1. General Procedure:

Studies were carried out with a Bruker AVIII 500 MHz Spectrometer equipped with a BCU-II chiller to enable strict temperature control. Once the desired temperature was reached and the system had stabilised, the NMR sample was inserted and an equilibration time of 5 min minimum was allowed for before running the experiment. Initial measurements were taken at 25 °C before measurements taken at 10 °C increments until -35 °C was reached. Once identified, further measurements at smaller intervals (2/3 °C) were taken around the temperature of coalescence.

5.2.1.1. Controlling Rotary Motion Through Protonation

Studies were performed at neutral pH first before the sample containing the cobalt sandwich complex was acidified with deuterated TFA (1.2 equiv.) before being subjected to further VT NMR studies. The sample was subsequently neutralised with pyridine (1.5 equiv.) and further NMR experiments conducted at 25 and -35 °C.

5.2.1.2. Controlling Rotary Motion Through Metal Cation Binding

Potassium hexafluorophosphate (2.5 equiv.) was added to the NMR sample before VT NMR analysis. Reversibility was assessed by VT NMR following addition of deuterated TFA (2.5 equiv.) and subsequently deuterated pyridine (3 equiv.) to the NMR sample.

5.3. Synthesis of Cyclidene Macrocyclic Complexes

5.3.1. Synthesis of Cyclidene Macrocycle:

5.3.1.1. Methyl Diformylacetate:

Known compound. Characterisation matches the literature data.[8]

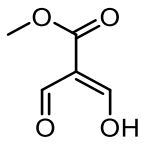

3.1

$POCl_3$ (8.95 ml, 96.00 mmols, 3 equiv.) was added dropwise to a stirred solution of dry DMF (50 ml). The solution is cooled to 0 °C before potassium monomethyl malonate (5.0 g, 32.00 mmol, 1 equiv.) was added in several portions over 30 min. The resulting mixture was heated at 90 °C for 4 h. The solvent was concentrated *via* vacuum distillation (58 °C) and the resulting dark brown liquid was poured onto ice (100 g). A saturated solution of potassium carbonate was added slowly until the pH equalled 11 and the resulting basic solution was subsequently stirred at rt for 16 h. The solution was washed with ethyl acetate (4 x 150 ml) before the organic washes were discarded and potassium chloride (12 g) was added to saturate the aqueous phase. Ice (50 g) was added and the mixture was further cooled on ice before conc. hydrochloric acid (150 ml) was added until pH 1 was reached. The aqueous phase was washed

with diethyl ether (6 x 200 ml), the organic washings were combined, and concentrated under reduced pressure. The organic solution was washed with aqueous potassium chloride solution (100 ml) before being dried over anhydrous sodium sulphate for 1 h. The drying agent was removed *via* filtration, combined with a diethyl ether (200 ml) wash of the desiccant, concentrated under reduced pressure to *ca* 500 ml and redried over anhydrous sodium sulphate. The desiccant was removed *via* filtration and the solvent removed under reduced pressure. Fractional distillation (58 °C) of the resulting orange liquid residue gave the desired product as a colourless liquid (1.520 g, 11.69 mmol, 37%). ^{1}H NMR (300 MHz, $CDCl_3$) δ 14.45 (s, 1H, O**H**), 9.14 (s, 2H*, C**H**OC=C**H***), 3.83 (s, 3H, O***C*H*₃**). ^{13}C NMR (101 MHz, $CDCl_3$) δ 186.7 (*H**C**=O*), 175.2 (*C=**C**OH*), 164.9 (***C**=O*), 109.3 (***C**=COH*), 51.7 (*O**C**H₃*). MS (TOF MS EI+) (m/z) calculated for $C_5H_6O_4$: 130.03 found: 130.0 M^+

5.3.1.2. Cyclidene Macrocycle:

Known compound. Characterisation matches the literature data.[9]

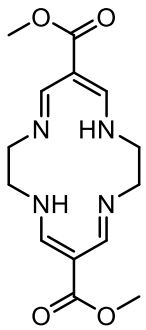

3.2

A solution of ethylene diamine (0.16 ml, 2.39 mmol, 1.03 equiv.) in methanol (5 ml) was added dropwise over 30 min to a stirred solution of methyl diformylacetate (0.325 g, 2.34 mmol, 1 equiv.) in methanol (1 ml) at rt. The resulting mixture was heated at 70 °C for 6 h. The reaction mixture was cooled to rt overnight before further cooling to -20 °C to induce crystallisation.

The resulting crystals were collected by filtration and dried under vacuum to yield the product as small, white, needle shaped crystals (0.195 g, 0.634 mmol, 54%). ^{1}H NMR (300 MHz, $CDCl_3$) δ 12.60 (s, 2H, *N**H***), 8.29 (d, J = 6.5 Hz, 4H, ***H**C=CC**H***), 3.72 (s, 6H, *OC**H₃***), 3.58 (s, 8H, *NC**H₂**C**H₂**N*). ^{13}C NMR (101 MHz, $CDCl_3$) δ 168.49 (***C**=O*), 157.80 (H***C**=**C**CH*), 94.93 (H*C=**C**CH*), 53.52 (*N**C**H₂**C**H₂N*), 50.79 (*O**C**H₃*). IR (neat) (cm^{-1}) *υ*: 2945.70 (*CH*), 2888.62 (*CH*), 2833.22 (*CH*), 1669.51 (*C=O*), 1628.77, 1592.38 (*C=C*). MS (TOF MS EI^{+}) (m/z) calculated for $C_{14}H_{20}O_4N_4$: 308.2 found: 309.2 $[M+H]^{+}$

5.3.2. Metal Complexation:

5.3.2.1. Nickel (II) Cyclidene Complex:

Known compound. Adapted from Rybka *et al*. Characterisation matches the literature data.[10]

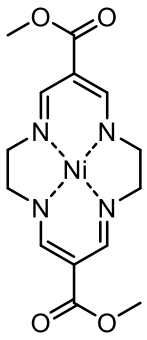

3.3Ni

Cyclidene macrocycle (0.741 g, 2.30 mmol, 1 equiv.) and nickel (II) acetate tetrahydrate (0.647 g, 2.60 mmol, 1.1 equiv.) were dissolved in dry methanol (160 ml) and heated at 70 °C for 1 h. The reaction mixture was cooled to rt before being cooled in the fridge at 4 °C overnight. The resulting orange precipitate was collected *via* filtration and dried under vacuum. The coloured filtrate was diluted with water (15 ml) and the remaining product was extracted with dichloromethane (3 x 15 ml). The organic washings were combined, washed with brine (10 ml), dried over anhydrous magnesium sulphate and concentrated under reduced

pressure. The orange precipitates collected were combined and dried under high vacuum to give the desired product as an orange solid (0.647 g, 1.78 mmol, 77%). ^{1}H NMR (300 MHz, $CDCl_3$) δ 7.81 (s, 4H, ***H***C=CC***H***), 3.73 (s, 6H, OC***H$_3$***), 3.38 (s, 8H, NC***H$_2$***C***H$_2$***N). ^{13}C NMR (101 MHz, $CDCl_3$) δ 168.41 (***C***=O), 154.94 (H***C***=C***C***H), 98.21 (HC=***C***CH), 58.74 (N***C***H$_2$***C***H$_2$N), 50.81 (O***C***H$_3$). IR (neat) (cm^{-1}) *υ*: 1668 (C=O), 1594 (C=C). m.p. (°C): 225-228. MS (TOF MS EI$^+$) (m/z) calculated for $C_{14}H_{18}O_4NiN_4$: 364.07 found: 364.07 $[M]^+$.

5.3.2.2. Copper (II) Cyclidene Complex:

Known compound. Adapted from Rybka *et al.* Characterisation matches literature data.[10]

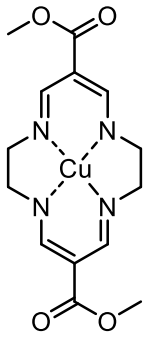

3.3Cu

Cyclidene macrocycle (0.691 g, 2.24 mmol, 1 equiv.) was dissolved in dry methanol (60 ml) before copper (II) acetate monohydrate (0.489 g, 2.69 mmol, 1.2 equiv.) was added, and the resulting mixture stirred at 75 °C for 1 h. The reaction was cooled to rt and the solvent removed under reduced pressure. The resulting precipitate was redissolved in dichloromethane (20 ml) and water added (20 ml). The aqueous layer was washed with dichloromethane (4 x 20 ml), before the organic washings were combined, washed with brine (15 ml) and dried over anhydrous magnesium sulphate. The solvent was removed under reduced pressure to give the product as dark pink crystals (0.763 g, 2.07 mmol, 92%). IR (neat)

(cm^{-1}) *υ*: 2947.58 (*CH*), 2926.93 (*CH*), 2840.62 (*CH*), 1671.75 (*C=O*), 1591.06 (*C=C*). m.p. (°C): 244-246. MS (TOF MS EI^+) (m/z) calculated for $C_{14}H_{18}O_4N_4Cu$: 369.06 found: 369.06 M^+.

5.3.3. Cyclidene Tag Complex Synthesis:

5.3.3.1. Cyclidene Tag Copper Complex:

Known compound. Adapted from Duprey *et al*. Characterisation matches literature data.[11]

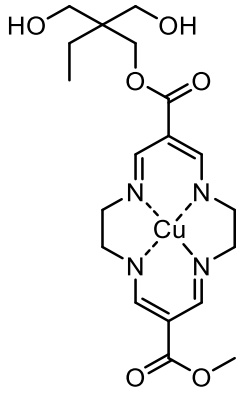

3.7Cu

1,1,1-tris(hydroxymethyl)propane (8.085 g, 65.9 mmol, 80 equiv.) was heated until melted, before cyclidene copper complex (0.301 g, 0.816 mmol, 1 equiv.) and sodium metal (0.189 g, 8.22 mmol, 10.1 equiv.) were added. The resulting mixture was stirred at 90 °C for 72 h. The reaction mixture was cooled to rt and methanol added (7.5 ml), before the mixture was further heated at 80 °C for 26 h. The reaction was cooled to rt, quenched with ice-water (100 ml) and left in the fridge at 4 °C overnight. The resulting pink precipitate was collected *via* filtration, washed with water (20 ml) and dried under vacuum. The remaining pink filtrate was washed with dichloromethane (3 x 20 ml) until colourless. The organic washings were combined, washed with brine (20 ml), dried over anhydrous magnesium sulphate and evaporated to dryness under reduced pressure. The crude precipitates were combined and purified by column chromatography (silica gel; gradient eluent system starting at 99:1

DCM:NEt_3, finishing at 96:3:1 DCM:MeOH:NEt_3). The second pink band was collected and the solvent removed under reduced pressure to yield the product as a pink solid (0.165 g, 0.349 mmol, 43 %). IR (neat) (cm^{-1}) *υ*: 3391.62 (*OH*), 2906.09 (*CH*) 1671.25 (*C=O*), 1589.91 (*C=C*). MS (TOF MS EI^+) (m/z) calculated for $C_{19}H_{28}O_6N_4Cu$: 471.13 found: 494.12 $[M+Na]^+$.

5.3.3.2. Tritylation of Copper Cyclidene Tag Diol:

Known compound. Adapted from Duprey *et al*. Characterisation matches literature values.[11]

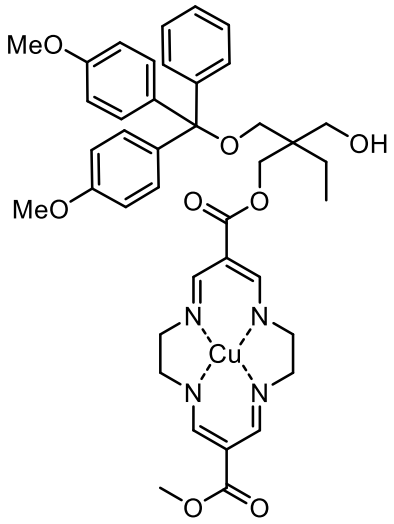

3.8Cu

Copper cyclidene tag diol (0.073 g, 0.155 mmol, 1 equiv.) was dissolved in dry pyridine (2 ml) before 4,4'-dimethoxytrityl chloride (0.042 g, 0.124 mols, 0.8 equiv.) was added in 3 portions over 5 min. The resulting mixture was stirred at rt for 4 h. The pyridine was removed under reduced pressure *via* coevaporation with toluene (3 x 10 ml) before the crude residue was purified by column chromatography (silica gel; eluent system of 1:1 hexane:ethyl acetate with 1% triethylamine). The second pink band was collected and the solvent removed under reduced pressure to yield the product as a fluffy pink solid (0.050 g, 0.065 mmol, 42 %). IR

(neat) (cm^{-1}) υ: 3442.3 (*OH*), 2920.79 (*CH*), 1676.24 (*C=O*) 1598.22 (*C=C*). MS (TOF MS EI^+) (m/z) calculated for $C_{40}H_{46}O_8N_4Cu$: 773.26 found: 773.26 M^+.

5.3.3.2.1. Regeneration of Copper Cyclidene Tag from Bistrityl Tag

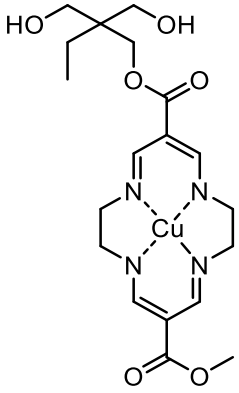

3.7Cu

Bistrityl copper cyclidene tag (0.100 g, 0.093 mmol, 1 equiv.) was dissolved in a dry dichloromethane:methanol solution (4:1, 5 ml) before trifluoroacetic acid (0.05 ml, 0.604 mmol, 6.5 equiv.) was added dropwise and the resulting mixture was stirred at rt for 16 h. The reaction mixture was neutralised with pyridine (0.05 ml, 0.651 mmol, 7 equiv.) before water (10 ml) was added and the solution washed with dichloromethane (3 x 10 ml). The organic washings were combined and washed with brine (10 ml) and dried over anhydrous magnesium sulphate. The solvent was removed under reduced pressure and the crude residue was purified by column chromatography (silica gel; eluent system of dichloromethane with 2% methanol and 1% triethylamine). The appropriate fractions were combined and evaporated to give a pink solid (0.040 g, 0.085 mmol, 91%).

5.3.3.3. Phosphitylation of Monotrityl Copper Cyclidene Tag:

Known compound. Adapted from Duprey *et al.* Characterisation matches literature values.[11]

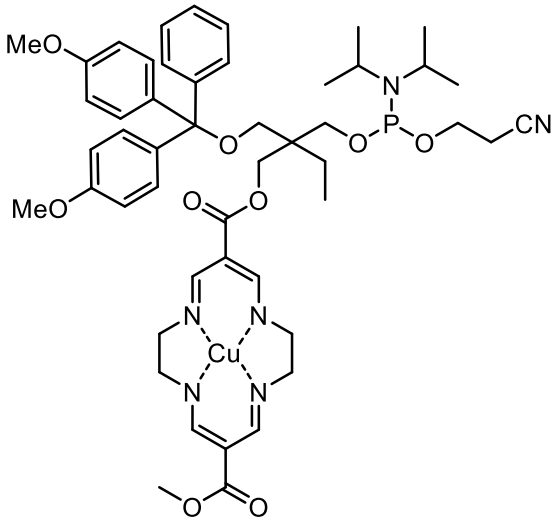

3.9Cu

Monotrityl copper cyclidene tag (0.122 g, 0.158 mmol, 1 equiv.) was azeotroped in dry dichloromethane (2 x 6 ml) before being redissolved in dry dichloromethane (7 ml). DIPEA (0.12 ml, 0.712 mmol, 4.5 equiv.) and 2-cyanoethyldiisopropylchlorophosphoramidite (0.05 ml, 0.222 mmol, 1.4 equiv.) were sequentially added dropwise and the resulting mixture was stirred at rt for 2.5 h. The reaction was diluted with deoxygenated ethyl acetate (20 ml), and the organic solution was washed with deoxygenated saturated sodium bicarbonate solution (20 ml), deoxygenated brine (10 ml) and dried over anhydrous sodium sulphate. The solvent was removed under reduced pressure and the crude residue was purified by column chromatography (silica gel; eluent system of deoxygenated 1:1 ethyl acetate:hexane with 1% triethylamine). The appropriate fractions were combined and evaporated to give a dark pink oil (0.136 g, 0.140 mmol, 88%). IR (neat) (cm^{-1}) υ: 2964.28 (*CH*), 2929.85 (*CH*), 1735.60 (*CN*),

1677.58 (*C=O*) 1600.02 (*C=C*). MS (TOF MS EI$^+$) (m/z) calculated for $C_{49}H_{63}O_9N_4Cu$: 973.37 found: 973.37 M^+.

5.3.4. Cyclidene Link Complex Synthesis:

5.3.4.1. Cyclidene Link Nickel Complex:

Known compound. Adapted from Duprey *et al* Characterisation matches literature values.[11]

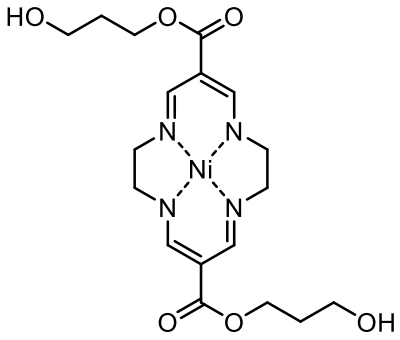

3.4Ni

Cyclidene nickel complex (0.569 g, 1.60 mmol, 1 equiv.) was stirred with 1,3-propandiol (60 ml) at rt before sodium metal (0.431 g, 18.70 mmol, 12 equiv.) was added and the resulting mixture was heated at 80 °C for 48 h. The reaction mixture was allowed to cool to rt, ice-water (250 ml) added and stored in the fridge at 4 °C overnight. The resulting orange precipitate was collected *via* filtration, washed with water (20 ml) and dried under vacuum. The remaining orange filtrate was washed with dichloromethane (3 x 10 ml) until the washings were colourless. The organic washings were combined, washed with brine (10 ml), dried over anhydrous magnesium sulphate and the solvent removed under reduced pressure. The orange precipitates were combined and purified by column chromatography (silica gel; eluent system of 95:4:1 DCM:MeOH:NEt_3). The appropriate fractions were combined and evaporated to yield an orange solid (0.607 g, 1.30 mmol, 86%). ^{1}H NMR (400 MHz, $CDCl_3$) δ

7.82 (s, 4H, ***H**C=CC**H***), 4.34 (t, J = 5.9 Hz, 4H, *COOC**H₂***), 3.66 (t, J = 5.7 Hz, 4H, *C**H₂**OH*), 3.39 (s, 8H, *NC**H₂**C**H₂**N*), 2.52 (s, 2H, *O**H***), 1.92 – 1.81 (m, 4H, *CH₂C**H₂**CH₂*). ^{13}C NMR (101 MHz, $CDCl_3$) δ 168.61 (***C**=O*), 155.06 (H***C**=C**C**H)*, 97.96 (H*C=**C**CH*), 59.82 (*COO**C**H₂)*, 58.79 (*N**C**H₂**C**H₂N*), 32.50 (***C**H₂OH)*, 29.72 (*CH₂**C**H₂CH₂)*. IR (neat) (cm^{-1}) *υ*: 3422 (*OH*), 2926 (*CH*), 1654 (*C=O*), 1595 (*C=C*). m.p. (°C): 179-181. MS (TOF MS EI^+) (m/z) calculated for $C_{18}H_{26}N_4NiO_6$: 452.12 found: $[M+Na]^+$: 475.11.

5.3.4.2. Tritylation of Nickel Cyclidene Link Diol:

Known compound. Adapted from Duprey *et al*. Characterisation matches literature values.[11]

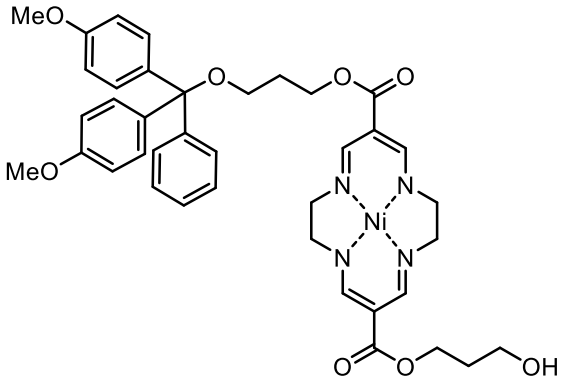

3.5Ni

Nickel cyclidene link diol (0.193 g, 0.427 mmol, 1 equiv.) was dissolved in dry pyridine (5 ml) before DMAP (0.0077 g, 0.063 mmol, 0.15 equiv.) and 4,4'-dimethoxytrityl chloride (0.081 g, 0.240 mmol, 1.2 equiv.) were sequentially added and the reaction mixture was stirred at rt for 3 h. Water (15 ml) was added and the mixture washed with dichloromethane (3 x 20 ml). The organic washings were combined, washed with brine (20 ml), dried over anhydrous magnesium sulphate and reduced under vacuum. The crude residue was purified by column chromatography (silica gel; eluent system of dichloromethane with 1% methanol and 1% triethylamine). The appropriate fractions were combined and the solvent removed under reduced pressure to afford the desired product as a fluffy orange solid (0.124 g, 0.164 mmol,

34%). ^{1}H NMR (400 MHz, $CDCl_3$) δ 7.82 (s, 2H, ***H****C=CC****H***), 7.70 (s, 2H, ***H****C=CC****H***), 7.45 – 7.41 (m, 2H, *DMT Ph C****H***), 7.34 – 7.29 (m, 4H, *DMT CH_3OPh C****H***), 7.27 – 7.26 (m, 2H, *DMT Ph C****H***), 7.22 – 7.18 (m, 1H, *DMT Ph C****H***), 6.83 – 6.78 (m, 4H, *DMT CH_3OPh C****H***), 4.38 - 4.29 (m, 4H, *COOC****H₂***), 3.79 (s, 6H, *DMT C****H₃****OPh*), 3.66 (t, *J* = 5.9 Hz, 2H, *C****H₂****OH*), 3.40 – 3.29 (m, 8H, *NC****H₂****C****H₂****N*), 3.18 (t, *J* = 20.1, 19.5 Hz, 2H, *C****H₂****ODMT*), 3.07 (s, 1H, *CH_2O****H***), 1.94 (q, *J* = 6.2 Hz, 2H, *CH_2C****H₂****CH_2*), 1.87 (q, *J* = 5.9 Hz, 2H, *CH_2C****H₂****CH_2*). ^{13}C NMR (101 MHz, $CDCl_3$) δ 168.65 (***C****=O*), 167.75 (***C****=O*), 158.32 (H***C****=C****C****H*), 154.95 (H***C****=C****C****H*), 145.20 (*DMT CH_3OPh ****C****OCH_3*), 136.42 (*DMT Ph ****C***), 130.06 (*DMT CH_3OPh ****C***), 128.16 (*DMT Ph ****C****H)*, 127.75 (*DMT Ph ****C****H*), 126.62 (*DMT CH_3OPh ****C****H*), 113.00 (*DMT CH_3OPh ****C****H*), 98.41 (H*C=****C****CH*), 97.89 (H*C=****C****CH*), 85.78 (*DMT O****C****Ar_3*), 60.75 (***C****H_2ODMT*), 59.90 (*COO****C****H_2)*, 59.79 (*COO****C****H_2)*, 58.81 (*N****C****H_2C****H₂****N*), 58.68 (*N****C****H_2C****H₂****N*), 55.23 (*DMT ****C****H_3OPh*), 32.51 (***C****H_2OH)*, 29.64 (*CH_2C****H₂****CH_2)*. IR (neat) (cm^{-1}) *υ*: 3435 (*OH*), 2930 (*CH*) 1676 (*C=O*), 1599 (*C=C*). m. p. (°C): 85-89. MS (TOF MS EI^+) (m/z) calculated for $C_{39}H_{44}N_4NiO_8$: 754.25 found: $[M+Na]^+$: 777.24.

5.3.4.3. Phosphitylation of Monotrityl Nickel Cyclidene Link:

Known compound. Adapted from Duprey *et al*. Characterisation matches literature values.[11]

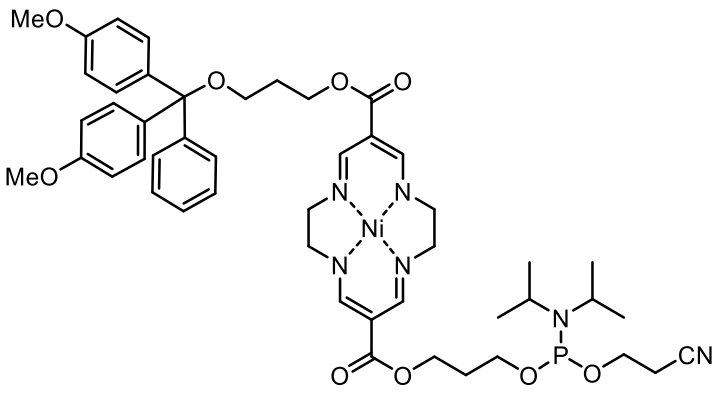

3.6Ni

Monotrityl nickel cyclidene link (0.090 g, 0.119 mmol, 1 equiv.) was azeotroped in dry dichloromethane (2 x 2 ml) before being redissolved in dry dichloromethane (4 ml). DIPEA (0.094 ml, 0.536 mmol, 4.5 equiv.) and 2-cyanoethyldiisopropylchlorophosphoramidite (0.040 ml, 0.143 mmol, 1.2 equiv.) were sequentially added dropwise and the reaction mixture was stirred at rt for 2 h. The reaction mixture was diluted with deoxygenated ethyl acetate (20 ml), washed with deoxygenated saturated sodium bicarbonate solution (2 x 20 ml) and deoxygenated brine (20 ml) and dried over anhydrous sodium sulphate. The solvent was removed under reduced pressure and the crude residue was purified by column chromatography (silica gel; eluent system of deoxygenated 1:1 ethyl acetate:hexane with 1% triethylamine). The first orange band was collected and dried under vacuum to afford the product as an orange oil (0.086 g, 0.090 mmol, 76%). ^{1}H NMR (400 MHz, CD_3CN) δ 7.80 (s, 2H, ***H**C=CC**H***), 7.66 (s, 2H, ***H**C=CC**H***), 7.44 – 7.41 (m, 2H, *DMT Ph C**H***), 7.32 – 7.27 (m, 4H, *DMT CH_3OPh C**H***), 7.25 – 7.20 (m, 3H, *DMT Ph C**H***), 6.87 – 6.82 (m, 4H, *DMT CH_3OPh C**H***), 4.24 – 4.15 (m, 4H, *COOC**H$_2$***), 3.78 (s, 6H, *DMT C**H$_3$**OPh*), 3.77 – 3.71 (m, 2H, *C**H$_2$**OP*), 3.65 – 3.57 (m,

2H, *C**H**₂**OP*), 3.39 – 3.27 (m, 8H, *NC**H**₂C**H**₂N*), 3.13 (t, *J* = 6.0 Hz, 2H, *C**H**₂**ODMT*), 2.77 – 2.58 (m, 2H, $^{i}Pr_2N$ C**H**), 2.64 (t, *J* = 6.4, 5.7 Hz, 2H, *C**H**₂**CN*), 1.92 – 1.88 (m, 4H, *CH₂C**H**₂CH₂*), 1.19 – 1.15 (m, 12H, $^{i}Pr_2N$ C**H₃**). ^{31}P NMR (121 MHz, CD_3CN) δ 147.10. MS (TOF MS EI$^+$) (m/z) calculated for $C_{48}H_{61}N_6NiO_9P$: 954.36 found $[M+Na]^+$: 977.36.

5.3.4.4. Cyclidene Link Copper Complex:

Known compound. Adapted from Duprey *et al.* Characterisation matches literature values.[11]

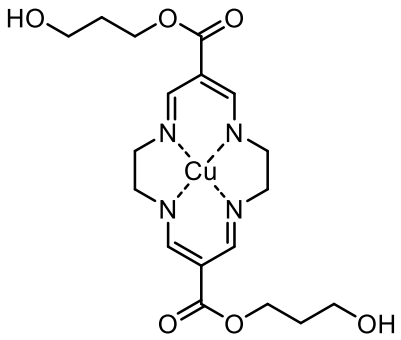

3.4Cu

Cyclidene copper complex (0.120 g, 0.325 mmol, 1 equiv.) was added to a stirred solution of 1,3-propandiol (22 ml) and sodium metal (0.075 g, 3.25 mmol, 10 equiv.) was added and the resulting mixture was heated at 100 °C for 48 h. The reaction mixture was allowed to cool to rt, ice-water (100 ml) added and stored in the fridge at 4 °C overnight. The resulting pink precipitate was collected *via* filtration, washed with water (20 ml) and dried under vacuum. The crude precipitate was purified by column chromatography (silica gel; eluent system of 96:4 dichloromethane:methanol). The appropriate fractions were combined and evaporated to yield a pink solid (0.094 g, 0.206 mmol, 63%). IR (neat) (cm^{-1}) *υ*: 3297.89 (*OH*), 2926.09 (*CH*) 1669.93 (*C=O*), 1594.15 (*C=C*). MS (TOF MS EI$^+$) (m/z) calculated for $C_{18}H_{26}N_4CuO_6$: 457.11 found: $[M+H]^+$: 458.12.

5.3.4.5. Tritylation of Copper Cyclidene Link Diol:

Known compound. Adapted from Duprey *et al.* Characterisation matches literature values.[11]

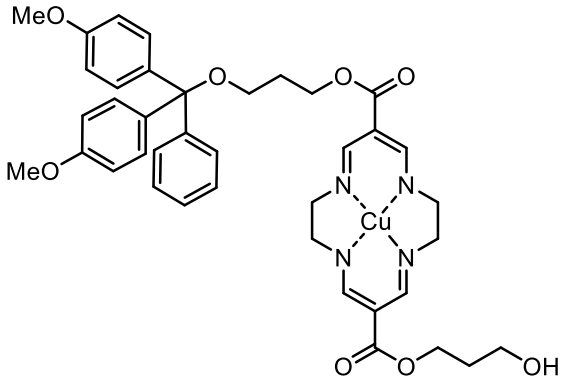

3.5Cu

Copper cyclidene link diol (0.352 g, 0.770 mmol, 1 equiv.) was dissolved in dry pyridine (8 ml) before DMAP (0.014 g, 0.115 mmol, 0.15 equiv.) was added. 4,4'-dimethoxytrityl chloride (0.287 g, 0.847 mmol, 1.1 equiv.) was added in portions over 10 min and the reaction mixture was stirred at rt for 3 h. Water (20 ml) was added and the mixture washed with dichloromethane (3 x 20 ml). The organic washings were combined, washed with brine (20 ml), dried over anhydrous magnesium sulphate and reduced under vacuum. The crude residue was purified by column chromatography (silica gel; eluent system of dichloromethane with 1% methanol and 0.5% triethylamine). The appropriate fractions were combined and the solvent removed under reduced pressure to afford the desired product as a pink oil (0.132 g, 0.174 mmol, 23%). IR (neat) (cm^{-1}) υ: 3407.97 (*OH*), 2934.05 (*CH*), 2899.55 (*CH*), 1649.52 (*C*=*O*), 1596.58 (*C*=*C*). MS (TOF MS EI^+) (m/z) calculated for $C_{18}H_{26}N_4CuO_6$: 759.25 found: $[M+H]^+$: 759.25.

5.3.4.6. Phosphitylation of Monotrityl Copper Cyclidene Link:

Known compound. Adapted from Duprey *et al*. Characterisation matches literature values.[11]

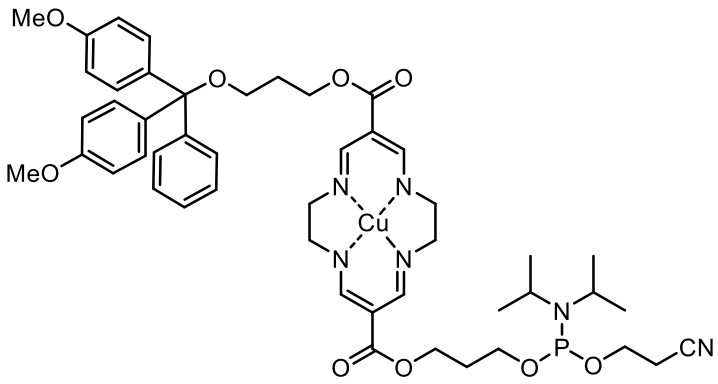

3.6Cu

Monotrityl copper cyclidene link (0.132 g, 0.174 mmol, 1 equiv.) was azeotroped in dry dichloromethane (2 x 6 ml) before being redissolved in dry dichloromethane (7 ml). DIPEA (0.14 ml, 0.782 mmol, 4.5 equiv.) and 2-cyanoethyldiisopropylchlorophosphoramidite (0.060 ml, 0.244 mmol, 1.4 equiv.) were sequentially added dropwise and the reaction mixture was stirred at rt for 2 h. The reaction mixture was diluted with deoxygenated ethyl acetate (20 ml), washed with saturated sodium bicarbonate solution (2 x 20 ml) and deoxygenated brine (20 ml) and dried over anhydrous sodium sulphate. The solvent was removed under reduced pressure and the crude residue was purified by column chromatography (silica gel; eluent system of deoxygenated 2:1 ethyl acetate:hexane with 1% triethylamine). The first pink band was collected and dried under vacuum to yield a pink oil (0.121 g, 0.126 mmol, 73%). IR (neat) (cm^{-1}) *υ*: 2964.89 (*CH*). 2928.89 (*CH*), 1735.60 (*CN*), 1675.32 (*C=O*), 1599.25 (*C=C*). MS (TOF MS EI^+) (m/z) calculated for $C_{48}H_{61}N_6CuO_9P$: 959.35 found: $[M+Na]^+$: 982.3.

5.4. Synthesis of Ferrocene Monomer

Synthetic procedure was adapted from the literature[12] and previous work within the group.[13]

Ferrocene diol and monotrityl ferrocene were synthesised by Lily Bailey.[14]

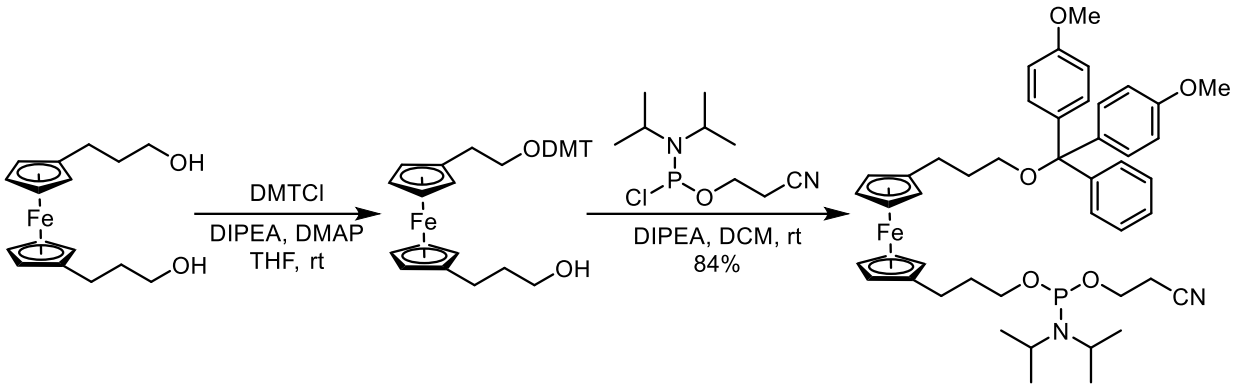

5.4.1. Phosphitylation of Monotrityl Ferrocene:

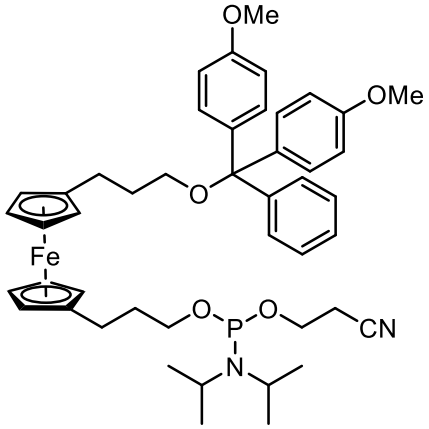

Monotrityl ferrocene (0.102 g, 0.169 mmol, 1 equiv.) was azeotroped with anhydrous dichloromethane (2 x 6 mL), before being redissolved in anhydrous dichloromethane (7 mL) under argon. To the resulting solution, *N,N*–diisopropylethylamine (0.075 mL, 0.422 mmol, 2.5 equiv.) and 2-cyanoethyl *N,N*–diisopropylchlorophosphoramidite (0.056 mL, 0.253 mmol, 1.5 equiv.) were added dropwise. The reaction was left for 2.5 h under argon. The reaction was then quenched with deoxygenated ethyl acetate (20 mL) and the mixture was washed

with deoxygenated sat. aqueous $NaHCO_3$ (20 mL) and deoxygenated brine (15 mL), before the organic layers were dried over anhydrous Na_2SO_4. This was then filtered, concentrated *in-vacuo* and product purified *via* column chromatography (silica gel, 3:2 hexane:ethyl acetate with 1% triethylamine) to yield the product as a yellow oil (84%, 0.114 g, 0.1422 mmol). ^{1}H NMR (300 MHz, CD_3CN) δ_H: 7.39 – 7.14 (m, 9H, *DMT*), 6.78 – 6.72 (m, 4H, *DMT*), 3.90 – 3.82 (m, 8H, *Fc Cp*), 3.76 – 3.67 (m, 8H, ***CH₂****CH₂CN*), 3.59 – 3.48 (m, 4H, ***CH₂****OP, NC****H***), 3.01 (t, *J* = 6.4 Hz, 2H, *CH₂ODMT*), 2.53 (t, *J* = 6.6 Hz, 2H, ***CH₂****CN*) 2.37 – 2.28 (m, 4H, *FcC****H₂***), 1.79 – 1.68 (m, 4H, *FcCH₂C****H₂***), 1.11 (dd, *J* = 6.8, 3.5 Hz, 12H, ***CH₃***). ^{31}P NMR (300 MHz, CD_3CN) δ_P: 147.37. IR (neat) (cm^{-1}) υ: 3084 (*CH*), 2964 (*CH*). MS (TOF MS EI$^+$) (m/z) calculated for $C_{46}H_{57}FeN_2O_5P$: 804.79. Found: 805.76 $[M+H]^+$.

5.5. Synthesis, Purification and Characterisation of DNA

5.5.1. Oligonucleotide Synthesis:

Oligonucleotides were synthesised on an Applied Biosystems ABI 394 (Foster City, CA, 30 U.S.A). Standard phosphoramidites of Pac-dA, iPr-Pac-dG, Ac-dC, dT were purchased from LGC Genomics and 3'-thiol-modifier 6 S-S CPG from Glen Research. The phosphoramidites (including cyclidene and ferrocene units) were dissolved in anhydrous acetonitrile to 0.1 M prior to synthesis. Strands were synthesised at a 1 μmol scale on SynBase™ CPG 1000/110 solid supports from LGC Genomics. Phosphoramidites were activated with 5-ethylthio-1H-tetrazole (ETT) (0.25 M) in acetonitrile prior to coupling with the previous nucleobase in the sequence. Coupling times of 25 seconds and 10 minutes were used for the nucleosides and organometallic modifications, respectively. Upon completion of coupling, phenoxyacetic anhydride and methylimidazole were added to cap any unreacted material, and iodine (0.02

M) in THF/pyridine/water (7:2:1) was added to oxidise the phosphotriester formed. Upon sequence completion, the resins were placed in freshly prepared 1 ml solutions of potassium carbonate (0.05 M) in dry methanol and left overnight to cleave the strands from the resin and remove the protecting groups. The solutions were neutralised with acetic acid (6 µl) and the solvent was removed on a Thermo Scientific speed vac. The dried powders were redissolved in 1 ml ultrapure water and desalted with a NAP-10 column (GE Healthcare) to remove any residual resin and potassium carbonate. The solutions were then concentrated to 1 ml and stored in the freezer before purification.

5.5.2. Oligonucleotide Purification:

Semi preparative HPLC purification was performed on an Agilent Technologies 1260 Infinity system using a Phenomenex Clarity 5 µm Oligo-RP LC 250 x 10 mm column. Collected fractions were evaporated to dryness, redissolved in Milli-Q water (1 ml) and desalted using a NAP-10 column (GE Healthcare), before being eluted from the column to 1.5 ml. Purity of oligonucleotides was determined by analytical HPLC using a Phenomenex Clarity 5 µm Oligo RP LC 250 x 4.6 mm column on an Agilent Technologies 1260 Infinity system. Solvent gradients used were identical to semi preparative HPLC. The UV/vis absorbance of each run was monitored at a wavelength of 260 nm.

Samples showing >95% purity by analytical HPLC were deemed sufficiently pure for use in experiments. Samples showing <95% purity were repurified by semi preparative HPLC. The characterisation of pure oligonucleotide samples was performed by negative mode electrospray mass spectrometry on a Waters Xevo G2-XS mass spectrometer. Sample concentrations were determined by optical density at 260nm using a BioSpecNano micro-volume UV-Vis spectrophotometer (nanodrop) from Shimadzu and the Beer Lambert law,

with extinction coefficients obtained from Integrated DNA Technologies' OligoAnalyzer and a value of 8294 mol^{-1} cm^{-1} used for the copper cyclidene complex, and 3300 mol^{-1} cm^{-1} for the ferrocene moiety.

5.5.2.1. Unmodified Oligonucleotide Sensing Probes and Targets:

The column was heated to 60 °C prior to sample injection and for the duration of the run. The UV/vis absorbance of each run was monitored at 260 nm. A solvent gradient system of HPLC grade acetonitrile (Fisher Scientific) and 0.1 M triethylamine acetate (TEAA) in HPLC grade water (Fisher Scientific) was employed for the purification of unmodified probes and targets, and is listed in the table below:

Table 5.1: HPLC solvent gradient system employed for the purification of unmodified oligonucleotide probes and targets.

Time / min	% 0.1 M TEAA	% Acetonitrile
0.00	95	5
30.00	82	18
30.01	0	100
40.00	0	100
40.01	95	5
45.00	95	5

5.5.2.2. Modified Oligonucleotide Sensing Probes:

The column was heated to 60 °C prior to sample injection and for the duration of the run. The UV/vis absorbance of each run was monitored at 260 nm and 428 nm, to monitor the DNA and ferrocene, respectively. A solvent gradient system of HPLC grade acetonitrile (Fisher Scientific) and 0.1 M triethylamine acetate (TEAA) in HPLC grade water (Fisher Scientific) was employed for the purification of modified probes, and is listed in the table below:

Table 5.2: HPLC solvent gradient system employed for the purification of modified oligonucleotide probes and NiLink10mer.

Time / min	% 0.1 M TEAA	% Acetonitrile
0.00	85	15
30.00	75	25
30.01	0	100
40.00	0	100
40.01	85	15
45.00	85	15

5.5.2.3. Nickel Cyclidene Modified Oligonucleotides:

The column was heated to 60 °C prior to sample injection and for the duration of the run. The UV/vis absorbance of each run was monitored at 260 nm. A solvent gradient system of HPLC grade acetonitrile (Fisher Scientific) and 0.1 M triethylamine acetate (TEAA) in HPLC grade water (Fisher Scientific) was employed for the purification of modified probes, and is listed in the table below:

Table 5.3: HPLC solvent gradient system employed for the purification of NiLink40mer and 3NiLink30mer..

Time / min	% 0.1 M TEAA	% Acetonitrile
0.00	95	5
40.00	70	30
40.01	0	100
50.00	0	100
50.01	95	5
55.00	95	5

5.5.3. Thermal Melting Studies:

Samples of oligonucleotide were made to a concentration of 10 µM, with 10 mM sodium phosphate buffer pH 7.0, 100 mM NaCl. 1 µL of 20 times concentration SsoAdvanced universal SYBR® green supermix (Bio-rad) was added to 19 µL of each 10 µM oligonucleotide sample. Samples were then heated from 20 °C to 90 °C and subsequently cooled from 90 °C to 20 °C at a rate of 1 °C per minute in a M550 double beam scanning UV/Vis spectrophotometer. Melting temperature values were then obtained from the maxima of the negative first derivative of the melting curve.

5.6. Electrochemistry

5.6.1. Equipment and Preparation:

Electrochemical measurements were performed on a BioAnalytical Systems Inc. (BASi, West Lafayette, IN, USA) EC epsilon potentiostat using a C3 cell stand. A traditional 3-electrode set-up, consisting of a Ag/AgCl reference electrode (3M KCl), platinum wire counter electrode and a polycrystalline gold disc, glass carbon or boron-doped diamond working electrode, was used throughout. Four gold working electrodes were used in each surface-based electrochemistry experiment, two with a 1.6 mm diameter, two with a 2.0 mm diameter. Reference electrodes and counter electrode were purchased from IJ Cambria (Llanelli, Wales), gold working electrodes were purchased from CH Instruments Inc. (Austin, TX, USA).

All water used was purified on a Merck Millipore Elix-Gradient A10 system (resistivity > 18 μΩ cm toc ≤ 5 ppb, Millipore, France), for both cleaning and solution preparation. All solutions were thoroughly deoxygenated with argon before use. All glassware and electrochemical cells were cleaned by soaking for several hours in a 1:1 mixture of ammonia (35%) and hydrogen peroxide (30%), before being copiously rinsed with ultrapure water and being left to soak overnight in ultrapure water. Following a final rinse in ultrapure water, the glassware was dried in an oven for several hours before use.

5.6.2. Solution-based Electrochemistry

The platinum wire counter electrode was flame annealed before use, whilst the reference electrode was thoroughly rinsed with ultrapure water. The glassy carbon and boron-doped diamond working electrodes were polished with successively finer grades of alumina slurry; 1.0 μm for 3 min, 0.3 μm for 3 min and finally 0.05 μm for 5 min on a polishing pad (BASi,

West Lafayette, IN, USA). Between each step the electrode was washed with ultrapure water. If further cleaning was required, the glassy carbon electrode was subjected to potential cycling in deoxygenated sulfuric acid (0.5 M) until consistent CVs were obtained (using a potential window between -0.35 V and 1.5 V at a scan rate of 4 V s^{-1}).

The analyte DNA (50 µM unless otherwise stated) was added to the specified buffer solution in the above described 3-electrode set-up. CVs were recorded at a range of scan rates to assess the scan rate dependence: 10, 20, 40, 60, 80, 100, 250, 500 and 1000 mV s^{-1} (unless otherwise stated).

5.6.3. Surface-based Electrochemistry

The platinum wire counter electrode was flame annealed before use, whilst the reference electrode was thoroughly rinsed with ultrapure water. The gold working electrodes were polished with a diamond suspension (1.0 µm) on a polishing pad (BASi, West Lafayette, IN, USA) for 3 min before subsequent polishing with successively finer grades of alumina slurry; 1.0 µm for 3 min, 0.3 µm for 3 min and finally 0.05 µm for 5 min. Between each step the electrode was washed with ultrapure water. The working electrode was then sonicated for 30 seconds in a deoxygenated 1:1 mixture of ultrapure water and ethanol.

The working electrodes were then subjected to electrochemical cleaning in deoxygenated sulfuric acid (0.5 M). Chronoamperometry was employed to hold the potential at first 2 V for 5 s, before -0.35 V for 10 s. A series of cyclic voltammograms (CV) were then recorded between -0.35 V and 1.5 V at scan rates of 4 V s^{-1} (until consistent, approximately 20 cycles) and 0.1 V s^{-1} (4 cycles), before a final CV was recorded at 0.5 V s^{-1}. From this final CV, the surface roughness and consequently the geometric area of the electrode were calculated

from the gold oxide reduction peak (using a literature value of 482 µC cm^{-2} to evaluate electrochemical area[15, 16]). Working electrodes were thoroughly rinsed with ultrapure water and dried under a stream of argon, before SAM fabrication.

5.6.3.1. Self-Assembled Monolayer Preparation:

2.0 µL of 100 µM DNA disulphide probe was centrifuged for 30 seconds with 2.0 µL of 10 mM TCEP and incubated at rt for 1 h. The solution was diluted to 200 µL (conc. of DNA is 1 µM) with 10 mM sodium phosphate buffer pH 7.0, 1 M sodium perchlorate. The gold working electrode was soaked in the solution for 2 h at rt. The electrode was then rinsed with ultrapure water and soaked in a 2 mM 6-mercapto-1-hexanol, 10 mM sodium phosphate buffer pH 7.0, 1 M sodium perchlorate solution overnight. The electrode was rinsed with ultrapure water, dried under a stream of argon and subjected to electrochemical sensing studies.

5.6.3.2. Electrochemical Sensing Procedure:

The working electrode (now functionalised with a SAM of DNA probes) was allowed to equilibrate for 5 min in the buffer before electrochemical measurements were taken. Square wave voltammetry (SWV) measurements were performed in triplicate, using an amplitude of 200 Hz and a step of 4 mV, before cyclic voltammograms were recorded. The target strand was added to the solution and 20 min were allowed for hybridisation, before electrochemical measurements are repeated.

The parameters for measurements were as follows: The potential window was dependent on the buffer conditions used, with a window of -75 mV to 525 mV used for 10 mM tris hydrochloride buffer pH 7.0, 100 mM sodium chloride, whilst a window of -75 mV to 550 mV

was used for 10 mM sodium phosphate buffer pH 7.0, 1 M sodium perchlorate. For SWV, a 4 mV potential step, 25 mV amplitude and 200 Hz frequency were employed. CVs were recorded at a range of scan rates to assess the scan rate dependence: 10, 20, 40, 60, 80, 100, 250, 500 and 1000 mV s^{-1}.

For ratiometric sensing, the ratio of the cyclidene complex current intensity to the reference ferrocene current intensity (Cyc:Fc) was used to assess the changes in current upon target binding. The CVs recorded at a scan rate of 1000 mV s^{-1} were used for these calculations because the peaks were largest at this scan rate, but any scan rate could be used. The data were processed using Origin Student 2019b software (Northampton, MA, USA).

5.6.3.3. Regeneration of the Unbound Probe:

Following measurements, the working electrode with probe was soaked in ultrapure water and sonicated for 1 min. The electrode was then rinsed with ultrapure water and returned to a solution of buffer before square wave and cyclic voltammogram measurements were made as previously stated.

5.7. References

1. M. D'auria, *Synth. Commun.*, 1992, **22**, 2393.
2. A. E. Koumbis, C. M. Kyzas, A. Savva and A. Varvoglis, *Molecules*, 2005, **10**, 1340.
3. Y. Wakatsuki and H. Yamazaki, *Inorg. Synth.*, 1989, **26**, 190.
4. A. M. Stevens and C. J. Richards, *Organometallics*, 1999, **18**, 1346.
5. D. J. Cassar, E.Nagaradja, D. C. D. Butler, D. Villemin and C. J. Richards, *Org. Lett.*, 2012, **14**, 894.
6. J. Li, K. Subramaniam, D. Smith, J. X. Qiao, J. J. Li, J. Qian-Cutrone, J. F. Kadow, G. D. Vite and B.-C. Chen, *Org. Lett.*, 2012, **14**, 214.
7. K. H. Ahn, C.-W. Cho, H.-H. Baek, J. Park and S. Lee, *J. Org. Chem.*, 1996, **61**, 4937.
8. C. R. Hutchinson, M. Nakane, H. Gollman and P. L. Knutson, *Org. Synth.*, 1986, **64**, 144.
9. S. Takamura, T. Yoshimiya, S. Kameyama, A. Nishida, H. Yamamoto and M. Noguchi, *Synthesis*, 2000, **5**, 637.
10. A. Rybka, R. Kolinski, J. Kowalski, R. Szmigielski, S. Domagała, K. Wozniak, A. Wieckowska, R. Bilewicz and B. Korybut-Daszkiewicz, *Euro. J. Inorg. Chem.*, 2007, 172.
11. J.-L. H. A. Duprey, J. Carr-Smith, S. L. Horswell, J. Kowalski and J. H. R. Tucker, *J. Am. Chem. Soc*, 2016, **138**, 746.
12. T. Ihara, D. Sasahara, M. Shimizu and A. Jyo, *Supramolecular Chemistry*, 2009, **21**, 207.
13. H. V. Nguyen, Z. Zhao, A. Sallustrau, S. L. Horswell, L. Male and J. H. R. Tucker, *Chem. Commun.*, 2012, **48**, 12165.
14. L. Bailey, MSci Dissertation, University of Birmingham, 2019.
15. U. Oesch and J. Janata, *Electrochimica Acta*, 1983, **28**, 1237.
16. J. C. Hoogvliet, M. Dijksma, B. Kamp and W. P. v. Bennekom, *Anal. Chem.*, 2000, **72**, 2016.

6. Appendix

6.1. Controlling the Rotary Motion of Cobalt Sandwich Complexes

6.1.1. Crystal Data for 2.15

Empirical formula	$C_{41}H_{39}CoO_6$
Formula weight	686.65
Temperature / K	100.00(10)
Crystal system	Monoclinic
Space group	$P2_1/n$
a / Å	12.3074(3)
b / Å	14.5432(3)
c / Å	19.5824(4)
α / °	90
β / °	107.117(2)
γ / °	90
Volume / $Å^3$	3349.76(13)
Z	4
ρ_{calc}g / cm^3	1.362
μ / mm^{-1}	0.561
F (000)	1440.0
Crystal size / mm^3	0.278 × 0.086 × 0.072
Radiation	MoKα (λ = 0.71073)
2Θ range for data collection / °	6.01 to 54.968
Index ranges	-15 ≤ h ≤ 15, -18 ≤ k ≤ 18, -25 ≤ l ≤ 24
Reflections collected	37265
Independent reflections	7611 [R_{int} = 0.0301, R_{sigma} = 0.0264]
Data / restraints / parameters	7611/0/440
Goodness-of-fit on F^2	1.042
Final R indexes [I>=2σ (I)]	R_1 = 0.0333, wR_2 = 0.0753
Final R indexes [all data]	R_1 = 0.0416, wR_2 = 0.0794
Largest diff. peak/hole / e $Å^{-3}$	0.34/-0.33

6.1.2. Variable Temperature NMR

6.1.2.1. Rotary System 2.10 in Methanol at Acidic pH

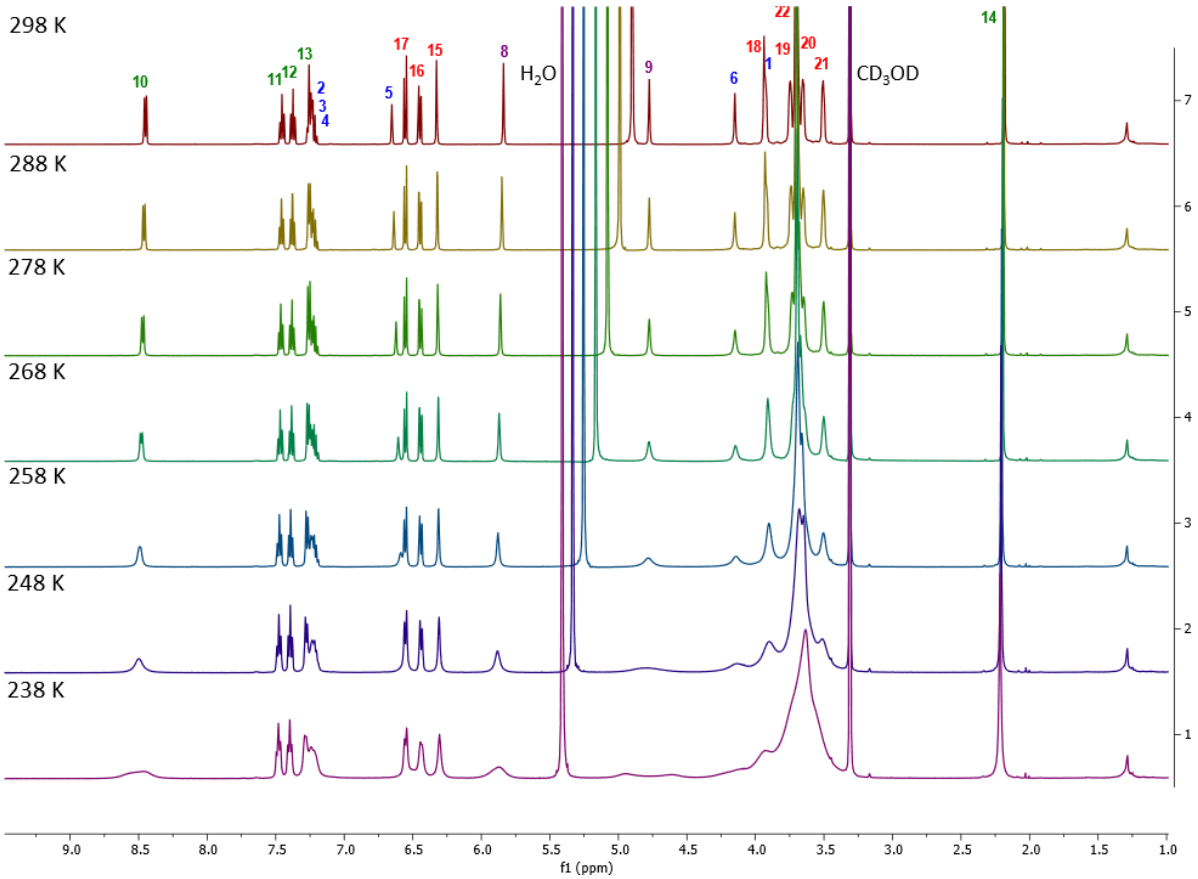

*Figure 6.1: Overlaid VT ^{1}H NMR spectra of rotary system **2.10** in deuterated methanol with 1.2 equiv. of deuterated TFA, recorded at 10-degree increments. Concentration of **2.10** is 8.93 x 10^{-3} mol dm^{-3}.*

6.1.2.2. Rotary System 2.10 T_c in Acetonitrile at Acidic pH

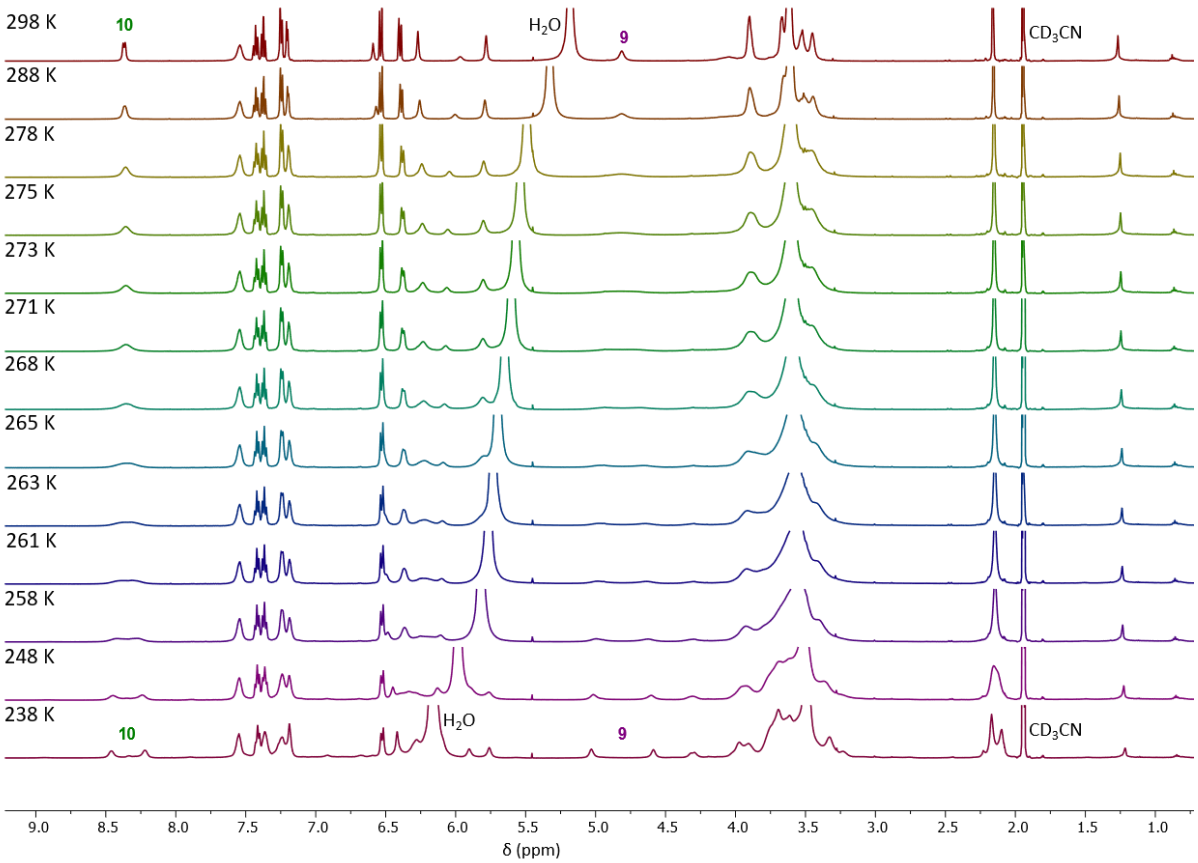

*Figure 6.2: Overlaid VT ^{1}H NMR spectra of rotary system **2.10** in deuterated acetonitrile with 1.2 equiv. of deuterated TFA, recorded at 10-degree increments, with additional measurements taken around the temperature of coalescence of signals 9 and 10. Concentration of **2.10** is 14.66 x 10^{-3} mol dm^{-3}.*

6.1.2.3. Rotary System 2.10 Under Cationic Control: Reversibility

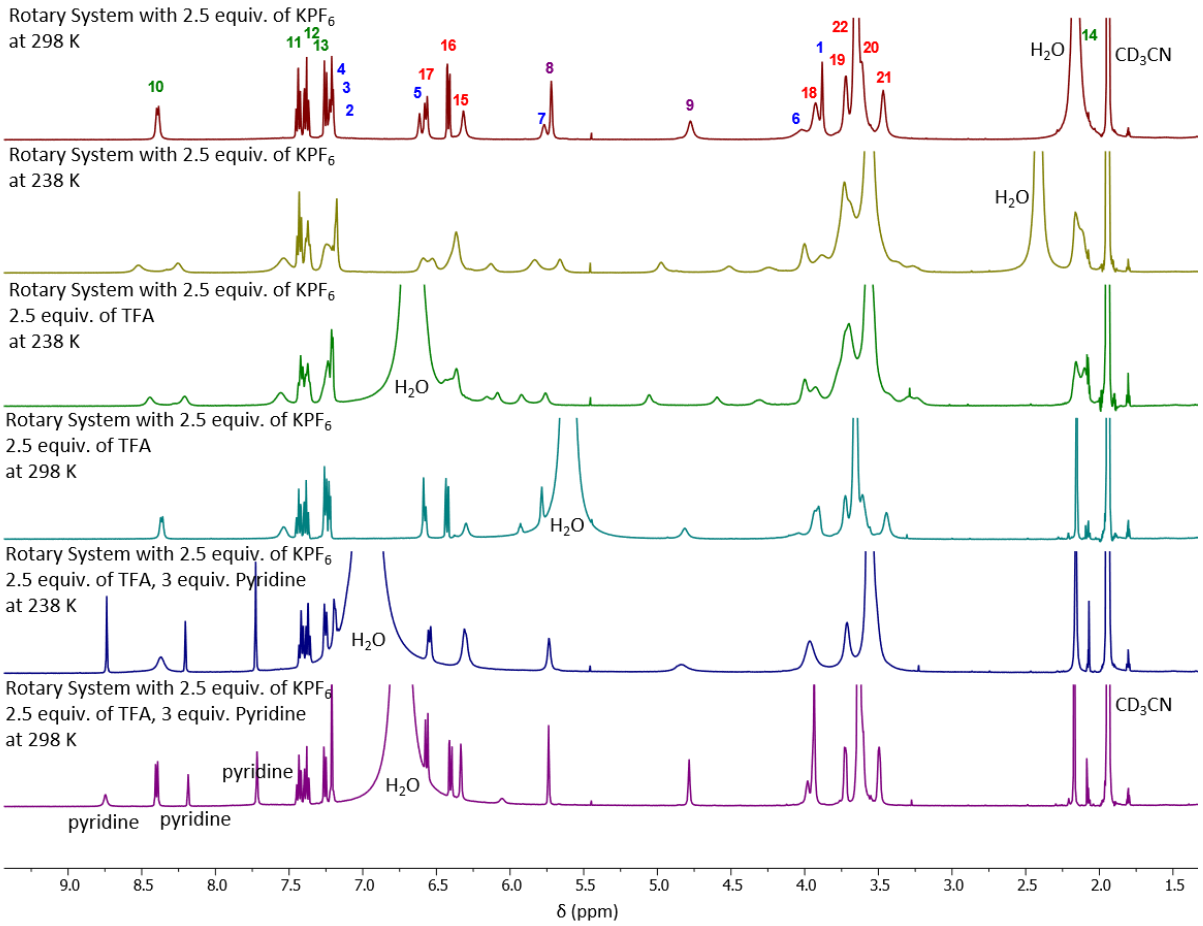

6.2. Metal-Modified Nucleic Acids

6.2.1. DNA Characterisation

Name	Sequence	Predicted Mass / m/z	Detected Mass / m/z	Purity by analytical HPLC / %
NiLink10mer	5' - CC GGG **X** CCC GG - 3'	3542.000	3542.635	99.72
NiLink40mer	5' – GCA ATA CTA TTT CGA TCT GG **X** AC ATG GTA GAA GGA GGA AAG – 3'	13046.514	13046.514	100.00
3NiLink30mer	5' - TTG TG - **X** - TT ATT GGT CA - **X** - TT AGG TTG AA - **X** - CC GAT - 3'	10895.320	10892.052	100.00
X = Nickel Cyclidene Link				

6.2.2. HPLC Traces:

The analytical HPLC traces of the purified modified oligonucleotides are included below. The purity is assessed by determining the percentage-area under the peak. Strands must be at least 95% pure to be used experimentally.

6.2.2.1. NiLink10mer

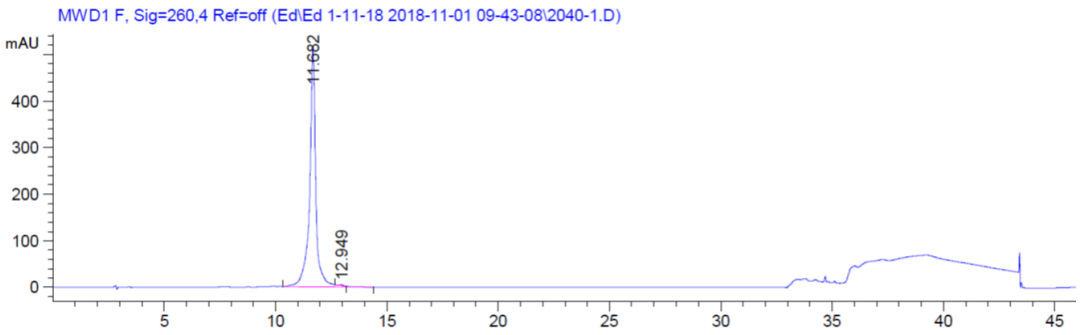

6.2.2.2. NiLink40mer

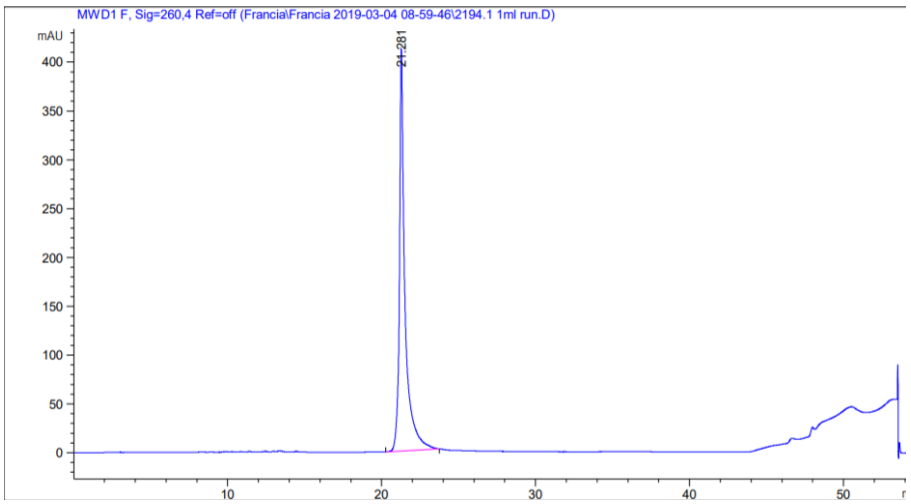

6.2.2.3. 3NiLink30mer

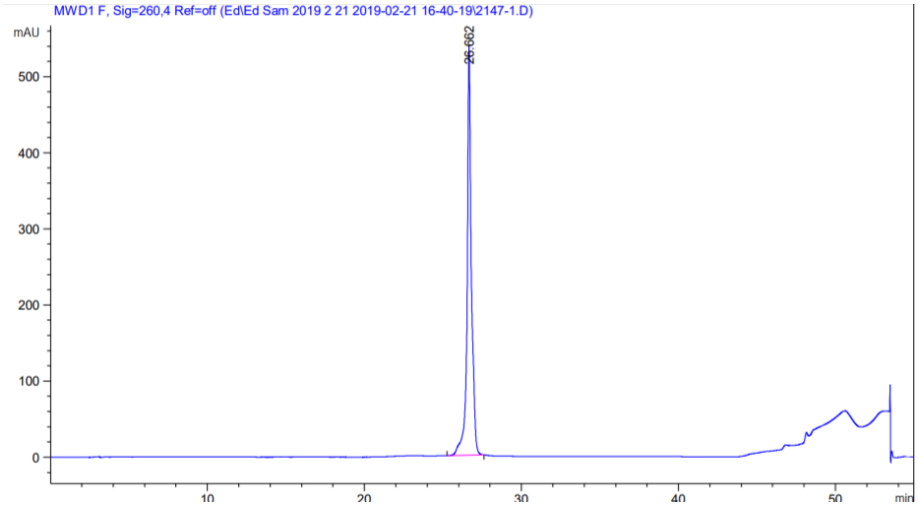

6.2.3. Electrochemistry

6.2.3.1. Nilink10mer

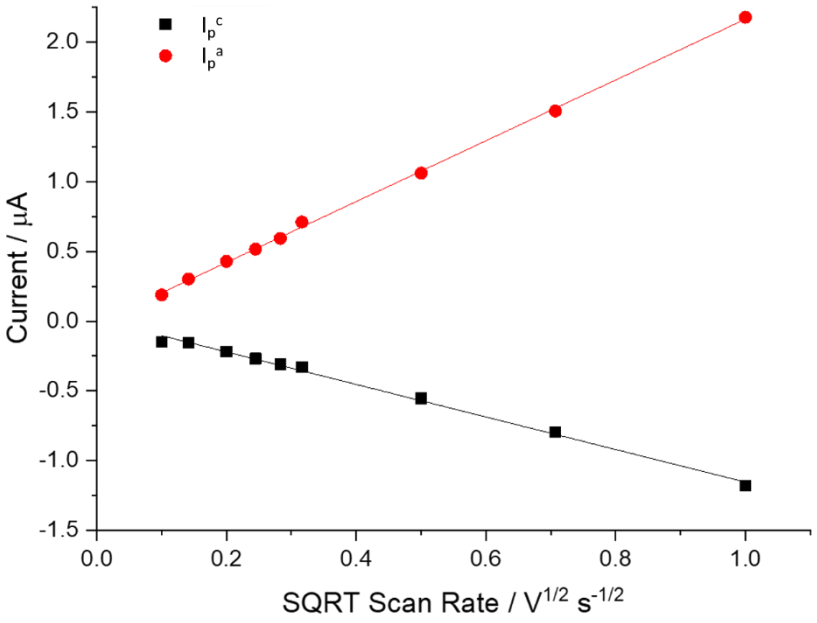

6.2.3.2. NiLink40mer

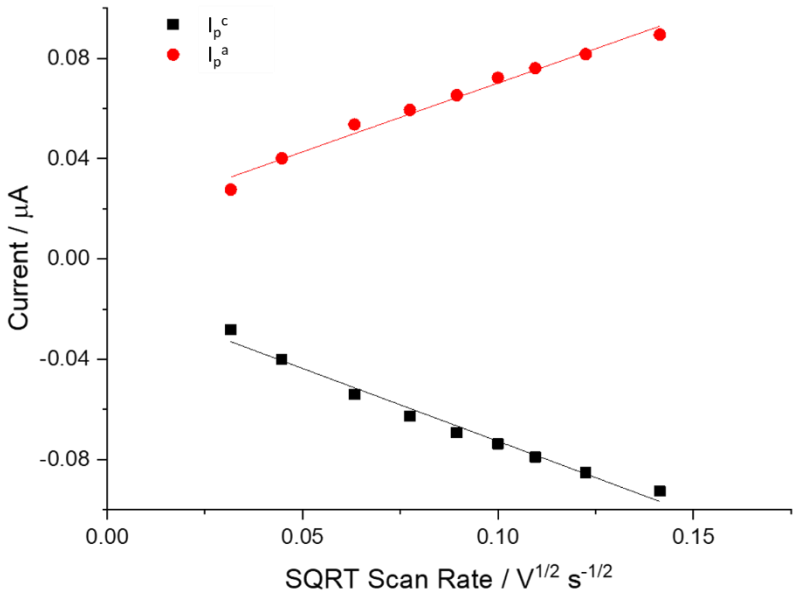

6.3. Electrochemical Sensing with Metal-Modified Nucleic Acid Probes

6.3.1. DNA Characterisation

6.3.1.1. Unmodified DNA

Name	Description	Sequence	Predicted Mass / m/z	Detected Mass / m/z	Purity by analytical HPLC / %
-	Unmodified NINA Probe	5'– TGG ACT CTC TCA ATG - 3'	4540.79	4540.66	98.79
Target-G	NINA G Target	5' – CAT TGA GGG AGT CCA – 3'	4614.81	4614.67	100.00
Target-C	NINA C Target	5' – CAT TGA GCG AGT CCA – 3'	4574.81	4574.67	100.00
Target-T	NINA T Target	5' – CAT TGA GTG AGT CCA – 3'	4589.81	4589.68	98.60
Target-A	NINA A Target	5' – CAT TGA GAG AGT CCA – 3'	4598.82	4598.69	97.60
Scrambled Target	Scrambled Target	5' – ACA GCT TCA TGG AAG – 3'	4598.82	4598.86	100.00
-	Unmodified BRAF Probe	5' - AGA TTT CAC TGT AGC – 3'	4564.80	4564.85	100.00
BRAF Target-T	BRAF T Wild Type Target	5' – GCT ACA GTG AAA TCT – 3'	4573.81	4573.67	100.00
BRAF Target-A	BRAF A Mutant Target	5' – GCT ACA GAG AAA TCT – 3'	4582.82	4582.69	100.00
-	Unmodified KRAS Probe	5' – TAC GCC ACC AGC TCC - 3'	4455.78	4456.07	100.00
KRAS Target-G	KRAS Wild Type G Target	5' – GGA GCT GGT GGC GTA – 3'	4686.81	4686.86	100.00
KRAS Target-T	KRAS Mutant T Target	5'– GGA GCT GTT GGC GTA – 3'	4661.80	4661.85	98.57
KRAS Target-A	KRAS Mutant A Target	5'– GGA GCT GAT GGC GTA – 3'	4670.82	4670.85	97.29

6.3.1.2. Modified DNA

Name	Description	Sequence	Predicted Mass / m/z	Detected Mass / m/z	Purity by analytical HPLC / %
FcCycNINA	NINA Fc Cyc Modified Probe	5'– Fc TGG ACT C Cyc C TCA ATG SS - 3'	5466.00	2465.730	100.00
CycNINA	NINA Cyc Modified Probe	5'– TGG ACT C Cyc C TCA ATG SS - 3'	4769.83	4769.673	98.90
FcNINA	NINA Fc Modified Probe	5' – Fc TGG ACT CTC TCA ATG SS – 3'	5237.21	5237.063	100.00
-	BRAF Cyc Modified Probe	5' – AGA TTT C Cyc C TGT AGC SS – 3'	5117.23	5116.727	98.15
FcCycBRAF	BRAF Fc Cyc Modified Probe	5' – Fc AGA TTT C Cyc C TGT AGC SS – 3'	5480.00	5480.758	100.00
FcCycKRAS	KRAS Fc Cyc Modified Probe	5' - Fc TAC GCC A Cyc C TCC SS – 3'	5396.00	5396.425	100.00
Fc = Ferrocene, Cyc = Copper Cyclidene Tag Complex, SS = 6 SS 3' disulphide					

6.3.2. HPLC Traces:

The analytical HPLC traces of the purified modified oligonucleotide probes are included below. The purity is assessed by determining the percentage-area under the peak. Strands must be at least 95% pure to be used experimentally.

6.3.2.1. FcCycNINA Probe:

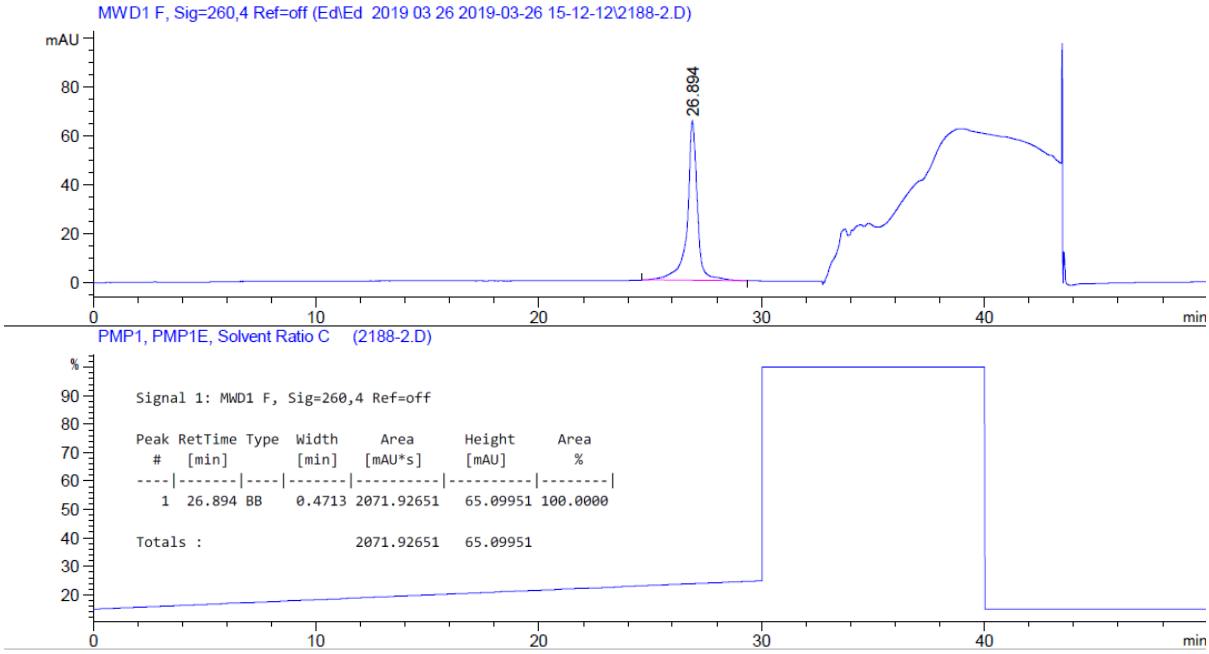

6.3.2.2. CycNINA Probe:

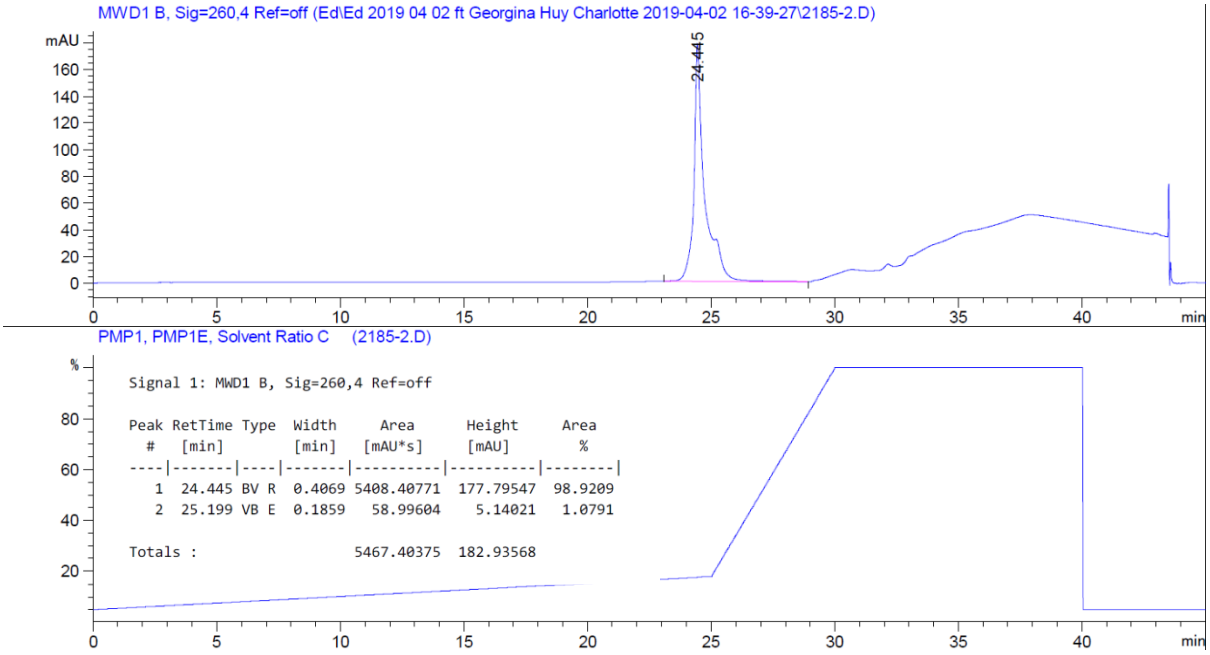

6.3.2.3. FcNINA Modified Probe:

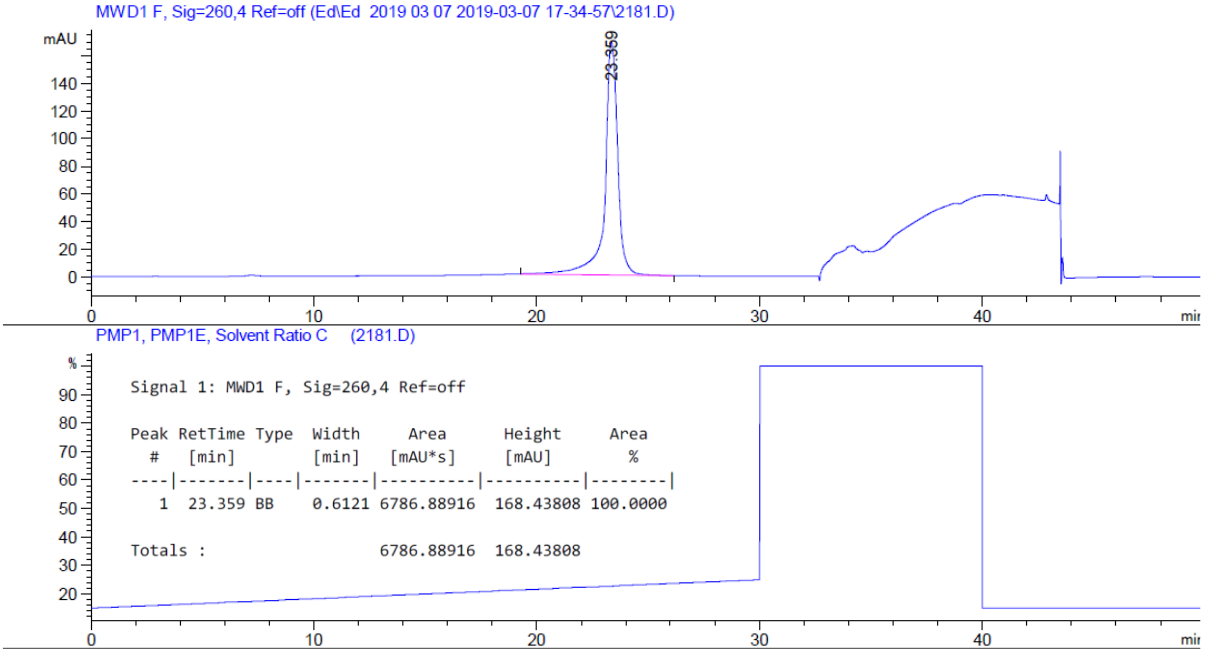

6.3.2.4. FcCycBRAF Probe:

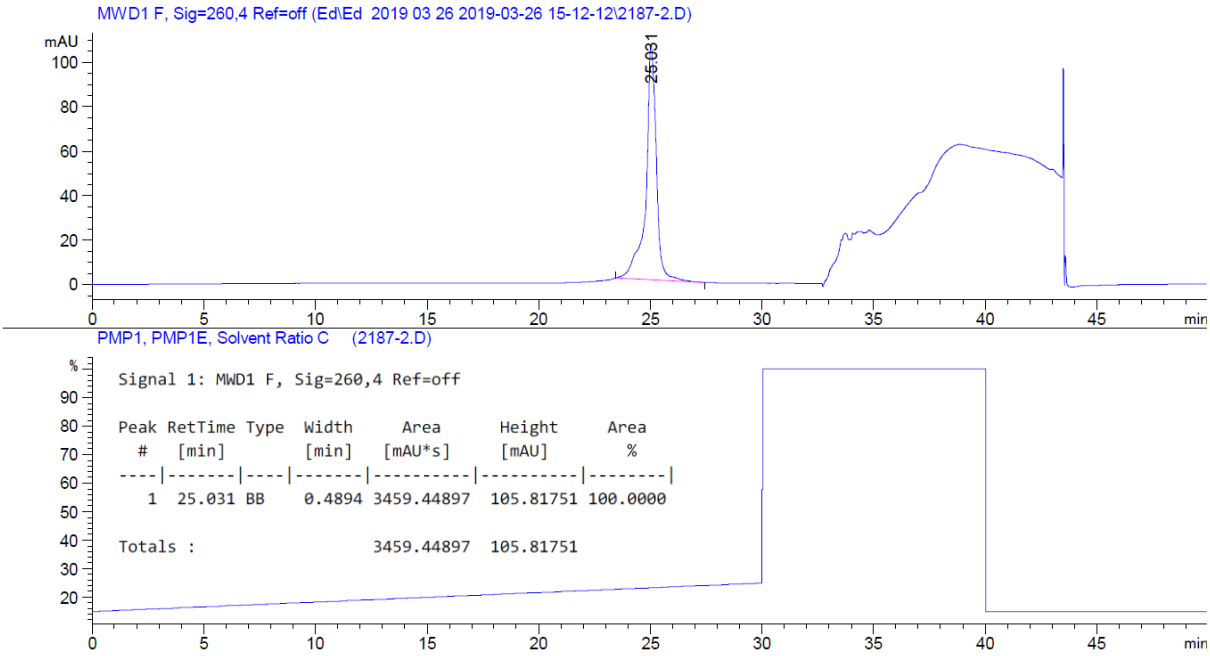

6.3.2.5. FcCycKRAS Probe:

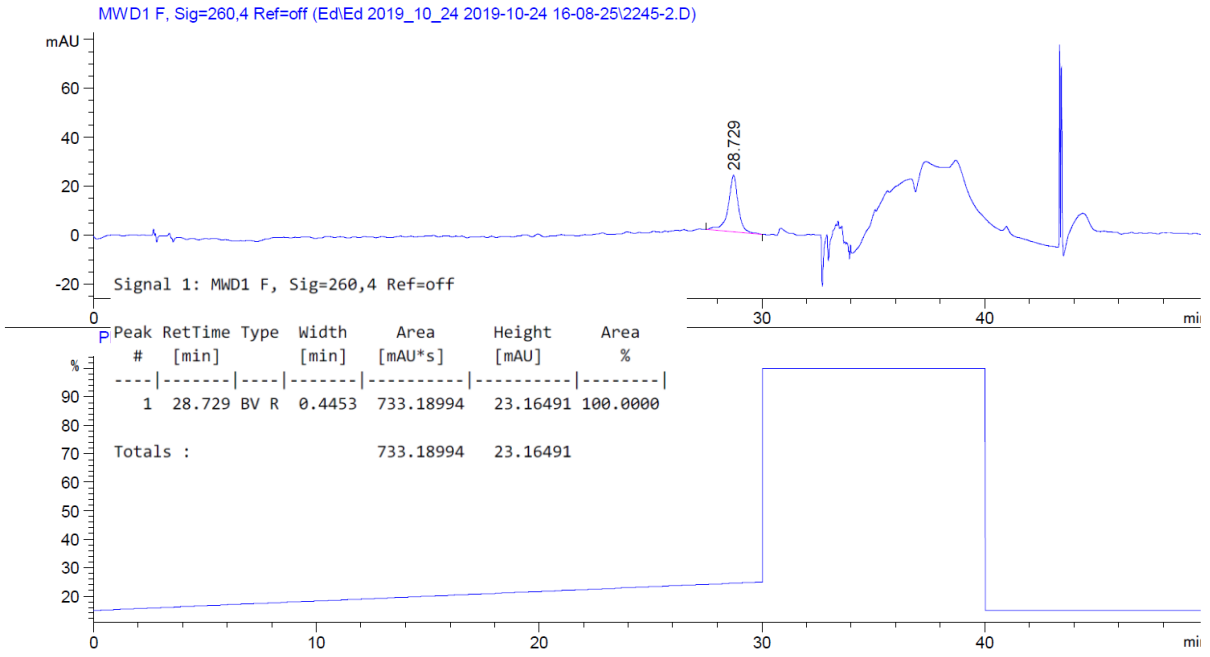

6.3.3. Electrochemical Sensing Summary

The values reported are the average percentage decrease observed in the Cyc:Fc ratio upon target binding. Each value was repeated at least in triplicate and across a variety of polycrystalline gold working electrodes. Due to the consistency of the electrochemical output, the average value incorporates measurements taken between 1 µM and 10 fM target concentrations across four polycrystalline gold working electrodes. Error values are reported at a 95% confidence level of the standard error of the mean.

Table 6.1: Sensing summary of ratiometric probes in 10 mM Tris HCl pH 7.0 100 mM NaCl Buffer. Values reported are the average % decreases in Cyc:Fc current ratio observed upon varying the nucleobase opposite the cyclidene. [Target] = 1 µM to 10 fM.

Probe	**T / %**	**A / %**	**G / %**	**C / %**
FcCycNINA Ratiometric	38.32 ± 0.64	26.11 ± 0.56	31.95 ± 0.64	33.53 ± 0.58
FcCycBRAF Ratiometric	16.38 ± 0.66	9.16 ± 1.43	n.d.	n.d.
FcCycKRAS Ratiometric	28.64 ± 0.96	22.09 ± 0.42	24.44 ± 0.55	n.d.

Table 6.2: Sensing summary of ratiometric probes in 10 mM Na Phosphate pH 7.0 1 M $NaClO_4$ Buffer. Values reported are the average % decreases in Cyc:Fc current ratio observed upon varying the nucleobase opposite the cyclidene. [Target] = 1 µM to 10 fM.

Probe	**T / %**	**A / %**	**G / %**	**C / %**
FcCycNINA Ratiometric	29.64 ± 0.76	20.89 ± 1.19	18.75 ± 0.90	23.55 ± 1.11
FcCycBRAF Ratiometric	13.80 ± 1.77	14.93 ± 2.97	n.d.	n.d.
FcCycKRAS Ratiometric	26.49 ± 0.95	22.73 ± 1.54	16.67 ± 1.23	n.d.

6.3.4. Cyclic Voltammograms

6.3.4.1. FcCycNINA

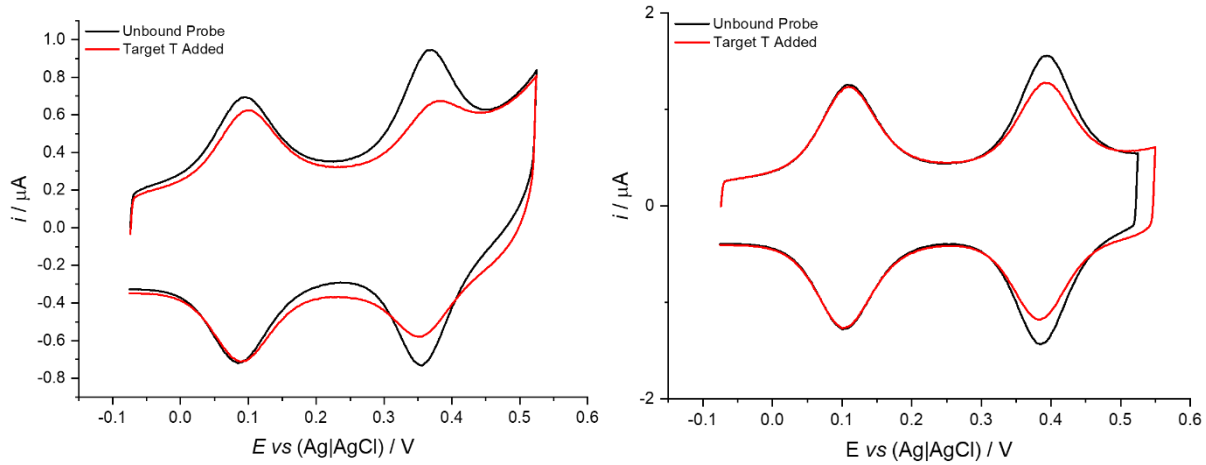

Figure 6.4: Cyclic Voltammograms of the FcCycNINA Ratiometric Probe with Target-T Strand in 10 mM Tris HCl Buffer 100 mM NaCl, [Target] = 100 nM (left) and 10 mM Na Phosphate Buffer 1 M $NaClO_4$, [Target] = 100 pM (right).

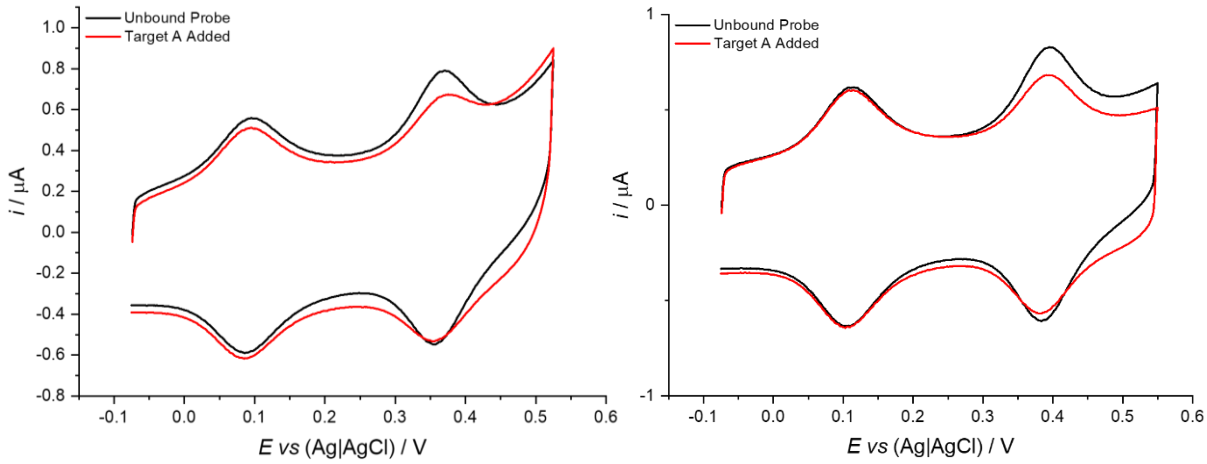

Figure 6.5: Cyclic Voltammograms of the FcCycNINA Ratiometric Probe with Target-A Strand in 10 mM Tris HCl Buffer 100 mM NaCl, [Target] = 100 pM (left) and 10 mM Na Phosphate Buffer 1 M $NaClO_4$, [Target] = 10 fM (right).

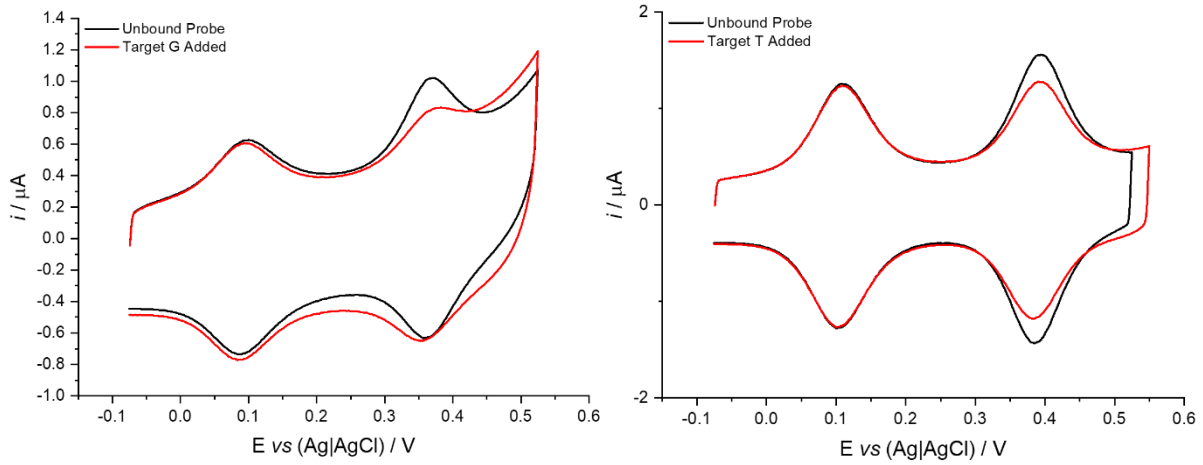

Figure 6.7: Cyclic Voltammograms of the FcCycNINA Ratiometric Probe with Target-G Strand in 10 mM Tris HCl Buffer 100 mM NaCl, [Target] = 10 nM (left) and 10 mM Na Phosphate Buffer 1 M $NaClO_4$, [Target] = 100 pM (right).

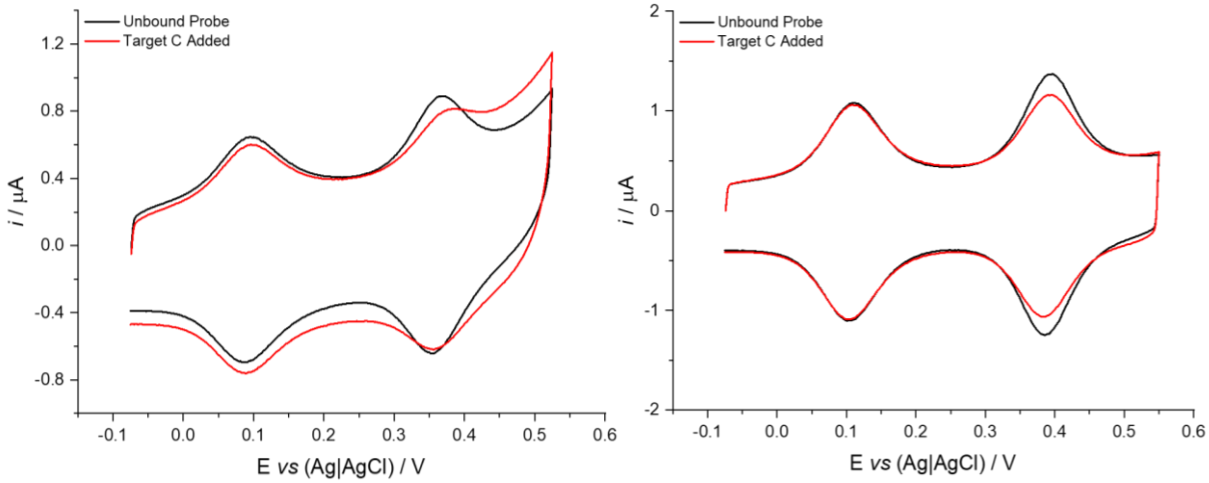

6.3.4.2. FcCycBRAF

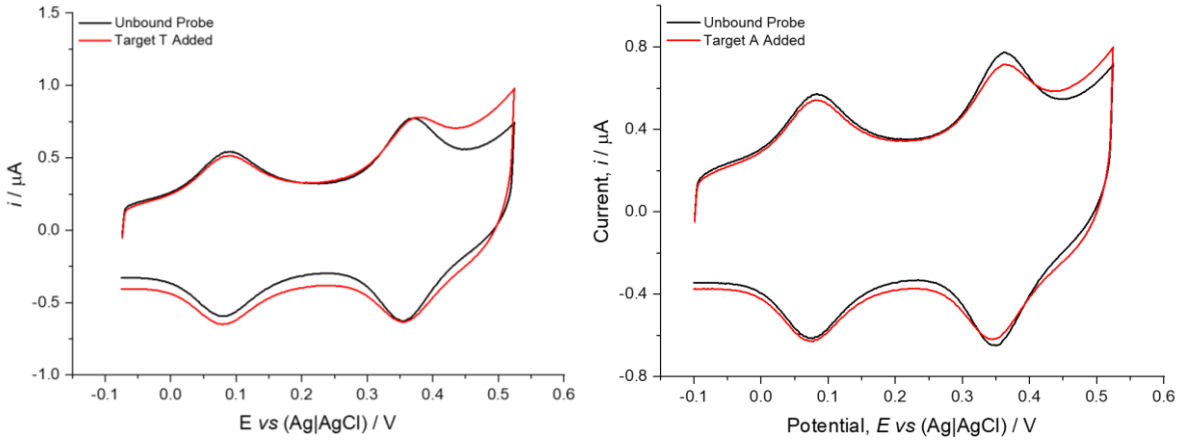

Figure 6.8: Cyclic Voltammograms of the FcCycBRAF Ratiometric Probe with Target-T Strand, [Target] = 100 pM (left) and Target-A Strand, [Target] = 10 fM (right) in 10 mM Tris HCl Buffer 100 mM NaCl.

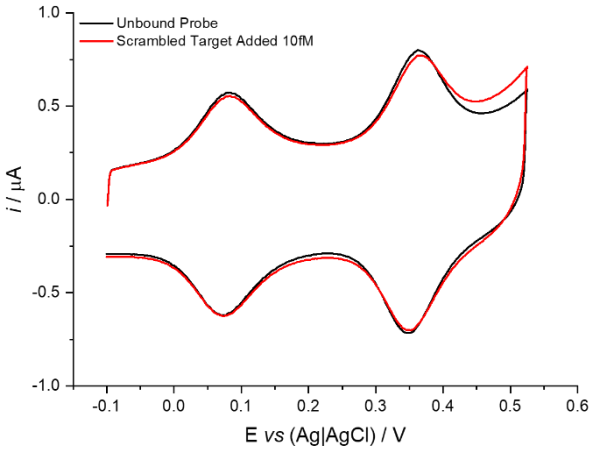

Figure 6.9: Cyclic Voltammogram of the FcCycBRAF Ratiometric Probe with Scrambled Target, [Target] = 10 fM in 10 mM Tris HCl Buffer 100 mM NaCl.

6.3.4.3. FcCycKRAS

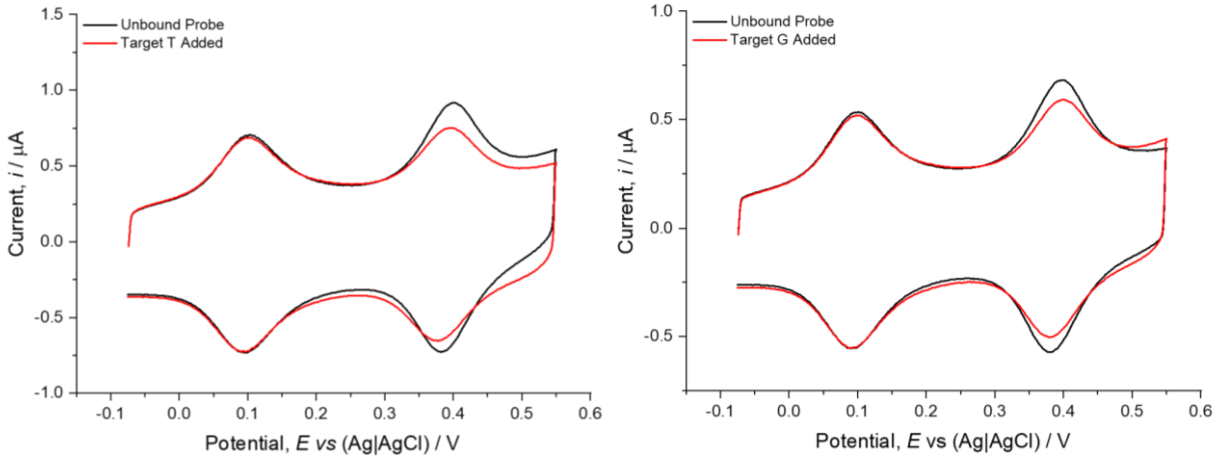

Figure 6.10: Cyclic Voltammograms of the FcCycKRAS Ratiometric Probe with Target-T Strand, [Target] = 10 fM (left) and Target-G Strand, [Target] = 10 fM (right) in 10 mM Na Phosphate Buffer 1 M $NaClO_4$.

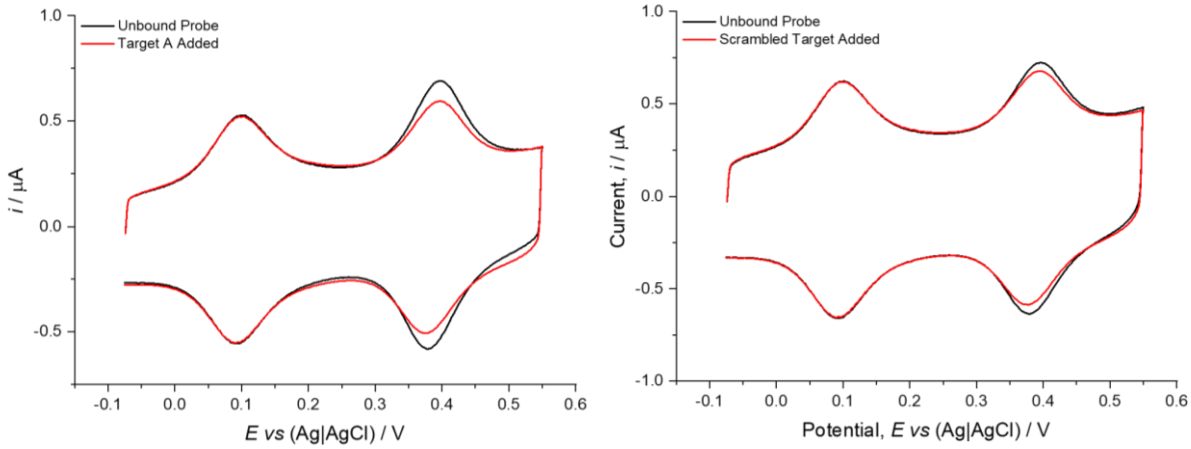

Figure 6.11: Cyclic Voltammograms of the FcCycKRAS Ratiometric Probe with Target-A Strand, [Target] = 10 fM (left) and Scrambled Target Strand, [Target] = 10 fM (right) in 10 mM Na Phosphate Buffer 1 M $NaClO_4$.

6.3.5. Electrochemical Sensing Buffer Summary

Table 6.3: Sensing summary of ratiometric probes. Values reported are the average % decreases in Cyc:Fc current ratio observed upon varying the nucleobase opposite the cyclidene. [Target] = 1 µM to 10 fM. Error values reported aat a 95% confidence level of the standard error of the mean.

Buffer Conditions	Average Percentage Decrease in Cyclidene:Ferrocene Current Ratio / %			
	T	A	G	C
10 mM Tris HCl Buffer (pH 7.0), 100 mM NaCl	38.32 ± 0.64	26.11 ± 0.56	31.95 ± 0.63	33.53 ± 0.58
10 mM Na Phosphate Buffer (pH 7.0), 1 M $NaClO_4$	29.64 ± 0.76	20.89 ± 1.19	18.75 ± 0.90	23.55 ± 1.11
10 mM Tris HCl Buffer (pH 7.0), 1 M $NaClO_4$	53.34 ± 1.37	43.65 ± 3.07	42.47 ± 3.63	45.93 ± 1.01
10 mM Na Phosphate Buffer (pH 7.0), 100 mM NaCl	25.29 ± 1.42	20.74 ± 1.02	13.45 ± 2.42	18.39 ± 1.33

6.3.6. Control Studies:

A control probe with the ferrocene on the 5' terminus without the cyclidene in the centre was synthesised, FcNINA, and subjected to electrochemical examination. As expected, the ferrocene redox signal behaved in an identical fashion to the sensing probes, confirming that its peak position and any variations in current are not affected by the cyclidene moiety in the DNA strand. Likewise, probes containing only the cyclidene unit, CycNINA, behave similarly in the absence of ferrocene as they do with ferrocene. Finally, 'blanks' were run of the working electrodes without a SAM of probe in the buffers used, and no redox peaks were observed in the regions where the Cu(II/III) redox couple of the cyclidene, and the Fe(II/III) redox couple of the ferrocene occur.

Table 6.4: The electrochemical potential shift exhibited by the probes vs Ag/AgCl reference electrode in the buffer conditions.

	Square Wave Voltammetry		**Cyclic Voltammetry**	
Probe	*10 mM Tris HCl Buffer 100 mM NaCl*	*10 mM Na Phosphate Buffer 1 M $NaClO_4$*	*10 mM Tris HCl Buffer 100 mM NaCl*	*10 mM Na Phosphate Buffer 1 M $NaClO_4$*
FcCyc NINA Ratiometric Probe	**Fc:** 0.089 V	0.109 V	0.092 V	0.109 V
	Cyc: 0.365 V	0.389 V	0.364 V	0.389 V
Fc NINA Modified Probe	0.093 V	0.105 V	0.093 V	0.108 V
CycNINA Modified Probe	0.364 V	0.389 V	0.363 V	0.390 V

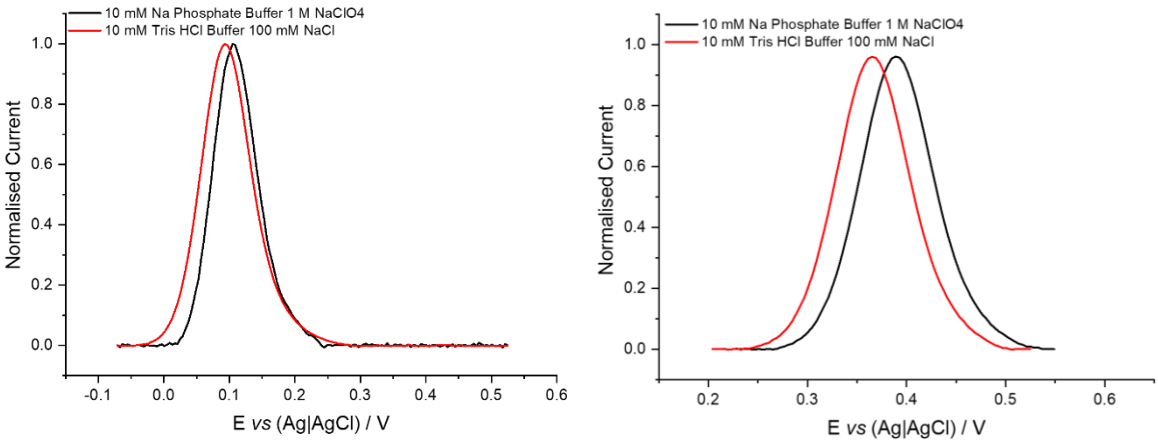

Figure 6.12: Square Wave Voltammograms of the FcNINA (left) and CycNINA (right) modified probes, exhibiting the impact of different buffer conditions on the electrochemical potential shift.

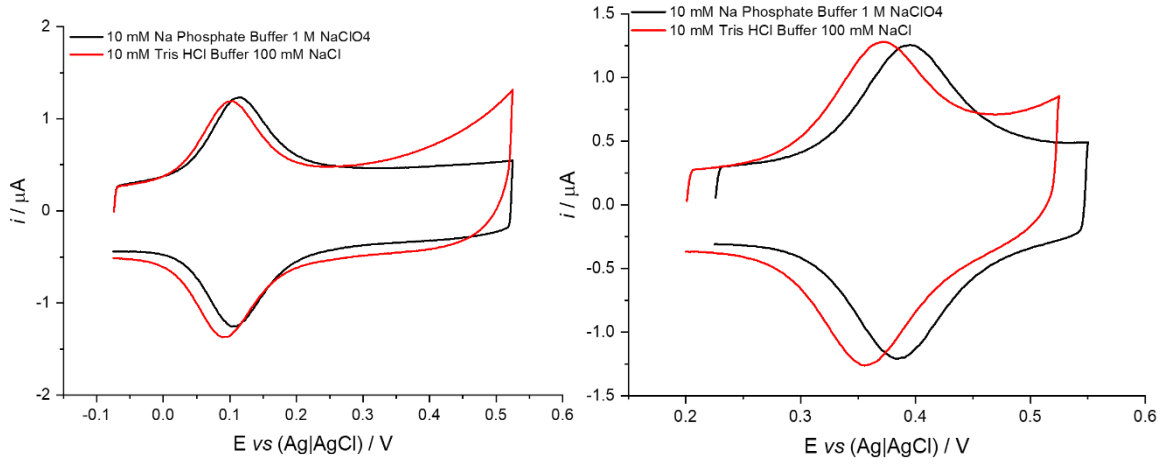

Figure 6.13: Cyclic Voltammograms of the FcNINA (left) and CycNINA (right) modified probes, showing the effect of different buffer conditions on the electrochemical potential shift.

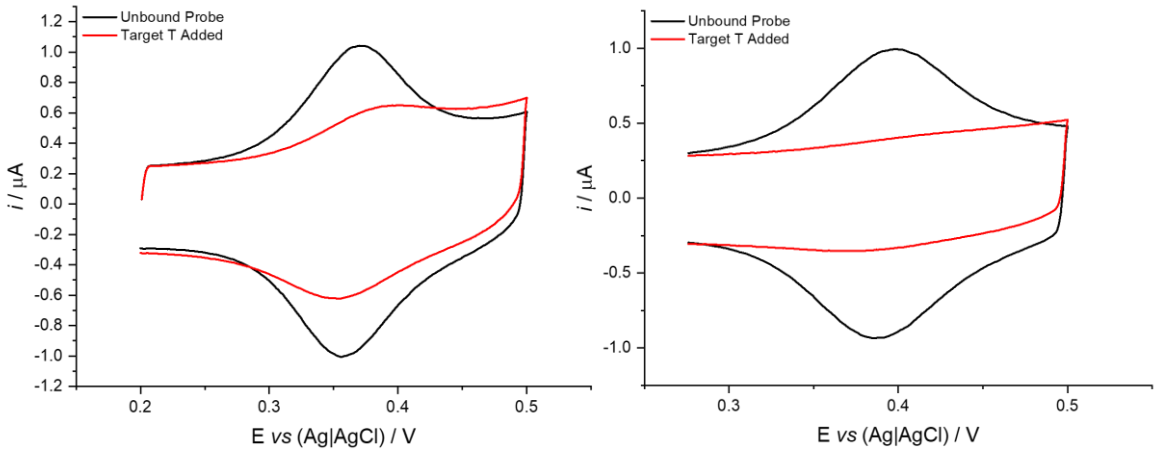

Figure 6.14: Cyclic Voltammograms of the CycNINA modified probe in 10 mM Tris HCl Buffer 100 mM NaCl (left) and 10 mM Na Phosphate Buffer 1 M $NaClO_4$ (right). Decrease in current signal is observed upon target addition.

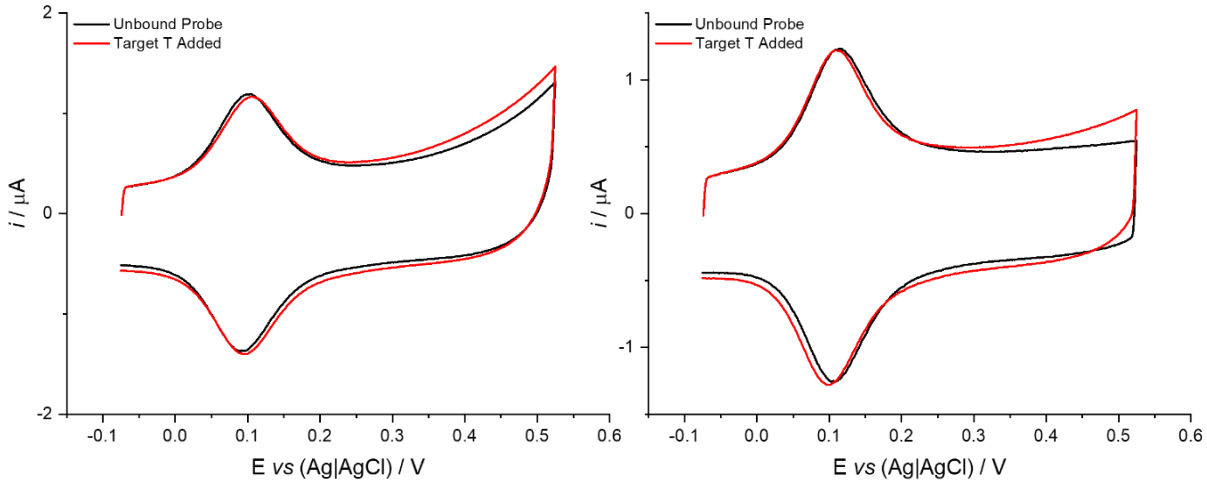

Figure 6.16: Cyclic Voltammograms of the FcNINA modified probe in 10 mM Tris HCl Buffer 100 mM NaCl (left) and 10 mM Na Phosphate Buffer 1 M $NaClO_4$ (right). Barely any change in current signal is observed upon target addition. This is a good example of the choice of buffers effect on the background signal; the NaCl buffer causes higher background, partly from chloride adsorption onto the electrode.

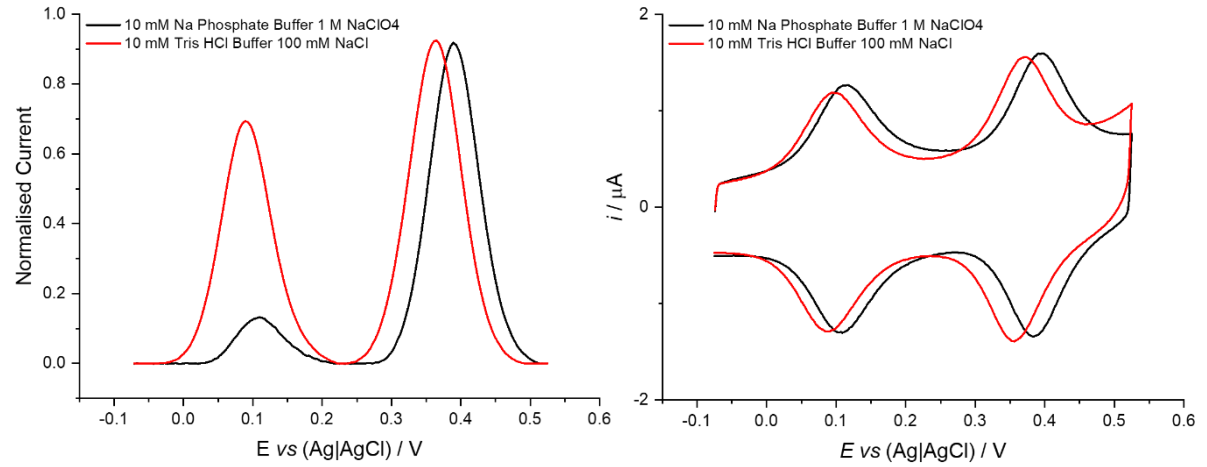

Figure 6.15: Square Wave Voltammograms (left) and Cyclic Voltammograms (right) of the Test Fc Cyc Ratiometric Probe, showing the effects of different buffers on the electrochemical potential shift.